UC Berkeley
UC Berkeley Electronic Theses and Dissertations

Title

Interrogation of the powdery mildew-host plant interaction at the intersection of cell cycle regulation and metabolism reveals insights into obligate biotrophy

Permalink

https://escholarship.org/uc/item/1wg4s80p

Author

McRae, Amanda Grace

Publication Date

2020

Peer reviewed|Thesis/dissertation

eScholarship.org Powered by the California Digital Library
University of California

Interrogation of the powdery mildew-host plant interaction at the intersection of cell cycle regulation and metabolism reveals insights into obligate biotrophy

By

Amanda Grace McRae

A dissertation submitted in partial satisfaction of the

requirements for the degree of

Doctor of Philosophy

in

Microbiology

in the

Graduate Division

of the

University of California, Berkeley

Committee in charge:

Professor Mary Wildermuth, Chair
Professor Georjana Barnes
Professor Jennifer Lewis
Professor Shauna Somerville

Summer 2020

Abstract

Interrogation of the powdery mildew-host plant interaction at the intersection of cell cycle regulation and metabolism reveals insights into obligate biotrophy

by

Amanda Grace McRae

Doctor of Philosophy in Microbiology

University of California, Berkeley

Professor Mary Wildermuth, Chair

Powdery mildew fungi are obligate biotrophs that obtain all nutrients from their plant host. This widespread pathogen infects agriculturally important crops like wheat, barley, cucurbits, and grapevine which can require numerous fungicide treatments to control. The powdery mildew *Golovinomyces orontii* infects the model plant *Arabidopsis thaliana*. Endoreduplication, or DNA replication without division, is induced in plant cells underlying its fungal feeding structure. This resulting enhanced DNA content supports its asexual reproduction. Fungal asexual reproductive structures contain chains of spores filled with lipid bodies. Elevated ploidy has long been associated with enhanced metabolic capacity, yet the induction of and metabolic changes resulting in this phenomenon remain underexplored. Here, metabolic and cell cycle contributors from the host and pathogen side are explored.

First, we show that a local ploidy-associated shift in plant primary metabolism to use the pyruvate dehydrogenase (PDH) bypass acts in a dose-dependent manner to support fungal reproduction. Not only are plant PDH bypass-derived lipids incorporated into fungal spore storage lipids, but they also act in a regulatory capacity to control the number of reproductive structures per colony, ensuring the fitness of spores that are formed. Evolutionarily distant plant and animal biotrophs require host lipids for their growth and/or reproduction. We provide a mechanism by which energy-dense host lipids are increased for microbial utilization. Next, spray-induced gene silencing (SIGS) methods were developed for powdery mildew fungi to investigate powdery mildew genetic contributors of disease. SIGS is an emerging tool being developed to protect crops from disease. It utilizes exogenously applied RNA designed to reduce expression of critical genes in plant pests using endogenous RNA interference machinery. For grape powdery mildew, dominant varieties are susceptible to powdery mildew and extensive resistance to fungicides has caused a need for new disease management strategies. *G. orontii*, was found to uptake RNA directly from its environment, independent of the host. SIGS methods using long double-stranded (dsRNA) and small interfering RNA (siRNA) were developed using *A. thaliana* whole plant and detached leaf assays. Methods were optimized against the azole-fungicide target, *CYP51*. Ten additional powdery mildew targets were screened identifying five genes that contribute to fungal proliferation: *lipase a, lipase 1*, *β-carotene 15,15'-dioxygenase, apoptosis-antagonizing transcription factor* (*AATF*), and *effector candidate 2*; four of which represent novel powdery mildew virulence targets. Translation of these methods to the *Erysiphe necator-Vitis vinifera*

pathosystem showed similar reduction in disease with SIGS against *CYP51* and the novel target *AATF* indicating high throughput screening of conserved powdery mildew targets in the *G. orontii*-*A. thaliana* pathosystem could prioritize targets for testing in grapevine powdery mildew and other systems. SIGS may be the future of controlling powdery mildew growth on crops because of its flexibility, resilience to resistance development, reduced environmental and health risks, and rapid transition from the bench to the field.

Lastly, powdery mildew effectors and host targets were examined in the context of powdery mildew-induced endoreduplication. Plant TCP transcription factors which regulate growth and development are heavily targeted by effectors of diverse plant pathogens; many of these TCPs have described roles in regulating cell expansion, proliferation, or endoreduplication. In a yeast-two hybrid screen between *A. thaliana* proteins and *Golovinomyces orontii* MPIPZ effectors, 34% of the interactions identified involved TCP proteins. In this study the contribution of TCPs and their targeting effectors to powdery mildew infection is ascertained. Four of the five TCPs targeted by effectors were found to suppress *G. orontii* MGH1 growth. Adult *A. thaliana* T-DNA mutants *tcp13*, *tcp14*, *tcp15*, and *tcp20* were more susceptible to *G. orontii* MGH1. Using SIGS, homologs of *G. orontii* effector candidates (OECs) in *G. orontii* MGH1 were targeted. SIGS against *OEC14*, *OEC60/OEC61*, and *OEC70* resulted in significantly reduced spore production compared to controls. With previous SIGS results above, a total of 7 novel powdery mildew targets have been identified. Homolog OEC60/OEC61 was investigated further. It encodes a short N-terminal domain originally annotated in *G. orontii* MPIPZ OEC60 and OEC61 coupled to a larger glycosyl hydrolase family 17 domain (GH17). To date, OEC60 and OEC61 homologs across all sequenced powdery mildews include the GH17 domain, suggesting the lack of GH17 domain in the MPIPZ isolate may be due to the incomplete nature of that genome. GH17 domain-containing proteins are found widely in plants and fungi. When homolog of *OEC60/OEC61* is targeted in the *E. necator*-grapevine system, significantly less spores were produced, providing evidence this is a conserved powdery mildew virulence factor. Using *Agrobacterium*-mediated transient expression assays in *Nicotiana benthamiana*, *G. orontii* MGH1 homolog of OEC60/OEC61 is shown to be nuclear-targeted and co-localizes with TCP13 and TCP14. Co-immunoprecipitation further shows OEC60/OEC61 interacts with TCP13 *in planta*. Additionally, *tcp14* mutants have enhanced endoreduplication at the site of powdery mildew infection which is known to correlate with enhanced powdery mildew asexual reproduction. Together, a role for OEC60/OEC61 in limiting TCP13/14 function to promote endoreduplication at the infection site is indicated. To further elucidate this interaction node, proteomic analysis (2-D LC MS/MS) of the MYC-purified protein complex from *G. orontii*-infected and uninfected plants expressing *G. orontii* MGH1 OEC60/OEC61-MYC was performed. These findings and tools may be used to further probe into powdery mildew-induced endoreduplication to uncover mechanisms of the complex transformations that occur in host tissue associated with biotrophs.

I dedicate this dissertation to my parents, Nancy and Brian.

Table of Contents

Chapter 1……..…….……..…….....1
Introduction

Chapter 2……....15
Ploidy-associated shift in host primary metabolism fuels and regulates fungal reproduction

Chapter 3……....38
Spray-induced gene silencing reduces powdery mildew disease

Chapter 4……67
Powdery mildew effectors targeting Arabidopsis TCP transcription factors contribute to disease

Chapter 5……....99
Conclusion

Appendices……..…….104

Appendix 1: Adapted Biotroph Manipulation of Plant Cell Ploidy published in Annual Review of Phytopathology……105

Appendix 2: Protocol for fungal spore neutral lipid comparison using flow cytometry……135

Appendix 3: Adult *Arabidopsis thaliana* powdery mildew spore quantification protocol……....137

Appendix 4: Quantification of *A. thaliana* powdery mildew infection site ploidy protocol…..…141

Acknowledgements

There are many people to thank for support and guidance over the course of my education. I had several mentors during my undergraduate studies who introduced me to lab research. I'd like to thank Govindaraj Dev Kumar, Anju Verma, Melissa Mitchum, and Zhongguo Xiong for mentoring me early on in my scientific career and giving me the opportunity to develop a great scientific foundation which I used to pursue graduate school.

I'd like to thank my advisor, Mary Wildermuth for mentoring me during my Ph.D. studies, giving me lots of room to explore ideas, and being my cheerleader. I really appreciate all the experiences and opportunities to grow as a scientist. All of the other Wildermuth lab members have been an invaluable resource of knowledge, advice, and encouragement. Johan and Jyoti have been amazing lab mates. Thanks to past lab members Becky, Mike, Kyungyong, Keshav, and Riley. A special thanks to all the undergraduate researchers I mentored. I've really enjoyed mentoring you all, it's been really rewarding to get to work together and have extra help in the lab. Thanks to Elizabeth, Megan, and Jon for their exceptional commitment to research.

Thanks to all the professors I've got to work with including Jenn Lewis and Brian Staskawicz who I rotated with during my first year of graduate school. I'd like to thank Shauna Somerville, Georjana Barnes, and Jenn Lewis for being on my thesis committee. I really appreciate all your feedback over these past few years.

There are also many people at UC Berkeley who have contributed to my growth as a scientist. The UC Berkeley core managers have been amazing resources and educators. Thanks to Hector Nolla from the Flow Cytometry Facility for helping me troubleshoot experiments. Thanks to Steve Ruzin and Denise Schichnes for their microscopy training and help over the years. The Dept. of Plant and Microbial Staff have been great advocates for us students. Thanks for helping us navigate our academics and special thanks to Rocio Sanchez for being an amazing person and graduate student advisor.

Finally, I'd like to thank my family and friends. Thanks to my best friends Morayma and Eugenia who were great companions in getting through graduate school. I have a wonderfully supportive family who has encouraged me academically for as long as I can remember. Thanks to my brother Mark, my parents, grandparents, aunts, and uncles for their care and support.

Chapter 1: Introduction

Powdery mildews

Powdery mildews are widespread obligate biotrophic pathogens of plants. There are hundreds of species that together infect over 10,000 plants including crops like wheat, barley, grape, and cucurbits, and ornamentals like rose (Agrios, 2004; Kuhn et al., 2016). Although they do not kill their host, they can significantly reduce crop yield and quality. Furthermore, infection by powdery mildew often increases likelihood or severity of secondary infections. Resistant varieties or costly integrated pest management strategies are frequently used to prevent infection in susceptible plants. Managing powdery mildew of California grapevine, for example, is quite costly with 74% of pesticide use directed to its control (Fuller et al., 2014). There are mixed opinions among wine grape growers on the use of powdery mildew-resistant varietals; although their use would save growers time and resources in managing powdery mildew, there are concerns about taste and having to label wine varietals differently (Fuller et al., 2014). With powdery mildew fungicide resistance emerging in several regions and the need to apply fungicides every 1-2 weeks, new options are desired (Frenkel et al., 2015).

Powdery mildews are filamentous ascomycetes belonging to the order Erysiphales, a monophyletic group within Leotiomycetes (Bélanger et al., 2003; Glawe, 2008). The Erysiphales are divided into 5 tribes based on host range and history (Takamatsu, 2004) and individual species have been renamed and classified as more molecular-based relationships have been uncovered. As obligate biotrophic pathogens, they must infect and feed from a living host in order to obtain nutrients and reproduce. The powdery mildew fungus, *Golovinomyces orontii*, historically known as *Erysiphe orontii,* infects the model plant *Arabidopsis thaliana*, tomato, tomatillo, sunflowers, and eggplant (Kallamadi and Mulpuri, 2020; Utkhede et al., 2001). *G. ororntii* MGH1 was first described by Plotnikova et al. after being isolated from a greenhouse at Massachusetts General Hospital (1998). Its lifecycle begins when an asexual spore (conidium) lands on a leaf surface. Within minutes, germination can begin (Micali et al., 2008; Fig. 1). A primary germ tube grows from the spore and develops into an appressorium which pierces through the tough cuticle surface of the leaf using turgor pressure. Unlike other pathogenic fungi, powdery mildews do not encode many cell wall degrading enzymes which are often secreted to facilitate entry into the plant (Spanu et al., 2010). This limits the amount of cell wall breakdown products produced upon entry which can elicit a defense response from the host. Before penetration into the plant, glycogen and lipids stored in the conidium are consumed to fuel its development (Both et al., 2005). After the powdery mildew enters the plant in the epidermal cell layer, a feeding structure (haustorium) develops and is enveloped by the plant cell membrane (Koh et al., 2005; Fig. 1). This is the primary site of nutrient uptake where glucose and other metabolites are acquired by the fungus. Hyphae grow epiphytically, branching out from the initial germinating conidium, with additional feeding sites supporting growth as the colony expands (Fig. 2a-b). Most powdery mildews develop in this fashion; however, there are two known species of powdery mildew that enter leaves through stomata to infect mesophyll cells instead of epidermal cells (Kuhn et al., 2016). By 5 days post infection (dpi), the *G. orontii* lifecycle is complete with the emergence of fully formed asexual reproductive structures (conidiophores). These conidiophores are stalk-like structures that grow from hyphae. They contain a basal cell and a chain of conidia that protrudes up and away from the leaf surface (Fig. 2c). The number of conidia per conidiophore varies with powdery mildew

species; for *G. orontii* MGH1, approximately 5 conidia per conidiophore are typically observed at 5 dpi (Chandran et al., 2010).

For *G. orontii* infection of *Arabidopsis* used in laboratory research, only asexual reproduction is observed, but many species reproduce sexually to remain viable during overwinter periods (Kuhn et al., 2016). After 5 dpi, the diameter of *G. orontii* colonies can be over 1 mm (Fig. 2b). Days later, the mass of spores produced becomes visible to the naked eye (Fig. 2d). In nature, these infective spores can be transferred by wind or animals, but in the lab, plants are often infected by dusting through mesh, brushing, or spraying spore suspensions (Kuhn et al., 2016; Micali et al., 2008).

Powdery mildew genomes and insights into obligate biotrophy

Spanu et al. were the first to sequence powdery mildew genomes: the wheat powdery mildew *Blumeria graminis* f.sp. *hordei*, the reference genome for powdery mildews, and draft genomes of dicot powdery mildews *Erysiphe pisi* and *G. orontii* (2010). Comparative analysis revealed significant gene loss and genome expansion compared to other related plant pathogenic fungi (Spanu et al., 2010). As obligate biotrophs, powdery mildews have evolved an intimate relationship with their hosts to acquire nutrients. This parasitism has led to the reliance on the host to provide specific metabolites, reducing the evolutionary pressure to maintain genes and complete metabolic pathways often conserved in ascomycetes. Other plant obligate biotrophs from diverse lineages also exhibit significant gene loss and shared loss of the same metabolic pathways or pathway components (Spanu, 2012). The genome size of the powdery mildews is significantly larger than other fungal genomes due to the proliferation of retrotransposons and the loss of mechanisms to control transposon propagation. Powdery mildew genomes can be over 120 Mb while other related fungal pathogens have an average genome size of 37 Mb. This proliferation has been left unchecked by the loss of genes responsible for repeat-induced point mutation mechanisms. Because their large genomes are full of repetitive elements, it has been difficult to sequence powdery mildew genomes. The DOE Joint Genome Institute (JGI) Community Service Program (CSP) #1657 Comparative Genomics of Powdery Mildews, led by Mary Wildermuth, with Shauna Somerville as co-lead, sought to sequence 11 diverse powdery mildews to provide high resolution genomic resources for this group of fungi. In addition, transcriptome profiling of powdery mildew-infected leaves over the course of infection was performed to provide insight on infection phase-specific patterns of expression for powdery mildew and plant host genes in parallel. Data from this DOE JGI CSP project is made publicly available, providing resources for the community. Genomes sequences and transcriptomes acquired as part of the JGI CSP #1657 are used in the research presented herein.

Enhanced plant ploidy fuels powdery mildew asexual reproduction

Transcriptional analysis of the *A. thaliana*-*G. orontii* interaction over the course of infection has provided numerous insights into host processes that limit powdery mildew growth, such as induction of salicylic acid (SA) defense responses and those manipulated by the powdery mildew to support its own growth and development (e.g. Chandran et al., 2010, 2009). Because *G. orontii* infection is highly localized and exhibits a defined temporal progression, infection stage-specific studies at the site of infection were undertaken (Chandran et al., 2010; Inada and Wildermuth, 2005). Chandran et al. used laser microdissection to isolate the approximately 20 cells at the infection site including the epidermal cell containing the haustorium and surrounding epidermal

and mesophyll cells at 5 dpi, concomitant with asexual reproduction (2010). This work revealed strong support for host cell cycle modification (Chandran et al., 2010). Synthesis (S)-phase genes, for example, are differentially regulated at the infection site (Chandran et al., 2010). These genes are regulated by TCPs, plant transcription factors that are generally characterized as regulating growth and development (Lopez et al., 2015). Genes containing a mitosis-specific activator element (MSA) in their promoter also have altered expression at the infection site (Chandran et al., 2010). Furthermore, the expression of *MYB3R4*, a transcription factor that regulates MSA elements to activate G_2/M cell cycle progression, is increased 2.5-fold (Chandran et al., 2010). Quantitative microscopic analysis of the cells associated with the *G. orontii* infection site revealed leaf mesophyll cells underlying the haustorium-occupied epidermal cell of an infection site have enhanced DNA content (Fig. 3a; Chandran et al., 2010). Furthermore, powdery mildew-induced endoreduplication is abrogated in *A. thaliana myb3r4* mutants which support less powdery mildew asexual reproduction (Fig. 3b). This suggests powdery mildew proliferation is directly dependent on enhanced endoreduplication in host tissues. Further work shows *G. orontii* host cell endoreduplication only occurs in the mesophyll cells underlying the infection site concomitant with the metabolically demanding process of asexual reproduction when lipids and sugars are stored as triacylglycerols and glycogen in the developing spores (Chandran et al., 2013). Additional Arabidopsis components impacting mesophyll ploidy and *G. orontii* asexual reproduction were identified and it was shown that the extent of *G. orontii* asexual reproduction is highly correlated with the DNA ploidy of mesophyll cells underlying the haustorium at 5 dpi (Fig. 3). This indicates *G. orontii*-induced localized host endoreduplication is an important susceptibility factor.

Metabolic analyses support powdery mildew transformation of infected tissue from a carbon source-to sink. In pea, sugar content increases in leaves after powdery mildew infection (Aked and Hall, 1993) and powdery mildew directly imports available glucose (Clark and Hall, 1998). In response to powdery mildew infection, leaf lipid content increases and there are more storage lipid compounds (Abood and Lösel, 1989). Transcriptional profiling provides further evidence that powdery mildews transform infected tissues from a carbon source-to-sink where photosynthesis is downregulated and glycolysis, respiration, and fermentation are upregulated (Chandran et al., 2010). Endoreduplication may be associated with this transformation to sink tissue and facilitate the increased expression of genes in metabolic pathways to accommodate the demand of fungal asexual reproduction.

Endopolyploidy is a widespread cell cycle variant observed in both plants and animals. Endoreduplication has been observed in tissues supporting embryogenesis including plant endosperm, *Drosophila melanogaster* nurse cells, and rodent trophoblast cells (Lee et al., 2010). This is thought to support the high metabolic demands of early development. In plants, there is a negative correlation between DNA content in cells and the highest ploidy level observed. This provides evidence plants use endopolyploidy as a compensatory mechanism to elevate the metabolic capacity of tissues in organisms with small genomes (Nagl, 1976). Rapid growth of hypocotyl tissue is fueled by endoreduplication in dark conditions before photosynthesis (Jakoby and Schnittger, 2004). Endoreduplication can also shield plants from abiotic stress like drought (Cookson et al., 2006). Endoreduplication of plant host tissue is also observed in diverse plant-biotroph interactions (See published review in Appendix 1; Wildermuth et al., 2017). Microbe-induced endoreduplication in host plant tissue appears to fuel the development of diverse

biotrophic pathogens and mutualistic microbes including rhizobia, arbuscular mycorrhizal fungi, nematodes, and Begomovirus in addition to powdery mildew fungi (Fig. 4; Wildermuth et al., 2017). There are many examples of microbial colonization, proliferation, or development being impaired when host plant tissue endopolyploidy is limited (Wildermuth, 2010; et al., 2017). In some interactions, specific components of cell cycle regulation that are manipulated by infection have been identified (Fig. 5). These include proteins required for endocycle entry, inhibition of cell division and cytokinesis, and endocycle progression (DNA replication and cell expansion). (Wildermuth et al., 2017).

Overview of research

In Chapter 2, the role of the pyruvate dehydrogenase (PDH) bypass, a pathway involved in primary metabolism that is upregulated in *A. thaliana* in response to powdery mildew infection is investigated. Increased expression is concomitant with induced endoreduplication in mesophyll cells at the infection site and appears to be part of the ploidy-associated shift in host primary metabolism to fuel fungal reproduction. When the PDH complex of cellular respiration is saturated, pyruvate decarboxylase activity in the PDH bypass can be favored and allow for increased flux (Conant and Wolfe, 2007). We hypothesize the upregulation of this pathway facilitates the production of precursors (acetate, acetyl-CoA) which can be taken up to fuel the synthesis of lipids in the fungus or used by the plant to produce lipids taken up by the fungus. Lipids accumulate in newly synthesized fungal spores and are presumed to fuel early colonization and development (Both et al., 2005). In this study we investigate the contribution the PDH bypass to fungal reproduction and the impact it has on spore lipid content and viability. We also determine if spore lipids contain carbon specifically derived from the PDH bypass.

There are limited resources to study the genetics of powdery mildews, as they are obligate biotrophs which cannot be cultured. In chapter 3, novel methods used to rapidly target powdery mildew genes and access their impact on spore production are described. Topically applied RNA is an emerging technique being used to study and prevent the growth of plant pathogens and pests including obligate biotrophs. This RNA may be uptaken by the target organism directly or mediated by feeding from the plant host that absorbed RNA (Sang and Kim, 2020). Once in the target organism, endogenous RNA interference mediates gene silencing of specific target genes. Here we describe spray-induced gene silencing (SIGS) methods that use RNA to target *G. orontii* and *Erysiphe necator*, the causal agent of grape powdery mildew, genes during infection of their respective hosts. Combined with spore quantification methods adapted from (Weßling and Panstruga, 2012) and the genomic resources provided from JGI CSP #1657, we create a gene discovery platform to identify important metabolic, regulatory, and effector genes.

Finally, in chapter 4, the link between secreted powdery mildew effectors and powdery mildew-induced endoreduplication is explored to elucidate induced host endoreduplication. Pathogen effectors are known to modulate the cell cycle in many systems (Wildermuth et al., 2017). In bacteria there is a group of effectors called “cyclomodulins” or “nucleomodulins” which inhibit cell cycle progression. These effectors, for example, arrest the cell cycle by misregulating protein degradation of cell cycle proteins or induce double-stranded DNA breaks in the host nucleus (Bierne and Cossart, 2012). Other effectors like AvrBs3, a transcription activator-like (TAL) effector of the plant pathogen *Xanthomonas campestris*, binds host promoters to induce hypertrophy (Kay et al., 2007). *Agrobacterium tumefaciens* can induce cell proliferation causing

crown gall via translocated effectors and DNA expressed in the host (Tarbah and Goodman, 1988). Using previously published interactions between *G. orontii* MPIPZ effector candidates (OECs) and *A. thaliana* proteins identified by yeast-two hybrid (Weßling et al., 2014) effectors targeting proteins involved in regulating the cell cycle were identified. We narrowed our focus to TCP transcription factors, which are already implicated by transcriptional analysis in altering expression of cell cycle genes in response to powdery mildew infection (Chandran et al., 2010). Some of these TCPs have been shown to modulate powdery mildew growth (Weßling et al., 2014). As regulators of growth and development, we hypothesize these host factors are manipulated by effectors to promote infection by modulating the host cell cycle (e.g. promoting localized endoreduplication). There is precedence for bacterial pathogen effector targeting of TCPs resulting in their degradation (Sugio et al., 2014;Yang et al., 2017).

The following research presented herein aims to describe the relationship between metabolism, host ploidy, and fungal reproductive success by identifying important genetic contributors to these processes. Gene silencing tools are developed which facilitate testing the contribution of over 15 powdery mildew genes described here and more tested by other researchers in the lab. This work elucidates fundamental knowledge of powdery mildew metabolic requirements and factors required to transform the plant host to facilitate powdery mildew growth and reproduction. Additionally, the potential of spray-induced gene silencing for powdery mildew management in agriculture is being explored.

References

Abood, J.K., Lösel, D.M., 1989. Effects of Powdery Mildew Infection on the Lipid Metabolism of Cucumber, in: Biological Role of Plant Lipids. Springer US, Boston, MA, pp. 597–601. https://doi.org/10.1007/978-1-4684-1303-8_136

Agrios, G., 2004. Plant Pathology, 5th ed. Elsevier Inc.

Aked, J., Hall, J.L., 1993. Effect of powdery mildew infection on concentrations of apoplastic sugars in pea leaves. New Phytologist 123, 283–288. https://doi.org/10.1111/j.1469-8137.1993.tb03737.x

Bélanger, R.R., Bushnell, W.R., Dik, A.J., Carver, T.L.W., 2003. The Powdery mildews: a comprehensive treatise, Choice Reviews Online. American Phytopathological Society, St. Paul. https://doi.org/10.5860/choice.40-5806

Bierne, H., Cossart, P., 2012. When bacteria target the nucleus: The emerging family of nucleomodulins. Cellular Microbiology 14, 622–633. https://doi.org/10.1111/j.1462-5822.2012.01758.x

Both, M., Csukai, M., Stumpf, M.P.H., Spanu, P.D., 2005. Gene Expression Profiles of Blumeria graminis Indicate Dynamic Changes to Primary Metabolism during Development of an Obligate Biotrophic Pathogen 17, 2107–2122. https://doi.org/10.1105/tpc.105.032631.1

Chandran, D., Inada, N., Hather, G., Kleindt, C.K., Wildermuth, M.C., 2010. Laser microdissection of Arabidopsis cells at the powdery mildew infection site reveals site-specific processes and regulators. Proceedings of the National Academy of Sciences of the United States of America 107, 460–465. https://doi.org/10.1073/pnas.0912492107

Chandran, D., Rickert, J., Cherk, C., Dotson, B.R., Wildermuth, M.C., 2013. Host Cell Ploidy Underlying the Fungal Feeding Site Is a Determinant of Powdery Mildew Growth and Reproduction. Molecular Plant-Microbe Interactions 26, 537–545. https://doi.org/10.1094/MPMI-10-12-0254-R

Chandran, D., Tai, Y.C., Hather, G., Dewdney, J., Denoux, C., Burgess, D.G., Ausubel, F.M., Speed, T.P., Wildermuth, M.C., 2009. Temporal Global Expression Data Reveal Known and Novel Salicylate-Impacted Processes and Regulators Mediating Powdery Mildew Growth and Reproduction on Arabidopsis. Plant Physiology 149, 1435–1451. https://doi.org/10.1104/pp.108.132985

Conant, G.C., Wolfe, K.H., 2007. Increased glycolytic flux as an outcome of whole-genome duplication in yeast. Molecular Systems Biology 3. https://doi.org/10.1038/msb4100170

Cookson, S.J., Radziejwoski, A., Granier, C., 2006. Cell and leaf size plasticity in Arabidopsis: What is the role of endoreduplication? Plant, Cell and Environment 29, 1273–1283. https://doi.org/10.1111/j.1365-3040.2006.01506.x

Frenkel, O., Cadle-Davidson, L., Wilcox, W.F., Milgroom, M.G., 2015. Mechanisms of resistance to an azole fungicide in the grapevine powdery mildew fungus, Erysiphe necator. Phytopathology 105, 370–377. https://doi.org/10.1094/PHYTO-07-14-0202-R

Fuller, K.B., Alston, J.M., Sambucci, O.S., 2014. The value of powdery mildew resistance in grapes: Evidence from California. Wine Economics and Policy 3, 90–107. https://doi.org/10.1016/j.wep.2014.09.001

Glawe, D.A., 2008. The Powdery Mildews: A Review of the World's Most Familiar (Yet Poorly Known) Plant Pathogens. Annual Review of Phytopathology 46, 27–51. https://doi.org/10.1146/annurev.phyto.46.081407.104740

Inada, N., Wildermuth, M.C., 2005. Novel tissue preparation method and cell-specific marker for laser microdissection of Arabidopsis mature leaf. Planta 221, 9–16. https://doi.org/10.1007/s00425-004-1427-y

Jakoby, M., Schnittger, A., 2004. Cell cycle and differentiation. Current Opinion in Plant Biology 7, 661–669. https://doi.org/10.1016/j.pbi.2004.09.015

Kallamadi, P.R., Mulpuri, S., 2020. Inheritance and molecular mapping of powdery mildew (Golovinomyces orontii) resistance gene(s) in sunflower (Helianthus annuus L.). 3 Biotech 10, 1–6. https://doi.org/10.1007/s13205-020-02224-2

Kay, S., Hahn, S., Marois, E., Hause, G., Bonas, U., 2007. A Bacterial Effector Acts as a Plant Transcription Factor and Induces a Cell Size Regulator. Science 318, 648–651. https://doi.org/10.1126/science.1144956

Koh, S., André, A., Edwards, H., Ehrhardt, D., Somerville, S., 2005. Arabidopsis thaliana subcellular responses to compatible Erysiphe cichoracearum infections. Plant Journal 44, 516–529. https://doi.org/10.1111/j.1365-313X.2005.02545.x

Kuhn, H., Kwaaitaal, M., Kusch, S., Acevedo-Garcia, J., Wu, H., Panstruga, R., 2016. Biotrophy at Its Best: Novel Findings and Unsolved Mysteries of the Arabidopsis-Powdery Mildew Pathosystem. The Arabidopsis Book 14, e0184. https://doi.org/10.1199/tab.0184

Lee, H.O., Davidson, J.M., Duronio, R.J., 2010. Endoreplication : polyploidy with purpose. Genes & Development 23, 2461–2477. https://doi.org/10.1101/gad.1829209.results

Micali, C., Göllner, K., Humphry, M., Consonni, C., Panstruga, R., 2008. The Powdery Mildew Disease of Arabidopsis: A Paradigm for the Interaction between Plants and Biotrophic Fungi. The Arabidopsis Book 6, e0115. https://doi.org/10.1199/tab.0115

Nagl, W., 1976. DNA endoreduplication and polyteny understood as evolutionary strategies. Nature 261, 614–615. https://doi.org/10.1038/261614a0

Plotnikova, J.M., Reuber, T.L., Ausubel, F.M., Pfister, D.H., 1998. Powdery mildew pathogenesis of Arabidopsis thaliana. Mycologia 90, 1009–1016. https://doi.org/10.1080/00275514.1998.12026999

Sang, H., Kim, J. il, 2020. Advanced strategies to control plant pathogenic fungi by host-induced gene silencing (HIGS) and spray-induced gene silencing (SIGS). Plant Biotechnology Reports 14, 1–8. https://doi.org/10.1007/s11816-019-00588-3

Spanu, P.D., 2012. The Genomics of Obligate (and Nonobligate) Biotrophs. Annual Review of Phytopathology 50, 91–109. https://doi.org/10.1146/annurev-phyto-081211-173024

Spanu, P.D., Abbott, J.C., Amselem, J., Burgis, T.A., Soanes, D.M., Stüber, K., van Themaat, E.V.L., Brown, J.K.M., Butcher, S.A., Gurr, S.J., Lebrun, M.H., Ridout, C.J., Schulze-Lefert, P., Talbot, N.J., Ahmadinejad, N., Ametz, C., Barton, G.R., Benjdia, M., Bidzinski, P., Bindschedler, L. v., Both, M., Brewer, M.T., Cadle-Davidson, L., Cadle-Davidson, M.M., Collemare, J., Cramer, R., Frenkel, O., Godfrey, D., Harriman, J., Hoede, C., King, B.C., Klages, S., Kleemann, J., Knoll, D., Koti, P.S., Kreplak, J., López-Ruiz, F.J., Lu, X., Maekawa, T., Mahanil, S., Micali, C., Milgroom, M.G., Montana, G., Noir, S., O'Connell, R.J., Oberhaensli, S., Parlange, F., Pedersen, C., Quesneville, H., Reinhardt, R., Rott, M., Sacristán, S., Schmidt, S.M., Schön, M., Skamnioti, P., Sommer, H., Stephens, A., Takahara, H., Thordal-Christensen, H., Vigouroux, M., Weßling, R., Wicker, T., Panstruga, R., 2010. Genome expansion and gene loss in powdery mildew fungi reveal tradeoffs in extreme parasitism. Science 330, 1543–1546. https://doi.org/10.1126/science.1194573

Sugio, A., Maclean, A.M., Hogenhout, S.A., 2014. The small phytoplasma virulence effector SAP11 contains distinct domains required for nuclear targeting and CIN-TCP binding and destabilization. New Phytologist 202, 838–848. https://doi.org/10.1111/nph.12721

Takamatsu, S., 2004. Phylogeny and evolution of the powdery mildew fungi (Erysiphales, Ascomycota) inferred from nuclear ribosomal DNA sequences. Mycoscience 45, 147–157. https://doi.org/10.1007/s10267-003-0159-3

Tarbah, F.A., Goodman, R.N., 1988. Anatomy of tumor development in grape stem tissue inoculated with Agrobacterium tumefaciens biovar 3, strain AG 63. Physiological and Molecular Plant Pathology 32, 455–466. https://doi.org/10.1016/S0885-5765(88)80037-7

Utkhede, R.S., Koch, C.A., Menzies, J.G., Ehret, D.L., 2001. Host range of a powdery mildew (Erysiphe orontii) on tomato. Canadian Journal of Plant Science 81, 179–182. https://doi.org/10.4141/P00-032

Weßling, R., Epple, P., Altmann, S., He, Y., Yang, L., Henz, S.R., McDonald, N., Wiley, K., Bader, K.C., Gläßer, C., Mukhtar, M.S., Haigis, S., Ghamsari, L., Stephens, A.E., Ecker, J.R., Vidal, M., Jones, J.D.G., Mayer, K.F.X., ver Loren Van Themaat, E., Weigel, D., Schulze-Lefert, P., Dangl, J.L., Panstruga, R., Braun, P., 2014. Convergent targeting of a common host protein-network by pathogen effectors from three kingdoms of life. Cell Host and Microbe 16, 364–375. https://doi.org/10.1016/j.chom.2014.08.004

Weßling, R., Panstruga, R., 2012. Rapid quantification of plant-powdery mildew interactions by qPCR and conidiospore counts. Plant Methods 8, 35. https://doi.org/10.1186/1746-4811-8-35

Wildermuth, M.C., 2010. Modulation of host nuclear ploidy: A common plant biotroph mechanism. Current Opinion in Plant Biology 13, 449–458. https://doi.org/10.1016/j.pbi.2010.05.005

Wildermuth, M.C., Steinwand, M.A., McRae, A.G., Jaenisch, J., Chandran, D., 2017. Adapted Biotroph Manipulation of Plant Cell Ploidy. Annual Review of Phytopathology 55, 537–564. https://doi.org/10.1146/annurev-phyto-080516-035458

Yang, L., Teixeira, P.J.P.L., Biswas, S., Finkel, O.M., He, Y., Salas-Gonzalez, I., English, M.E., Epple, P., Mieczkowski, P., Dangl, J.L., 2017. Pseudomonas syringae Type III Effector HopBB1 Promotes Host Transcriptional Repressor Degradation to Regulate Phytohormone Responses and Virulence. Cell Host Microbe 21, 156–168. https://doi.org/10.1016/j.chom.2017.01.003

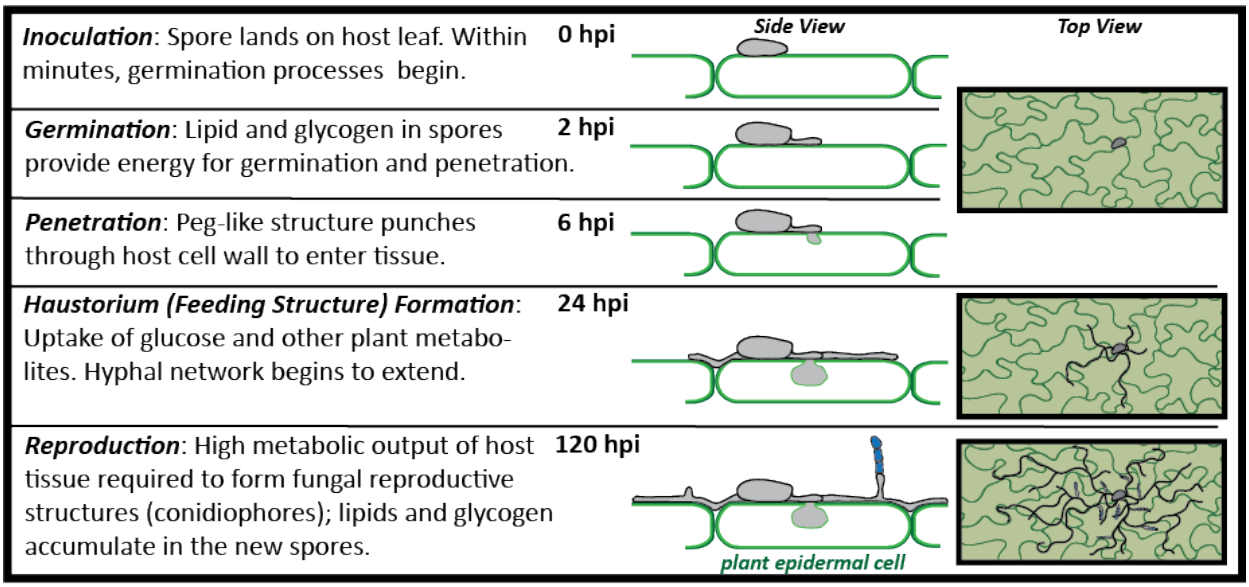

Fig. 1. Developmental timeline of *Golovinomyces orontii* on *Arabidopsis thaliana.* Modified from Both et al., 2005 for this system.

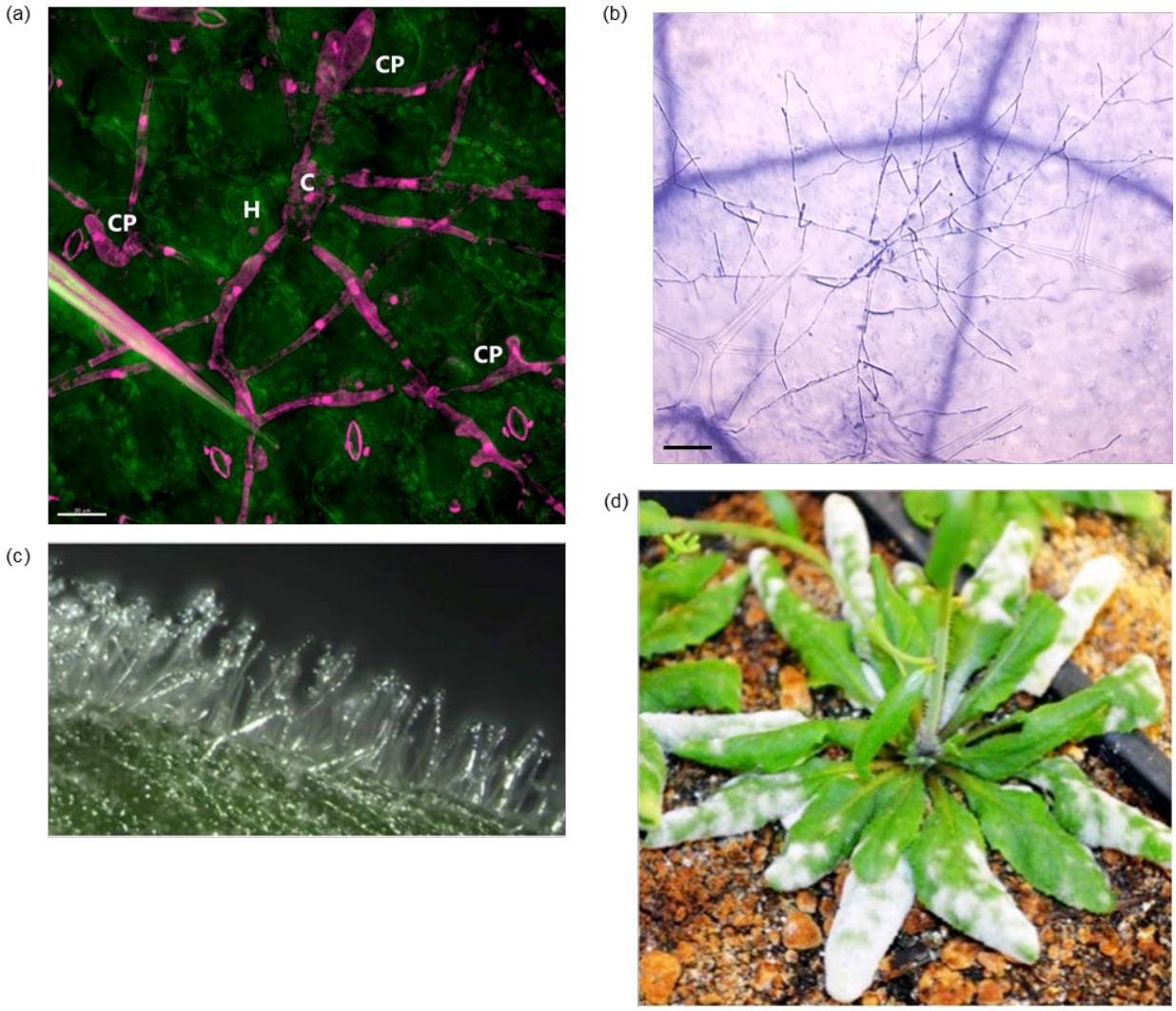

Fig. 2. *Golovinomyces orontii* MGH1 infection of *Arabidopsis thaliana* Col-0. (a) Center of powdery mildew infection site at 5 dpi showing infecting conidium (C), primary haustorium (H), and several conidiophores (CP). Scale bar is 20 µm. (b) Trypan Blue-stained fungal colony at 5 dpi. Scale bar is 100 µm. (c) Mass of conidiophores growing up and away from the leaf surface. Image credit: Jyoti Taneja. (d) *A. thaliana* infected with *G. orontii*, at 15 days post infection (dpi). The visible white powdery mildew is comprised of masses of asexual reproductive structures (conidiophores). Image credit: Jyoti Taneja.

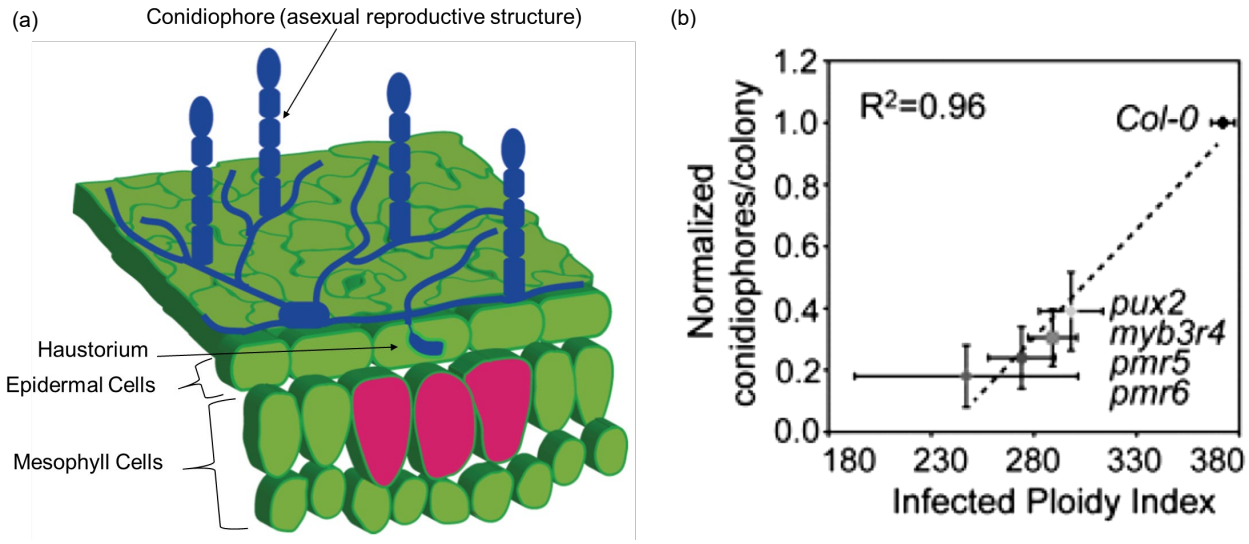

Fig. 3. Endoreduplication at the *G. orontii-A. thaliana* infection site is positively correlated with pathogen growth. (a) Cross section of powdery mildew infection site. Mesophyll cells that undergo endoreduplication are pink. (b) *G. orontii*-induced endoreduplication is directly correlated with fungal reproductive output (Chandran et al., 2013). Col-0 is WT. Mutants *myb3r4* and *pmr5* have WT basal DNA content but no *G. orontii*-induced endoreduplication. Mutants *pux2* and *pmr6* have reduced basal DNA content but a WT increase in DNA content in response to *G. orontii* infection.

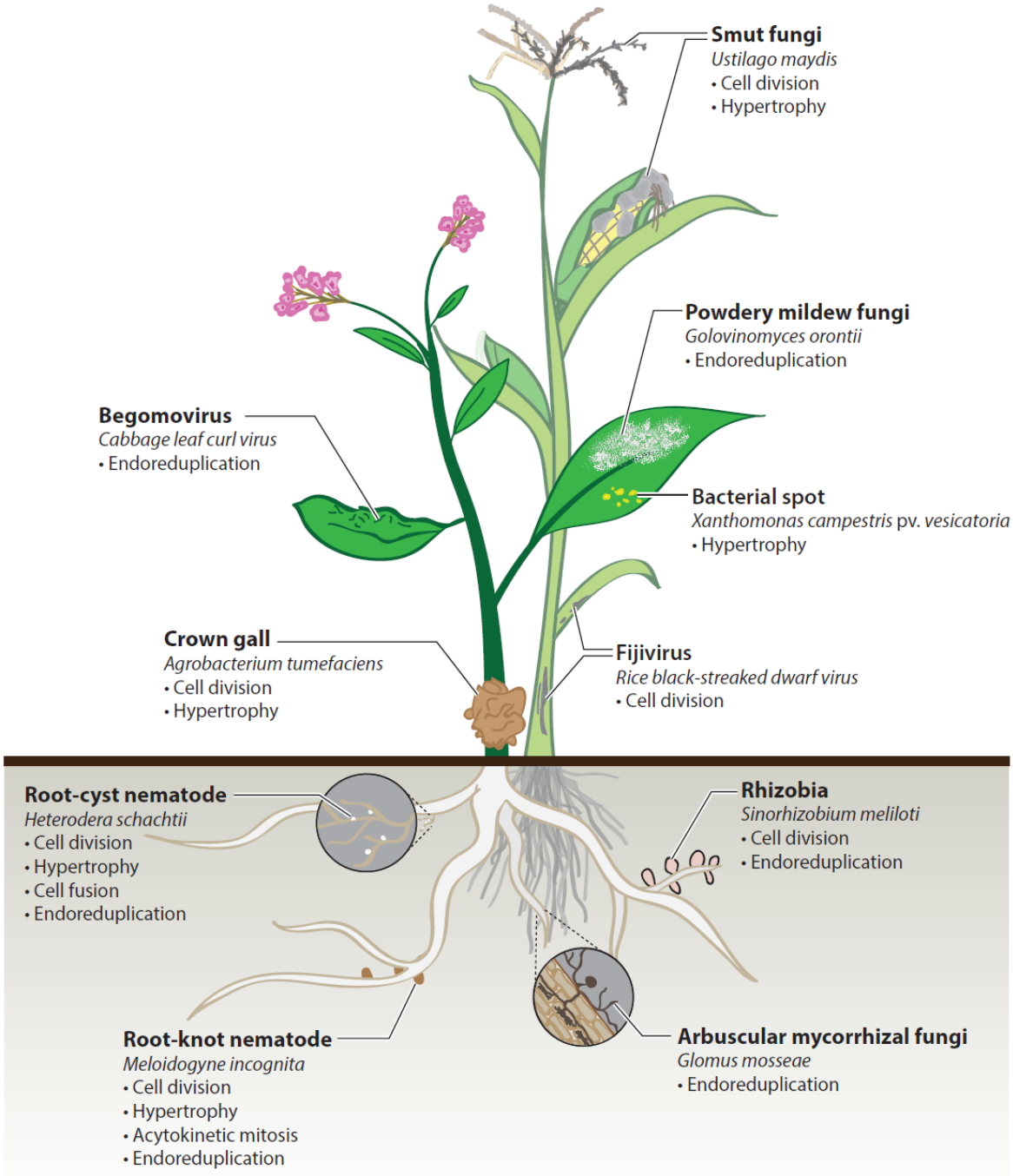

Fig. 4. Diverse plant biotrophs manipulate the host cell cycle to promote their colonization, development, and proliferation. Manipulated cell fates of susceptible hosts include enhanced cell division, hypertrophy (hyper cell-expansion), acytokinetic mitosis (cytokinesis does not occur, resulting in two separate nuclei within one cell for each event), endoreduplication (cytokinesis and cell division do not occur, resulting in DNA content increased by 2C with each cycle), and cell fusion. Note that cell death is not induced by plant biotrophs. Image from Appendix 1; Wildermuth et al., 2017.

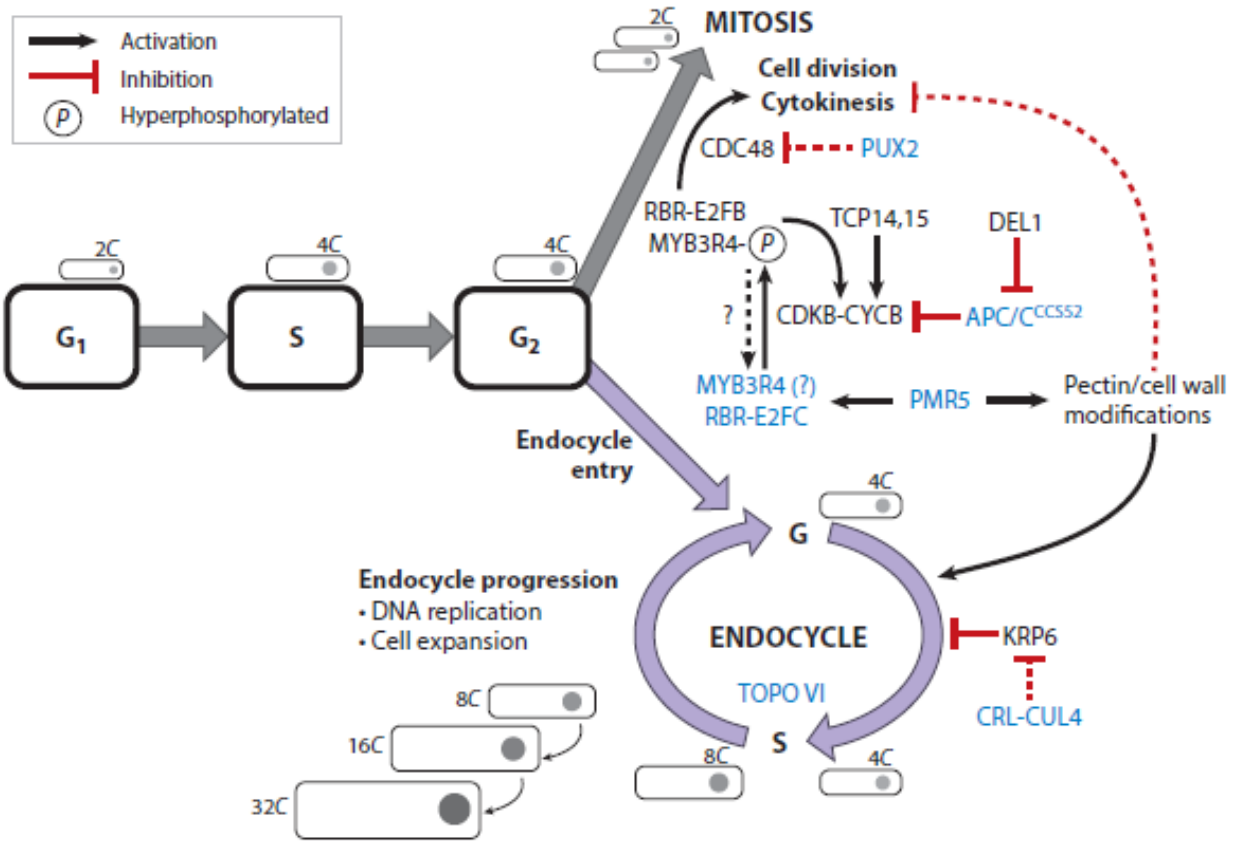
Activation
Inhibition
P
Hyperphosphorylated
2C
MITOSIS
Cell division
Cytokinesis
CDC48
PUX2
RBR-E2FB
MYB3R4-P
TCP14,15
DEL1
2C
4C
4C
G1
S
G2
?
CDKB-CYCB
APC/CCCS52
MYB3R4 (?)
RBR-E2FC
PMR5
Pectin/cell wall
modifications
Endocycle
entry
4C
G
Endocycle progression
• DNA replication
• Cell expansion
ENDOCYCLE
KRP6
TOPO VI
CRL-CUL4
8C
16C
32C
8C
S
4C

Fig. 5. Modulation of host cell cycle machinery by adapted plant biotrophs to promote endoreduplication. The mitotic cell cycle progresses through gap (G) and DNA synthesis (S) phases to mitosis (M). The endocycle is a variant of the cell cycle in which DNA is replicated but mitosis does not occur, resulting in a doubling of DNA content with each endocycle round. A simplified model showing the proposed function of identified host factors in promoting endocycle entry and progression is presented. Endocycle entry is controlled at the G2-M boundary to promote the endocycle and inhibit mitosis in the specific context of each interaction. MYB3R4-P is the promitotic hyperphosphorylated form of MYB3R4; hyperphosphorylation by the B-type cyclin-dependent kinase-cyclin B (CDKB-CYCB) complex is shown. CDK-CYC complexes other than CDKB-CYCB and E2F dimerization partners are omitted for simplicity. Inhibition of CDKB-CYCB complex accumulation promotes endoreduplication. This can be achieved through (*a*) degradation of CDKB-CYCB via the activated APC/C-CCS52 complex, (*b*) decreased expression of *CDKB* or *CYCB* via degradation or inhibition of promitotic transcriptional activators MYB3R4-P, TCP14, and TCP15, or (*c*) inhibition of cyclin-dependent kinase activity via CDK inhibitors, such as KRP2 (*not shown*). RBR1-MYB3R-E2FC repressive complexes restrict the expression of M-phase genes in G1-S. (*not shown*). Here, we propose that un(der)phosphorylated MYB3R4 complexed with RBR-E2FC inhibits M-phase gene expression to promote the endocycle. Although factors that control CDKB-CYCB accumulation and thus MYB3R4-P are known, direct MYB3R4-P dephosphorylation via a phosphatase remains a theoretical possibility. PMR5 likely acts upstream of MYB3R and HDZips (*not shown*) to promote endoreduplication and cell expansion. In addition to PMR5, PMR6 and PME3 (*not shown*) also modify pectin/cell wall with impacts that suggest an inhibitory effect on mitosis (cytokinesis) and promotion of the endocycle. Similarly, PUX2 is an adapter of the AAA-ATPase CDC48 that is co-localized to the cell division plane during cytokinesis. Endocycle progression involves repeated cycles of G-S, which presumably require alternating low and high levels of A-type cyclin-dependent kinase (CDKA)-CYC to allow licensing of replication origins and S-phase transcription, respectively. CRL-CUL4 proteolysis of KRPs, which inhibit specific CDK complexes, could then promote or inhibit endocycle progression in a context-dependent manner, as proposed for KRP6. DNA replication appears to specifically utilize DNA topoisomerase VI (TOPO VI). Proteins in blue promote endoreduplication. Dashed lines are proposed functions. Image from Appendix 1; Wildermuth et al., 2017.

Chapter 2: Ploidy-associated shift in host primary metabolism fuels and regulates fungal reproduction

M.Y. Lee*, J. Jaenisch*, A.G. McRae*, C. Hirai, K. Louie, L. Silva, B.P. Bowen, T.R. Northen, and M.C. Wildermuth
*Authors contributed equally to this work

Permission was granted from primary co-authors to include this work as part of this dissertation.

Preface

My role in this project was to characterize the role of *PYRUVATE DECARBOXYLASE-2* (*PDC2*), an *Arabidopsis thaliana* gene that is part of the pyruvate dehydrogenase bypass (PDH), during powdery mildew infection. I explored the impact of the PDH bypass on powdery mildew spore energy accumulation and viability. First, I developed a method to compare the lipid content of spores (Appendix 2) to determine if spores growing on *pdc2* mutants impacted the ability of powdery mildews to accumulate and store lipids. I also used a spore germination assay to describe the germination rate of spores shed from *pdc2* mutants and wildtype plants. My work showed that though the number of asexual reproductive structures and spores that develop is decreased when *G. orontii* develops on *pdc2* mutants compared to wild type plants, the spores that do develop have similar lipid storage content to those that develop on wild type plants. Similarly, the spores that develop on *pdc2* mutants show no defect in germination. This indicates that not only does the powdery mildew acquire precursors derived from the plant PDH bypass pathway to make spore storage lipids, but also that a PDH bypass product regulates the number of asexual reproductive structures formed so that those that are formed develop normally with fit spores.

Abstract

Powdery mildew fungi are obligate biotrophs that obtain all nutrients from their plant host. The powdery mildew *Golovinomyces orontii* induces endoreduplication, resulting in enhanced DNA content in plant cells underlying its fungal feeding structure to support its asexual reproduction. Asexual reproductive structures contain chains of spores filled with lipid bodies. Elevated ploidy has long been associated with enhanced metabolic capacity, yet the metabolic changes resulting in this phenomenon are underexplored. We show a local ploidy-associated shift in plant primary metabolism, to use the pyruvate dehydrogenase (PDH) bypass, acts in a dose-dependent manner to support fungal reproduction. Not only are plant PDH bypass-derived lipids incorporated into fungal spore storage lipids, but they also act in a regulatory capacity to control the number of reproductive structures per colony, ensuring the fitness of spores that are formed. Evolutionarily distant plant and animal biotrophs require host lipids for their growth and/or reproduction. We provide a mechanism by which energy-dense host lipids are increased for microbial utilization.

Main Text

Powdery mildews are widespread fungal pathogens with a significant impact on agricultural productivity (Glawe, 2008). Furthermore, they are among the most rapidly-spreading pests (Bebber et al., 2014). As obligate plant biotrophs, powdery mildew fungi can only grow and reproduce on living plants. They alter plant cellular architecture and metabolism to acquire all nutrients from the plant, while limiting plant defense. The powdery mildew *Golovinomyces orontii* infects *Arabidopsis thaliana*, the resource-rich model plant dicot (Micali et al., 2008; Plotnikova

et al., 1998). Infection of an *Arabidopsis* leaf begins with germination and differentiation of the spore, penetration of the plant cell wall, and establishment of a fungal feeding structure in the host epidermal cell by 1 day post inoculation (dpi). The fungus then proliferates forming a surface hyphal network, with fully mature asexual reproductive structure (conidiophore) production first apparent at 5 dpi (Fig. 1a). Conidiophores contain newly formed spores (conidia) filled with lipid bodies (Fig. 1a-c), making their formation a metabolically demanding process. Subsequent catabolism of these energy rich storage compounds is associated with spore germination and differentiation (Both et al., 2005).

Concomitant with fungal asexual reproduction (conidiation), *G. orontii* induces endoreduplication in plant mesophyll cells underlying the fungal feeding structure (Fig. 1a; Chandran et al., 2010). Multiple rounds of endoreduplication (DNA replication without mitosis) result in elevated ploidy with on average 16-fold elevated DNA content in these plant cells. Furthermore, analysis of a set of *Arabidopsis* mutants with reduced ploidy in the cells underlying the fungal feeding structure found the number of conidiophores per powdery mildew colony to be highly correlated with host cell DNA content in these plant cells (Chandran et al., 2013). This suggests ploidy-dependent enhanced host metabolism is needed to support the metabolically demanding process of powdery mildew asexual reproduction. In both plants and animals, developmental endoploidy occurs in cells of tissue associated with nutrient supply and/or enhanced metabolic demand including developing plant hypocotyls, seed endosperm, *Drosophila* follicle and nurse cells, and rodent trophoblasts (Lee et al., 2009). Furthermore, local biotroph-induced plant cell endoreduplication has emerged as a common means by which adapted plant biotrophs augment nutrient/energy supply to promote particularly metabolically demanding phases of their life cycle (Wildermuth 2010; et al., 2017). Although increased endoploidy has long been associated with nutrient supply and enhanced metabolism (Lee et al., 2009; Nagl, 1976), the metabolic changes resulting in this phenomenon are underexplored.

To identify potential ploidy-associated shifts in metabolism associated with enhanced metabolic capacity, transcriptome plant datasets with a locally induced increase in ploidy in the context of plant development or interaction with an adapted biotroph were analyzed (Wildermuth, 2010). Glycolysis, respiration, and fermentation metabolic pathways showed a statistically significant enhancement in expression across systems; this included the *G. orontii-Arabidopsis* interaction site at 5 dpi, concomitant with induced endoreduplication and asexual reproduction. Enhanced glycolysis and respiration could facilitate the increased generation of carbon and energy metabolites required by the fungus to fuel conidiation. However, when glucose/pyruvate levels are high, as inferred at the powdery mildew infection site (Fotopoulous, 2003; Swarbrick et al., 2006), respiratory capacity via the pyruvate dehydrogenase (PDH) complex can be saturated (Conant and Wolfe, 2007). In this situation, pyruvate decarboxylase (PDC, EC 4.1.1.1) activity can be favored. Fermentation occurs when the PDC product acetaldehyde is subsequently converted to ethanol via the reversible enzyme alcohol dehydrogenase (ADH, EC 1.1.1.1; Fig. 1d). Fermentation could provide additional ATP while also regenerating NAD+ when the PDH complex is saturated or its activity is otherwise limited, e.g. in anoxic/hypoxic conditions (Kursteiner et al., 2003). Of interest, barley ADH appears to positively influence barley powdery mildew penetration success, perhaps by promoting fermentative metabolism at the penetration site (Kasbauer et al., 2018; Pathuri et al., 2011) where reactive oxygen species are produced (Trujillo et al., 2006). Alternatively, acetaldehyde can be converted to acetate via acetaldehyde dehydrogenase (ALDH, EC 1.2.1; Fig.

1d). The conversion of pyruvate to acetate via PDC and ALDH, referred to as the PDH bypass, could provide additional acetyl-CoA and lipids when pyruvate is abundant (Fig. 1d). For example, the PDH bypass has been shown to support the highly demanding metabolic process of pollen tube elongation (Gass et al., 2005; Mellema et al., 2002). A closer look at the expression of *Arabidopsis* genes at the powdery mildew infection site at 5 dpi when *G. orontii* asexual reproduction occurs shows that while genes involved in the PDH bypass exhibit enhanced expression, the *Arabidopsis ADH1* required for fermentation does not (Fig. 1d; Chandran et al., 2010).

To experimentally assess whether PDC and/or ADH activity are important to *G. orontii* asexual reproduction, we developed a detached leaf system that allowed us to supply biochemical inhibitors of PDC or ADH through the *Arabidopsis* leaf petiole. Fully expanded mature leaves from 4 week old *Arabidopsis* plants inoculated with powdery mildew were detached at 2 dpi when the powdery mildew feeding structure had formed, but asexual reproduction had not yet occurred. The petioles were placed in agarose with varying concentrations of each inhibitor, from 0 to 100 μM. After an additional 5 days, the number of conidiophores (cp) per powdery mildew colony were counted for each leaf. Inhibitors supplied to the leaf via the petiole were not in direct contact with the fungus. Furthermore, powdery mildews including *G. orontii* do not contain *PDC* nor *ADH* genes in their genomes (Spanu, 2012). We found PDC inhibition reduced the number of powdery mildew cp/colony by 5-fold, to <20% of uninhibited levels (Fig. 1e). Furthermore, the impact of the PDC chemical inhibitor on fungal conidiation was dose-dependent with a minimal inhibitory concentration $(MIC)_{50}$ of 27 μM for the experiment shown and a mean MIC_{50} of 34 μM. This MIC_{50} is similar to that found for the bovine parasite *Tritrichomonas foetus* when its growth is dependent on PDC and to the IC_{50} of the purified PDC enzyme (Sutaket al., 2004). By contrast, ADH inhibition did not reduce powdery mildew asexual reproduction (Fig. 1e). Instead the number of cp/colony was enhanced, likely due to increased acetaldehyde available to go through the PDH bypass. These results suggest host PDC operates in a dose-dependent manner through the PDH bypass to support fungal reproduction and that PDC is not used in fermentation but in the PDH bypass.

To further examine whether the host PDH bypass supports fungal asexual reproduction, we obtained mutants with reduced expression of specific PDH bypass genes. *Arabidopsis thaliana* has four *PDC* genes. Only *AtPDC2* (At5g54960) exhibits enhanced expression in response to powdery mildew infection at 5 dpi (Chandran et al., 2010). Furthermore, AtPDC2 is most similar to the petunia PDC2 shown to play a role in the PDH bypass (Gass et al., 2005). AtPDC2 has a K_m for pyruvate of 3.5 mM (Ye and Cohen, 2009), compared with the K_m for pyruvate of 45 μM for AtPDH (Hirani et al., 2011), which would allow for greatly enhanced utilization of pyruvate when it is abundant. The *Arabidopsis pdc2-1* mutant (*pdc2*) contains a T-DNA insertion in the 5'UTR of the *PDC2* gene, resulting in a dramatic reduction in powdery mildew-induced *PDC2* expression at 5 dpi. The *Arabidopsis* PDH bypass then utilizes the mitochondrial ALDHs ALDH2B4 (At3g48000) and B7 (At1g23800) to convert acetaldehyde to acetate (Wei et al., 2009). *ALDH2B4* expression is enhanced in response to powdery mildew at 5 dpi, while *ALDH2B7* expression remains very low (Chandran et al., 2010). Because the *aldh2B4,B7* double null mutant (*aldhB2*), disrupted in both genes, was previously shown to be required for a strong PDH-bypass associated phenotype (Wei et al., 2009), we initially employed it in our studies.

We found *pdc2* plants have a visible decrease in powdery mildew growth and reproduction, with

significantly less visible leaf coverage (Fig. 2a). Microscopic analysis of the number of cp/colony show a significant decrease in asexual reproductive structures formed by powdery mildew that develop on *pdc2* compared to wild type (WT) plants (Fig. 2b). Complementation of *pdc2* with *PDC2* restores cp/colony to WT levels. Similar to *pdc2*, the mitochondrial *aldh2B* double mutant supports less visible growth of the powdery mildew compared to WT (Fig. 2d), with fewer cp/colony (47% of WT). Decreased powdery mildew asexual reproduction is not associated with mesophyll cell death in *pdc2* or *aldh2B* (Fig. 2c). In addition, the *pdc2* and *aldh2B* plants do not exhibit dwarfism. Because *ALDH2B4* was specifically induced at the powdery mildew infection site at 5 dpi (Chandran et al., 2010), we then assessed the *aldh2B4-1* single null mutant (Wei et al., 2009) for altered powdery mildew reproduction. We employed a more rapid complementary assay to assess powdery mildew asexual reproduction: total powdery mildew spore production per gram leaf fresh weight as in (Weßling et al., 2014). Powdery mildew spore production is on average 24% of WT for *aldh2B4* (Fig. 2d), consistent with the enzyme encoded by this gene playing a dominant role in powdery mildew-induced use of the PDH bypass**.** Furthermore, a null mutant in the single *Arabidopsis ADH* gene, *ADH1* (At1g77120), showed no difference in spore production (Fig. 2d**)** affirming the importance of the PDH bypass, not fermentation, to powdery mildew asexual reproduction.

Increased ploidy provides an effective mechanism for increasing activity through a pathway as copy number increases for all pathway components. Biochemical inhibition of PDC activity supports this dosage-dependence (Fig. 1e). To further explore the impact of *PDC* dosage on spore production, a genetic approach comparing powdery mildew asexual reproduction on the *pdc* mutant, WT, and WT plants with an additional copy of *PDC2* was employed. We found fungal spore production to increase proportionally with *PDC* dosage (Fig. 2e).

Newly formed powdery mildew spores are filled with lipid bodies containing storage lipids (Fig. 1c). Because the PDH bypass is known to provide precursors for lipid production during metabolically demanding processes, we postulated that the host plant PDH bypass is used to enhance the production of lipids required by the fungus during spore formation (aka conidiation). In order to determine whether C derived from the plant PDH-bypass pathway is incorporated into newly formed powdery mildew spore lipids, we used an experimental setup similar to that used for our biochemical inhibition experiments and tracked incorporation of supplied ^{13}C-ethanol into lipids of the detached washed leaf and newly formed powdery mildew spores that develop on the leaf (Fig. 3a). Because only the ADH enzymatic reaction is reversible, supplied ^{13}C-ethanol would be utilized by the induced PDH bypass (Fig. 1d). Wei et al. successfully used this approach to confirm contribution of the *Arabidopsis* PDH bypass to fatty acid synthesis in seedlings (2009). It should be noted that the ^{13}C- ethanol, or unlabeled ethanol, is provided via the leaf petiole to the leaf and therefore not directly accessible to the powdery mildew. Furthermore, as mentioned above, powdery mildew genomes including *G. orontii* MGH1 do not contain an *ADH* gen**e.**

Triacylglycerols (TG) are the dominant storage lipid in lipid bodies, therefore, lipid analysis by LC-MS/MS focused on TGs. We identified sixty-seven TGs in powdery mildew spores, ranging from 47:0 to 64:7 (Fig. 3b). Ninety- seven percent of conidial TG abundance exhibits statistically significant ^{13}C enrichment indicating the extensive contribution of the plant PDH bypass to TGs in newly formed spores. Conidial TGs containing exclusively fully saturated acyl chains are the exception and show no ^{13}C enrichment. Similarly, only fully saturated leaf TGs show no ^{13}C

enrichment with ^{13}C-ethanol feeding. Examination of the MS2 spectra for these TGs confirmed the lack of ^{13}C incorporation. ^{13}C enrichment calculations are based on M_{0+1}/M_0 to enhance specificity but thereby underestimate actual ^{13}C enrichment as we see multiple label incorporation into TGs. For example, MS spectra and associated isotopolog analysis show multiple labels are incorporated into TG 56:6 of spores that developed on ^{13}C-ethanol supplied leaves resulting in an overall 4.3-fold increase in label relative to TG 56:6 of spores that developed on leaves supplied with unlabeled ethanol, compared with a 1.6-fold increase analyzing only the M_0+1 label (Fig. 3c).

While dominant leaf TGs are highly abundant in spores**,** conidial TGs do not simply parallel leaf TG profiles (Fig. 3b). TGs with longer acyl chains (e.g. 58:x to 64:x) are more abundant in conidia, while in leaves they are often near the detection limit. TG MS2 analysis of a subset of the longer acyl chain TGs shows they include C20-C24 acyl chains, which have been reported to be highly prevalent in powdery mildew conidia (Johnson et al., 1976; Muchembled et al., 2005; Tulloch and Ledingham, 1960). In addition, conidial TGs tend to have acyl chains that are slightly more saturated than leaf TGs, though not fully saturated (Fig. 3b). Taken together our data shows the plant PDH bypass provides precursors for use in fungal spore TGs. The enhanced abundance of spore TGs with longer fatty acid acyl chains that are slightly more saturated, but not fully saturated, compared to leaf TGs suggests that the fungus does not merely take up locally-produced leaf TGs and store them in developing spores. Instead active lipid remodeling by the fungus is implicated. This could include fungal uptake of plant TGs, partial catabolism, remodeling of acyl chains, and TG reformation, and/or fungal uptake of plant TG precursors that are remodeled and incorporated into TGs.

In fungi, lipids can act in a regulatory capacity (Singh and Del Poeta, 2011; Tsitsigiannis and Keller, 2007). We established that decreased function of the plant PDH bypass results in fewer cp per powdery mildew colony or spore production in a dose-dependent manner (Fig. 1e, 2b, d-e). To investigate whether plant PDH bypass-derived lipids also act to control conidiophore development once initiated, we microscopically evaluated cp development. *G. orontii* cp development consists of formation of a basal foot cell, followed by a generative cell that successively elongates and divides to produce a conidium in its upper section (Fig. 1b). This process is repeated resulting in a chain of conidia with the oldest at the tip. We found cp development is not impacted for either powdery mildew colonies developed on i) WT leaves with no PDC inhibitor compared with inhibitor (at the IC_{50}) (Fig. 4a) or ii) WT versus *pdc2* plant leaves (Fig. 4b). These results indicate cp initiation but not subsequent development is dependent on *Arabidopsis* PDH bypass function.

To then ascertain whether the lipid content of those conidia that do form is impacted by reduced plant PDH bypass function, we used flow cytometry analysis of spores with BODIPY505/515 neutral lipid staining (Fig. 4c). We found no difference in conidia lipid content for powdery mildew that develop on WT compared with *pdc2* plants (Fig. 4d). Qualitative microscopic comparisons also showed no difference in conidia lipid body content or morphology. Because conidia storage lipids decrease with conidial germination and fungal TG lipases are expressed at this time, it is likely that catabolism of spore storage lipids provides nutrients/energy for conidial germination and germ tube differentiation (Both et al., 2005). Therefore, we ascertained whether the germination rate of powdery mildew conidia that develop on *pdc2* plants differs from those that develop on WT plants. No difference in spore germination rates is detected (Fig. 4e).

Taken together, we show a local ploidy-associated shift in plant primary metabolism, to use the PDH bypass, acts in a dose- dependent manner to support fungal asexual reproduction. Not only are plant PDH bypass-derived lipids incorporated into fungal spore storage lipids, but they also act in a regulatory capacity to control the number of conidiophores per powdery mildew colony. Those conidiophores that are initiated develop normally forming fully competent spores filled with lipid bodies. In this way, host lipid availability via the PDH bypass is linked to the extent of reproductive output, while ensuring the fitness of spores that are formed.

Final Discussion

Host lipid acquisition by biotrophic pathogens and symbionts of animals has emerged as a common mechanism by which these organisms support demanding phases of their life cycles. Obligate intracellular bacterial pathogens of mammals (e.g. *Mycobacterium tuberculosis*, *Chlamydia trachomatis, Coxiella burnetii* reviewed in Toledo and Benach, 2014; Vromman and Subtil, 2014), mammalian *Apicomplexa* intracellular parasites (e.g. *Toxoplasma gondii*, causative agent of toxiplasmosis in Caffaro and Boothroyd, 2011; Nolan et al., 2017) and *Plasmodium*, causative agent of malaria, (Itoe et al., 2014), and the insect endosymbiotic bacteria *Spiroplasma poulsonii* (Herren et al., 2014) provide just a few examples.

Recent studies extend this mechanism of nutrient/energy acquisition to plant biotrophs (Keymer and Gutjahr, 2018). For example, arbuscular mycorrhizal fungi (AMF) are endosymbionts that colonize roots of a broad array of plant species, facilitating plant uptake of phosphate and nitrogen from the soil, while acquiring host sugars – and lipids (MacLean et al., 2017). As part of their study with AMF, Jiang et al. found powdery mildews also utilize host lipids (2017). A specific alteration of plant host lipid composition resulting in the early release of fatty acids from acyl carrier protein (ACP) as C:12 lauric acid resulted in a similar alteration in fungal lipid composition (Jiang et al., 2017). In addition, mutants in KAR1 and KASI, part of the core plant fatty acid biosynthetic machinery (plastidic fatty acid synthase (FAS) complex), and FatB, which releases free fatty acids (16:0, 18:0, and 18:1) from ACP, supported less powdery mildew asexual reproduction. However, these mutants had pleotropic phenotypes including cell death, known to limit powdery mildew growth and reproduction (Micali et al., 2008), complicating interpretation.

Both AMF (Bago et al., 2002) and powdery mildew (Fig. 1c; Both et al., 2005) store lipids in lipid bodies to support growth and/or reproduction. For AMF, 16:0 β-monoacylglycerol or a derivative appears to be the dominant plant lipid acquired by the fungus (Bravo et al., 2017; Keymer et al., 2017; Luginbuehl et al., 2017). Fungal remodeling via desaturation and elongation produces a variety of lipids including TGs. For *G. orontii,* the specific lipid(s) trafficked to the powdery mildew remains to be elucidated. Our TG analyses indicate that *G. orontii* conidial TGs do not simply parallel leaf TG composition (Fig. 3b). Similar to AMF, there is evidence of fungal lipid remodeling, including desaturation of fully saturated species and elongation. Furthermore, obligate biotrophs sequenced to-date, like the AMF *Rhizophagus irregularis* (Wewer et al., 2014), contain genes encoding proteins that elongate and desaturate >C16 fatty acids. For example, the grapevine powdery mildew *E. necator* contains fatty acid desaturases and elongases that exhibit dramatically increased expression concurrent with asexual reproduction (Jones et al., 2014).

Because of the highly localized and defined temporal progression of *G. orontii* growth and asexual reproduction, we were able to uncover the role of ploidy and the PDH bypass in conidiation. When

pyruvate is highly abundant, use of the PDH bypass can dramatically increase the synthesis of lipid precursors. PDC activity is not limited by O_2 availability as is PDH. In *Arabidopsis*, PDC2 has a >75-fold higher K_m for pyruvate than PDH (Hirani et al., 2011; Ye and Cohen, 2009). Furthermore, similar to yeast PDC, it appears to exhibit substrate cooperativity (Ye and Cohen, 2009) and likely has a greater V_{max} than PDH resulting in dramatically enhanced flux when pyruvate levels are high (Conant and Wolfe, 2007). Indeed, the PDH bypass has been engineered to increase the production of acetyl-CoA derived biotechnology products from acetyl-CoA (Chen et al., 2013; Shiba et al., 2007;). And, we see that ^{13}C-label supplied via the plant PDH bypass supplies lipid precursors that are incorporated into highly labeled TGs in developing powdery mildew spores (Fig. 3b-c).

Metabolic control theory supports increased ploidy as mechanism for increasing activity through a pathway as copy number increases for all pathway components. Not only are plant cell PDH bypass genes preferentially induced concomitant with locally induced ploidy and powdery mildew asexual reproduction (Fig. 1d; Chandran et al., 2010), but the extent of powdery mildew asexual reproduction is highly correlated with PDC dosage as assessed by biochemical inhibition (Fig. 1e) or altered copy number (Fig. 2e). Similar to *G. orontii*, other plant biotrophs including AMF and *Plasmodiophora brassicae* that induce host plant cell endoreduplication (Carotenuto et al., 2019; Chandran et al., 2010; Olszak et al., 2019; Wildermuth et al., 2017), exhibit enhanced expression of plant PDH bypass genes (Chandran et al., 2010; Gomez et al., 2009; Gravot et al., 2016, Wildermuth, 2010), and acquire lipids from their host. Furthermore, the protist *P. brassicae*, causative agent of a root gall disease known as clubroot, is a fatty acid auxotroph (Schwelm et al., 2015) that exhibits reduced clubroot symptoms and spore formation on the *Arabidopsis pdc2* mutant compared to WT, with no difference in disease on the *adh* mutant (Gravot et al., 2016). Taken together, biotroph-induced host cell endoreduplication and use of the PDH bypass may be a general means by which obligate plant biotrophs increase host lipid precursor supply for their own gain. This manipulation of primary plant metabolism occurs upstream of the core plant fatty acid biosynthetic machinery to increase lipid biosynthetic capacity. Importantly, reduction in powdery mildew asexual reproduction for the PDH bypass mutants occurs in the absence of cell death or other dramatic pleotropic phenotypes (Fig. 2c). Specific plant host lipids acquired by distinct biotrophs can then evolve based on their individualized interaction demands.

Obligate intracellular bacterial pathogens of mammals including *Mycobacterium tuberculosis* and *Plasmodium*, causative agent of malaria, also require host lipids for their growth and/or reproduction. Induced endoploidy is much more common in plants than mammals, however, mammals contain endopolyploid cells in critical tissues such as the liver, heart, and placenta where polyploidy serves to enhance nutrient/energy supply and plasticity (Schoenfelder and Fox, 2015). *Plasmodium* preferentially infect polyploid hepatocytes, with infection rates positively correlated with ploidy level independent of cell size (Austin et al., 2014). Analysis of expression changes associated with hepatocycte polyploidy show enhanced glycolysis, non-respiratory acetyl-CoA formation, and cholesterol biosynthesis (Anatskaya and Vinogradov, 2007). *M. tuberculosis* induces granuloma macrophage differentiation that includes polyploid cells; these also exhibit increased expression of genes involved in cholesterol biosynthesis (Herrtwich et al., 2016). In mammals, increased host lipid synthesis could result from increased dosage associated with polyploidy as well as ploidy-associated specific impacts on gene expression (e.g. via methylation, acetylation in Shi et al., 2015) and utilized pathways, as we see in plants (Wildermuth, 2010). Although mammals do not encode PDH bypass genes *per se*, mammalian cells can also bypass the

PDH pathway to produce acetate and acetyl-CoA for lipid production from glucose-derived pyruvate (Liu et al., 2018). Therefore, our work suggests a mechanistic link between increased host cell ploidy and enhanced host lipid availability that is broadly used to support obligate biotrophic parasite and symbiont nutrient acquisition.

Methods

Plants

All *Arabidopsis thaliana* mutants are in the Col-0 background except for the *aldh2B4-1, aldh2B7-1* double mutant which is in the Ws-0 background. The appropriate WT control is used in all experiments. Homozygous *pdc2-1* (SALK_066678C), *aldh2B4-2* (SALK_078568), and *adh1-1* (SALK_066824) T-DNA insertion lines (Alonso et al., 2003), were obtained from the Arabidopsis Biological Resource Center. *aldh2B4-1/B7-1* double mutant and *aldh2B4-2* lines were previously characterized as null mutants (Wei et al., 2009) as was *adh1-1* (Hwang et al., 2011). To generate stable transgenic plants, constructs were introduced into *Agrobacterium* and transformed into WT Col-0 or *pdc2-1* by floral dip (Clough and Bent, 1998). The 2523 bp product containing the *PDC2* promoter (*PDC2pro*) and *PDC2* gene was amplified from *A. thaliana* Col-0 genomic DNA and introduced into pCAMBIA 1300 in frame with previously introduced enhanced GFP (pEGFP-N1, Clonetech, CA) and *CaMV* 35S terminator site. All PCR products were verified by DNA sequencing. The plasmid containing *PDC2pro::PDC2-eGFP* (below) was introduced into *Agrobacterium tumefaciens* strain GV3101 and transformed into *Arabidopsis pdc2-1* and WT. Lines with insertions were selected by resistance to Hygromycin and GFP expression, and inserted sequences were verified. Homozygous stable transgenic lines with one introduced copy of *PDC2* in *pdc2 (PDC2pro::PDC2-eGFP/pdc2-1*) referred to as *PDC2/pdc2* were used for the complementation experiment, while lines with one introduced copy of *PDC2* in WT (*PDC2pro::PDC2-eGFP/*WT*)* referred to as *PDC2/*WT was used for the dosage experiment.

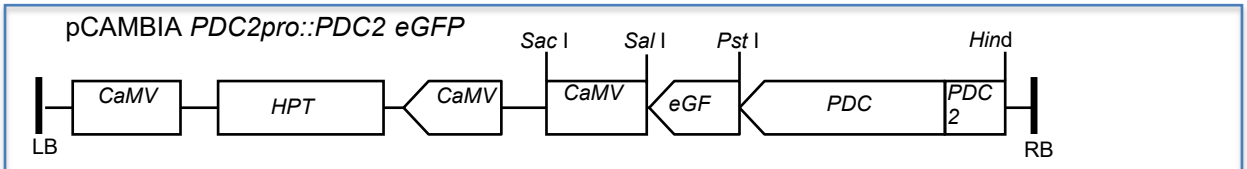

Schematic diagram of pCAMBIA 1300-derived plasmid with inserted PDC2pro*::PDC2-eGFP.*

LB, left border; RB, right border; *CaMV,* Cauliflower Mosaic Virus*; HPT II,* hygromycin phosphotransferase

Powdery mildew assays

A. thaliana WT and mutants were grown, evenly spaced, using an alternating pattern with 12 plants per box in Percival AR66L environmental chambers at 22C, 70% RH, and 12 h photoperiod with photosynthetically active radiation (PAR) of 120-150 µmol/m^2 s. At 4 weeks, each box was infected with conidia from 2 half-covered leaves (10-14 dpi) of *G. orontii* MGH1 isolate (Plotnikova et al., 1998) using a uniform settling tower method with mesh screen as in Chandran et al., 2009. Visual and microscopic powdery mildew disease phenotypes were performed as described in Chandran et al., 2009, with visual disease phenotypes scored at 10-11 dpi based on percent visible coverage of the leaf. 20-25 plants were evaluated per genotype for one experiment. For microscopic analysis, three fully expanded leaves per plant (leaves approximately 7-9 post emergence) were excised at 5 dpi, cleared and stained with trypan blue for visualization of fungus and counting of asexual reproductive structures (conidiophores) per colony, or cell death. Leaves from four plants per genotype were analyzed with at least 30 powdery mildew colonies assessed.

Conidiophore developmental stage was noted at the time of assessment, and ranged from Stage 1 (initial nub of the basal foot cell is visible microscopically) to Stage 4 containing progressively more conidia. Independent experiments gave similar results.

For powdery mildew spore counting, the procedure of Weßling et al., was optimized to enhance reproducibility (2014; Appendix 3). At 8-10 dpi following a moderate to heavy inoculation dose (3-4 fully covered leaves), three fully expanded mature leaves per plant for 5-6 plants of each genotype in a box were excised, weighed, and vortexed with 15 ml 0.01% Tween-80. Following leaf removal, the solution was filtered through a 40 µm mesh (Sysmex) and conidia in the filtrate were pelleted at 4,000 x g for 5 min. Pellets were resuspended in 200-600 µL final volume ddH_20 and 10 µl aliquots used in an IMPROVED NEUBAUER 0.1 mm deep Brightline Houser Scientific hemacytometer. All 9 fields were independently counted and the mean and standard deviation calculated to ensure sample counts were reproducible. In addition, a lower threshold of 80,000 spores/gFW (fresh weight) for WT was utilized to improve reproducibility. Note that each planted box is an independent biological sample directly comparing WT and mutant plant lines. 4-6 independent biological samples were assessed per mutant vs WT comparison. Student's T-Test was utilized for statistical analysis of paired comparisons (e.g. WT vs. mutant cp/colony or spores/gFW). For assessing differences in distributions, Pearson's Chi-squared test with Yates continuity correction was utilized.

Biochemical inhibition and ethanol feeding experiments

4 week old WT plants were grown in environmental chambers and infected with a moderate dose of *G. orontii* conidia using settling towers, as above. At 2 dpi, three fully expanded leaves were excised and the petioles were placed in semi-solid media (1/2 MS salts, 0.8% BactoAgar, with either inhibitor or ethanol) in 100 mm x 100 mm x 15 mm square petri dishes, sealed with micropore tape (3M), with 12 leaves per dish for inhibitor experiment and 20 leaves per dish for ethanol feeding experiment. The petri dishes were then placed back in the environmental chamber. For the biochemical inhibition studies, the PDC inhibitor omeprazole (Sigma-Aldrich) or the ADH inhibitor pyrazole (Sigma-Aldrich) was dissolved in DMSO to make a working stock solution and added to the agar media solution just before pouring. Volumes added were adjusted with DMSO for consistency across all concentrations including no inhibitor. The series of concentrations were assessed on separate plates in the same experiment. Five days later (7 dpi), leaves were removed from agar and stained for microscopic counting of cp/colony as above. At least 45 colonies were counted per inhibitor dose, with on average 5 colonies observed from each of 9 leaves. Independent experiments gave similar results.

For the ethanol feeding experiment, 10 mM ^{13}C-ethanol (Sigma-Aldrich) or ethanol was added to the agar media just before pouring. Five days later (7 dpi), leaves were removed from the agar and washed in 0.01% Tween-80. The resulting solution was filtered through 40µm mesh (Corning), spun down at 4,000 x g for 5 min. to pellet the spores, resuspended in 500 µL ddH_20 and spun down. The pelleted spores were weighed, frozen using liquid Nitrogen, finely ground using a TissueLyserII (Qiagen) with 3 mm size balls, and immediately extracted for lipid analysis (below). Three biological replicates per experiment, with approximately 50 infected leaves per replicate resulting in approximately 0.17 gFW spores per sample. For the washed leaves, a subset of the washed pool of leaves of approximately 0.075 gFW leaf material was used per sample, ground as above, and immediately extracted for lipid analysis (below). For one independent experiment,

three spore samples and three washed leaf samples from both control ethanol and ^{13}C-ethanol plates were analyzed. An independent repeat of entire experiment confirmed findings.

Lipid LC-MS/MS analyses

Lipids were extracted from spore and washed leaf samples from ethanol or ^{13}C-ethanol agar plates using a modified Bligh & Dyer extraction (1:1:0.9 methanol:chloroform:H_20) (Li-Beisson et al., 2010). 300 µL of the chloroform phase was recovered per leaf or spore sample, and dried under Nitrogen. The dried extracts were re-suspended in 200 µL of 3:3:4 IPA:ACN:MeOH, and run immediately with LC-MS. A triacylglyceride (TG) internal standard mix (LM6000, Avanti) was added to resuspended extracts to ensure retention time reproducibility. LM-MS was performed using an Agilent 1290 (Agilent Technologies, Santa Clara, CA) UHPLC connected to a QExactive mass spectrometer (Thermo Fisher Scientific, San Jose, CA) with the following chromatographic method, in both positive and negative mode. 2 µL of lipid exptracts were injected onto a reversed phase C18 column (50 mm x 2.1 mm, 1.8 µm Zorbax Rapid Resolution High Definition, Agilent Technologies) with a 21 min. gradient and 0.4 mL/min. flow rate, with 2 µL injections. The mobile phases used were A: 60:40 H_2O:ACN with 5 mM ammonium acetate, 0.1% formic acid, and B: 90:10 IPA:ACN with 5 mM ammonium acetate (0.2% H_2O), 0.1% formic acid. The system was held at 20% B for 1.5 min, followed by an increase to 55% B over 2.5 min, and a subsequent increase to 80% B over 6 min. The system was then held at 80% B for 2 min., before being flushed out with 100% B for 5 min., and re-equilibrated at 20% B over 5 min. The QExactive parameters were as follows: MS resolution was set to 70,000, and data was collected in centroid mode from 80-1200 m/z. MS/MS data was collected at a resolution of 17,500 with a collision energy step gradient of 10, 20, and 30. All solvents were HPLC grade unless specified.

Lipid Data Analysis: Lipids, focused on TGs, were identified by comparing accurate mass and MS/MS fragmentation patterns in positive ion mode to standards either run in-house, the NIST 11 Mass Spectral Library (Kind et al., 2009), or from several online databases, including LipidMaps (Fahy et al., 2007) and Metlin (Smith et al., 2005), as well as identification of neutral loss fragments corresponding to fatty acid tails in MS-MS fragmentation spectra. Calculations used peak height of NH_4^+ adducts, run in positive ion mode. Relative abundance = unlabeled mean M_0 peak height/mg leaf FW, with n=3. M_0 peak heights of <1E05 were considered to be below reliable detection threshold. A two-tailed T- Test (unpaired with equal variance) was used to assess statistical significance between treatments; n=3 per treatment. Percent ^{13}C enrichment = (Mean/mgFW ^{13}C-ethanol supplied M_0+1/M_0 – Mean/mgFW unlabeled ethanol supplied M_0+1/M_0)/Mean/mgFW unlabeled M_0+1/M_0). Percent label incorporation = (M_0+1 + M_0+2*2 + M_0+3*3 ….)/((M_0 + M_0+1+ M_0+2 + M_0+3...)*# of mass isotopologues), calculated as in Doomun et al., 2016. Data is available at the EMBL-EBI Metabolights data repository (Haug et al., 2013), with ID www.ebi.ac.uk/metabolights/MTBLS1114.

Powdery mildew spore lipid analysis using flow cytometry

See Appendix 2 for more detailed methods. As above, *Arabidopsis* plants were grown in a Percival using an alternating pattern of WT and mutant genotypes within each box to ensure equal growing conditions and even inoculation. At 4 weeks, *A. thaliana* was settling tower-inoculated with a moderate inoculum of *G. orontii* MGH1 per box. Nine days later, three fully expanded mature leaves per plant were harvested from 9 plants per genotype pooled from 2 boxes. To liberate spores, leaves were vortexed in 0.01% Tween-80 in ddH_20 for 30 seconds. Spore suspensions were filtered

through 40 µm mesh and centrifuged at 4000 x g. To concentrate spores further, the spore pellet was layered on top of a sucrose gradient (20, 30, 40, 50, and 60%) and centrifuged at 4000 x g for 5 min. Layers corresponding to approximately 20-30% sucrose were highly enriched for spores and collected for analysis. The neutral lipid dye BODIPY 505/515 (ThermoFisher Scientific D3921) at a final concentration of 1µg/mL was added to spore suspensions which are then analyzed using LSR Fortessa X20 flow cytometer. Samples were interrogated with a 488 nm laser and signal captured with a FITC (505LP 530/30) filter. Sample acquisition uses BD FACSDiva Software (v7.0) with subsequent gating of spores via FlowJo (v10.1); see Fig. 4. Each biological replicate measured the fluorescence intensity of 200 (±10%) spores shed from WT or mutant *pdc2* plants. Fluorescence intensity distributions were compared using Chi-Squared T(x) statistical analysis in FlowJo v.10 software. Two additional independent experiments were performed with a similar result.

Powdery mildew spore germination assay

At 11 dpi, three mature fully expanded leaves from WT and *pdc2* plants were harvested and tapped over a glass slide to collect spores. Leaves from three plants per genotype were utilized. Slides were stacked in a petri dish with 3 mL ddH_2O water to ensure high relative humidity, closed, and covered with aluminum foil for 1 hr. Petri dishes were then exposed to light for 5 hr. At least 100 spores were observed per slide, with three slides per genotype. A Student's T-Test (Two- Tailed, Two-Sample Assuming Equal Variance) was used to compare germination rates between genotypes. Two additional independent experiments showed similar results.

Acknowledgements

This work was supported by National Science Foundation grants IOS-0958100 to M.C.W. and MCB-1617020 to M.C.W and T.R.N. T.R.N. also acknowledges funding from the U.S. Department of Energy, Office of Science, Office of Biological & Environmental Research Microbial Community Analysis and Functional Evaluation in Soils Program at Lawrence Berkeley National Laboratory DE-AC02-05CH11231. The work conducted by the U.S. Department of Energy Joint Genome Institute, a DOE Office of Science User Facility, is supported by the Office of Science of the U.S. Department of Energy under Contract No. DE-AC02-05CH11231. We thank Dr. Hans van Veen (Utrecht University, Netherlands) for assistance with statistical analyses of disease scoring distributions. M.C.W. also thanks Drs. Divya Chandran and Jyoti Taneja for their contributions to mentoring and training of Wildermuth lab personnel.

Author contributions

M.Y.L. and C.H. contributed the powdery mildew disease assays including inhibition analyses and characterized the *pdc2* mutant. M.Y.L. also created the complemented and overexpressed *PDC2* plant lines. J.J. performed the ^{13}C feeding experiment, lipid extraction, and lipid data calculations; he also analyzed powdery mildew spore production on mutant plant lines. A.G.M. contributed the spore FACS and germination rate analyses and confirmatory powdery mildew disease assays using spore production for *PDC* complementation and dosage experiments. L.S., K.L., and B.P.B. performed LC-MS/MS analysis of lipids under the direction of T.R.N. M.C.W. conceptualized and directed the research, analyzed data and created figures with the primary experimentalists, and wrote the manuscript with J.J. and A.G.M., with review by all authors.

References

Alonso et al. (2003) Genome-wide insertional mutagenesis of *Arabidopsis thaliana*. *Science* 301:653-657.

Anatskaya, O.V. & Vinogradov, A.E. Genome multiplication as adaptation to tissue survival: evidence from gene expression in mammalian heart and liver. *Genomics* 89, 70-80 (2007).

Austin, L.S., Kaushansky, A. & Kappe, S.H. Susceptibility to Plasmodium liver sTGe infection is altered by hepatocyte polyploidy. *Cell Microbiol.* 16, 784-95. doi: 10.1111/cmi.12282 (2014).

Bago, B., Zipfel, W., Williams, R.M., Jun, J., Arreola, R., Lammers, P.J., Pfeffer, P.E. & Shachar-Hill, Y. Translocation and utilization of fungal storage lipid in the arbuscular mycorrhizal symbiosis. *Plant Physiol.* 128, 108-24 (2002).

Bebber, D.P., Holmes, T. & Gurr, S.J. The global spread of crop pests and pathogens. *Global Ecol Biogeograph* 23, 1398- 1407, doi:10.1111/geb.12214 (2014).

Both, M., Csukai, M., Stumpf, M.P.H., & Spanu, P.D. Gene expression profiles of Blumeria graminis indicate dynamic changes to primary metabolism during development of an obligate biotrophic pathogen. *The Plant Cell* 17, 2107-2122 (2005).

Bravo, A., Brands, M., Wewer, V., Dörmann, P. & Harrison, M.J. Arbuscular mycorrhiza-specific enzymes FatM and RAM2 fine-tune lipid biosynthesis to promote development of arbuscular mycorrhiza. *New Phytol.* 214, 1631-1645, doi: 10.1111/nph.14533 (2017).

Caffaro, C.E. & Boothroyd, J.C. Evidence for host cells as the major contributor of lipids in the intravacuolar network of Toxoplasma-infected cells. *Eukaryot Cell.* 10, 1095-9, doi: 10.1128/EC.00002-11 (2011).

Chandran D., Tai Y.C., Hather G., Dewdney J., Denoux C., Burgess D.G., Ausubel F.M., Speed T.P., Wildermuth M.C. (2009) Temporal global expression data reveal known and novel salicylate-impacted processes and regulators mediating powdery mildew growth and reproduction on Arabidopsis. *Plant Physiol.* 149:1435-51.

Chandran, D., Inada, N., Hather, G., Kleindt, C.K., & Wildermuth, M.C. Laser microdissection of Arabidopsis cells at the powdery mildew infection site reveals site-specific processes and regulators. *Proc. Natl. Acad. Sci. USA* 107, 460-5, doi:10.1073/pnas.1013020107 (2010).

Chandran, D., Rickert, J., Cherk, C., Dotson, B.R. & Wildermuth, M.C. Host cell ploidy underlying the fungal feeding site is a determinant of powdery mildew growth and reproduction. *Mol Plant Microbe Interact.* 26, 537-45, doi: 10.1094/MPMI-10-12-0254-R (2013).

Chen, Y., Daviet, L., Schalk, M., Siewers, V., & Nielsen, J. Establishing a platform cell factory through engineering of yeast acetyl-CoA metabolism. *Metab Eng.* 15, 48-54, doi: 10.1016/j.ymben.2012.11.002 (2013).

Clough S.J. & Bent A.F. (1998) Floral dip: a simplified method for Agrobacterium-mediated transformation of Arabidopsis thaliana. *Plant J.* 16:735–743.

Conant, G.C. & Wolfe, KH. Increased glycolytic flux as an outcome of whole-genome duplication in yeast. *Mol Syst Biol.* 3, 129 (2007).

Doomun N.E., Loke S., O'Callaghan S., Callahan D.L. (2016) A simple method for measuring carbon-12 fatty acid enrichment in major lipid classes of microalgae using GC-MS. *Metabolites* 6:42.

Fahy E., Sud M., Cotter D., Subramaniam S. (2007) LIPID MAPS online tools for lipid research. *Nucleic Acids Research* 35:W606-W612.

Fotopoulos, V., Gilbert, M.J., Pittman, J.K., Marvier, A.C., Buchanan, A.J., Sauer, N., Hall, J.L., & Williams, LE. The monosaccharide transporter gene, AtSTP4, and the cell-wall

invertase, Atbetafruct1, are induced in Arabidopsis during infection with the fungal biotroph Erysiphe cichoracearum. *Plant Physiol.* 132, 821-9 (2003).

Gass, N., Glagotskaia, T., Mellema, S., Stuurman, J., Barone, M., Mandel, T., Roessner-Tunali, U., & Kuhlemeier, C. Pyruvate decarboxylase provides growing pollen tubes with a competitive advanTGe in petunia. *Plant Cell.* 17, 2355-68, doi:10.1105/tpc.105.033290 (2005).

Glawe, D.A. The powdery mildews: a review of the world's most familiar (yet poorly known) plant pathogens. *Annu. Rev. Phytopathol*. 46, 27-51, doi:10.1146/annurev.phyto.46.081407.104740 (2008).

Gomez, S.K., Javot, H., Deewatthanawong, P., Torres-Jerez, I., Tang, Y., Blancaflor,E.B., Udvardi, M.K., & Harrison, M.J. *Medicago truncatula* and *Glomus intraradices* gene expression in cortical cells harboring arbuscules in the arbuscular mycorrhizal symbiosis. *BMC Plant Biol*. 9, 10 (2009).

Gravot, A., Richard, G., Lime, T., Lemarie, S., Jubault, M., Lariagon, C., Lemoine, J., Vicente, J., Robert-Seilaniantz, A., Holdsworth, M.J., and Manzanares-Dauleux, M.J. (2016) Hypoxia response in Arabidopsis roots infected by Plasmodiophora brassicae supports the development of clubroot. *BMC Plant Biology* 16:251.

Haug K. et al. (2013) MetaboLights-- an open-access general-purpose repository for metabolomics studies and associated meta-data. *Nucl. Acids Res.* 41:D781-6.

Herren, J.K., Paredes, J.C., Schüpfer, F., Arafah, K., Bulet, P. & Lemaitre, B. Insect endosymbiont proliferation is limited by lipid availability. *Elife*. 3, e02964, doi: 10.7554/eLife.02964 (2014).

Herrtwich, L., Nanda, I., Evangelou, K., Nikolova, T., Horn, V., Sagar, Erny, D., Stefanowski, J., Rogell, L., Klein, C., Gharun, K., Follo, M., Seidl, M., Kremer, B., Münke, N., Senges, J., Fliegauf, M., Aschman, T., Pfeifer, D., Sarrazin, S., Sieweke, M.H., Wagner, D., Dierks, C., Haaf, T., Ness, T., Zaiss, M.M., Voll, R.E., Deshmukh, S.D., Prinz, M., Goldmann, T., Hölscher, C., Hauser, A.E., Lopez-Contreras, A.J., Grün, D., Gorgoulis, V., Diefenbach, A., Henneke, P. & Triantafyllopoulou, A. DNA Damage Signaling Instructs Polyploid Macrophage Fate in Granulomas. *Cell* 167, 1264- 1280.e18, doi: 10.1016/j.cell.2016.09.054 (2016).

Hirani, T.A., Tovar-Méndez, A., Miernyk, J.A., & Randall, DD. Asp295 stabilizes the active-site loop structure of pyruvate dehydrogenase, facilitating phosphorylation of ser292 by pyruvate dehydrogenase-kinase. *Enzyme Res.* 2011, 939068., doi:10.4061/2011/939068 (2011).

Hwang J.H., Lee, M.O., Choy, Y.-H., Ha-Lee, Y.-M., Hong C.B., Lee, D.-H. (2011) Expression profile analysis of hypoxia responses in Arabidopsis roots and shoots. *Journal of Plant Biology* 54:373.

Itoe, M.A., Sampaio, J.L., Cabal, G.G., Real, E., Zuzarte-Luis, V., March, S., Bhatia, S.N., Frischknecht, F., Thiele, C., Shevchenko, A., & Mota, M.M. Host cell phosphatidylcholine is a key mediator of malaria parasite survival during liver sTGe infection. *Cell Host Microbe.* 16, 778-86, doi: 10.1016/j.chom.2014.11.006 (2014).

Jiang, Y., Wang, W,. Xie, Q., Liu, N., Liu, L., Wang, D., Zhang, X., Yang, C., Chen, X., Tang, D. & Wang, E. Plants transfer lipids to sustain colonization by mutualistic mycorrhizal and parasitic fungi. *Science* 356, 1172-1175, doi: 10.1126/science.aam9970 (2017).

Johnson, D., Weber, D.J., & Hess, W.M. Lipids from conidia of Erysiphe graminis tritici (powdery mildew). *Trans. Br. mycol. Soc.* 66, 35-43 (1976).

Jones, L., Riaz, S., Morales-Cruz, A., Amrine, K.C., McGuire, B., Gubler, W.D., Walker, M.A. & Cantu, D. Adaptive genomic structural variation in the grape powdery mildew pathogen, Erysiphe necator. *BMC Genomics* 15, 1081, doi: 10.1186/1471-2164-15-1081 (2014).

Käsbauer, C.L., Pathuri, I.P., Hensel, G., Kumlehn, J., Hückelhoven, R., Proels, R.K. Barley ADH-1 modulates susceptibility to Bgh and is involved in chitin-induced systemic resistance. *Plant Physiol Biochem.* 123, 281-287, doi: 10.1016/j.plaphy.2017.12.029 (2018).

Keymer, A., Pimprikar, P., Wewer, V., Huber, C., Brands, M., Bucerius, S.L., Delaux, P.M., Klingl, V., Röpenack-Lahaye, E.V., Wang, T.L., Eisenreich, W., Dörmann, P., Parniske, M. & Gutjahr, C. Lipid transfer from plants to arbuscular mycorrhiza fungi. *Elife* 6. pii: e29107, doi:10.7554/eLife.29107 (2017).

Keymer, A. and Gutjahr, A. (2018) Cross-kingdom lipid transfer in arbuscular mycorrhiza symbiosis and behyond. *Curr. Opin. Plant Biol*. 44:137-144.

Kind T., Wohlgemuth G., Lee D.Y., Lu Y., Palazoglu M., Shahbaz S., Fiehn O. (2009). FiehnLib: mass spectral and retention index libraries for metabolomics based on quadrupole and time-of-flight gas chromatography/mass spectrometry. *Analytical Chemistry* 81:10038-10048.

Kürsteiner, O., Dupuis, I., & Kuhlemeier, C. The pyruvate decarboxylase1 gene of Arabidopsis is required during anoxia but not other environmental stresses. *Plant Physiol.* 132, 968-78, doi:10.1104/pp.102.016907 (2003).

Lee, H.O., Davidson, J.M., & Duronio, R.J. Endoreduplication: ploidy with purpose. *Genes Dev.* 23, 2461-77, doi: 10.1101/gad.1829209 (2009).

Li-Beisson Y. et al. (2010) Acyl-Lipid Metabolism,*The Arabidopsis Book* 2010:e0133.

Liu, X., Cooper, D.E., Cluntun, A.A., et al. (2018) Acetate production from glucose and coupling to mitochondrial metabolism in mammals. *Cell* 175:502-513.

Luginbuehl, L.H., Menard, G.N., Kurup, S., Van Erp, H., Radhakrishnan, G.V., Breakspear, A., Oldroyd, G.E.D. & Eastmond, P.J. Fatty acids in arbuscular mycorrhizal fungi are synthesized by the host plant. *Science* 356, 1175-1178, doi: 10.1126/science.aan0081 (2017).

MacLean, A.M., Bravo, A. & Harrison, M.J. Plant Signaling and Metabolic Pathways Enabling Arbuscular Mycorrhizal Symbiosis. *Plant Cell* 29, 2319-2335, doi: 10.1105/tpc.17.00555 (2017).

Mellema, S., Eichenberger, W., Rawyler, A., Suter, M., Tadege, M., & Kuhlemeier, C. The ethanolic fermentation pathway supports respiration and lipid biosynthesis in tobacco pollen. *The Plant J.* 30, 329-336 (2002).

Micali, C., Göllner, K., Humphry, M., Consonii, C. & Panstruga, R. The powdery mildew disease of Arabidopsis: a paradigm for the interaction between plants and biotrophic fungi. *The Arabidopsis Book* e0115, 1-19, doi: 10.1199/tab.0115 (2008).

Muchembled, J., Sahraoui, A.L., Laruelle, F,. Palhol, F., Couturier, D., Grandmougin-Ferjani, A., & Sancholle, M. Methoxylated fatty acids in Blumeria graminis conidia. *Phytochemistry* 66, 793-6 (2005).

Nagl, W. DNA endoreduplication and polyteny understood as evolutionary strategies. *Nature* 261, 614-615 (1976).

Nolan, S.J., Romano, J.D. & Coppens, I. Host lipid droplets: An important source of lipids salvaged by the intracellular parasite Toxoplasma gondii. *PLoS Pathog.* 13, e1006362, doi:10.1371/journal.ppat.1006362 (2017).

Olszak, M. Truman, W., Stefanowicz, K., Silwinska, E., Ito, M., Walerowski, P., Rolfe, S., and Malinowski, R. (2019) Tranascriptional profiling identifies critical steps of cell cycle

programming necessary for Plasmodiophora brassicae-driven gall formation in *Arabidopsis*. *The Plant Journal* 97:715-729.
Pathuri, I.P., Reitberger, I.E., Hückelhoven, R., & Proels, R.K. Alcohol dehydrogenase 1 of barley modulates susceptibility to the parasitic fungus Blumeria graminis f.sp. hordei. *J Exp Bot.* 62, 3449-57, doi: 10.1093/jxb/err017 (2011).
Plotnikova, J.M., Reuber, T.L., Ausubel, F.M. & Pfister, D.H. Powdery mildew pathogenesis of Arabidopsis thaliana. *Mycologia* 90, 1009-1016, doi:10.2307/3761274 (1998).
Schoenfelder, K.P. & Fox, D.T. The expanding implications of polyploidy. *J Cell Biol.* 209, 485-91, doi: 10.1083/jcb.201502016 (2015).
Shi, X., Zhang, C., Ko, D.K. & Chen, Z.J. Genome-Wide Dosage-Dependent and -Independent Regulation Contributes to Gene Expression and Evolutionary Novelty in Plant Polyploids. *Mol Biol Evol.* 32, 2351-66, doi: 10.1093/molbev/msv116 (2015).
Shiba, Y., Paradise, E.M., Kirby, J., Ro, D.K. & Keasling, J.D. Engineering of the pyruvate dehydrogenase bypass in Saccharomyces cerevisiae for high-level production of isoprenoids. *Metab Eng.* 9, 160-8 (2007).
Singh, A., & Del Poeta, M. Lipid signalling in pathogenic fungi. *Cell Microbiol.* 13, 177-85, doi: 10.1111/j.1462- 5822.2010.01550.x (2011).
Smith C.A., Maille G.O., Want E.J., Qin C., Trauger S.A., Brandon T.R., Custodio D.E., Abagyan R., Siuzdak G. (2005) Metlin: a metabolite mass spectral database. *Therapeutic Drug Monitoring* 27:747-751.
Spanu, P.D. (2012) The genomics of obligate (and nonobligate) biotrophs. *Annu. Rev. Phytopathol.* 50:91-109.
Sutak, R. Tachezy, J, Kulda, J., & Hrdy, I. Pyruvate decarboxylase, the target for omeprazole in metronidazole-resistant and iron-restricted tritichomonas foetus. Antimicrobial Agents and Chemotherapy, June 2004, 2185-2189 (2004). doi: 10.1128/AAC.48.6.2185–2189.2004
Swarbrick, P.J., Schulze-Lefert, P., & Scholes, J.D. Metabolic consequences of susceptibility and resistance (race-specific and broad-spectrum) in barley leaves challenged with powdery mildew. *Plant Cell Environ*. 29, 1061-76 (2006).
Toledo, A., & Benach, J.L. Hijacking and use of host lipids by intracellular pathogens. *Microbiol Spectr*. 3, doi: 10.1128/microbiolspec.VMBF-0001-2014 (2015).
Trujillo, M., Altschmied, L., Schweizer, P., Kogel, K.H., & Hückelhoven, R. Respiratory burst oxidase homologue A of barley contributes to penetration by the powdery mildew fungus Blumeria graminis f. sp. hordei. *J Exp Bot*. 57, 3781-91, doi:10.1093/jxb/erl191 (2006).
Tsitsigiannis, D.I. & Keller, N.P. Oxylipins as developmental and host-fungal communication signals. *Trends Microbiol.* 15, 109-18 (2007).
Tulloch, A.P. & Ledingham, G.A. The component fatty acids of oils found in spores of plant rusts and other fungi. *Can J Microbiol.* 6, 425-34 (1960).
Vromman, F., & Subtil, A. Exploitation of host lipids by bacteria. *Curr Opin Microbiol.* 17, 38-45, doi: 10.1016/j.mib.2013.11.003 (2014).
Weßling R. & Panstruga, R. (2014) Rapid quantification of plant-powdery mildew interactions by qPCR and conidiospore counts. Plant Methods 8:35.
Wei, Y., Lin, M., Oliver, D.J., & Schnable, P.S. The roles of aldehyde dehydrogenases (ALDHs) in the PDH bypass of Arabidopsis. *BMC Biochemistry* 10, 7, doi: 10.1186/1471-2091-10-7 (2009).
Wewer, V., Brands, M. & Dörmann, P. Fatty acid synthesis and lipid metabolism in the obligate biotrophic fungus Rhizophagus irregularis during mycorrhization of Lotus japonicus. *Plant*

J. 79, 398-412, doi: 10.1111/tpj.12566 (2014).
Wildermuth, M.C. Modulation of host nuclear ploidy: a common plant biotroph mechanism. *Curr. Opin. Plant Biol.* 13, 449-58, 10.1016/j.pbi.2010.05.005 (2010).
Wildermuth, M.C., Steinwand, M.A., McRae, A.G., Jaenisch, J., & Chandran, D. Adapted Biotroph Manipulation of Plant Cell Ploidy. *Annu Rev Phytopathol.* 55, 537-564, doi:10.1146/annurev-phyto-080516-035458 (2017).
Ye, S. & Cohen, J.D. Identification of pyruvate decarboxylase/indole pyruvate decarboxylase gene family members from Arabidopsis thaliana. Ph.D. Dissertation, University of Minnesota (2009).

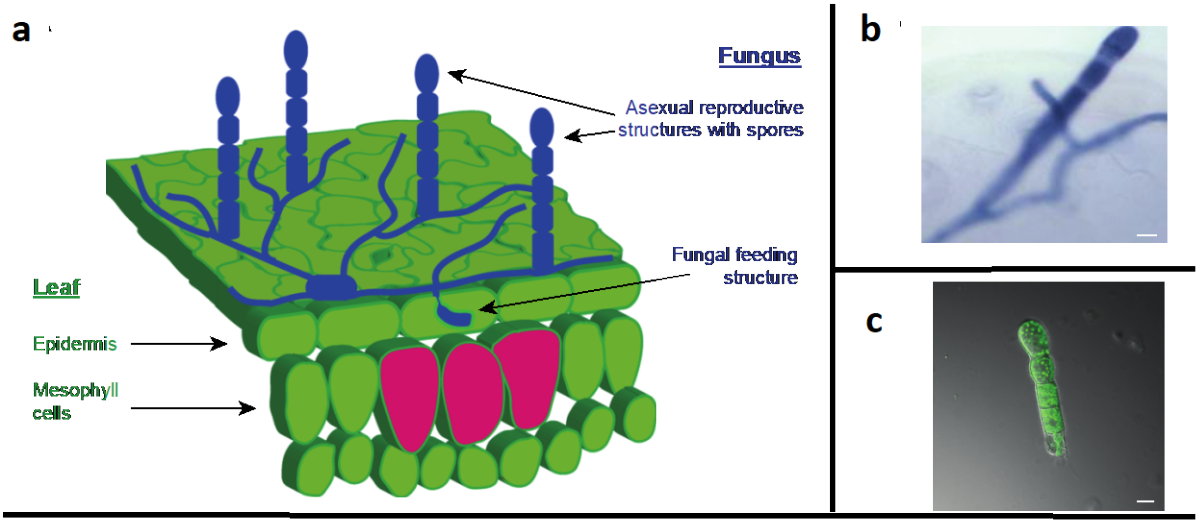
a
Fungus
Asexual reproductive structures with spores
Fungal feeding structure
Leaf
Epidermis
Mesophyll cells
b
c

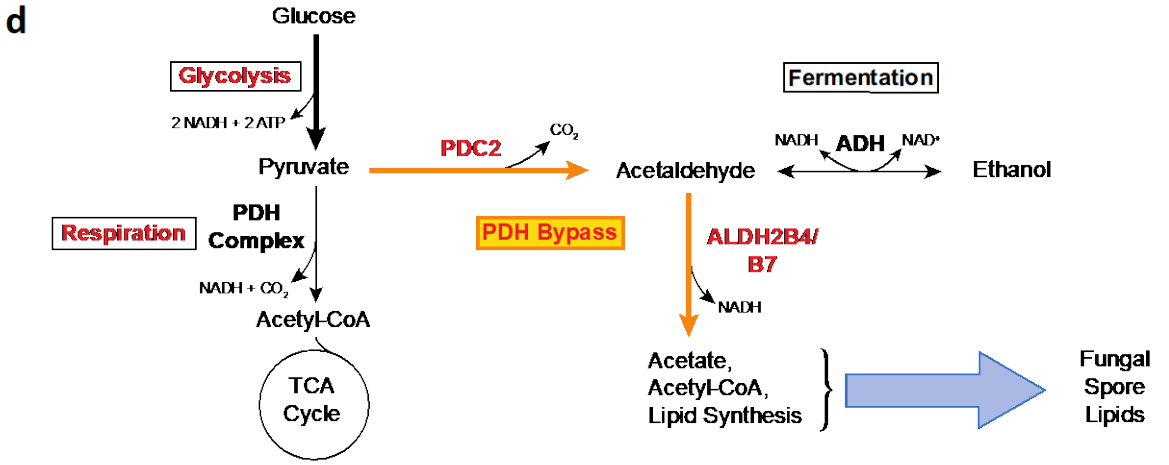
d
Glucose
Glycolysis
2 NADH + 2 ATP
Pyruvate
PDC2
CO2
Acetaldehyde
Fermentation
NADH
ADH
NAD+
Ethanol
Respiration
PDH Complex
NADH + CO2
Acetyl-CoA
TCA Cycle
PDH Bypass
ALDH2B4/ B7
NADH
Acetate, Acetyl-CoA, Lipid Synthesis
Fungal Spore Lipids

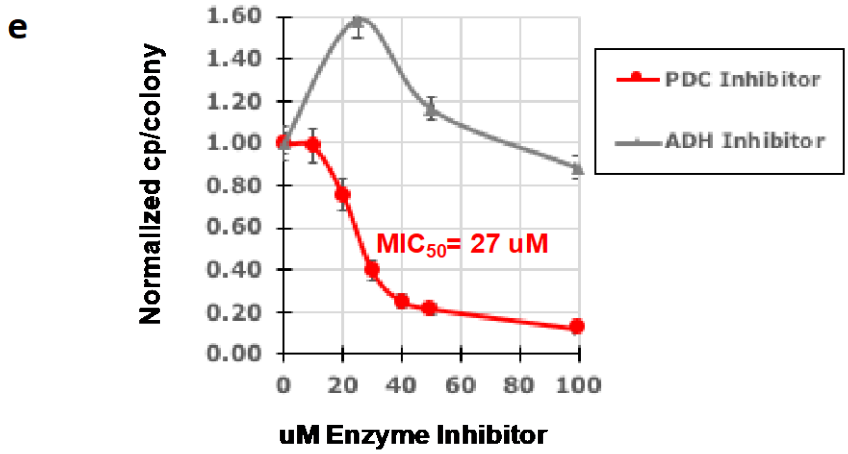
e
Normalized cp/colony
1.60
1.40
1.20
1.00
0.80
0.60
0.40
0.20
0.00
0
20
40
60
80
100
uM Enzyme Inhibitor
PDC Inhibitor
ADH Inhibitor
MIC50= 27 uM

Fig. 1. *Arabidopsis* PDH bypass at the powdery mildew infection site concurrent with asexual reproduction. (a) Side view depiction of powdery mildew infection of *Arabidopsis* leaf at 5 dpi. Magenta leaf mesophyll cells exhibit powdery mildew-induced endoreduplication at 5 dpi, resulting in an 8- to 64-fold increase in cellular DNA content (Chandran et al., 2010). (b-c) Microscopic visualization of conidiophore, the asexual reproductive structure, stained with trypan blue (b) or BODIPY 505/515 neutral lipid staining fluorescent dye (c) bar=20 μm. (d) Simplified view of *Arabidopsis* primary metabolism highlighting the PDH bypass contribution to fungal spore lipids. Annotated processes with statistically significant enhanced ploidy-associated expression are boxed in black (Wildermuth, 2010). Red indicates enhanced expression of processes/PDH bypass genes at 5 dpi with powdery mildew (Chandran et al., 2010). *ADH* did not show enhanced expression in response to powdery mildew; therefore, Fermentation process is not in red. (e) Impact of chemical inhibition of PDC or ADH enzymes on powdery mildew asexual reproduction (conidiophore (cp)/colony). Mean ±SE is shown for one independent experiment, with 45 colonies assessed per concentration. Independent experiments gave similar results.

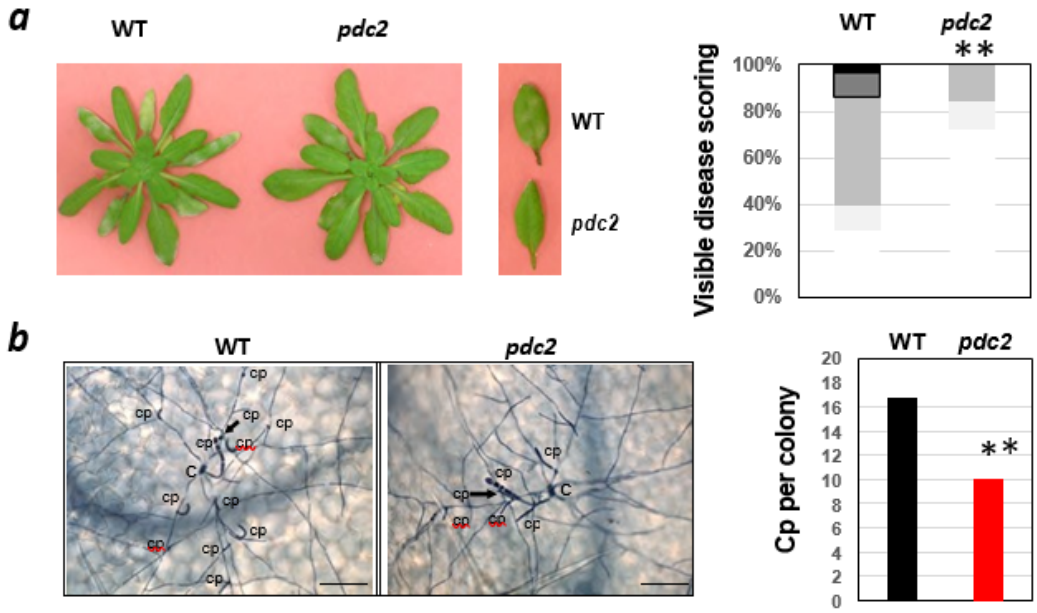
a
WT
pdc2
WT
pdc2
Visible disease scoring
100%
80%
60%
40%
20%
0%
**
b
WT
pdc2
cp
C
WT
pdc2
Cp per colony
20
18
16
14
12
10
8
6
4
2
0
**
c
WT
pdc2
C
d
WT
aldh2B4,B7
Visible disease scoring
100%
80%
60%
40%
20%
0%
*
WT
aldh2B4,B7
Cp per colony
14
12
10
8
6
4
2
0
**
WT
pdc2
aldh2B4
adh1
Normalized asexual reproductive output
120
100
80
60
40
20
0
**
**
e
pdc2
WT
PDC2/WT
Normalized asexual reproductive output
200
150
100
50
0
*
**

Fig. 2. Powdery mildew growth and reproduction is reduced on *Arabidopsis* PDH bypass mutants. (a) Powdery mildew-infected whole plants and representative leaves were photographed for wild-type (WT) and *pdc2* mutant at 10 dpi. (a, d) Visible disease scoring comparing WT and mutant is shown as percent with each disease rating: White = no visible symptoms of infection; light grey = isolated spots of powdery mildew; gray = isolated spots of powdery mildew; dark gray = 20% leaf coverage; black = 50% leaf coverage. 20-25 plants were evaluated per genotype for one experiment. Multiple independent experiments gave similar results. (b,d) Microscopic analysis of leaves harvested at 5 dpi and stained with trypan blue for analysis of fungal asexual reproduction (coniophore (cp) per colony) or (c) cell death. C is initial germinated conidia. Bar = 100 µm. Mean is shown for one independent experiment, with at least 30 powdery mildew colonies analyzed per genotype. Independent experiments gave similar results. (d-e) Mean percent powdery mildew spores per gFW leaf on mutant compared to WT are shown for one experiment with multiple independent biological replicates. Independent experiments gave similar results. (e) Plant lines with increasing *PDC2* dosage were used; *PDC2/WT* is homozygous plant line with native *PDC2* stably introduced into WT. Statistical significance was assessed using Student's T-Test. **p*-value $\leq$0.05. ***p*-value $\leq$0.001.

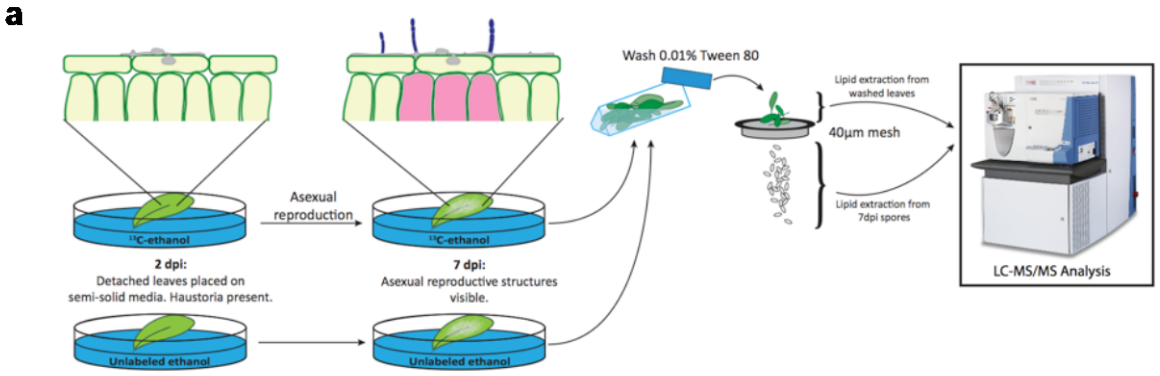
a
Wash 0.01% Tween 80
Lipid extraction from washed leaves
40µm mesh
Lipid extraction from 7dpi spores
LC-MS/MS Analysis
Asexual reproduction
13C-ethanol
13C-ethanol
2 dpi:
Detached leaves placed on semi-solid media. Haustoria present.
7 dpi:
Asexual reproductive structures visible.
Unlabeled ethanol
Unlabeled ethanol

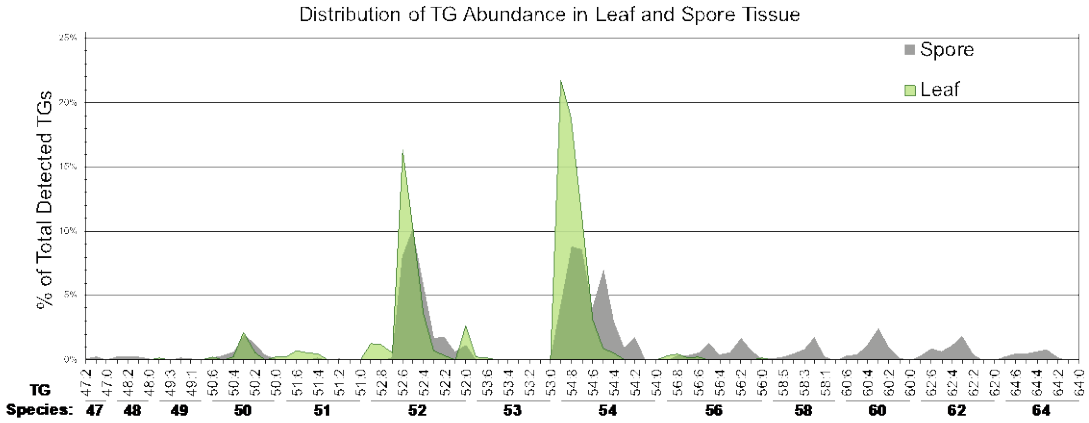
b
Distribution of TG Abundance in Leaf and Spore Tissue
Spore
Leaf
% of Total Detected TGs
TG Species: 47 48 49 50 51 52 53 54 56 58 60 62 64

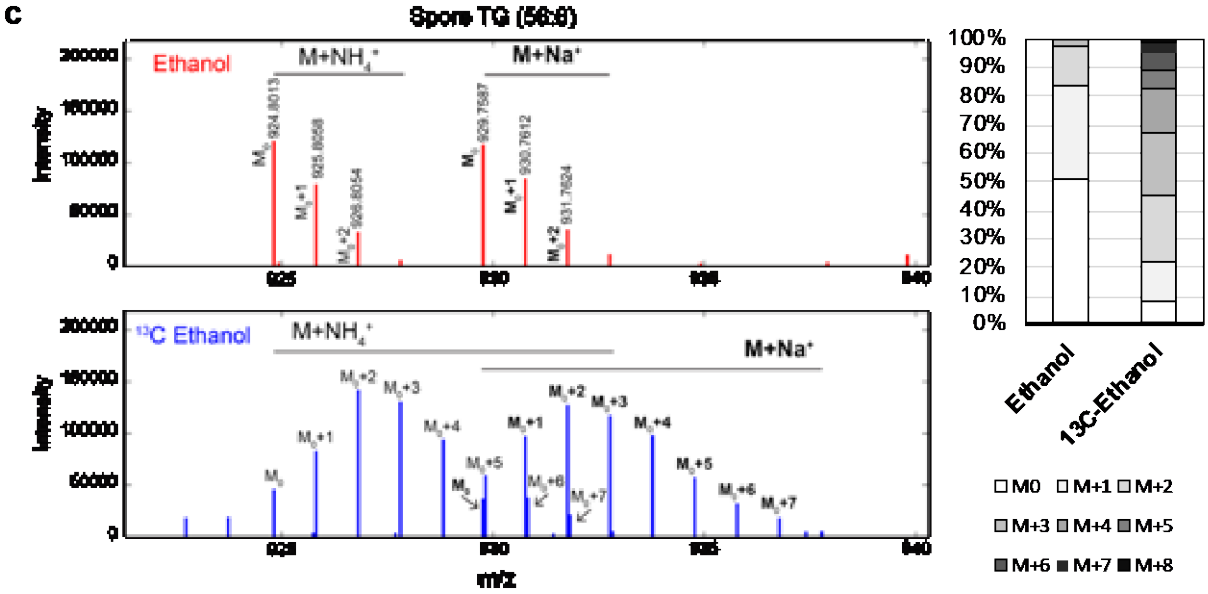
c
Spore TG (56:8)
Ethanol
M+NH4+
M+Na+
13C Ethanol
M+NH4+
M+Na+
Intensity
m/z
100%
90%
80%
70%
60%
50%
40%
30%
20%
10%
0%
Ethanol
13C-Ethanol
M0 M+1 M+2
M+3 M+4 M+5
M+6 M+7 M+8

Fig. 3. Incorporation of plant PDH precursors into fungal spore triacylglycerols. (a) Overview of experimental design. Mature fully expanded Arabidopsis leaves 2 days post inoculation with powdery mildew are detached and placed in agar containing either ^{13}C-ethanol or unlabeled ethanol. At 2 dpi, the fungal feeding structure has formed, but asexual reproduction has not occurred. Five days later, at 7 dpi, leaves from agar plates are removed for processing. Leaves are washed to remove fungal spores and spores are filtered through a 40 μm mesh to remove other debris. Lipid extraction was performed on three biological replicates from each treatment and tissue type, followed by LC-MS/MS. (b) Relative abundance of TGs in leaf and spore tissue is calculated based on value of unlabeled mean M_0 peak height per mg fresh weight (FW) tissue; n=3. LC-MS/MS analysis was performed using a reverse phase C18 column. TG species were identified by accurate mass and MS/MS fragmentation patterns corresponding to neutral loss of fatty acid tails, and quantified using peak height in positive ion mode. (c) Representative MS1 spectra for spore TGs from agar plates with unlabeled ethanol (top) or ^{13}C-ethanol (bottom). Relative contribution of each isotopologue to total (sum of isotopologues) shown for NH4+ adducts. Independent experiments gave similar results. See Methods for further detail.

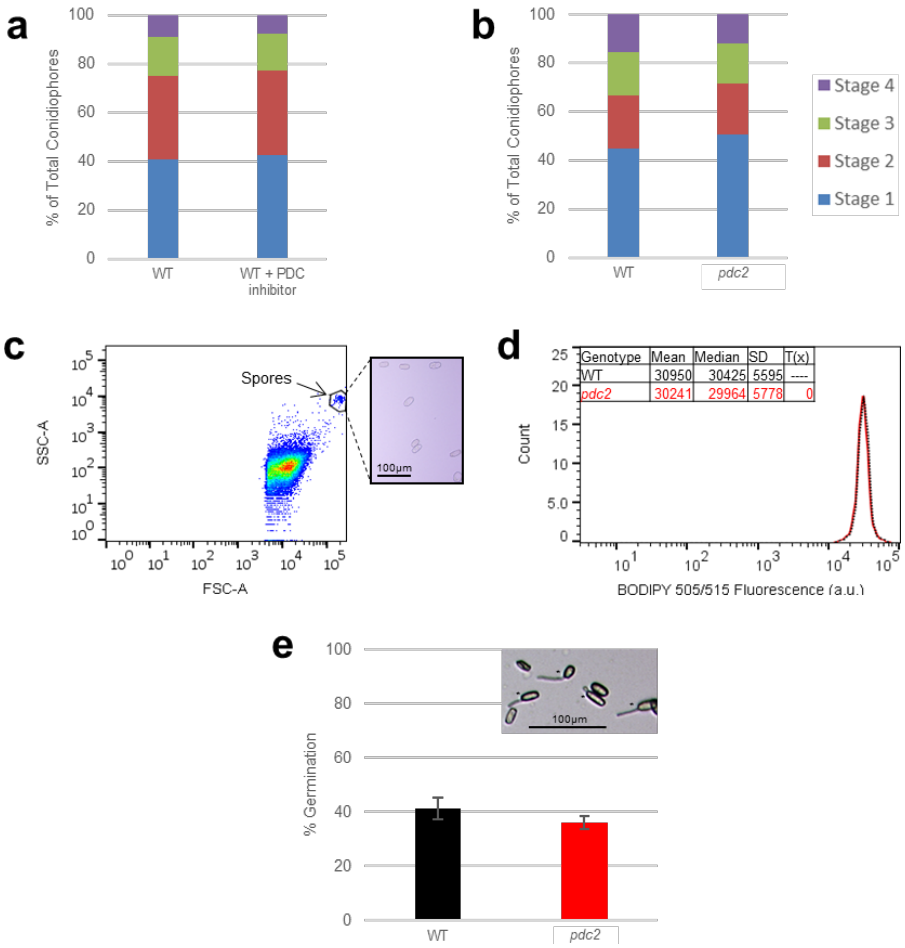

Fig. 4. *Arabidopsis* PDC2 does not impact powdery mildew conidiophore development and spore fitness. (a-b) Mean percent of total conidiophores (cp) at each developmental stage at 5 dpi. Stage 1(basal foot cell) to Stage 4, containing progressively more conidia. Powdery mildew developed on (a) wild type (WT) leaves with and without PDC inhibitor at the MIC_{50} from or (b) WT compared with *pdc2* mutant plant leaves from. Data shown is for one independent experiment. Pearson's Chi-squared analysis found no statistical difference. An independent experiment gave similar results. (c) Spores from powdery mildew that developed on WT and *pdc2* plants were stained with the neutral lipid dye, BODIPY 505/515, and fluorescence was measured using a flow cytometer (LSR Fortessa X20, 488 nm laser (505LP 530/30 filter). Spore suspension was visualized by forward scatter (FSC-A) and side scatter (SSC-A) to identify spores (gated). Inset shows spores sorted by a BD Influx Sorter to verify gating methods. (d) The fluorescence of 200 (±10%) spores developed on WT (black) and *pdc2* (red) were measured. Fluorescence intensity distributions were compared using Chi-Squared T(x) statistical analysis in FlowJo v.10 software. Analysis shows no significant difference (T(x)=0). Two additional independent experiments show a similar result. (e) The mean germination rate ± SE of spores that developed on WT and *pdc2* plants is displayed, n=3. Student's T-Test of the germination rates shows no significant difference ($p \geq 0.05$). Two additional independent experiments show similar results. Inset shows spores in germination assay; * indicates germinated spore.

Chapter 3: Spray-induced gene silencing reduces powdery mildew disease

A.G. McRae*, J. Taneja*, and M.C. Wildermuth
*Authors contributed equally to this work

Permission was granted from all co-authors to include this work as part of this dissertation.

Preface

Mary, Jyoti, and I worked together to develop gene silencing methods for powdery mildews. We all contributed intellectually to the experimental design and interpreted experiments to troubleshoot the methodologies. The research was performed by Jyoti and me; I focused on whole plant *A. thaliana* and RNA uptake experiments while Jyoti focused on detached leaf experiments, hyphal length quantification, and translating the methods to grape powdery mildew. I also optimized a powdery mildew spore quantification assay (Appendix 3) extensively used in these experiments.

Keywords: powdery mildew, spray-induced gene silencing (SIGS), dsRNA, Golovinomyces orontii, Arabidopsis thaliana, Erysiphe necator, grapevine

Abstract

Spray-induced gene silencing (SIGS) is an emerging tool being developed to protect crops from disease. It utilizes exogenously applied RNA designed to reduce gene expression of critical genes in plant pests using endogenous RNA interference machinery. The widespread obligate biotrophic pathogen, powdery mildew, infects agriculturally important crops like wheat, barley, cucurbits, and grapevine which can require numerous fungicide treatments to control. For grape powdery mildew, dominant varieties are susceptible to powdery mildew and extensive resistance to fungicides has caused a need for new disease management strategies. In this study we developed SIGS methods for powdery mildews and identified novel gene targets that significantly contribute to fungal growth. *Golovinomyces orontii*, a powdery mildew that infects *Arabidopsis thaliana*, was found to uptake RNA directly from its environment, independent of the host. SIGS methods using long double-stranded (dsRNA) and small interfering RNA (siRNA) were developed using whole plant and detached leaf assays. Method optimization utilized the azole-fungicide target *CYP51*. Ten additional powdery mildew targets were screened identifying 5 novel genes that contribute to fungal proliferation: *lipase a, lipase 1*, *β-carotene 15,15'-dioxygenase, apoptosis-antagonizing transcription factor* (*AATF*), and *effector candidate 2*. Translation of these methods to the *Erysiphe necator-Vitis vinifera* pathosystem showed similar reduction in disease with SIGS against *CYP51*. Furthermore, SIGS of the novel target *AATF* identified in the *G. oronti-A. thaliana* pathosystem also showed reduced fungal proliferation in grapevine suggesting high throughput screening of targets in the *G. orontii-A. thaliana* pathosystem could prioritize targets for testing in the grapevine powdery mildew system. SIGS may be the future of controlling powdery mildew growth on crops because of its flexibility, resilience to resistance development, reduced environmental and health risks, and rapid transition from the bench to the field.

Introduction

Powdery mildews are widespread obligate biotrophic pathogens that infect a variety of agriculturally important crops (Agrios, 2004). Hosts like grapevine require fungicides to control

infection, though there are increasing needs for other options to manage disease due to fungicide resistance and increasing human health and environmental concerns associated with fungicide application (Calvert et al., 2008; Frenkel et al., 2015; Jones et al., 2014; Zubrod et al., 2014). *Erysiphe necator*, which causes grape powdery mildew, is especially troublesome for California grape growers as dominant cultivars are susceptible. Powdery mildew disease management accounts for 74% of pesticide use amounting to 9% of table and raisin grape production costs and up to 20% of wine grape production costs of highly susceptible cultivars like chardonnay wine grapes in the Central Coast of California (Fuller et al., 2014). Sulfur is heavily used in the grape industry to prevent fungal disease. Although cheap and effective, sulfur is routinely applied during high disease pressure every 7-10 days (Jones et al., 2014) which can cause respiratory symptoms in workers and people living in the area (Raanan et al., 2017). In addition, some wine producers are concerned about a potential impact of sulfur on taste when applied repeatedly later in the growing season. Fungicides including azole-fungicides (demethylase inhibitors) are also used to control powdery mildew disease. These fungicides inhibit *CYP51* function, which is required for sterol biosynthesis, a component of fungal cell membranes (Frenkel et al., 2015). Powdery mildew isolates that have increased resistance to azole-fungicides have increased expression of *CYP51* and acquire mutations that decrease azole-fungicide sensitivity (Frenkel et al., 2015; Jones et al., 2014).

RNA interference (RNAi) strategies are being developed to offer additional solutions to combat plant disease. These tools utilize conserved eukaryotic host and/or pathogen RNAi machinery to mediate silencing of pathogen genes by degrading messenger RNA (Majumdar et al., 2017). Double-stranded RNA (dsRNA) can be provided by the host plant using host-induced gene silencing (HIGS) and has been demonstrated to be effective in reducing barley powdery mildew infection (Pliego et al., 2013) and other fungal diseases like Fusarium head blight (Machado et al., 2018), wheat stripe rust (Zhu et al., 2017), and grey mold (Xiong et al., 2019) suggesting plant-mediated RNA uptake is widespread. HIGS, however, requires the use of transgenic crops which can require years of engineering to create the transgenic host contributing to high production costs. Despite years of advancement, there are limited RNAi based plant products in the marketplace (Bramlett et al., 2020). Spray-induced gene silencing (SIGS) offers a higher throughput and adaptable strategy that is not transgenic. Much like HIGS, it relies on endogenous RNAi machinery to mediate gene silencing of critical pathogen genes. The necrotrophic fungus *Botrytis cinerea* has been shown to directly uptake RNA from the environment. Both long dsRNA and small RNAs (sRNAs) applied onto plants limited infection of *B. cinerea* (Wang et al., 2016). This strategy has the potential to be readily adaptable to more than one crop or pest. It requires that the pest is able to take up dsRNA and/or siRNA, has endogenous RNAi machinery, and has sequenced transcripts to target. SIGS has been shown to be effective in reducing disease in many fungal and oomycete pathogens with various lifestyles including obligate biotrophs, *Hyaloperonospora arabidopsidis* (Bilir et al., 2019) and *Phakopsora pachyrhizi* (Hu et al., 2020), the hemibiotroph, *Fusarium graminearum* (Koch et al., 2016), and the necrotroph, *B. cinerea* (Wang et al., 2016).

In this study, we developed SIGS methods in the *Golovinomyces orontii-Arabidopsis thaliana* model system using *CYP51* as the positive control gene target (Koch et al., 2016) and translated these methods to the agriculturally relevant system, *Vitis vinifera-Erysiphe necator*. SIGS phenotypes can be detected at early time points in infection using microscopic hyphal length measurements or at later stages by quantifying fungal spore production. Both siRNAs (small interfering RNAs) and long dsRNAs were shown to be effective in reducing powdery mildew

growth and reproduction. After screening methods were optimized, ten additional conserved powdery mildew genes were selected for testing. SIGS against five of these targets significantly reduce spore production and represent diverse target genes that function as metabolic enzymes, regulatory genes, and secreted protein effectors. Of these five, *AATF*, was then silenced in grapevine, with results similar to *Arabidopsis,* showing findings in *Arabidopsis* translates to other agronomic species. Through this research we can rapidly identify important powdery mildew gene targets suitable for RNAi-based control of powdery mildew disease.

Results

G. orontii spores can take up environmental RNA

To determine if *G. orontii* can uptake RNA directly from its environment, germinated conidia were incubated with *in vitro* transcribed Fluorescein-labeled β-actin-Mouse RNA (300 bp) using methods adapted from (Wang et al., 2016). To ensure RNA signal was intracellular, RNases were added before imaging. Powdery mildew uptake of RNA is rapid and observed within 1.5 hours of application demonstrating powdery mildews can uptake RNA independent from the host plant. Fluorescein was observed in all tissues present: germinated conidia, germ tubes of germinated conidia, and ungerminated conidia (Fig. 1). Not all spores observed had fluorescein signal, possibly indicating more time would be required to observe uptake in all cells or not all spores were at the appropriate stage for uptake.

siRNA and long dsRNA design

siRNA and/or long dsRNA was designed for each gene target selected (Fig. 2, Table 1). The online resource pssRNAit (See Methods) was used to minimize off-target silencing in the host (*A. thaliana* or *V. vinifera*) and identify efficient siRNAs and dsRNAs *in silico* (Fig. 2). Known features of efficient siRNAs were incorporated into siRNA design (Mittal, 2004; Reynolds et al., 2004; Ui-Tei et al., 2004). Long dsRNAs in this study were 199-449 bps and siRNAs were composed of 21 base long sense and antisense strands that anneal over 19 bases with 2 base overhangs at the 3' ends. Where applicable, dsRNAs were also designed to anneal to multiple copies of the gene where possible as there are varying degrees of sequence conservation among copies.

siRNA and dsRNA designed to target _G. orontii CYP51_ significantly reduces spore production in _A. thaliana_ whole plant and detached leaf assays

SIGS methods were optimized (Fig. 2) using the *G. orontii* MGH1 gene target, *CYP51*, which has been successfully silenced using SIGS to reduce growth of the fungal pathogen, *F. graminearum* (Koch et al., 2016). CYP51 function is required for sterol biosynthesis, a component of fungal cell membranes, and an azole-fungicide target (Frenkel et al., 2015). In *G. orontii*, there are two copies of *CYP51* with 98.1% sequence identity. Two 21 bp siRNAs, siRNA-1 and siRNA-2, and two long dsRNAs, dsRNA-1 and dsRNA-2, targeting different regions of *CYP51* were designed (Fig. 3a).

The spraying methods, amount of RNA, number of RNA applications, timing of RNA application, RNA purification methods, and detached leaf or whole plant protocols were troubleshooted as part of SIGS protocol development to improve the efficiency and reproducibility of results (Fig. 2). The impact of SIGS on growth was measured by determining the asexual reproductive output as measured by harvesting infected tissue, liberating spores in 0.01% Tween-80, and determining the concentration of spores in suspensions. We focused on phenotyping fungal growth by measuring

spore production as spores are what propagate the fungus and it can be rapidly assessed. For all experiments, results from control treatments with buffer alone were compared with the RNA-treated samples.

In whole plant and detached leaf experiments using *CYP51* dsRNA-1, spore production decreased by an average of 46% and 30% respectively (Fig. 3b) and visually less powdery mildew coverage and density was observed on dsRNA-sprayed plants than buffer control-sprayed plants (Fig. 3c). Spore production was similarly reduced on average by 35% and 40% in whole plant and detached leaf *CYP51* siRNA-1 treated samples, respectively (Fig. 3b). These results show that SIGS against the *G. orontii CYP51* target can reproducibly limit powdery mildew disease on *Arabidopsis*.

By contrast, the *CYP51* dsRNA-2 and siRNA-2 treated samples did not affect fungal growth as spore production was similar to the control samples (Fig. 3b). This is in accordance with previous findings that a negative result does not mean the targeted transcript is not important to the phenotype assessed; instead, the negative result can be due to poor silencing efficiency of a particular siRNA or long dsRNA for reasons not yet understood (Wu et al., 2004). The lack of impact of *CYP51* dsRNA-2 and siRNA-2 on *G. orontii* spore production also indicates that the addition of dsRNA or siRNA alone does not impact powdery mildew growth.

Targeting *CYP51* significantly reduces *G. orontii* hyphal length on *A. thaliana* detached leaves

To see the impact of SIGS on early *G. orontii* colony development, we measured the impact of *CYP51* siRNA-1 on hyphal length at 2 and 3 dpi in *A. thaliana* detached leaf assays. Observing the hyphal length of colonies is more time consuming compared to measuring spore production, requiring fixing and staining of harvested leaves, fluorescence microscopy, and image analysis, but may reveal early infection phenotypes masked at later points in infection. The average total hyphal length of *CYP51* siRNA-1 colonies was significantly reduced at 2 and 3 dpi by 56% and 45% respectively compared to control samples (Fig. 3e). Although the length was reduced, the branching architecture was not altered (Fig. 3d). Coupled with the similar decrease in spore production with *CYP51* siRNA-1 treatment (Fig. 3b), this suggests the SIGS treatment against the cell membrane sterol biosynthetic enzyme *CYP51* target was reproducibly effective in limiting powdery mildew growth, but was unable to fully prevent it. This could be due to a number of factors including RNA stability, design, uptake efficiency, and mobility that can be further optimized. In summary, the optimized SIGS protocol provides a high throughput means of screening for key powdery mildew targets of import to its proliferation. The extent of growth limitation for given target can be subsequently optimized. Finally, those targets without a powdery mildew disease phenotype are not necessarily unimportant; additional dsRNA and/or siRNAs would need to be designed and tested.

dsRNA designed to target metabolic, regulatory, and effector genes identifies novel powdery mildew targets that contribute to *G. orontii* spore production on *A. thaliana*

To identify novel powdery mildew genes that contribute to its growth and development, metabolic, regulatory, and effector genes were targeted using SIGS to determine their impact on proliferation (spore production). Spore production was chosen for screening as it results in the propagation of the infection in the field and therefore is most relevant as an agricultural disease outcome

assessment. dsRNA was chosen for initial screening as multiple siRNAs are generated from each dsRNA increasing the likelihood of a successful silencing outcome.

The gene targets were chosen based on their annotation and potential function such as maintaining essential cell function, mobilizing spore energy reserves early in powdery mildew development and/or manipulating the plant host. In addition, pattern and magnitude of expression of the genes through development, number of highly similar genes, and putative positioning in a metabolic or regulatory pathway was considered (Table 1, Fig. 5, SI Fig. 1.). In addition to *CYP51*, powdery mildew gene targets tested consist of *G. orontii* MGH1 homologs of *unidentified transcript 4* (*UTR4), glycogen debranching enzyme 1* (*GDB1*), *glycogen phosphatase 1* (*GPH1*), *lipase 1* (*LIP1*), *lipase a* (*LIPA*), *diglyceride acyltransferase* (*DGAT*), *β-carotene 15,15'-dioxygenase* (*BCDO*), *glucose-induced degradation 9* (*GID9*), *apoptosis-antagonizing transcription factor* (*AATF*), and *effector candidate 2* (*EC2*) (Table 1, Fig. 4). A brief rationale on why these targets were selected is presented in Table 1. All targets were tested using *A. thaliana* whole plant assays. A portion of those genes were also tested in the detached leaf assay to compare the outcome based on the assay type. SIGS against four out of these ten targets tested reproducibly and significantly reduced fungal proliferation (Fig. 4). For initial screening, this gives a 40% success rate in identifying single powdery mildew targets important to fungal proliferation.

As previously shown, SIGS against *CYP51* involved in maintaining cell function (membrane component generation) resulted in an average spore reduction of 46% when compared to control treatment (Fig. 4). Consistent with its essential cellular function, normalized *CYP51* expression (to total RNA) is essentially stable across the infection timeline (Black box, Fig. 5). The metabolic gene, *UTR4*, an enzyme in the methionine salvage pathway (Pirkov et al., 2008), allows cells to regenerate methionine and reuse sulfur (Table 1). *UTR4* expression levels are very high and unlike *CYP51*, *UTR4* expression dramatically peaked at 6 hpi (Grey box, Fig. 5). This suggests it is utilized early in development before the haustorium is developed and plant nutrients are acquired. No SIGS phenotype was observed with the tested dsRNA against *UTR4* (Fig. 4). However, SIGS using additional *UTR4* dsRNAs and dsRNAs against other powdery mildew genes in the methionine salvage pathway should be explored.

A number of targets were chosen because they could play a role in breaking down and mobilizing/metabolizing spore glycogen or storage lipids to provide energy and metabolic precursors for early development and growth of the fungus before the haustorium has fully developed (Fig. 2). As shown in Fig. 5 (blue box), the genes encoding biosynthetic enzymes GDB1 and GPH1 and the regulatory enzyme GID9 all exhibit peaks of expression before the haustorium is fully developed. These enzymes are postulated to play a role in mobilizing energy and precursors from spore glycogen (Table 1). SIGS against these targets did not impact spore production (Fig. 4). The impact of other dsRNAs targeting these genes and this process remains to be explored. However, the similar findings for all three targets tested suggests that spore glycogen mobilization is not the prime contributor to spore germination and early colonization events.

Three metabolic genes involved in storage lipid metabolism were targeted with SIGS: lipases *LIP1* and *LIPA* and *DGAT*. Triacylglycerol lipases hydrolyze triacylglycerols producing fatty acids and glycerol while diglyceride acyltransferases form triglycerides from diacylglycerol and acyl-CoA. Triacylglycerols are stored in lipid droplets in spores and are degraded to build membranes and

fuel cellular metabolism (Subramoni et al., 2010). SIGS of *LIP1* reduced growth an average of 22% and 51% in whole plant and detached leaf experiments, respectively (Fig. 4). SIGS of *LIPA* reduced growth an average of 41% and 67% in whole plant and detached leaf experiments, respectively (Fig. 4). There are 2 copies of *LIPA* and 2 copies of *LIP1;* the dsRNA was designed to silence both copies. All copies of these lipases are most highly expressed within 12 hpi (Light blue box, Fig. 5). This suggests these lipases may be especially important for obligate biotrophs before the haustorium is fully developed. In contrast to the glycogen mobilization targets, initial screening of storage lipid mobilization targets resulted in 2 of 3 tested with a reproducible significant reduction in powdery mildew spore production. This suggests spore storage lipid breakdown/mobilization may contribute more to initial powdery mildew growth and development than glycogen breakdown/mobilization.

Manipulation of the plant host by pathogens can take many forms and is a key feature of the evolved interaction of an obligate biotroph with its host. Carotenoid oxygenases (members of the BCDO family) are enzymes responsible for cleaving carotenoids and have been identified in plants, fungi, animals, and bacteria (Ahrazem et al., 2016; Tan et al., 2003). They can function in diverse roles including signaling in response to environmental cues, regulation, and biosynthesis. In *G. orontii* MGH1, the targeted *BCDO* is further specified as a 9-cis-epoxycarotenoid dioxygenase (EC 1.1.3.11.51) involved in ABA biosynthesis (SI Fig. 2). In addition, another ABA biosynthetic gene encoding xanthoxin dehydrogenase (EC 1.1.1.288) is also annotated as being present in *G. orontii* MGH1. The low and variable expression of this target gene as shown in Fig. 5 (green box) does not allow us to further postulate on its involvement in a specific phase of infection. However, SIGS using long dsRNA targeting *G. orontii* MGH1 *BCDO* had a significant impact on growth, reducing spore production by 50% in whole plant experiments, the highest average reduction observed among the whole plant experiments (Fig. 4). Reduction was also seen in detached leaf assays with long dsRNA reducing spore production by 54% (Fig. 4).

The powdery mildew apoptosis antagonizing transcription factor, AATF, could mediate fungal response to plant-induced cell stress (Table 1). Alternately, it could be secreted into the plant by a yet unknown mechanism to limit cell death. *AATF* expression increases with infection through 24 hpi and then remains elevated (Fig. 5, green box). SIGS of *AATF* was found to reduce spore production an average of 21% and 32% in whole plant and detached leaf assays, respectively (Fig. 4). Only the detached leaf experiment showed the reduced growth to be statistically significant (Fig. 4). This reduction in spore production is close to the resolution of spore counting. However, based on its potential functions, it remains an interesting target for further analysis.

Effectors are secreted proteins that manipulate plant functions. EC2 is a widely conserved powdery mildew effector protein first described in *B. graminis* f.sp. *hordei* as BEC2 (CSEP0214; (Schmidt et al., 2014). Both copies of *EC2* in *G. orontii* MGH1 are extremely highly expressed, with one copy being the most highly expressed gene in the fungal transcriptome (Fig. 5, green box). SIGS using long dsRNA against *EC2* did not impact spore production (Fig. 4). However, given the fact that expression of EC2 in transgenic *A. thaliana* increased non-host powdery mildew penetration (Schmidt et al., 2014), we decided to further test it using siRNA (below).

siRNA targeting *BCDO* and *EC2* significantly reduces *G. orontii* spore production on *A. thaliana* detached leaves

The efficacy of siRNAs was further tested using the gene targets *BCDO* and *EC2* in *A. thaliana* detached leaf assays (Fig. 6a). siRNA targeting *BCDO* was tested because the long dsRNA SIGS experiments consistently showed very strong suppression of spore production (Fig. 4). SIGS of *EC2* did not show reduced spore production (Fig. 4) using dsRNA, but given its demonstrated role in powdery mildew pathogenesis (Schmidt et al., 2014), it was worth testing another silencing RNA (Fig. 4). *BCDO* siRNA sprayed leaves visually had less powdery mildew growth and chlorosis (Fig. 6b). Spore production was reduced an average of 42% (Fig. 6c), providing further confirmation for the role of BCDO in promoting powdery mildew proliferation. SIGS using siRNA-1 *EC2* reduced growth an average of 66% (Fig. 6c), showing *EC2* does promote powdery mildew proliferation and the *EC2* dsRNA previously tested (Fig. 4) was not effective. This result shows that known powdery mildew effectors, even those that are very highly expressed, can be targeted via SIGS to reduce powdery mildew growth and development.

SIGS methods and gene target *AATF* translate to the *Erysiphe necator-Vitis vinifera* pathosystem

With SIGS methods optimized and gene targets identified, we sought to translate these methods and targets to grape powdery mildew (Fig. 2). New long dsRNAs were designed for each target tested as there is significant sequence divergence between *G. orontii* MGH1 and *E. necator* c. First, procedures were optimized for the grapevine system by silencing *CYP51*. Spore production was reduced by 62% and 45% in grapevine whole plant and leaf disc assays, respectively when treated with long dsRNA against the same region of *CYP51* as dsRNA-1 against *G. orontii* MGH1 *CYP51* (Fig. 2; Fig. 7a). In addition, visual inspection showed infected grape leaves had less powdery mildew coverage and density when sprayed with dsRNA targeting *CYP51* than with buffer alone (Fig. 7b). We chose to also test SIGS against *AATF* in the grapevine system, as we were interested in ascertaining whether it would show a statistically significant difference in grape powdery mildew spore production. The SIGS target, *AATF*, exhibited on average of 53% reduced spore production in *E. necator* when silenced with long dsRNA (Fig. 7a). The average reduction of powdery mildew spore production for SIGS against *CYP51* and *AATF* was greater in *E. necator* compared to *G. orontii* (Fig. 4 and Fig. 7). One notable difference is *G. orontii* has 2 copies each of *CYP51* and *AATF* while *E. necator* has 1 copy of each of these genes. These results indicate we can successfully translate work performed using the *Arabidopsis* powdery mildew system to the grapevine powdery mildew system.

Discussion

We developed a high-throughput assay to silence powdery mildew genes and determine their contribution to disease (Fig. 2). Our success in SIGS of powdery mildew targets is consistent with HIGS working in the powdery mildew, *B. graminis* (Pliego et al., 2013), and genes encoding the required endogenous RNAi machinery being annotated in *G. orontii* MGH1 v4.0 genome. Screening gene targets in *Arabidopsis* powdery mildew is rapid (Fig. 2) and provides insight into genes important for powdery mildews, as about 86% of dicot powdery mildew and 77% of dicot and monocot powdery mildew genes are conserved (Wu et al., 2018). Furthermore, as obligate biotrophs, powdery mildews have few genes relative to other Ascomycota (Wu et al., 2018) making target testing using the *G.orontii-A. thaliana* pathosystem an efficient means of prioritizing targets to test in other powdery mildew-plant host interactions. *A. thaliana* plants have a quick

generation time, can be highly controlled in growth chambers, and require little space for multiple replicates compared to many powdery mildew-impacted crops making this system valuable in quickly identifying novel gene targets.

In this study we also demonstrated SIGS methods and conserved targets in *G. orontii* can translate to the grape powdery mildew *E. necator* and we anticipate they can translate to other powdery mildews. The gene target *AATF* was found to contribute to *G. orontii* spore production (Fig. 4) with an even greater impact on *E. necator* (Fig. 7). *AATF* expression is modulated upon pathogen infection (Benakanakere et al., 2019; Kaul et al., 2009) and in cancer cells (Iezzi and Fanciulli, 2015) to prolong the life of a cell. If the powdery mildew AATF is secreted into the plant, by a yet undefined means, it could potentially prolong plant cell life and inhibit cell death, features of critical import to obligate biotrophy. If it functions in the fungi, it could act to maintain normal cellular function in the presence of plant-induced stress. Other regulators of cell fate should be tested via SIGS to identify additional important targets.

Using SIGS we probed the importance of ten metabolic, regulatory, and effector genes and identified five powdery mildew targets that impact G. orontii MGH1 spore production (Fig. 4, 6). When screening targets, multiple long dsRNAs or siRNAs may need to be tested in order to determine the contribution of a gene. The efficiency of siRNA mediated silencing depends on several factors including the accessibility of target region, structural features of the siRNA leading to efficient loading of antisense strand of siRNA into RISC complex (Reynolds et al., 2004; Ui-Tei et al., 2004). Our preliminary screen also highlights the importance of screening multiple genes involved in a process in an initial screen to increase the likelihood of identifying at least one with a powdery mildew phenotype when screened with an initial dsRNA. For example, 2/3 genes tested involved in storage lipid metabolism exhibited reduced spore production when sprayed with long dsRNA (Fig. 4). By contrast, 3/3 genes involved in glycogen metabolism did not show reductions in powdery mildew proliferation when sprayed with long dsRNA suggesting this process is not as critical to the success of the infection.

Homologs of lipases *lipase a* and *lipase 1* proved to be significant contributors to powdery mildew growth on *A. thaliana*. In the powdery mildew, *Blumeria graminis* f. sp. *hordei*, lipases fall into 3 distinct expression patterns. Group III lipase expression remains constant throughout infection while group I lipase expression is elevated in ungerminated spores and at 4 hpi, decreasing as the infection progresses and group II expression is suppressed in haustoria tissue (Both et al., 2005). Lipid staining of developing powdery mildew spores reflects the activity of class I lipases suggesting lipids are consumed to fuel development before nutrient acquisition from the host begins (Both, et al. 2005). Later in infection these lipases or others can potentially be used for lipid remodeling for triacylglycerol storage in newly formed spores (Laureano et al., 2018), suggesting lipases have various functions and are regulated by development. The early expression of *LIPA* and *LIP1* (Fig. 5) indicates they behave like group I lipases which are presumably required early in development to facilitate mobilization of energy. *Extracellular lipase, LIP1,* in the necrotrophic pathogen *B. cinerea* is induced by exposure to grape cuticle, but *lip1* mutants do not have reduced lesion formation (Subramoni et al., 2010). Similarly, *lip1* mutants of the hemibiotrophic pathogen, *F. graminearum*, does not impact virulence (Subramoni et al., 2010). For a biotrophic pathogen such as powdery mildew, dependent initially on its own spore reserves for early growth and development, it appears that LIPA and LIP1 may play more critical roles.

SIGS against the powdery mildew BCDO-family gene provided the most dramatic reduction in powdery mildew proliferation of the targets tested (Figs. 4, 6). Carotenoid-cleaving enzymes can have diverse functions in plants, fungi, animals, and bacteria (Ahrazem et al., 2016; Tan et al., 2003). In *G. orontii* MGH1, the targeted *BCDO* is further specified as a 9-cis-epoxycarotenoid dioxygenase (EC 1.1.3.11.51) involved in ABA biosynthesis (SI Fig. 2). In addition, another ABA biosynthetic gene encoding xanthoxin dehydrogenase (EC 1.1.1.288) is also annotated as being present in *G. orontii* MGH1 supporting this putative function. Diverse fungi have been described to produce ABA, though this trait appears restricted to plant-associated fungi (Asselbergh et al., 2008). Expression of *A. thaliana* genes in this pathway is modulated in response to powdery mildew infection (Chandran et al., 2010). These changes may promote the formation of violaxanthin from zeaxanthin (upstream of ABA formation) via *NPQ4* which is down-regulated in high-light conditions. Not only is this shift providing precursors for ABA biosynthesis but also provides additional support for the source to sink transition imposed by infection. In the rice-*Magnaporthe oryzae* interaction, exogenous application of ABA promotes germination and fungal ABA biosynthesis mutants have impaired lesion formation on rice (Spence et al., 2015).

Powdery mildews and other fungal pathogens can have hundreds of putative effectors identified through genomics with few having any annotated domains (de Jonge et al., 2011). These effector repertoires expand and contract in fungal pathogens allowing new adaptations to emerge at the host-pathogen interface (Fouché et al., 2018). The effector EC2 is a highly expressed powdery mildew effector (Fig. 5) with a cysteine-rich fungal extracellular membrane (CFEM) domain. CFEM domains have proposed roles in fungal pathogenesis (Kulkarni et al., 2003). Transgenic *A. thaliana* expressing *EC2* have increased entry by non-adapted powdery mildew (Schmidt et al., 2014), demonstrating its contribution to pathogenesis of powdery mildews as well. *EC2* also significantly contributes to *G. orontii* growth and reproduction on *A. thaliana* (Fig. 6). In *G. orontii*, *EC2* is expressed 1-2 orders of magnitude higher than the other genes targeted in this study (Fig. 5). Despite being highly expressed, SIGS against *EC2* still had a significant impact on powdery mildew proliferation. *EC2* is highly expressed by many fungal pathogens suggesting it may represent a broad fungal target for an RNA-based pesticide.

SIGS has the potential to revolutionize agriculture if RNA pesticides prove to be efficacious in controlling pathogen growth. SIGS methods were translated to identify agriculturally important targets to be used for pest management. Using SIGS we can rapidly identify novel targets and adapt RNA constructs to the strain-specific sequences of target genes present in the field. We anticipate these RNA pesticides are more evolutionarily robust to resistance compared to chemical fungicides. Pathogens challenged with RNA pesticides would have to accumulate many mutations in the targeted gene sequence to avoid silencing, while pathogens challenged with azole-fungicides, for example, may only require a mutation in the enzyme binding site to avoid inhibition. If resistance does develop to an RNA pesticide, other dsRNAs targeting other parts of the gene can be developed to effectively silence the same gene or dsRNAs targeting other genes in the same pathway or cellular process can be designed and tested. Additionally, pathogens could downregulate RNAi processes to develop resistance to RNA pesticides, however, silencing RNAi machinery during fungal infection also impairs growth (Werner et al., 2020). Multiple required cellular processes could potentially be targeted at once by multiplexing dsRNAs. Or dsRNAs against multiple genes in a given process or pathway could be multiplexed to further increase

efficacy. Finally, the efficiency of uptake and duration of gene silencing may be improved, for example by encapsulating dsRNAs in liposomes or complexing dsRNAs to clay nanosheets (Cagliari et al., 2019).

The optimization of SIGS in powdery mildews provides a novel and versatile approach to study genetics in the obligate biotroph, powdery mildew. To our knowledge, this is the first report of SIGS in powdery mildew fungi. Using this high-throughput SIGS and disease assay pipeline, we can more rapidly assess the importance of a gene on powdery mildew growth and development, removing the plasmid construction steps required for virus-induced gene silencing (VIGS) and the transformation steps required for HIGS. SIGS provides a rapid methodology to study gene function in powdery mildews which are not culturable apart from the host and not genetically tractable. Given the conservation of retained genes and essential processes in obligate biotrophs (Spanu 2012), targets identified in the powdery mildew-plant host system may translate to other plant (obligate) biotrophs as well as human intracellular pathogens.

Methods

***Arabidopsis* growth and *G. orontii* inoculation**

A. thaliana ecotype Col-0 were grown in growth chambers at 22°C, 70% relative humidity, and a 12 hour photoperiod with photosynthetically active radiation = 150µmol/(m^2 x s). Plants for whole plant assays were grown in 4-inch pots (4 plants per pot). Detached leaf assays plants were grown in plant trays with 16.6 x 12.4 x 5.8-cm insert boxes (12 plants per box). Before infection, leaves were plucked and petiole was inserted into medium with half strength Murashige and Skoog salts and 0.8% agar with Whatman 1.0 sheet placed on top of medium. Two plates with 12 leaves each, were prepared with leaves from the same planting boxes for control and RNA spayed samples. At 4-4.5 weeks plant tissue was inoculated by settling tower (Reuber et al., 1998) with *G. orontii* isolate MGH1 performed at 2:30 pm +/- 1.5 hrs. The control and RNA sprayed samples were inoculated in the same tower to ensure equal inoculation for each replicate. For spore counting assays, plants were inoculated with a heavy dose (conidia from 4-5 fully infected leaves at 10-14 dpi). For microscopic analysis, plants were inoculated with a low to moderate dose (conidia from 1-2 half covered leaves).

Grape growing and *E. necator* maintenance and inoculations

The grape powdery mildew *E. necator* isolate c was regularly maintained on detached leaves of Chardonnay and Carignan grapevine varieties. The hard cuttings of grapevine varieties were received from Foundation Plant Services, UC Davis, CA and were grown at the UC Berkeley Oxford Tract Greenhouse facility. The cuttings were rooted on a mist bench and then transferred to 2-gallon pots with supersoil and fertilized with Osmocote. Grapevine plants are sprayed with sulfur every week to keep them mildew free. For *E. necator* isolate maintenance and for grapevine leaf disc assays, the 3rd or 4th node leaf was collected, sterilized with 50% bleach for 30 seconds, washed with sterile water 3 to 4 times, and then placed on 1% agar medium. For maintenance, chains of conidia were transferred to sterile leaves under the microscope in a laminar hood, every 12 to 14 days. For grapevine leaf disc assays, 12-15 10 mm leaf discs were cut from sterile leaves and placed on Whatman sheet 1.0 over 1% agar plates. The leaf discs were inoculated with a heavy dose by settling tower (Reuber et al., 1998). For whole plant grapevine assays, 4 month old potted Chardonnay grapevine plant were used. Three leaves from the 3rd or 4th node on each plant were sprayed with approximately 60,000 spores/mL. For each treatment 3 to 5 plants were used.

RNA fluorescence labeling and uptake

Fluorescein-labeled 300 base long β-actin-Mouse was synthesized using MAXIscript T7 Transcription Kit (AM1312, Invitrogen by Fisher Scientific, Waltham, Massachusetts) and Fluorescein RNA Labeling Mix (11685619910, Roche, Basel, Switzerland). To induce germination, spores were tapped onto a glass slide, placed in a petri dish containing water, covered in foil for 1 hour, then unwrapped and left overnight in ambient light. Spores were then blotted onto a 1% agar pad on a glass slide before 20 µL water or water plus Fluorescein-labeled RNA (800 ng) was spotted onto spores. Spores were incubated with RNA for 1.5 hours before imaging with a Zeiss Axio Imager fluorescence microscope. For RNase treated samples, 1 µL each of Benzoase Nuclease and RNase A was added 30 minutes before microscopy.

RNA-Sequencing

For RNA-Seq analysis, RNA was prepared from 4 week old *A. thaliana* Col-0 plants heavily infected with 14 day old *G. orontii* spores through settling tower (Reuber et al., 1998) and three leaves were harvested for each time point at 6 hpi, 12 hpi, 24 hpi, 3 dpi and 5 dpi. RNA was extracted using Qiagen RNeasy Plant Mini Kit (#74903/74904, Qiagen, Hilden, Germany). Briefly, leaf samples were grinded using two 3 mm stainless steel balls for 1 min at 25 hertz/s and were immediately frozen in liquid nitrogen. RNA was isolated following directions from manufacturer's protocol and the on-column DNase digestion was performed using Qiagen RNase-Free DNase Set (#79254, Qiagen, Hilden, Germany). Samples were submitted to the DOE Joint Genome Institute as part of JGI CSP #1657. Stranded RNA-Seq library(s) were created and quantified by qPCR. Sequencing was performed using Illumina HiSeq-2500 1TB 2x151. Raw fastq file reads were filtered and trimmed using the JGI QC pipeline resulting in the filtered fastq file. Quality trimming was performed using the phred trimming method set at Q6. Finally, following trimming, reads under the length threshold were removed with a minimum length 25 bases or one-third of the original read length, whichever is longer. Filtered reads from each library were aligned to the reference genome using HISAT2 version 2.1.0 [2] (BAMs/ directory) and FPKM normalized gene counts were calculated.

RNA design and spray

pssRNAit (https://plantgrn.noble.org/pssRNAit/) was used to identify efficient siRNAs and dsRNAs and limit off-target gene silencing in the host *A. thaliana* or *V. vinifera.* Genes in *G. orontii* MGH1 (https://mycocosm.jgi.doe.gov/Golor4/Golor4.home.html4.0) and *E. necator* c (https://mycocosm.jgi.doe.gov/Erynec1/Erynec1.home.html) were identified in MycoCosm (Grigoriev et al., 2014). Template for *in vitro* transcriptions was amplified from powdery mildew infected tissue cDNA using Phusion polymerase (M0530S/L, New England Biolabs, Ipswich, Massachusetts) and the T7 promoter (5'- TAATACGACTCACTATAGGGGG-3') was added to both ends. dsRNA was generated using the HiScribe T7 High Yield RNA Synthesis Kit (E2040S, New England Biolabs, Ipswich, Massachusetts), purified using the Monarch RNA Cleanup Kit (T2050S/L, New England Biolabs, Ipswich, Massachusetts), reannealed by heating to 94°C and slowly cooling to room temperature over 50 minutes, and quantified by nanodrop (dsRNA A_{260} x 46.7ng/µL). 21 bp siRNAs were synthesized by Horizon Discovery (Lafayette, Colorado) and prepared as directed. In all cases, plant samples were infected with powdery mildew, then sprayed with RNA dissolved in nuclease-free water or nuclease-free water.

Staining, microscopy and hyphal length measurements

Infected leaves or leaf discs were fixed, cleared in 3:1 (v/v) ethanol:acetic acid, and stained with calcofluor (CF) to visualize and quantify fungal growth. A CF stock solution of 3 mg/mL (F3543, Sigma-Aldrich, St. Louis, Missouri) was prepared. The working solution of 6 µg/mL CF was prepared in 50% glycerol. Leaves were cleared in 1:3 acetic acid/ethanol for 1-2 days and either stored in 70% ethanol for later use or immediately stained with CF. Cleared leaves were washed with water for 5 minutes, stained with 6 µg/mL CF solution for 15 min, rinsed with water for 10 minutes, and mounted on slides in 50% glycerol. Fungal colonies were imaged at 10X using a Zeiss Axio Imager fluorescence microscope, Qimaging QiClick and Micropublisher cameras, and Sutter Instruments Lambda LS Light Source using a DAPI Long Pass filter set. Hyphal lengths were measured using the image analysis software Fiji: ImageJ:https://imagej.net/Fiji/Downloads.

Spore quantification

Spore counting was performed to assess fungal spore production as described by (Weßling and Panstruga, 2012) summarized here with the following modifications. For *A. thaliana* experiments, 12-15 leaves were harvested per condition at 8-10 dpi. For grapevine leaf disc assays, 12-15 leaf discs were collected at 14-21 dpi. Tissue was vortexed in 15 mL 0.01% Tween-80 then filtered through 40 µm mesh before centrifugation. Spore pellets were resuspended to 200 µL to 1,200 µL depending on spore yield. For each sample, nine 1 x 1 mm^2 fields of a Neubauer-improved hemocytometer were counted and normalized to the weight of the plant tissue to determine spore concentration. The average spore count was normalized to the control for each replicate. An unpaired, two-tailed Student's T-test was used to compare control and normalized RNA sprayed spore counts with $n \geq 3$ and $p \leq 0.05$ indicating statistical significance. For grapevine whole plant assays, 3 infected leaves were collected at approximately 16 dpi. Each leaf was vortexed in 15 mL 0.01% Tween-80 as above. Suspensions from the 3 leaves were filtered and combined before centrifugation.

Author Contributions

A.G.M., J.T., and M.C.W. planned and designed the research, analyzed and interpreted the data, and wrote the manuscript. A.G.M. and J.T. conducted the laboratory work.

References

Agrios, G., 2004. Plant Pathology, 5th ed. Elsevier Inc.

Ahrazem, O., Gómez-Gómez, L., Rodrigo, M.J., Avalos, J., Limón, M.C., 2016. Carotenoid cleavage oxygenases from microbes and photosynthetic organisms: Features and functions. International Journal of Molecular Sciences 17. https://doi.org/10.3390/ijms17111781

Aked, J., Hall, J.L., 1993. Effect of powdery mildew infection on concentrations of apoplastic sugars in pea leaves. New Phytologist 123, 283–288. https://doi.org/10.1111/j.1469-8137.1993.tb03737.x

Asselbergh, B., de Vleesschauwer, D., Höfte, M., 2008. Global switches and fine-tuning-ABA modulates plant pathogen defense. Molecular Plant-Microbe Interactions 21, 709–719. https://doi.org/10.1094/MPMI-21-6-0709

Benakanakere, M.R., Zhao, J., Finoti, L., Schattner, R., Odabas-Yigit, M., Kinane, D.F., 2019. MicroRNA-663 antagonizes apoptosis antagonizing transcription factor to induce apoptosis in epithelial cells. Apoptosis 24, 108–118. https://doi.org/10.1007/s10495-018-01513-9

Bilir, Ö., Telli, O., Norman, C., Budak, H., Hong, Y., Tör, M., 2019. Small RNA inhibits infection by downy mildew pathogen Hyaloperonospora arabidopsidis. Molecular Plant Pathology 20, 1523–1534. https://doi.org/10.1111/mpp.12863

Both, M., Csukai, M., Stumpf, M.P.H., Spanu, P.D., 2005. Gene Expression Profiles of Blumeria graminis Indicate Dynamic Changes to Primary Metabolism during Development of an Obligate Biotrophic Pathogen 17, 2107–2122. https://doi.org/10.1105/tpc.105.032631.1

Bramlett, M., Plaetinck, G., Maienfisch, P., 2020. RNA-Based Biocontrols—A New Paradigm in Crop Protection. Engineering 6, 522–527. https://doi.org/10.1016/j.eng.2019.09.008

Braun, B., Pfirrmann, T., Menssen, R., Hofmann, K., Scheel, H., Wolf, D.H., 2011. Gid9, a second RING finger protein contributes to the ubiquitin ligase activity of the Gid complex required for catabolite degradation. FEBS Letters 585, 3856–3861. https://doi.org/10.1016/j.febslet.2011.10.038

Cagliari, D., Dias, N.P., Galdeano, D.M., dos Santos, E.Á., Smagghe, G., Zotti, M.J., 2019. Management of Pest Insects and Plant Diseases by Non-Transformative RNAi. Frontiers in Plant Science 10. https://doi.org/10.3389/fpls.2019.01319

Calvert, G.M., Karnik, J., Mehler, L., Beckman, J., Morrissey, B., Sievert, J., Barrett, R., Lackovic, M., Mabee, L., Schwartz, A., Mitchell, Y., Moraga-McHaley, S., 2008. Acute pesticide poisoning among agricultural workers in the United States, 1998-2005. American Journal of Industrial Medicine 51, 883–898. https://doi.org/10.1002/ajim.20623

Chandran, D., Inada, N., Hather, G., Kleindt, C.K., Wildermuth, M.C., 2010. Laser microdissection of Arabidopsis cells at the powdery mildew infection site reveals site-specific processes and regulators. Proceedings of the National Academy of Sciences of the United States of America 107, 460–465. https://doi.org/10.1073/pnas.0912492107

de Jonge, R., Bolton, M.D., Thomma, B.P.H.J., 2011. How filamentous pathogens co-opt plants: The ins and outs of fungal effectors. Current Opinion in Plant Biology 14, 400–406. https://doi.org/10.1016/j.pbi.2011.03.005

Fouché, S., Plissonneau, C., Croll, D., 2018. The birth and death of effectors in rapidly evolving filamentous pathogen genomes. Current Opinion in Microbiology 46, 34–42. https://doi.org/10.1016/j.mib.2018.01.020

Frenkel, O., Cadle-Davidson, L., Wilcox, W.F., Milgroom, M.G., 2015. Mechanisms of resistance to an azole fungicide in the grapevine powdery mildew fungus, Erysiphe necator. Phytopathology 105, 370–377. https://doi.org/10.1094/PHYTO-07-14-0202-R

Fuller, K.B., Alston, J.M., Sambucci, O.S., 2014. The value of powdery mildew resistance in grapes: Evidence from California. Wine Economics and Policy 3, 90–107. https://doi.org/10.1016/j.wep.2014.09.001

Grigoriev, I. v., Nikitin, R., Haridas, S., Kuo, A., Ohm, R., Otillar, R., Riley, R., Salamov, A., Zhao, X., Korzeniewski, F., Smirnova, T., Nordberg, H., Dubchak, I., Shabalov, I., 2014. MycoCosm portal: Gearing up for 1000 fungal genomes. Nucleic Acids Research 42, 699–704. https://doi.org/10.1093/nar/gkt1183

Hu, D., Chen, Z.Y., Zhang, C., Ganiger, M., 2020. Reduction of Phakopsora pachyrhizi infection on soybean through host- and spray-induced gene silencing. Molecular Plant Pathology 21, 794–807. https://doi.org/10.1111/mpp.12931

Iezzi, S., Fanciulli, M., 2015. Discovering Che-1/AATF: A new attractive target for cancer therapy. Frontiers in Genetics 6, 1–7. https://doi.org/10.3389/fgene.2015.00141

Jones, L., Riaz, S., Morales-Cruz, A., Amrine, K.C., McGuire, B., Gubler, W., Walker, M., Cantu, D., 2014. Adaptive genomic structural variation in the grape powdery mildew pathogen, Erysiphe necator. BMC Genomics 15, 1081. https://doi.org/10.1186/1471-2164-15-1081

Kaul, D., Ahlawat, A., Gupta, S.D., 2009. HIV-1 genome-encoded hiv1-mir-H1 impairs cellular responses to infection. Molecular and Cellular Biochemistry 323, 143–148. https://doi.org/10.1007/s11010-008-9973-4

Koch, A., Biedenkopf, D., Furch, A., Weber, L., Rossbach, O., Abdellatef, E., Linicus, L., Johannsmeier, J., Jelonek, L., Goesmann, A., Cardoza, V., McMillan, J., Mentzel, T., Kogel, K.H., 2016. An RNAi-Based Control of Fusarium graminearum Infections Through Spraying of Long dsRNAs Involves a Plant Passage and Is Controlled by the Fungal Silencing Machinery. PLoS Pathogens 12, 1–22. https://doi.org/10.1371/journal.ppat.1005901

Kulkarni, R.D., Kelkar, H.S., Dean, R.A., 2003. An eight-cysteine-containing CFEM domain unique to a group of fungal membrane proteins. Trends in Biochemical Sciences 28, 118–121. https://doi.org/10.1016/S0968-0004(03)00025-2

Laureano, G., Figueiredo, J., Cavaco, A.R., Duarte, B., Caçador, I., Malhó, R., Sousa Silva, M., Matos, A.R., Figueiredo, A., 2018. The interplay between membrane lipids and phospholipase A family members in grapevine resistance against Plasmopara viticola. Scientific Reports 8, 1–15. https://doi.org/10.1038/s41598-018-32559-z

Lievens, L., Pollier, J., Goossens, A., Beyaert, R., Staal, J., 2017. Abscisic acid as pathogen effector and immune regulator. Frontiers in Plant Science 8, 1–15. https://doi.org/10.3389/fpls.2017.00587

Machado, A.K., Brown, N.A., Urban, M., Kanyuka, K., Hammond-Kosack, K.E., 2018. RNAi as an emerging approach to control Fusarium head blight disease and mycotoxin contamination in cereals. Pest Management Science 74, 790–799. https://doi.org/10.1002/ps.4748

Majumdar, R., Rajasekaran, K., Cary, J.W., 2017. RNA interference (RNAi) as a potential tool for control of mycotoxin contamination in crop plants: Concepts and considerations. Frontiers in Plant Science 8. https://doi.org/10.3389/fpls.2017.00200

Martínez-Cruz, J., Romero, D., de Vicente, A., Pérez-García, A., 2018. Transformation by growth onto agro-infiltrated tissues (TGAT), a simple and efficient alternative for transient transformation of the cucurbit powdery mildew pathogen Podosphaera xanthii. Molecular Plant Pathology 19, 2502–2515. https://doi.org/10.1111/mpp.12722

Mittal, V., 2004. Improving the efficiency of RNA interference in mammals. Nature Reviews Genetics 5, 355–365. https://doi.org/10.1038/nrg1323

Pirkov, I., Norbeck, J., Gustafsson, L., Albers, E., 2008. A complete inventory of all enzymes in the eukaryotic methionine salvage pathway. FEBS Journal 275, 4111–4120. https://doi.org/10.1111/j.1742-4658.2008.06552.x

Pliego, C., Nowara, D., Bonciani, G., Gheorghe, D.M., Xu, R., Surana, P., Whigham, E., Nettleton, D., Bogdanove, A.J., Wise, R.P., Schweizer, P., Bindschedler, L. v., Spanu, P.D., 2013. Host-induced gene silencing in barley powdery mildew reveals a class of ribonuclease-like effectors. Molecular Plant-Microbe Interactions 26, 633–642. https://doi.org/10.1094/MPMI-01-13-0005-R

Raanan, R., Gunier, R.B., Balmes, J.R., Beltran, A.J., Harley, K.G., Bradman, A., Eskenazi, B., 2017. Elemental sulfur use and associations with pediatric lung function and respiratory

symptoms in an agricultural community (California, USA). Environmental Health Perspectives 125, 1–8. https://doi.org/10.1289/EHP528

Ramanujam, R., Calvert, M.E., Selvaraj, P., Naqvi, N.I., 2013. The Late Endosomal HOPS Complex Anchors Active G-Protein Signaling Essential for Pathogenesis in Magnaporthe oryzae. PLoS Pathogens 9. https://doi.org/10.1371/journal.ppat.1003527

Regelmann, J., Schüle, T., Josupeit, F.S., Horak, J., Rose, M., Entian, K.-D., Thumm, M., Wolf, D.H., 2003. Catabolite Degradation of Fructose-1,6-bisphosphatase in the Yeast Saccharomyces cerevisiae : A Genome-wide Screen Identifies Eight Novel GID Genes and Indicates the Existence of Two Degradation Pathways. Molecular Biology of the Cell 14, 1652–1663. https://doi.org/10.1091/mbc.e02-08-0456

Reuber, T.L., Plotnikova, J.M., Dewdney, J., Rogers, E.E., William Wood, B., Ausubel, F.M., 1998. Correlation of defense gene induction defects with powdery mildew susceptibility in Arabidopsis enhanced disease susceptibility mutants. Plant Journal 16, 473–485. https://doi.org/10.1046/j.1365-313X.1998.00319.x

Reynolds, A., Leake, D., Boese, Q., Scaringe, S., Marshall, W.S., Khvorova, A., 2004. Rational siRNA design for RNA interference. Nature Biotechnology 22, 326–330. https://doi.org/10.1038/nbt936

Schmidt, S.M., Kuhn, H., Micali, C., Liller, C., Kwaaitaal, M., Panstruga, R., 2014. Interaction of a Blumeria graminis f. sp. hordei effector candidate with a barley ARF-GAP suggests that host vesicle trafficking is a fungal pathogenicity target. Molecular Plant Pathology 15, 535– 549. https://doi.org/10.1111/mpp.12110

Spence, C.A., Lakshmanan, V., Donofrio, N., Bais, H.P., 2015. Crucial roles of abscisic acid biogenesis in virulence of rice blast fungus Magnaporthe oryzae. Frontiers in Plant Science 6, 1–13. https://doi.org/10.3389/fpls.2015.01082

Subramoni, S., Suárez-Moreno, Z.R., Venturi, V., 2010. Lipases as Pathogenicity Factors of Plant Pathogens, in: Handbook of Hydrocarbon and Lipid Microbiology. Springer Berlin Heidelberg, Berlin, Heidelberg, pp. 3269–3277. https://doi.org/10.1007/978-3-540-77587-4_248

Tan, B.C., Joseph, L.M., Deng, W.T., Liu, L., Li, Q.B., Cline, K., McCarty, D.R., 2003. Molecular characterization of the Arabidopsis 9-cis epoxycarotenoid dioxygenase gene family. Plant Journal 35, 44–56. https://doi.org/10.1046/j.1365-313X.2003.01786.x

Ui-Tei, K., Naito, Y., Takahashi, F., Haraguchi, T., Ohki-Hamazaki, H., Juni, A., Ueda, R., Saigo, K., 2004. Guidelines for the selection of highly effective siRNA sequences for mammalian and chick RNA interference. Nucleic Acids Research 32, 936–948. https://doi.org/10.1093/nar/gkh247

Wang, M., Weiberg, A., Lin, F.M., Thomma, B.P.H.J., Huang, H. da, Jin, H., 2016. Bidirectional cross-kingdom RNAi and fungal uptake of external RNAs confer plant protection. Nature Plants 2, 1–10. https://doi.org/10.1038/nplants.2016.151

Werner, B.T., Gaffar, F.Y., Schuemann, J., Biedenkopf, D., Koch, A.M., 2020. RNA-Spray-Mediated Silencing of Fusarium graminearum AGO and DCL Genes Improve Barley Disease Resistance. Frontiers in Plant Science 11, 1–11. https://doi.org/10.3389/fpls.2020.00476

Weßling, R., Panstruga, R., 2012. Rapid quantification of plant-powdery mildew interactions by qPCR and conidiospore counts. Plant Methods 8, 35. https://doi.org/10.1186/1746-4811-8- 35

Wu, W., Hodges, E., Redelius, J., Höög, C., 2004. A novel approach for evaluating the efficiency of siRNAs on protein levels in cultured cells. Nucleic acids research 32, 1–6. https://doi.org/10.1093/nar/gnh010

Wu, Y., Ma, X., Pan, Z., Kale, S.D., Song, Y., King, H., Zhang, Q., Presley, C., Deng, X., Wei, C.I., Xiao, S., 2018. Comparative genome analyses reveal sequence features reflecting distinct modes of host-adaptation between dicot and monocot powdery mildew 06 Biological Sciences 0604 Genetics. BMC Genomics 19, 1–20. https://doi.org/10.1186/s12864-018-5069-z

Xiong, F., Liu, M., Zhuo, F., Yin, H., Deng, K., Feng, S., Liu, Y., Luo, X., Feng, L., Zhang, S., Li, Z., Ren, M., 2019. Host-induced gene silencing of BcTOR in Botrytis cinerea enhances plant resistance to grey mould. Molecular Plant Pathology 20, 1722–1739. https://doi.org/10.1111/mpp.12873

Zhu, X., Qi, T., Yang, Q., He, F., Tan, C., Ma, W., Voegele, R.T., Kang, Z., Guo, J., 2017. Host-induced gene silencing of the MAPKK gene PsFUZ7 confers stable resistance to wheat stripe rust. Plant Physiology 175, 1853–1863. https://doi.org/10.1104/pp.17.01223

Zubrod, J.P., Baudy, P., Schulz, R., Bundschuh, M., 2014. Effects of current-use fungicides and their mixtures on the feeding and survival of the key shredder Gammarus fossarum. Aquatic Toxicology 150, 133–143. https://doi.org/10.1016/j.aquatox.2014.03.00

Table 1. Gene information for *G. orontii* MGH1 targets selected for spray-induced silencing. [1]*G. orontii* MGH1 (v4.0) genome annotated and accessed through MycoCosm (Grigoriev et al., 2014), [2](Koch et al., 2016), [3](Both et al., 2005), [4](Lievens et al., 2017), [5](Chandran et al., 2010), [6](Pirkov et al., 2008), [7](Braun et al., 2011), [8](Regelmann et al., 2003), [9](Aked and Hall, 1993), [10](Iezzi and Fanciulli, 2015) [11](Benakanakere et al., 2019), [12](Kaul et al., 2009), [13](Schmidt et al., 2014).

Gene Category	Putative Gene Symbol	Putative Gene Name	Copy Number[1]	Annotated Domains[1]	Rationale
Metabolic	*CYP51*	*cytochrome P450 51*	2	cytochrome P450	Encodes the azole-fungicide target, sterol 14α-demethylase. It is critical for ergosterol synthesis which is required for fungal cell membranes. *Fusarium graminearum* infection of barley is reduced by spray-induced gene silencing of *CYP51*.[2]
	GDB1	*glycogen debranching enzyme*	2	amylo-alpha-1,6-glucosidase, glycogen debranching enzyme (glucanotransferase domain), N-terminal and central domain from the human glycogen debranching enzyme	Glycogen is broken down in germinating and developing powdery mildew conidia.[3] It is thought to fuel development from germination to penetration. Glycogen breakdown can be visualized with Lugol staining, showing reduced glycogen content in germinated spores.[3]
	GPH1	*glycogen phosphorylase*	2	carbohydrate phosphorylase	
	LIP1	*lipase 1*	2	carboxylesterase family	Lipid droplets are components of powdery mildew conidia that are consumed and mobilized during germination of powdery mildew conidia.[3]
	LIPA	*lipase A*	2	lipase (class 3)	
	DGAT	*diglyceride acyltransferase*	2	MBOAT (membrane-bound O-acyltransferase family)	
	BCDO	*β-carotene 15,15' -dioxygenase*	1	retinal pigment epithelial membrane protein (carotenoid oxygenase)	Abscisic acid (ABA) promotes biotic fungal interactions with plants and decreases plant immunity. Many pathogens are known to produce or modulate ABA biosynthesis in host plants.[4] *G. orontii* may require host ABA precursor as most genes are lost in carotenoid biosynthesis.[1] *A. thaliana* ABA biosynthetic gene expression is modulated at the powdery mildew infection site.[5]
	UTR4	*unidentified transcript 4*	2	haloacid dehalogenase-like hydrolase	*UTR4* is a 2,3-dioxomethiopentane- 1-phosphate enolase /phosphatase involved in the methionine salvage pathway which allows cells to regenerate methionine and reuse sulfur. Saccharomyces cerevisiae *utr4* mutants grow poorly on media lacking methionine and have a significantly lower growth rate.[6]

Regulatory	*GID9*	*glucose-induced degradation 9*	2	LisH, CTLH/CRA C-terminal to LisH motif domain	Involved in proteasome-dependent catabolite inactivation of gluconeogenic enzymes fructose-1,6-bisphosphatase, phosphoenolpyruvate carboxykinase, and cytoplasmic malate dehydrogenase.[7,8] Glucose and sucrose concentrations are enhanced in powdery mildew infected leaf apoplast.[9]
	AATF/ Che-1	*apoptosis-antagonizing transcription factor*	2	apoptosis-antagonizing transcription factor (C-terminal), apoptosis antagonizing transcription factor	Required for proliferation in mammalian systems and involved in many cellular processes including cell stress response and cell cycle control.[10] Pathogens manipulate the expression of AATF.[11,12]
Effector	*EC2*	*effector candidate 2*	2	CFEM domain	Transgenic *A. thaliana* expressing *EC2* have increased entry by non-adapted powdery mildew.[13] *EC2* is among the most highly expressed genes in *G. orontii* MGH1 and is widely conserved in powdery mildews[1].

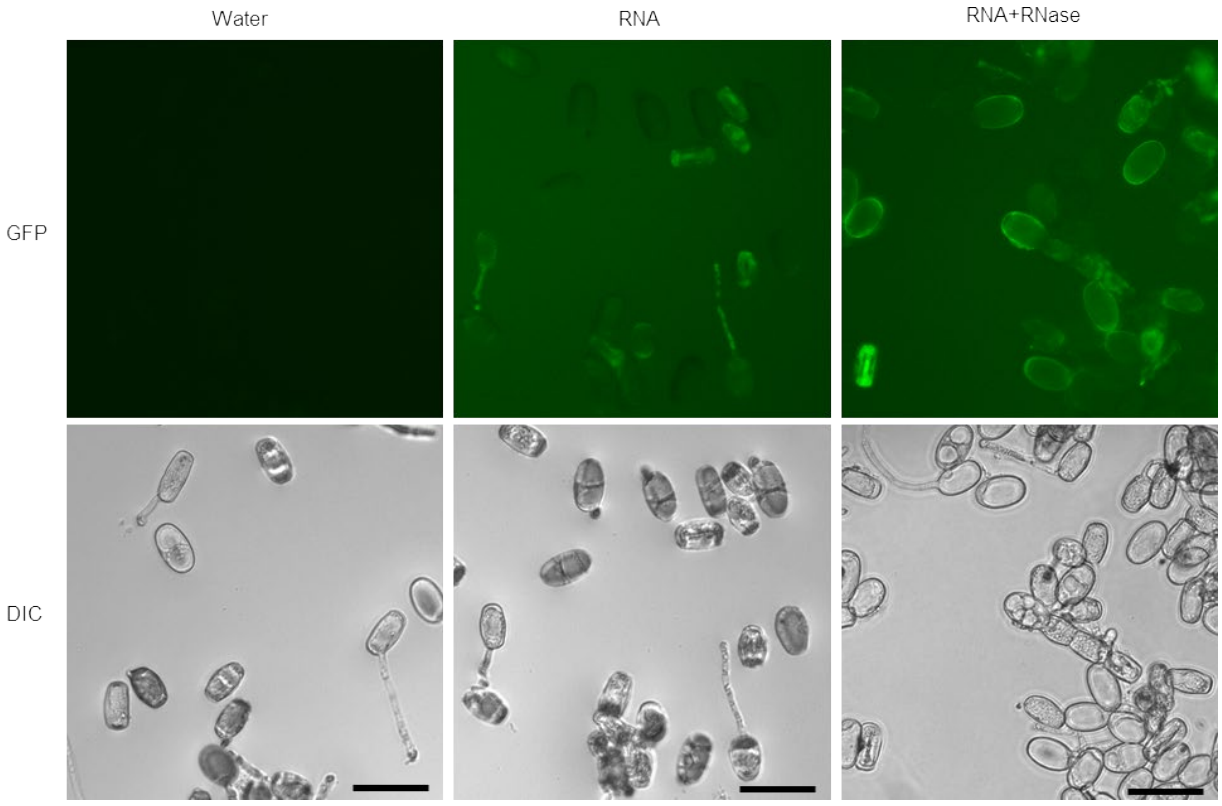

Fig. 1. *G. orontii* MGH1 uptakes extracellular RNA. Germinated spores were blotted onto a 1% agar pad and incubated with RNA containing fluorescein-conjugated UTPs or water for 90 minutes. 30 min. before imaging RNases were added. Images taken with Zeiss Axio Imager using the 20X objective. DIC = Differential Interference Contrast. GFP = Green Fluorescent Protein Filter Set. Scale bar = 50 μm.

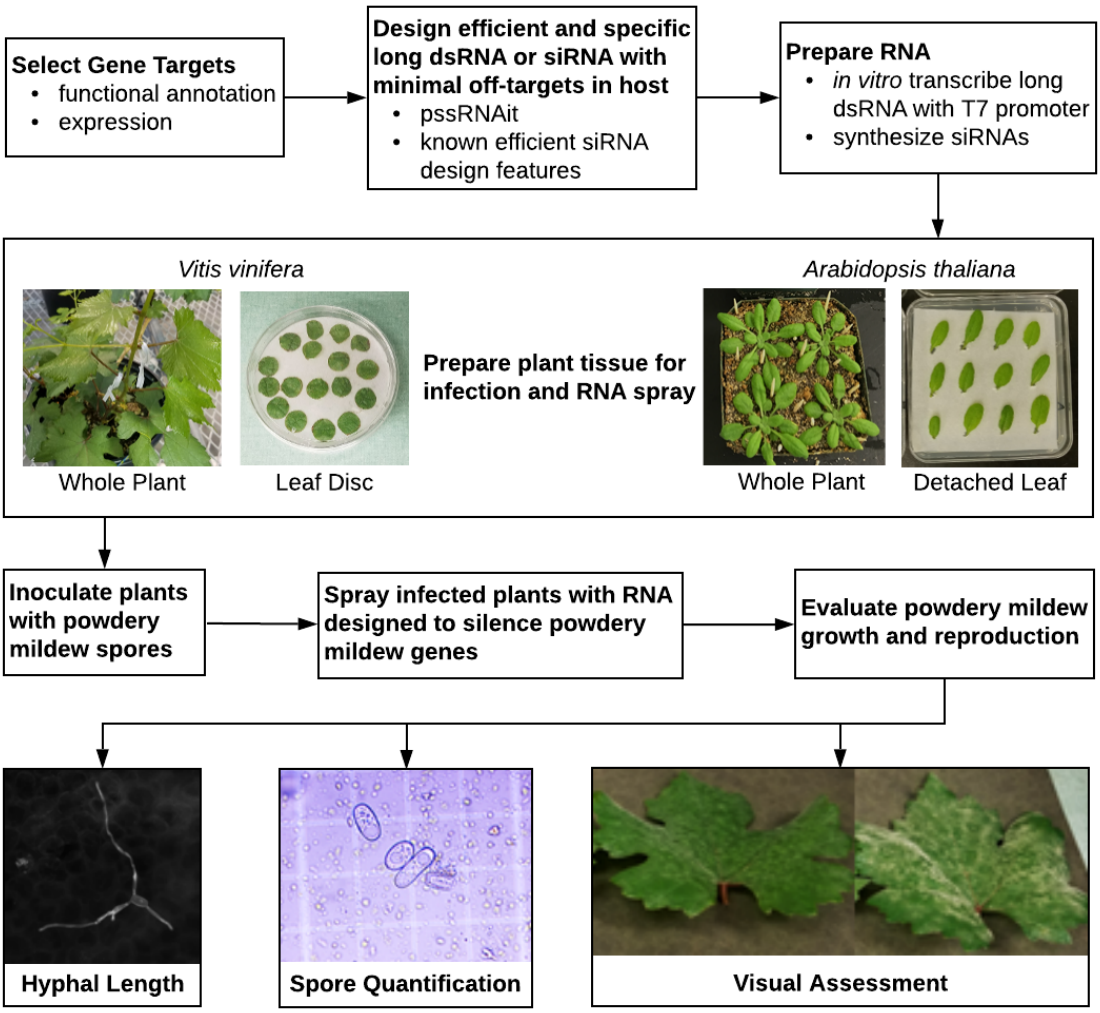

Fig. 2. Overview of spray-induced gene silencing methodology. The flowchart outlines target gene selection, siRNA and long dsRNA design, spray-induced gene silencing protocol, and methods used to identify powdery mildew infection phenotypes.

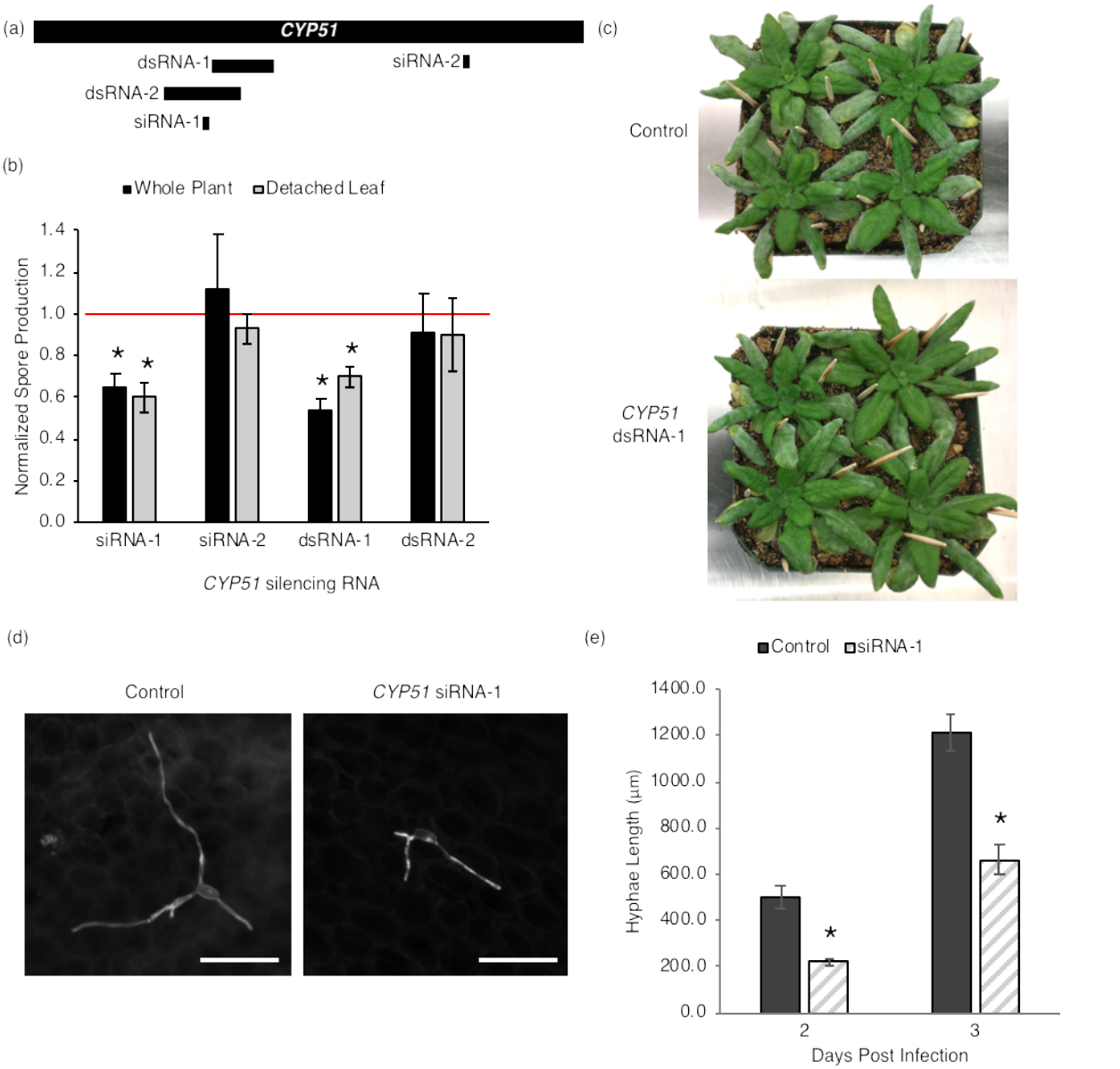

Fig. 3. siRNA and long dsRNA targeting *CYP51* reduces spore production and hyphal length. (a) Diagram of *CYP51* and targeting RNAs. *CYP51* (Protein IDs: 2912305 and 2918117) is 1578 bp. (b) Average normalized spore production displayed from n ≥ 3. Spore suspension concentrations were normalized to the input tissue weight (g) before being normalized to the control. Error bars± SEM. *p<0.05 by Student's T-Test (unpaired, 2-sided) compared to control. (c) Less powdery mildew coverage and density observed on *CYP51* dsRNA-1 sprayed *A. thaliana* plants. Image taken 9 days post infection. (d) *G. orontii* MGH1 hyphal length is reduced by siRNAs targeting *CYP51* on *A. thaliana*. Calcofluor-stained *G. orontii* imaged with a Zeiss Axio Imager using a 10X objective and DAPI long pass filter set. Scale bar is 100 µm. (e) Average total hyphal length of colonies at 2 and 3 dpi from detached leaf experiments using 1% agar plates. Error bars ± SEM. *p<0.05 by Student's T-Test (unpaired, 2-sided) compared to control. Similar results observed in an independent experiment.

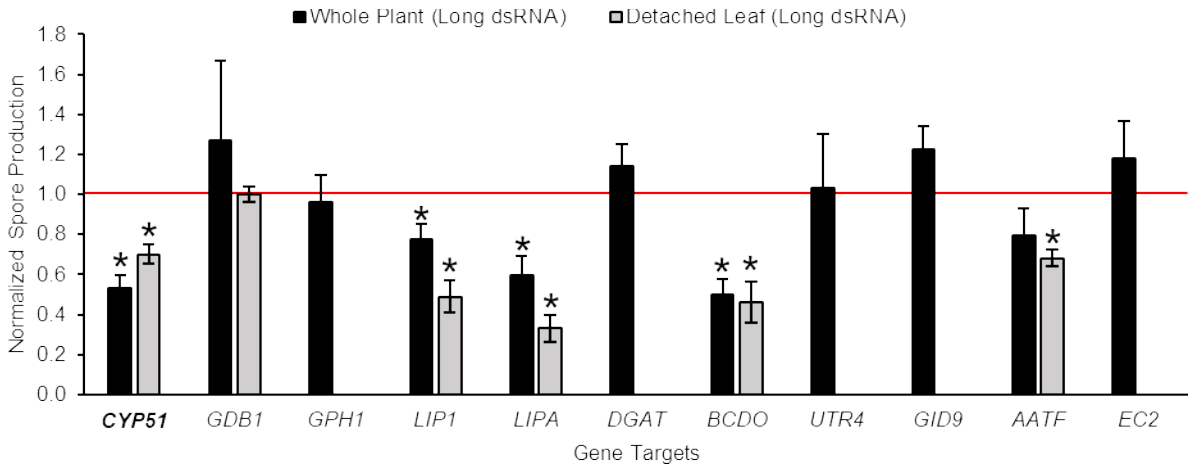

Fig. 4. *G. orontii* MGH1 spore production is impacted by long dsRNA targeting metabolic, regulatory, and effector genes on *A. thaliana* whole plant and detached leaf assays. Average normalized spore production displayed from n ≥ 3. Spore suspension concentrations were normalized to the input tissue weight (g) before being normalized to the control. Error bars ± SEM. *p<0.05 by Student's T-Test (unpaired, 2-sided) compared to control.

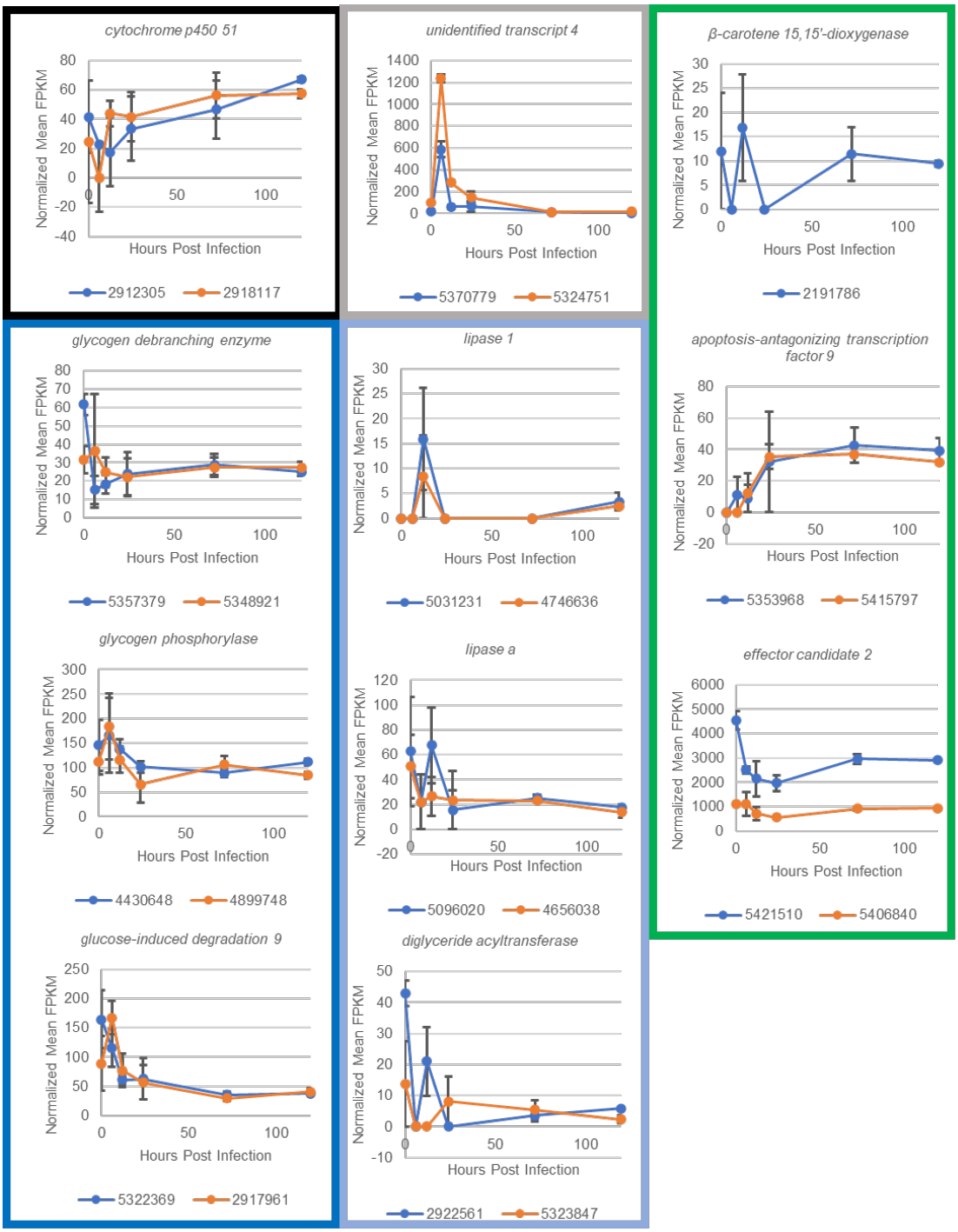

Fig. 5. *G. orontii* MGH1 gene expression for spray-induced gene silencing targets at 0, 6, 12, 24, 72, and 120 hours post infection. Mean normalized FPKM (fragments per kilobase of exon per million reads) with n=3 is displayed for each gene +/- SE. Golor4 annotated genome can be accessed through MycoCosm (Grigoriev et al., 2014). Black and gray box denote central metabolic functions (cell membrane biosynthesis, methionine salvage pathway). Genes involved in glycogen metabolism are in blue box. Light blue box encloses genes involved in storage lipid metabolism. Green box includes genes expected to be involved in fungal manipulation of plant processes or response to plant-induced stress.

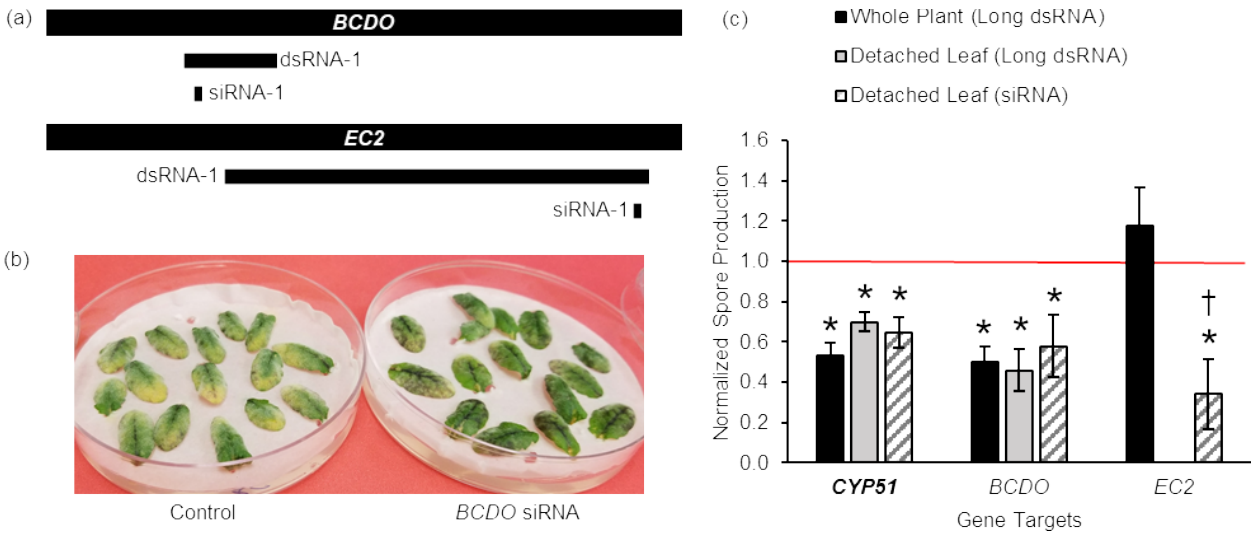

Fig. 6. *G. orontii* MGH1 spore production is reduced by siRNAs targeting *EC2* and *BCDO* on *A. thaliana*. (a) Diagram of siRNAs and long dsRNAs targeting *BCDO* and EC2. Total transcript length for BCDO and EC2 are 1869 and 420 respectively. (b) Detached leaves sprayed with BCDO siRNA have reduced powdery mildew and less chlorosis than the control at 8 days post infection. (c) Average normalized spore production displayed from $n \geq 3$. Spore suspension concentrations were normalized to the input tissue weight(g) before being normalized to the control. Error bars ± SEM. *$p<0.05$ by Student's T-Test (unpaired, 2-sided) compared to control. † n=2, each experiment $p<0.00005$.

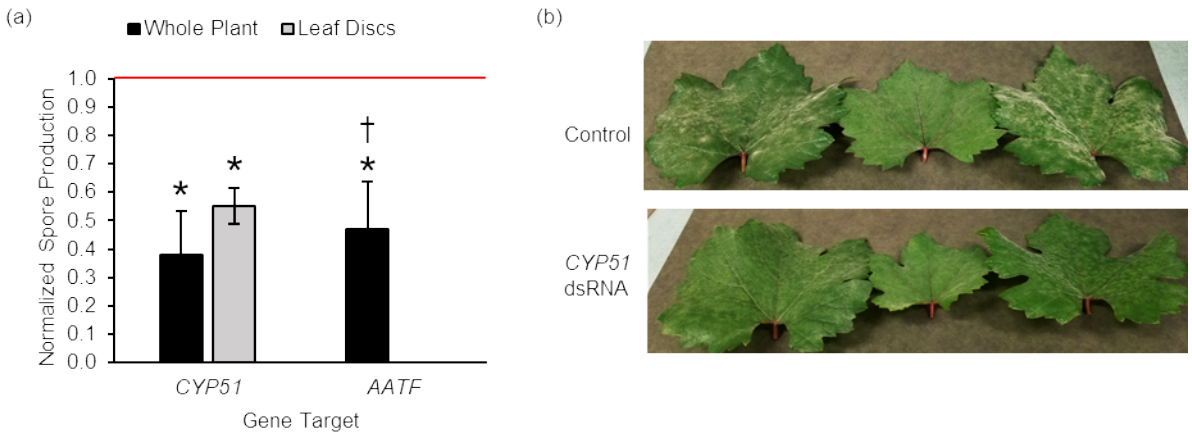

Fig. 7. Long dsRNA targeting genes in *E. necator* reduces spore production on *V. vinifera*. (a) Average normalized spore production displayed from n ≥ 3. Spore suspension concentrations were normalized to the input tissue weight (g) before being normalized to the control. Error bars ± SEM. *p<0.05 by Student's T-Test (unpaired, 2-sided) compared to control. † n=2, each experiment p<0.05. (b) Less powdery mildew density observed on *CYP51* long dsRNA sprayed *V. vinifera* 9 days post infection.

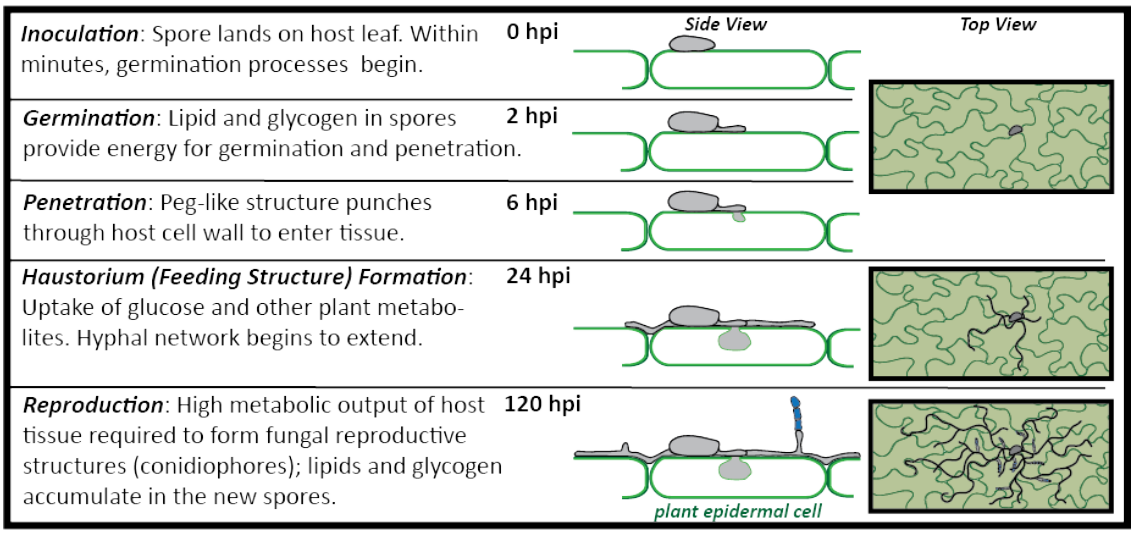

SI Fig. 1. *G. orontii* developmental timeline. Modified from Both et al., 2005.

(a)

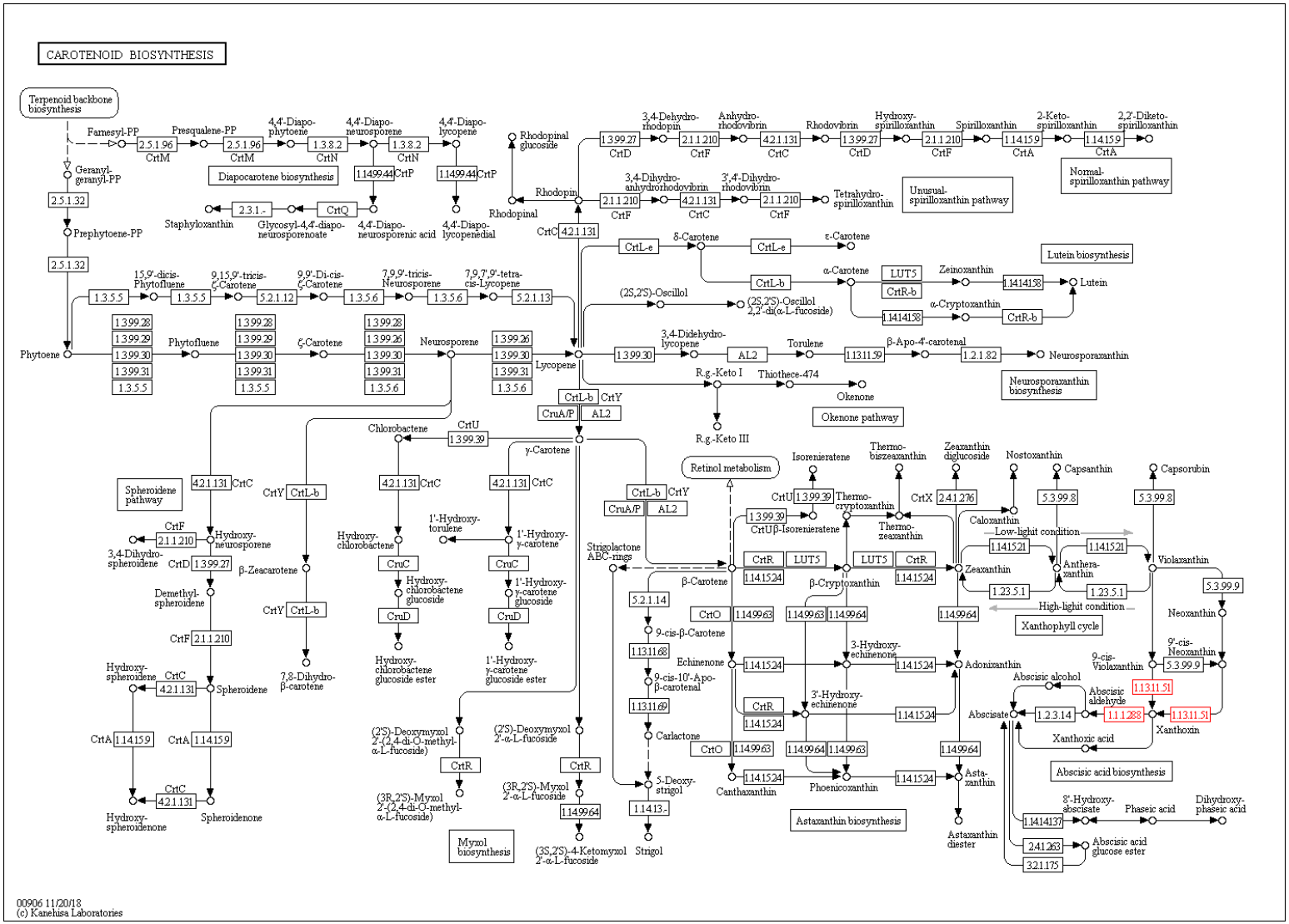
CAROTENOID BIOSYNTHESIS
Terpenoid backbone biosynthesis
Farnesyl-PP
Presqualene-PP
4,4'-Diapo-phytoene
4,4'-Diapo-neurosporene
4,4'-Diapo-lycopene
Diapocarotene biosynthesis
Geranyl-geranyl-PP
Prephytoene-PP
Staphyloxanthin
Glycosyl-4,4'-diapo-neurosporenoate
4,4'-Diapo-neurosporenic acid
4,4'-Diapo-lycopenedial
Rhodopinal glucoside
Rhodopin
Rhodopinal
3,4-Dehydro-rhodopin
Anhydro-rhodovibrin
Rhodovibrin
Hydroxy-spirilloxanthin
Spirilloxanthin
2-Keto-spirilloxanthin
2,2'-Diketo-spirilloxanthin
Normal-spirilloxanthin pathway
3,4-Dihydro-anhydrorhodovibrin
3',4'-Dihydro-rhodovibrin
Tetrahydro-spirilloxanthin
Unusual-spirilloxanthin pathway
Phytoene
Phytofluene
ζ-Carotene
Neurosporene
Lycopene
15,9'-dicis-Phytofluene
9,15,9'-tricis-ζ-Carotene
9,9'-Di-cis-ζ-Carotene
7,9,9'-tricis-Neurosporene
7,9,7',9'-tetra-cis-Lycopene
δ-Carotene
ε-Carotene
α-Carotene
β-Carotene
Lutein
Zeinoxanthin
α-Cryptoxanthin
Lutein biosynthesis
(2S,2'S)-Oscillol
(2S,2'S)-Oscillol 2,2'-di(α-L-fucoside)
3,4-Didehydro-lycopene
Torulene
β-Apo-4'-carotenal
Neurosporaxanthin
Neurosporaxanthin biosynthesis
R.g.-Keto I
Thiothece-474
Okenone
Okenone pathway
R.g.-Keto III
Chlorobactene
γ-Carotene
Spheroidene pathway
Hydroxy-chlorobactene
1'-Hydroxy-torulene
1'-Hydroxy-γ-carotene
Hydroxy-chlorobactene glucoside
1'-Hydroxy-γ-carotene glucoside
Hydroxy-chlorobactene glucoside ester
1'-Hydroxy-γ-carotene glucoside ester
3,4-Dihydro-spheroidene
Hydroxy-neurosporene
β-Zeacarotene
Demethyl-spheroidene
7,8-Dihydro-β-carotene
Hydroxy-spheroidene
Spheroidene
Hydroxy-spheroidenone
Spheroidenone
(2'S)-Deoxymyxol 2'-(2,4-di-O-methyl-α-L-fucoside)
(3R,2'S)-Myxol 2'-(2,4-di-O-methyl-α-L-fucoside)
(2'S)-Deoxymyxol 2'-α-L-fucoside
(3R,2'S)-Myxol 2'-α-L-fucoside
(3S,2'S)-4-Ketomyxol 2'-α-L-fucoside
Myxol biosynthesis
Retinol metabolism
Strigolactone ABC-rings
9-cis-β-Carotene
9-cis-10'-Apo-β-carotenal
Carlactone
5-Deoxy-strigol
Strigol
Isorenieratene
Thermo-biszeaxanthin
Zeaxanthin diglucoside
Nostoxanthin
Capsanthin
Capsorubin
Thermo-cryptoxanthin
Thermo-zeaxanthin
Caloxanthin
Low-light condition
High-light condition
Xanthophyll cycle
Zeaxanthin
Anthera-xanthin
Violaxanthin
Neoxanthin
9'-cis-Neoxanthin
9-cis-Violaxanthin
Echinenone
3-Hydroxy-echinenone
3'-Hydroxy-echinenone
Adonixanthin
Canthaxanthin
Phoenicoxanthin
Asta-xanthin
Astaxanthin diester
Astaxanthin biosynthesis
Abscisic alcohol
Abscisic aldehyde
Abscisate
Xanthoxic acid
Xanthoxin
Abscisic acid biosynthesis
8'-Hydroxy-abscisate
Phaseic acid
Dihydroxy-phaseic acid
Abscisic acid glucose ester
00906 11/20/18
(c) Kanehisa Laboratories

(b)

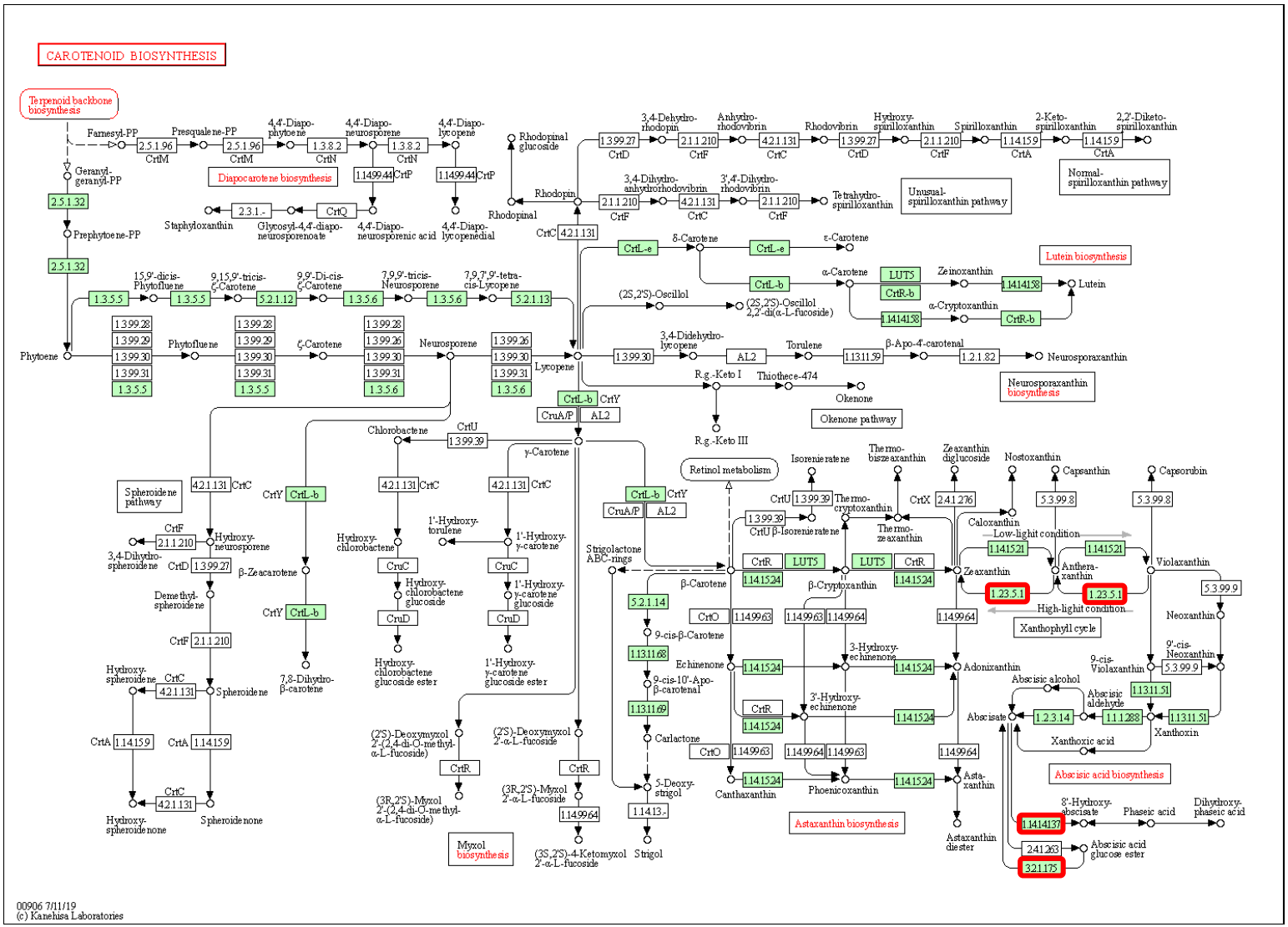
CAROTENOID BIOSYNTHESIS
Terpenoid backbone biosynthesis
Farnesyl-PP
Presqualene-PP
4,4'-Diapo-phytoene
4,4'-Diapo-neurosporene
4,4'-Diapo-lycopene
Geranyl-geranyl-PP
Diapocarotene biosynthesis
Staphyloxanthin
Glycosyl-4,4'-diapo-neurosporenoate
4,4'-Diapo-neurosporenic acid
4,4'-Diapo-lycopenedial
Prephytoene-PP
Phytoene
Phytofluene
ζ-Carotene
Neurosporene
Lycopene
Rhodopinal glucoside
Rhodopin
Rhodopinal
3,4-Dehydro-rhodopin
Anhydro-rhodovibrin
Rhodovibrin
Hydroxy-spirilloxanthin
Spirilloxanthin
2-Keto-spirilloxanthin
2,2'-Diketo-spirilloxanthin
Normal-spirilloxanthin pathway
3,4-Dihydro-anhydrorhodovibrin
3',4'-Dihydro-rhodovibrin
Tetrahydro-spirilloxanthin
Unusual-spirilloxanthin pathway
δ-Carotene
ε-Carotene
Lutein biosynthesis
α-Carotene
Zeinoxanthin
Lutein
α-Cryptoxanthin
(2S,2'S)-Oscillol
(2S,2'S)-Oscillol 2,2'-di(α-L-fucoside)
3,4-Didehydro-lycopene
Torulene
β-Apo-4'-carotenal
Neurosporaxanthin
Neurosporaxanthin biosynthesis
R.g.-Keto I
Thiothece-474
Okenone
Okenone pathway
R.g.-Keto III
Chlorobactene
γ-Carotene
Spheroidene pathway
Hydroxy-neurosporene
3,4-Dihydro-spheroidene
β-Zeacarotene
Demethyl-spheroidene
7,8-Dihydro-β-carotene
Hydroxy-spheroidene
Spheroidene
Hydroxy-spheroidenone
Spheroidenone
Hydroxy-chlorobactene
Hydroxy-chlorobactene glucoside
Hydroxy-chlorobactene glucoside ester
1'-Hydroxy-torulene
1'-Hydroxy-γ-carotene
1'-Hydroxy-γ-carotene glucoside
1'-Hydroxy-γ-carotene glucoside ester
(2'S)-Deoxymyxol 2'-(2,4-di-O-methyl-α-L-fucoside)
(3R,2'S)-Myxol 2'-(2,4-di-O-methyl-α-L-fucoside)
(2'S)-Deoxymyxol 2'-α-L-fucoside
(3R,2'S)-Myxol 2'-α-L-fucoside
(3S,2'S)-4-Ketomyxol 2'-α-L-fucoside
Myxol biosynthesis
Strigolactone ABC-rings
9-cis-β-Carotene
9-cis-10'-Apo-β-carotenal
Carlactone
5-Deoxy-strigol
Strigol
Retinol metabolism
Isorenieratene
β-Isorenieratene
Thermo-cryptoxanthin
Thermo-biszeaxanthin
Thermo-zeaxanthin
Zeaxanthin diglucoside
Nostoxanthin
Caloxanthin
Capsanthin
Capsorubin
Low-light condition
High-light condition
Xanthophyll cycle
β-Carotene
β-Cryptoxanthin
Zeaxanthin
Anthera-xanthin
Violaxanthin
Neoxanthin
9'-cis-Neoxanthin
9-cis-Violaxanthin
Echinenone
3-Hydroxy-echinenone
3'-Hydroxy-echinenone
Adonixanthin
Abscisic alcohol
Abscisic aldehyde
Abscisate
Xanthoxic acid
Xanthoxin
Abscisic acid biosynthesis
Canthaxanthin
Phoenicoxanthin
Astaxanthin
Astaxanthin diester
Astaxanthin biosynthesis
8'-Hydroxy-abscisate
Phaseic acid
Dihydroxy-phaseic acid
Abscisic acid glucose ester
00906 7/11/19
(c) Kanehisa Laboratories

SI Fig. 2. Carotenoid biosynthesis enzymes annotated in *G. orontii* MGH1 and *A. thaliana*. (a) Enzyme classes in red-colored boxes represent genes identified in *G. orontii*. (b) Enzyme classes in boxes highlighted green represent genes present in *A. thaliana*. Among abscisic acid biosynthesis genes, genes in red boxes are down-regulated ($p<0.05$) at the infection site during *G. orontii* infection at 5 dpi (Chandran et al., 2010). Down-regulated genes infected:uninfected expression ratios were: 0.2 for EC 1.23.5.1 (AT1G08550, *NPQ4*), 0.1 for EC 1.14.14.137 (AT3G19270, *CYP707A4*), and 0.3 for EC 3.2.1.175 (AT1G52400, *BGLU18*). Carotenoid Biosynthesis maps (00906) were accessed through KEGG.

Chapter 4: Powdery mildew effectors targeting Arabidopsis TCP transcription factors contribute to disease

A.G. McRae, J. Taneja, E. Applegate, J. Liu, M. Kan, and M. C. Wildermuth

Permission was granted from all primary co-authors to include this work as part of this dissertation.

Preface

All experimental work in this manuscript was performed by me or by undergraduates Elizabeth Applegate, Jonathan Liu, and Megan Kan under my mentorship and supervision with the exception of the grape powdery mildew spray-induced gene silencing experiments which were performed by Dr. Jyoti Taneja. Powdery mildew disease on *Arabidopsis thaliana* mutants was quantified using the spore counting protocol (Appendix 3). An updated protocol for the confocal quantification of ploidy is provided in Appendix 4.

Keywords: effector, TCP transcription factors, spray-induced gene silencing, powdery mildew, Arabidopsis thaliana, *Golovinomyces orontii, Erysiphe necator,* glycosyl hydrolase family 17 (GH17) domain

Abstract

Plant TCP transcription factors which regulate growth and development are heavily targeted by effectors of diverse plant pathogens. In a yeast-two hybrid screen between *Arabidopsis thaliana* proteins and *Golovinomyces orontii* MPIPZ effectors, 34% of the interactions identified involved TCP proteins. In this study the contribution of TCPs and their targeting effectors during infection is measured. Four of the five TCPs targeted by effectors were found to suppress *G. orontii* MGH1 growth. Adult *A. thaliana* T-DNA mutants *tcp13, tcp14, tcp15*, and *tcp20* were more susceptible to *G. orontii* MGH1. Using spray-induced gene silencing (SIGS), homologs of OECs in *G. orontii* MGH1 were targeted. When *OEC14*, *OEC60/OEC61*, and *OEC70* were targeted via SIGS, significantly less spores were produced. Homolog *OEC60/OEC61* was investigated further. It encodes a short N-terminal domain originally annotated in *G. orontii* MPIPZ OEC60 and OEC61 coupled to a larger glycosyl hydrolase family 17 domain (GH17). To date, OEC60 and OEC61 homologs across all sequenced powdery mildews include the GH17 domain, suggesting the lack of GH17 domain in the MPIPZ isolate may be due to the incomplete nature of that genome. GH17 domain-containing proteins are found widely in plants and fungi. When homolog of *OEC60/OEC61* is silenced in the *Erysiphe necator*-grapevine system, significantly less spores are also produced, providing evidence this is a conserved powdery mildew virulence factor. Using *Agrobacterium*-mediated transient expression assays in *Nicotiana benthamiana, G. orontii* MGH1 homolog of OEC60/OEC61 was shown to be nuclear-targeted and co-localize with TCP13 and TCP14. Furthermore, co-immunoprecipitation shows OEC60/OEC61 interaction with TCP13 *in planta*. An analysis of available TCP13 and TCP14 Arabidopsis protein interaction data reveals a majority of targets interact with both TCP13 and 14; these targets are highly enriched in development and gene expression ontology. *tcp14* mutants have enhanced endoreduplication at the site of powdery mildew infection which is known to correlate with enhanced powdery mildew asexual reproduction. Together, these results support a role for OEC60/OEC61 in limiting TCP13/14 function to promote endoreduplication at the infection site. To further elucidate this

interaction node, proteomic analysis (2-D LC MS/MS) of the MYC-purified protein complex from *G. orontii*-infected and uninfected plants expressing *G. orontii* MGH1 OEC60/OEC61-MYC was performed. TCP13 and TCP14 protein interactions suggest OEC60/OEC61 interacts with TCP13 and TCP14 to alter gene expression associated with endoreduplication including endocycle reentry, inhibition of cell division and cytokinesis, and endocycle progression. Manipulation of the endocycle is important for the proliferation of powdery mildew and the growth and development of diverse biotrophs. These findings provide fundamental insights on regulation of the eukaryotic cell cycle.

Introduction

Plant TCP transcription factors regulate growth and development (Lopez et al., 2015). The TCP gene family is named after the first 3 genes identified in this family: TEOSINTE BRANCHED1 in maize (*Zea mays*), CYCLOIDEA in snapdragon (*Antirrhinum majus*), and PCF (proliferating cell nuclear antigen factor) in rice (*Oryza sativa*) (Lopez et al., 2015). TCPs emerged 650-800 million years ago, predating land plants, and have been identified in moss and algae in addition to angiosperms which are more well studied (Navaud et al., 2007). *Arabidopsis thaliana* has 24 TCPs containing the 59 amino acid TCP domain (basic helix-loop-helix domain) which mediates DNA-binding (Lopez et al., 2015). TCPs are divided into two classes; class I TCPs are known to promote cell proliferation and class II TCPs act antagonistically to suppress growth (Li, 2015). They are highly interactive proteins within and outside their protein family (BioGRID; Stark et al., 2006). They interact within their protein family to form homo- and hetero-dimers which controls affinity and specificity in DNA-binding (Li, 2015). Together these transcription factors act redundantly and antagonistically to regulate leaf development, plant hormone biosynthesis, and plant immunity (Lopez et al., 2015). This regulation may be critical in balancing growth when stressed to protect the fitness of the plant.

TCPs are emerging as plant pathogen immunity modulators heavily acted upon by secreted pathogen effectors from diverse pathogens. In a yeast-two hybrid screen performed by (Weßling et al., 2014), effectors from *Hyaloperonospora arabidopsidis* (downy mildew, oomycete), *Pseudomonas syringae* DC3000 (bacterium), and *Golovinomyces orontii* MPIPZ (powdery mildew fungus) were screened against a library of *A. thaliana* proteins. Among 9 proteins that were targeted by effectors from all three pathogens, 3 of them were TCPs (TCP13, TCP14, and TCP15). TCP14 was the most highly targeted host protein with 52 effectors targeting it, primarily effectors from the obligate biotrophic pathogens downy and powdery mildews (Weßling et al., 2014). Furthermore, *tcp13* and *tcp14* mutants challenged by *P. syringae* DC3000 had opposite susceptibility phenotypes compared with challenge by obligate biotrophs (Weßling et al., 2014). Together this suggests TCPs function in lifestyle specific manners to impact plant immunity and/or pathogen virulence.

Within the 42 *G. orontii* MPIPZ effector candidate (OEC)-TCP interactions, several effectors were found to interact with multiple TCPs by yeast two-hybrid and all 5 targeted TCPs interacted with multiple effectors (Weßling et al., 2014). This represents 34% of all *A. thaliana* protein-OEC interactions. Suffice to say, there is much to uncover about the mechanism and function of these interactions. In this study we measure the genetic contribution of TCPs and OECs in the context of powdery mildew infection utilizing the *G.orontii* MGH1-*Arabidopsis thaliana* pathosystem.

Homologs of OECs in the related strain *G. orontii* MGH1 were identified for investigation in the annotated *G. orontii* MGH1 v4.0 genome accessed through MycoCosm (Grigoriev et al., 2014).

Spray-induced gene silencing is used to rapidly assess the contribution of OECs to powdery mildew spore production, prioritizing highly connected OECs that interact with TCPs that control powdery mildew susceptibility. Mutants in the five targeted *TCP* genes are also challenged with powdery mildew to identify novel *TCP* genes that contribute to spore production. The results of these disease assays along with bioinformatic analysis prioritizes *G. orontii* MGH1 homolog of OEC60 and OEC61 for further investigation.

The reproductive success of the powdery mildew fungus, *G. orontii*, is also tied to the ploidy state of the surrounding host tissues being co-opted to provide nutrients. Enhanced endoreduplication, or DNA replication without cell division, is observed in *A. thaliana* mesophyll cells underlying the infection site (Chandran et al., 2010). Additionally, several *A.* thaliana mutants with reduced or abrogated endoreduplication at the site of infection support less growth of the powdery mildew, with the extent of powdery mildew asexual reproduction highly correlated with infection site plant cell DNA ploidy levels (Chandran et al., 2013). Endoreduplication is proposed to increase the cells ability to provide energy rich metabolites to the powdery mildew during the metabolically demanding process of spore formation. It may also be associated with a metabolic shift from a source tissue to a sink tissue. TCPs, particularly class I TCPs, have many described roles in regulating the cell cycle. Powdery mildew infection assays are performed on four class I *tcp* mutants: *tcp9, 14, 15,* and *tcp20.* Of the 5 TCPs targeted by effectors, TCP14 and TCP15 have the most well described role in regulating endoreduplication (Peng et al., 2015). TCP14 and TCP15 redundantly suppress endoreduplication; single mutants have wildtype ploidy but double mutants have enhanced ploidy. DA1, DAR1, and DAR2 modulate the stability of TCP14 and TCP15 which represses the gene expression of *RBR* and *CYCA3;2* among others whose expression promotes endoreduplication (Peng et al., 2015). Effectors targeting these TCPs could interfere with TCP mediated suppression of these genes. TCP20 is also a known regulator of the cell cycle and binds the *CYCB1;1* promoter to regulate G_2/M transition (Gutie et al., 2005) and TCP13, a class II TCP, suppresses cell expansion via suppression of *ATHB12* expression (Hur et al., 2019). ATHB12 promotes expression of *EXPANSIN* (*EXPA*) a regulator of leaf expansion and *CELL-CYCLE SWITCH 52A* (*CCS52A*), an activator of the anaphase-promoting complex/cyclosome that promotes endoreduplication and has been implicated in biotroph-induced plant cell endoreduplication (Vercruysse et al., 2020; Wildermuth et al., 2017). The prevalence of effectors acting upon TCP nodes regulating growth and immunity indicates the import and complexity of their role in plant-pathogen interactions. Herein we provide evidence for a model by which powdery mildew effectors act on the TCP13-TCP14 node to promote localized host cell endoreduplication.

Results

G. orontii effectors converge on *A. thaliana* TCP transcription factors

G. orontii MGH1 effector homologs of *G. orontii* MPIPZ effector candidates (OECs) that interact with *A. thaliana* TCPs via yeast 2-hybrid (Weßling et al., 2014) were identified (SI Fig. 1) using *G. orontii* MGH1 v4.0 genome (See Methods) accessed through MycoCosm (Grigoriev et al., 2014). The TCP-OEC interaction map (Fig. 1a) contains all *G. orontii* MPIPZ effectors identified in *G. orontii* MGH1 and their interacting TCPs (Weßling et al., 2014). Some OECs of interest have

distinct OEC names but are homologs. When naming OEC homologs in *G, orontii* MGH1, OEC names are grouped together to indicate the homologs identified are related to multiple OECs (Table 1). For example, OEC60 and OEC61 are homologs. In *G. orontii* MGH1, two homologs were identified and are referred to as homologs of OEC60/OEC61. The *OEC60/OEC61 G. orontii* MGH1 homologs of *OEC60/OEC61* also contain a large glycosyl hydrolase family 17 (GH17) domain belonging to the enzyme class 3.2.1.58 (EC 3.2.1.58). *OEC60/OEC61* homologs in other powdery mildews also include the GH17 domain; therefore, *G. orontii* MPIPZ *OEC60* and *OEC61* homologs may be missing this domain due to the incomplete nature of the *G. orontii* MPIPZ genome sequence (Spanu et al., 2010).

***A. thaliana tcp13, tcp14, tcp15,* and *tcp20* have enhanced susceptibility to *G. orontii* MGH1**

Of the five TCPs found to interact with *G. orontii* MPIPZ effectors via yeast 2-hybrid (Fig. 1a; Table 2; Weßling et al., 2014), *A. thaliana* T-DNA insertion mutants in three exhibited a powdery mildew phenotype in seedling assays. *tcp13*, *tcp14*, and *tcp15* exhibited enhanced disease susceptibility (eds) to *G. orontii* MPIPZ. However, only *tcp13* and *tcp14* exhibited eds using adult plants (Weßling et al., 2014), the focus of our study.

Using a modified spore quantification protocol developed for *G. orontii* MGH1 (Appendix 3), powdery mildew disease was quantified on *tcp9, tcp13, tcp14, tcp15,* and *tcp20* adult plants compared with wild type plants (Fig. 1b-c). *A. thaliana tcp13, tcp14, tcp15,* and *tcp20* have enhanced susceptibility to *G. orontii* MGH1 (Fig. 1c), meaning they support higher fungal proliferation. *tcp15* exhibits the smallest statistically significant increase in powdery mildew spore production of the tested TCPs, with 24% more spores formed per gram fresh weight on average than wild type plants. This suggests our assay is able to resolve small differences in powdery mildew disease not previously identified. *tcp13* and *14* exhibit similar increases in spore production of 48% and 39%, respectively, compared to wild type plants, and the previously untested *tcp20* mutant allows the greatest increase in spore production (56%).

***G. orontii* MGH1 effector homologs OEC14, OEC60/OEC61, and OEC70 contribute to spore production**

OEC homologs in *G. orontii* MGH1 (Table 1, SI Table 1) were selected for spray-induced silencing assays (SIGS) based on their ability to target multiple TCPs (Fig. 1a-b) or target TCPs that contribute to spore production (Fig. 1c). For each of the seven OEC homologs tested, a single long dsRNA was designed and synthesized for SIGS in *A. thaliana* whole plant powdery mildew disease assays. As a control, we show the reduction in spore production with SIGS against the known azole-fungicide target, *CYP51* (Fig. 1d), a gene required for membrane synthesis (Zhang et al., 2019). SIGS targeting *G. orontii* MGH1 homologs of *OEC14, OEC60/OEC61,* and *OEC70* significantly reduced spore production in *G. orontii* MGH1 infection of *A. thaliana* compared to buffer only controls (Fig. 1d).

All OECs were originally identified based on their secretion signal and not having homology outside powdery mildews (Weßling et al., 2014), among other criteria. As such the effectors silenced are specific to powdery mildews except for the glycosyl hydrolase family 17 (GH17) domain of *G. orontii* MGH1 *OEC60/OEC61* (Fig. 2a). The GH17 protein domain has been identified in plants and fungi (Gaudioso-Pedraza and Benitez-Alfonso, 2014). Among other fungi accessed via MycoCosm, we found GH17 domain-containing proteins to be often secreted and

have multiple copies (Grigoriev et al., 2014). The predicted protein structure of *G. orontii* MGH1 *OEC60/OEC61* is similar to a glycoside hydrolase family 17 beta-1,3-glucanosyltransferase in *Rhizomucor miehei* (Fig. 2b). Furthermore, it contains the catalytic amino acid identified in barley β-glucan endohydrolases that is also present in *Saccharomyces cerevisiae* (Chen et al., 1993).

Spray-induced gene silencing of homolog of *OEC60/OEC61* in *Erysiphe necator* reduces grape powdery mildew spore production

As the full *G. orontii* MGH1 OEC60/OEC61 is conserved in other powdery mildews (Table 1) and has the potential to interact with both TCP13 and TCP14, we tested whether findings in the *G. orontii MGH1-Arabidopsis* pathosystem can translate to an agriculturally important pathosystem, powdery mildew of grapevine. To do so, we identified an *OEC60/OEC61* homolog in *E. necator* c (Jones et al., 2014) and designed a long dsRNA to target this gene in the same region effective for *G. orontii* (Fig. 2a). Targeting of *OEC60/OEC61* in *Erysiphe necator* by SIGS reduces grape powdery mildew production on *V. vinifera* leaves to 71% of control treated plants (Fig. 3), similar to the reduction seen with the *Arabidopsis* powdery mildew (Fig. 1d).

***G. orontii* MGH1 OEC60/OEC61 is nuclear-targeted effector that colocalizes and interacts with TCP13**

Agrobacterium-mediated transient expression experiments were performed in *Nicotiana benthamiana* to investigate the localization of *G. orontii* MGH1 homolog of OEC60/OEC61. OEC60/OEC61-CFP was strongly localized to the nucleus of plant cells (Fig. 4). Co-infiltrations experiments showed OEC60/OEC61-CFP colocalized in the nucleus with YFP-TCP13 (Fig. 4). Subnuclear foci could not be resolved to indicate specific co-localization of YFP-TCP13 and OEC60/OEC61-CFP. Although TCPs are transcription factors known to localize to the nucleus, TCP13 was found to primarily localize to chloroplasts in tobacco plants and to function as a regulator of chloroplast encoded genes like *psbD* (Baba et al., 2001). Co-localization should be further explored in mesophyll cells where chloroplasts are prevalent and in response to infection, which could alter localization. Additional co-infiltrations were performed to confirm a physical biochemical interaction *in planta* via co-immunoprecipitation (co-IP). A western blot shows YFP-TCP13 and OEC60/OEC61-3xHA interact *in planta* (Fig. 5). *G. orontii* MPIPZ OEC60 was previously shown to co-localize in sub-nuclear foci and interact *in planta*, confirmed by co-IP, with TCP14 (Weßling et al., 2014). In addition, TCP13 and TCP14 have been found to interact with each other via yeast-two hybrid (Danisman et al., 2013; Dreze et al., 2011) suggesting they could both function in the nucleus.

Transgenic *A. thaliana* expressing *G. orontii* MGH1 OEC60/OEC61-MYC created to identify protein interaction network

To identify novel protein interactions with *G. orontii* MGH1 OEC60/OEC61, we transformed *A. thaliana* pGWB17-OEC60/OEOC61 (protein ID 4531743). pGWB17 contains a T-DNA that expresses genes of interest constitutively under the control of the CaMV35s and adds a C-terminal MYC epitope. Transformants do not have any noticeable or severed developmental phenotype. Using stable transgenic lines, we performed co-IP of OEC60/OEC61 from the host plant in uninfected and powdery mildew-infected leaf tissue (Fig. 6a). Multiple proteins were detected in infected and uninfected MYC co-IP protein purifications by Coomassie staining of protein run on an SDS-PAGE gel (Fig. 6b) cut and sent for proteomic analysis (2-D LC MS/MS). We anticipate

many proteins to be complexed with OEC60/OEC61 during infection including other effectors that interact with their TCP and other host targets.

A. thaliana tcp14 mutant has enhanced endoreduplication in leaf mesophyll cells underlying the *G. orontii* MGH1 feeding structure.

TCP proteins have numerous described roles in regulating plant immunity and the cell cycle (Lopez et al., 2015). Pathogens of various lifestyles throughout the tree of life are known to induce cell cycle-related changes in host tissue to promote infection (Appendix 1; Wildermuth et al., 2017). These changes include inducing cell hypertrophy, cell proliferation, and endoreduplication (Wildermuth et al., 2017). Endoreduplication is a cell cycle variant where DNA is replicated without subsequent cell division. Endoreduplicating cells are found at the infection site of many biotrophic interactions with plants. This includes both pathogenic and mutualistic microbes like arbuscular mycorrhizal fungi, plant parasitic nematodes, *Cabbage leaf curl virus*, rhizobia, and powdery mildew fungi with numerous others remaining to be explored (Wildermuth et al., 2017).

In the *G.orontii* MGH1- *Arabidopsis* pathosystem, endoreduplication is induced in mesophyll cells underlying the fungal feeding structure at five days post infection (dpi) when asexual spores are formed (Chandran et al., 2010); the ploidy (DNA content) of those mesophyll cells increases on average from 8C to 32C. *A. thaliana* mutants with reduced or abrogated endoreduplication at the site of infection support less growth of *G. orontii* (Chandran et al., 2013). Furthermore, the extent of asexual reproduction is highly correlated with the ploidy level (DNA content). In the powdery mildew-plant interaction, locally induced endoreduplication is postulated to increase the metabolic output of the plant tissue to support the metabolically demanding process of spore development (Chandran and Wildermuth, 2016; Wildermuth, 2010).

Given that the Arabidopsis TCPs targeted by *G. orontii* MGH1 effectors (TCP9, 13, 14, 15, and 20) have described roles regulating the cell cycle and that localized cell cycle modulation is critical to powdery mildew proliferation, we explored DNA ploidy in the *tcp9, tcp13, tcp14, tcp15,* and *tcp20* mutant lines. Whole leaf ploidy (leaf 8) of adult plants was assessed by flow cytometry for mutants compared with wild type plants (SI Fig. 2). DNA content levels were assigned 2C-64C and ploidy index was calculated to compare the ploidy levels of the mutant to the wildtype. No *tcp* mutants had altered DNA ploidy (SI Fig. 2) in uninfected mature fully expanded leaves. At the whole leaf level, flow cytometry analysis could not resolve a change in ploidy with powdery mildew infection. This is likely because there are few endoreduplicated mesophyll cells underlying the fungal feeding structures compared to the total number of cells in the leaf.

Therefore, similar to Chandran et al., 2010, 2013, we used confocal microscopy to measure the fluorescence of DAPI stained nuclei in mesophyll cells underlying epidermal cells containing the primary feeding structure (first haustorium established at the beginning of colony development) (Fig. 7). *tcp14* mutant plants were found to have significantly enhanced endoreduplication in this tissue (Fig. 7b) in one experiment. This mutant even had 128C nuclei at the site of infection; higher DNA content than has been quantified in wild type infected tissue analyzed in the same manner (Chandran et al., 2013, 2010). This finding remains to be confirmed in an independent experiment; however, statistically significant differences in DNA ploidy at the powdery mildew infection site for other mutants were reproducible in separate experiments (Chandran et al., 2013). In addition, the localized ploidy index for the *tcp14* mutant extends the high correlation between plant cell

ploidy at the powdery mildew infection site and the extent of spore production seen for other mutants with altered ploidy indices (Fig. 7b). This supports the enhanced endoreduplication phenotype as the primary driver of the powdery mildew phenotype for *tcp14*.

TCP13 and TCP14 protein interactions overlap significantly and regulate transcription and development

To investigate the TCP13/TCP14 interaction node, known protein interactions were analyzed in BioGRID (Stark et al., 2006). TCP13 has 225 and TCP14 has 312 unique protein interactions cataloged. 143 of these protein targets are targeted by both TCP13 and TCP14 (SI Table 2). 64% of TCP13 and 46% of TCP14 protein targets are conserved. Gene ontology analysis of this common set of protein interactors reveals regulation of development and transcription to be dramatically statistically over-represented (PANTHER Overrespresentation Test version 15.0). Protein targets in common include KNAT1, CUC2, and DA1 (SI Table 2) which are implicated in regulating endoreduplication. Together these interactions may be utilized during powdery mildew infection to promote localized endoreduplication and asexual reproduction (Fig. 8).

Discussion

TCPs and their targeting effectors are important modulators of susceptibility in *A. thaliana*-*G. ororntii* interactions. Our findings suggest these interactions promote infection site reprogramming to support powdery mildew proliferation. The adapted spore quantification assay and ploidy determination experiments proved to be quite sensitive to resolve the impact of single cell cycle component genes and effectors despite the prevalence of redundancy. The *tcp14* mutant, for example, supported more powdery mildew growth and had enhanced ploidy at the site of infection (Fig. 1c; Fig. 7b) despite being functionally redundant in developmentally-associated ploidy. *tcp14* and *tcp15* single mutants do not impact ploidy in leaves, but double mutants have enhanced ploidy (Peng et al., 2015). Similarly, a single mutant in *MYB3R4* was abrogated in powdery mildew-induced ploidy and supported less powdery mildew asexual reproduction whereas a double mutant was required to observe a leaf ploidy phenotype (Chandran et al., 2010). These findings highlight the ability of the powdery mildew system to identify individual components of the complex cell machinery governing cell fate.

TCP15, TCP20, OEC14, OEC60/OEC61, and *OEC70* were identified as novel targets regulating powdery mildew asexual reproduction in adult plants. Interestingly, most of the TCPs investigated here are not upregulated at the site of infection (Chandran et al., 2013). This suggests effector-targeted TCPs are modulated at the protein level - and not transcriptionally. This is supported by the finding that the yeast 2-hybrid screen of *G. orontii* MPIPZ OEC60/OEC61 and OEC70 identified eight interacting *Arabidopsis* proteins in total, including three TCPs as shown in Fig. 1a and three proteins involved in protein modification (CSN5A, RCN1, and UBQ-like) (Weßling et al., 2014).

Prioritizing effectors targeting TCPs via SIGS has been extremely fruitful with 43% of targets contributing to spore production. Furthermore, those that did not have a phenotype via SIGS could be tested with long dsRNAs or siRNAs designed against different regions of the transcript or in combination with another dsRNA against a similarly interacting OEC. This is especially relevant for *OEC27/OEC39* which has 7 copies identified in *G. orontii* MGH1 with significant divergence. The dsRNA designed and used in this study primarily targeted the 2 copies (protein IDs 4163222

and 4575775) most closely related to *G. orontii MPIPZ OEC27*. All other copies were expressed an order of magnitude lower (SI Fig. 3). *G. orontii* MGH1 homologs of ten other OEC proteins that interact with TCPs by yeast 2-hybrid remain to be tested (Fig. 1a). Three additional untested OECs belong to the same subclade (OEC16a, OEC123, and OEC125) and encode RNAse-like effectors. There are 12 copies of *OEC16a/OEC123/OEC125* homologs in *G. orontii* MGH1 and 5 copies in the closely related powdery mildew *G. cichoracearum* (Grigoriev et al., 2014).

G. orontii MGH1 OEC70 which did contribute to spore production (Fig. 1d) is very highly expressed (SI Fig. 3). As such, it may be an important conserved powdery mildew virulence factor. Future work will explore the role of OEC70 in the grape powdery mildew as was done with OEC60/OEC61. OEC14 which has a nuclear localization signal and is annotated as an RNAse-like effector (Table 1) also impacts spore production. Unlike the other effectors investigated, it only has one known target, TCP20. The impact of SIGS targeting OEC14 on grapevine powdery mildew proliferation will be assessed on its own and in combinations with OEC70 and/or OEC60/OEC61 targets.

OEC60/OEC61 emerged as an important effector in both the *Arabidopsis* and grapevine powdery mildew systems. Co-immunoprecipitation of this effector *in planta* can uncover additional protein interactions that influence this TCP 13-14 node. It can identify both host and pathogen effector proteins not originally included in the yeast-two hybrid screen (Weßling et al., 2014). *OEC60/OEC61* gene structure requires further investigation. The OEC60/OEC61 sequence that is responsible for TCP interaction via yeast 2-hybrid is completely independent of the GH17 domain, but both have implications in pathogenicity. In both plants and fungi, GH17 domain containing proteins are involved in immunity (Minic, 2008). One reported activity of this enzyme class is to break down callose which is deposited at plasmodesmata controlling the size exclusion limit of plasmodesmata and impacting pathogen susceptibility(Gaudioso-Pedraza and Benitez-Alfonso, 2014). However, the substrate of glycans can be hard to predict and would need to be experimentally validated. It is tempting to believe GH17 could be involved in post translational modification of TCPs. For example, TCP15 can be glycosylated to promote cytokinin responses (Steiner et al., 2016, 2012).

TCP13 and TCP14 are highly interactive proteins known to each target hundreds of proteins. These interactions modify their activity in regulating transcription. In the context of powdery mildew infection, these proteins are heavily targeted which may impact their protein and DNA binding capacities fine-tuning their role in this specific context. Several proteins that co-interact with both TCP13 and TCP14 are implicated in modulating the cell cycle (Fig. 8). *KNAT1* is highly expressed in hypocotyl tissue (Klepikova et al., 2016) which undergoes endoreduplication to support the growth of the plant before photosynthesis can take place (Jakoby and Schnittger, 2004). DA1 directly regulates endoreduplication by controlling the stability of TCP14 and TCP15 (Peng et al., 2015). CUC2 binds the *DA1* promoter to promote its expression (Li et al., 2020). As our findings suggest, effectors could play a role in transiently modulating these interactions to guide TCP network outcomes. There are many examples of TCPs being targeted by pathogen effectors to promote infection. The *P. syringae* effector HopBB1 has been identified as a jasmonic acid (JA) regulator, facilitating the degradation of two negative regulators of JA, JAZ3 and TCP14, to promote virulence (Yang et al., 2017). Aster Yellows phytoplasma strain Witches' Broom (AY-WB) also encode effectors known to degrade TCPs. Specifically, effector SAP11 degrades class

II sub group CIN-TCPs like TCP13 (Sugio et al., 2014). Expression of SAP11 in *A. thaliana* severely impacts development, phenocopying disease symptoms for which the disease is named after, Witches' Broom (Sugio et al., 2011). However, we found OEC60/OEC61 expression in plants does not lead to severe defects in plant development. SAP11 and OEC60/OEC61 are unrelated effectors originating in different domains of life but still converge on these TCP nodes.

The nature of OEC60/OEC61 interaction with TCPs remains to be described but similar to the two above examples, it is likely to inhibit/limit the function of the targeted TCPs by degradation, impairing DNA-binding affinity, interfering with TCP protein-interaction, or altering localization (e.g. for TCP13). In Fig. 8, a model is presented which identifies potential protein interactions and transcriptional regulators that could modulate powdery mildew-induced endoreduplication. This model remains to be tested (Fig. 8). OEC60/OEC61 could inhibit TCP13/14 function in transcriptional activation/repression and TCP-protein interactions to promote the expression of genes promoting endoreduplication. DA1 and CUC2 interact with both TCP13 and TCP14 (Stark et al., 2006). CUC2 promotes expression of *DA1* (Li et al., 2020). DA1 degrades TCP14 which suppresses expression of endocycle promoters, *CYCA3;2* and *RBR* (Peng et al., 2015). Transcriptional implications of TCP13 interactions with DA1 and CUC2 remains unexplored, however, TCP13 is linked to the endocycle through another transcriptional network. TCP13 degradation could promote *ATHB12* expression which promotes endoreduplication via expression of genes such as *EXPA* and genes involved in G_2/M modulation (e.g. *CCS52A*, an activator of the anaphase promoting complex) (Hur et al., 2019; Vercruysse et al., 2020). One important outcome of the *G. orontii* MGH1 effector-TCP interaction network is that it appears to be involved in the coordination of localized powdery mildew-induced endoreduplication, concomitant with asexual reproduction. Fundamental understanding of the complex network of interactions controlling cell fate (e.g. endoreduplication) has broad applications to powdery mildew disease management, to other biotroph-host interactions where induced endoreduplication promotes growth and development of the biotroph, to crops with endopolyploid products (such as cotton), and to cancer treatment.

Acknowledgements
Thanks to Steve Ruzin and Denise Schichnes for their expert advice and training to use the microscopes at the Biological Imaging Facility. Thanks to Hector Nolla at the Flow Cytometry Facility for training and troubleshooting experiments.

Methods

Arabidopsis growth and _G. orontii_ inoculation

A. thaliana ecotype Col-0 were grown in growth chambers at 22°C, 70% relative humidity, and a 12 hour photoperiod with photosynthetically active radiation = 150µmol/(m2 x s). Plant mutants were obtained from The Arabidopsis Biological Research Center: *tcp9* (SALK_201398c), *tcp13* (CS313854), *tcp14* (CS856207), *tcp15* (SALK_011491c), and *tcp20* (SALK_041906c). Plants for spray-induced gene silencing assays were grown in 4-inch pots (4 plants per pot). Plants for *tcp* mutant experiments were grown in plant trays with 16.6 x 12.4 x 5.8-cm insert boxes (12 plants per box). At 4-4.5 weeks plant tissue was inoculated by settling tower (Reuber et al., 1998) with *G. orontii* isolate MGH1 performed at 2:00 pm. The control and RNA sprayed samples were inoculated in the same tower to ensure equal inoculation for each replicate. For spore counting assays, plants were inoculated with a heavy dose (conidia from 4-5 fully covered leaves at 10-14

dpi). For microscopic ploidy analysis, plants were inoculated with a moderate dose (conidia from 2 half-covered leaves).

Grape growing and *E. necator* maintenance and inoculations

The grape powdery mildew *E. necator* isolate c was regularly maintained on detached leaves of Chardonnay and Carignan grapevine varieties. The hard cuttings of grapevine varieties were received from Foundation Plant Services, UC Davis, CA and were grown at the UC Berkeley Oxford Tract Greenhouse facility. The cuttings were rooted on a mist bench and then transferred to 2-gallon pots with supersoil and fertilized with Osmocote. Grapevine plants are sprayed with sulfur every week to keep them mildew free. For *E. necator* isolate maintenance and for grapevine leaf disc assays, the 3rd or 4th node leaf was collected, sterilized with 50% bleach for 30 seconds, washed with sterile water 3 to 4 times, and then placed on 1% agar medium. For maintenance, chains of conidia were transferred to sterile leaves under the microscope in a laminar hood, every 12 to 14 days. For grapevine leaf disc assays, 12-15 10 mm leaf discs were cut from sterile leaves and placed on Whatman sheet 1.0 over 1% agar plates. The leaf discs were inoculated with a heavy dose by settling tower (Reuber et al., 1998). For each treatment 3 to 5 plants were used.

RNA design and synthesis and spraying

pssRNAit (https://plantgrn.noble.org/pssRNAit/) was used to identify efficient dsRNAs and limit off-target gene silencing in the host *A. thaliana* or *V. vinifera.* Genes in *G. orontii* MGH1 (https://mycocosm.jgi.doe.gov/Golor4/Golor4.home.html4.0) and *E. necator* c (https://mycocosm.jgi.doe.gov/Erynec1/Erynec1.home.html) were identified in MycoCosm (SI Table 1, Grigoriev et al., 2014). Template for *in vitro* transcriptions was amplified from powdery mildew infected tissue cDNA using Phusion polymerase (M0530S/L, New England Biolabs, Ipswich, Massachusetts) and the T7 promoter (5'- TAATACGACTCACTATAGGGGG-3') was added to both ends. dsRNA was generated using the HiScribe T7 High Yield RNA Synthesis Kit (E2040S, New England Biolabs, Ipswich, Massachusetts), purified using the Monarch RNA Cleanup Kit (T2050S/L, New England Biolabs, Ipswich, Massachusetts), reannealed by heating to 94°C and slowly cooling to room temperature over 50 minutes, and quantified by nanodrop (dsRNA A_{260} x 46.7ng/µL). Plant samples were infected with powdery mildew, then sprayed with RNA or buffer in which the RNA was dissolved.

Spore counts

Spore counting was performed to assess fungal spore production as described by (Weßling and Panstruga, 2012) summarized here with the following modifications (Appendix 3). For *A. thaliana* experiments, 12-15 leaves were harvested per condition at 8-10 dpi. For grapevine leaf disc assays, 12-15 leaf discs were collected at 14-21 dpi. Tissue was vortexed in 15 mL 0.01% Tween-80 then filtered through 40 µm mesh before centrifugation. Spore pellets were resuspended to 200 µL to 1,200 µL depending on spore yield. For each sample, nine 1 x 1 mm2 fields of a Neubauer-improved hemocytometer were counted and normalized to the weight of the plant tissue to determine spore concentration. The average spore count was normalized to the control for each replicate. An unpaired, two-tailed Student's T-test was used to compare control and normalized RNA sprayed spore counts with $n \geq 3$ and $p < 0.05$ indicating statistical significance.

Gateway Cloning
Effector genes were cloned from *G. orontii* MGH1-infected *A. thaliana* cDNA. *TCPs* were cloned from The Arabidopsis Biological Research Center bacterial clones: *TCP9* (TOPO-U07-F11), *TCP13* (TOPO-U09-E02), *TCP14* (TOPO-U04-A09), *TCP15* (TOPO-U03-D12), and *TCP20* (TOPO-U15-G05). Genes were prepared for Gateway cloning into pDODR221 by adding *attB* sites to 5' and 3' of template using PCR. *Escherichia coli* was transformed with the pDONR221 plasmids. Genes were subsequently Gateway cloned from pDONR221 into pEARLEYGATE102 (C-CFP), pEARLEYGATE104 (N-YFP) (Earley et al., 2006), pGWB14 (C-3xHA), and/or pGWB17 (C-4xMYC) (Tanaka et al., 2012). Plasmids were purified from transformants and transformed into *Agrobacterium tumefaciens* (strain GV3101 or C58C1).

Agrobacterium-mediated transient expression in *N. benthamiana* and transformation of *A. thaliana*
A. tumefaciens transformants were grown in 5 mL liquid LB with appropriate antibiotics overnight at 28°C, pelleted, resuspended in induction media (10 mM MES pH 5.6, 10 mM $MgCl_2$, 150 µM acetosyringone) to an OD_{600} of 0.4-0.60 for transient expression, and incubated in induction media for approximately 3-4 hours before infiltration in *N. benthamiana* leaves. For co-infiltrations, 2 cultures were mixed 1:1 before infiltration. For *A. thaliana* transformation, floral dip methods were used as in (Clough and Bent, 1998).

Co-localization
The Zeiss LSM710 was used for imaging transiently expressed fluorescent proteins in *Nicotiana benthamiana*. Intensity profiles for colocalization and Z-stacks were generated using ZEN2010.

Nuclear DNA quantification at *G. orontii* infection sites
A. thaliana tissue was prepared and imaged with a Zeiss LSM 710 using methods from (Chandran et al., 2010) with modifications noted in Appendix 4. Ploidy quantitation was performed using Imaris 9.5.1 Surfaces (Appendix 4).

***A. thaliana* whole leaf ploidy analysis using flow cytometry**
Nuclei were isolated from the eight leaf of 4.5 week old *A. thaliana*, with n=3 for each experiment. Nuclei were isolated using methods described in (Vlieghe et al., 2005). Tissue was chopped on ice in 600 µL of nuclei isolation buffer (45 mM $MgCl_2$, 30 mM sodium citrate, 20 mM 3-[N-morpholino] propanesulfonic acid (pH 7), and 0.1% Triton X-100) and stained with 2 µL of 1 mg/mL DAPI. For each replicate, a sample of 5,000 nuclei were collected with flow cytometry (405nm Violet laser, Pacific Blue filter 450/50 BP) using the BD LSR II. Samples were gated on a logarithmic ploidy levels (2C, 4C, 8C, 16C, 32C, 64C) and clustered ploidy levels (8C+, 16C+, 32C+) between samples and controls. Ploidy index was also calculated and used overall metric of endoreduplication (ploidy index = 0[%2C]+1[%4C]+2[%8C]+3[%16C]+4[%32C]+5[%64C]). Two-tailed, unpaired T-tests were calculated to compare the average ploidy index of samples and controls, with $p<0.05$.

Co-immunoprecipitation
A. thaliana and *N. benthamiana* protein was extracted, co-immunoprecipitated, and probed using methods described in (Weßling et al., 2014). 1 mL protein extraction was run through a single

μMACS (Miltenyi Biotec) column after labeling for *N. benthamiana* co-IP. 2 mL protein extraction was split into 2 columns for *A. thaliana* co-IP. Blots were probed with 1:500 dilutions of primary α-MYC (9E10, BioRad, Hercules, CA), 1:1.000 dilutions of α-GFP (Sigma-Aldrich), 1:1.000 dilutions of α-HA (Sigma-Aldrich), 1:10,000 dilutions of secondary anti-mouse IgG (A9044-2ML, Sigma-Aldrich, St. Louis, MO), and/or 1:10,000 of dilutions secondary anti-rabbit IgG.

RNA-Sequencing

For RNA-Seq analysis, RNA was prepared from 4 week old *A. thaliana* Col-0 plants heavily infected with 14 day old *G. orontii* spores through settling tower (Reuber et al., 1998) and three leaves were harvested for each time point at 6 hpi, 12 hpi, 24 hpi, 3 dpi, and 5 dpi. RNA was extracted using Qiagen RNeasy Plant Mini Kit (#74903/74904, Qiagen, Hilden, Germany). Briefly, leaf samples were ground using two 3 mm stainless steel balls for 1 min at 25 hertz/s and were immediately frozen in liquid nitrogen. RNA was isolated following directions from manufacturer's protocol and the on-column DNase digestion was performed using Qiagen RNase-Free DNase Set (#79254, Qiagen, Hilden, Germany). Stranded RNA-Seq library(s) were created and quantified by qPCR by DOE Joint Genome Institute as part of DOE JGI CSP #1657. Sequencing was performed at the JGI using Illumina HiSeq-2500 1TB 2x151. Raw fastq file reads were filtered and trimmed using the JGI QC pipeline resulting in the filtered fastq file. Quality trimming was performed using the phred trimming method set at Q6. Finally, following trimming, reads under the length threshold were removed with a minimum length 25 bases or one-third of the original read length, whichever is longer. Filtered reads from each library were aligned to the reference genome using HISAT2 version 2.1.0 [2] (BAMs/ directory) and FPKM normalized gene counts were calculated.

References

Baba, K., Nakano, T., Yamagishi, K., Yoshida, S., 2001. Involvement of a nuclear-encoded basic helix-loop-helix protein in transcription of the light-responsive promoter of psbD. Plant Physiology 125, 595–603. https://doi.org/10.1104/pp.125.2.595

Bernhofer, M., Goldberg, T., Wolf, S., Ahmed, M., Zaugg, J., Boden, M., Rost, B., 2018. NLSdb-major update for database of nuclear localization signals and nuclear export signals. Nucleic Acids Research 46, D503–D508. https://doi.org/10.1093/nar/gkx1021

Chandran, D., Inada, N., Hather, G., Kleindt, C.K., Wildermuth, M.C., 2010. Laser microdissection of Arabidopsis cells at the powdery mildew infection site reveals site-specific processes and regulators. Proceedings of the National Academy of Sciences of the United States of America 107, 460–465. https://doi.org/10.1073/pnas.0912492107

Chandran, D., Rickert, J., Cherk, C., Dotson, B.R., Wildermuth, M.C., 2013. Host Cell Ploidy Underlying the Fungal Feeding Site Is a Determinant of Powdery Mildew Growth and Reproduction. Molecular Plant-Microbe Interactions 26, 537–545. https://doi.org/10.1094/MPMI-10-12-0254-R

Chandran, D., Wildermuth, M.C., 2016. Modulation of Host Endocycle During Plant–Biotroph Interactions, Enzymes. https://doi.org/10.1016/bs.enz.2016.09.001

Chen, L., Fincher, G.B., Hoj, P.B., 1993. Evolution of polysaccharide hydrolase substrate specificity. Catalytic amino acids are conserved in barley 1,3-1,4- and 1,3-β-glucanases. Journal of Biological Chemistry 268, 13318–13326.

Clough, S.J., Bent, A.F., 1998. Floral dip: A simplified method for Agrobacterium-mediated transformation of Arabidopsis thaliana. Plant Journal 16, 735–743. https://doi.org/10.1046/j.1365-313X.1998.00343.x

Danisman, S., van Dijk, A.D.J., Bimbo, A., van der Wal, F., Hennig, L., de Folter, S., Angenent, G.C., Immink, R.G.H., 2013. Analysis of functional redundancies within the Arabidopsis TCP transcription factor family. Journal of Experimental Botany 64, 5673–5685. https://doi.org/10.1093/jxb/ert337

Dreze, M., Carvunis, A.-R., Charloteaux, B., Galli, M., Pevzner, S.J., Tasan, M., Ahn, Y.-Y., Balumuri, P., Barabasi, A.-L., Bautista, V., Braun, P., Byrdsong, D., Chen, H., Chesnut, J.D., Cusick, M.E., Dangl, J.L., de los Reyes, C., Dricot, A., Duarte, M., Ecker, J.R., Fan, C., Gai, L., Gebreab, F., Ghoshal, G., Gilles, P., Gutierrez, B.J., Hao, T., Hill, D.E., Kim, C.J., Kim, R.C., Lurin, C., MacWilliams, A., Matrubutham, U., Milenkovic, T., Mirchandani, J., Monachello, D., Moore, J., Mukhtar, M.S., Olivares, E., Patnaik, S., Poulin, M.M., Przulj, N., Quan, R., Rabello, S., Ramaswamy, G., Reichert, P., Rietman, E.A., Rolland, T., Romero, V., Roth, F.P., Santhanam, B., Schmitz, R.J., Shinn, P., Spooner, W., Stein, J., Swamilingiah, G.M., Tam, S., Vandenhaute, J., Vidal, M., Waaijers, S., Ware, D., Weiner, E.M., Wu, S., Yazaki, J., 2011. Evidence for Network Evolution in an Arabidopsis Interactome Map. Science 333, 601–607. https://doi.org/10.1126/science.1203877

Earley, K.W., Haag, J.R., Pontes, O., Opper, K., Juehne, T., Song, K., Pikaard, C.S., 2006. Gateway-compatible vectors for plant functional genomics and proteomics. Plant Journal 45, 616–629. https://doi.org/10.1111/j.1365-313X.2005.02617.x

Gaudioso-Pedraza, R., Benitez-Alfonso, Y., 2014. A phylogenetic approach to study the origin and evolution of plasmodesmata-localized glycosyl hydrolases family 17. Frontiers in Plant Science 5, 1–14. https://doi.org/10.3389/fpls.2014.00212

Grigoriev, I. v., Nikitin, R., Haridas, S., Kuo, A., Ohm, R., Otillar, R., Riley, R., Salamov, A., Zhao, X., Korzeniewski, F., Smirnova, T., Nordberg, H., Dubchak, I., Shabalov, I., 2014. MycoCosm portal: Gearing up for 1000 fungal genomes. Nucleic Acids Research 42, 699–704. https://doi.org/10.1093/nar/gkt1183

Gutie, R.A., Doerner, P., Li, C., Colon-Carmona, A., Potuschak, T., 2005. Arabidopsis TCP20 links regulation of growth and cell division control pathways. Proceedings of the National Academy of Sciences of the United States of America 102, 12978–12983.

Hur, Y.S., Kim, J., Kim, S., Son, O., Kim, W.Y., Kim, G.T., Ohme-Takagi, M., Cheon, C.I., 2019. Identification of TCP13 as an upstream regulator of ATHB12 during leaf development. Genes 10. https://doi.org/10.3390/genes10090644

Jakoby, M., Schnittger, A., 2004. Cell cycle and differentiation. Current Opinion in Plant Biology 7, 661–669. https://doi.org/10.1016/j.pbi.2004.09.015

Jones, L., Riaz, S., Morales-Cruz, A., Amrine, K.C., McGuire, B., Gubler, W., Walker, M., Cantu, D., 2014. Adaptive genomic structural variation in the grape powdery mildew pathogen, Erysiphe necator. BMC Genomics 15, 1081. https://doi.org/10.1186/1471-2164-15-1081

Klepikova, A. v., Kasianov, A.S., Gerasimov, E.S., Logacheva, M.D., Penin, A.A., 2016. A high resolution map of the Arabidopsis thaliana developmental transcriptome based on RNA-seq profiling. Plant Journal 88, 1058–1070. https://doi.org/10.1111/tpj.13312

Koyama, T., Mitsuda, N., Seki, M., Shinozaki, K., Ohme-takagi, M., 2010. TCP Transcription Factors Regulate the Activities of ASYMMETRIC LEAVES1 and miR164 , as Well as the

Auxin Response , during Differentiation of Leaves in Arabidopsis 22, 3574–3588. https://doi.org/10.1105/tpc.110.075598
Li, S., 2015. The Arabidopsis thaliana TCP transcription factors: A broadening horizon beyond development. Plant Signaling and Behavior 10, 1–12. https://doi.org/10.1080/15592324.2015.1044192
Li, Yu, Xia, T., Gao, F., Li, Yunhai, 2020. Control of Plant Branching by the CUC2/CUC3-DA1-UBP15 Regulatory Module. The Plant Cell 32, 1919–1932. https://doi.org/10.1105/tpc.20.00012
Lopez, J.A., Sun, Y., Blair, P.B., Mukhtar, M.S., 2015. TCP three-way handshake : linking developmental processes with plant immunity. Trends in Plant Science. https://doi.org/10.1016/j.tplants.2015.01.005
Minic, Z., 2008. Physiological roles of plant glycoside hydrolases. Planta 227, 723–740. https://doi.org/10.1007/s00425-007-0668-y
Navaud, O., Dabos, P., Carnus, E., Tremousaygue, D., Hervé, C., 2007. TCP transcription factors predate the emergence of land plants. Journal of Molecular Evolution 65, 23–33. https://doi.org/10.1007/s00239-006-0174-z
Peng, Y., Chen, L., Lu, Y., Wu, Y., Dumenil, J., Zhu, Z., 2015. The Ubiquitin Receptors DA1 , DAR1 , and DAR2 Redundantly Regulate Endoreduplication by Modulating the Stability of TCP14 / 15 in Arabidopsis 27, 649–662. https://doi.org/10.1105/tpc.114.132274
Reuber, T.L., Plotnikova, J.M., Dewdney, J., Rogers, E.E., William Wood, B., Ausubel, F.M., 1998. Correlation of defense gene induction defects with powdery mildew susceptibility in Arabidopsis enhanced disease susceptibility mutants. Plant Journal 16, 473–485. https://doi.org/10.1046/j.1365-313X.1998.00319.x
Spanu, P.D., Abbott, J.C., Amselem, J., Burgis, T.A., Soanes, D.M., Stüber, K., van Themaat, E.V.L., Brown, J.K.M., Butcher, S.A., Gurr, S.J., Lebrun, M.H., Ridout, C.J., Schulze-Lefert, P., Talbot, N.J., Ahmadinejad, N., Ametz, C., Barton, G.R., Benjdia, M., Bidzinski, P., Bindschedler, L. v., Both, M., Brewer, M.T., Cadle-Davidson, L., Cadle-Davidson, M.M., Collemare, J., Cramer, R., Frenkel, O., Godfrey, D., Harriman, J., Hoede, C., King, B.C., Klages, S., Kleemann, J., Knoll, D., Koti, P.S., Kreplak, J., López-Ruiz, F.J., Lu, X., Maekawa, T., Mahanil, S., Micali, C., Milgroom, M.G., Montana, G., Noir, S., O'Connell, R.J., Oberhaensli, S., Parlange, F., Pedersen, C., Quesneville, H., Reinhardt, R., Rott, M., Sacristán, S., Schmidt, S.M., Schön, M., Skamnioti, P., Sommer, H., Stephens, A., Takahara, H., Thordal-Christensen, H., Vigouroux, M., Weßling, R., Wicker, T., Panstruga, R., 2010. Genome expansion and gene loss in powdery mildew fungi reveal tradeoffs in extreme parasitism. Science 330, 1543–1546. https://doi.org/10.1126/science.1194573
Stark, C., Breitkreutz, B.J., Reguly, T., Boucher, L., Breitkreutz, A., Tyers, M., 2006. BioGRID: a general repository for interaction datasets. Nucleic acids research 34, 535–539. https://doi.org/10.1093/nar/gkj109
Steiner, E., Efroni, I., Gopalraj, M., Saathoff, K., Tseng, T., Kieffer, M., Eshed, Y., Olszewski, N., Weiss, D., 2012. The Arabidopsis O -Linked N- Acetylglucosamine Transferase SPINDLY Interacts with Class I TCPs to Facilitate Cytokinin Responses in Leaves and Flowers 24, 96–108. https://doi.org/10.1105/tpc.111.093518
Steiner, E., Livne, S., Kobinson-Katz, T., Tal, L., Pri-Tal, O., Mosquna, A., Tarkowská, D., Mueller, B., Tarkowski, P., Weiss, D., 2016. The putative O-linked N-acetylglucosamine

transferase SPINDLY inhibits class I TCP proteolysis to promote sensitivity to cytokinin. Plant Physiology 171, 1485–1494. https://doi.org/10.1104/pp.16.00343

Sugio, A., Kingdom, H.N., MacLean, A.M., Grieve, V.M., Hogenhout, S.A., 2011. Phytoplasma protein effector SAP11 enhances insect vector reproduction by manipulating plant development and defense hormone biosynthesis. Proceedings of the National Academy of Sciences of the United States of America 108, 1–10. https://doi.org/10.1073/pnas.1105664108

Sugio, A., Maclean, A.M., Hogenhout, S.A., 2014. The small phytoplasma virulence effector SAP11 contains distinct domains required for nuclear targeting and CIN-TCP binding and destabilization. New Phytologist 202, 838–848. https://doi.org/10.1111/nph.12721

Tanaka, Y., Kimura, T., Hikino, K., Goto, S., Nishimura, M., Mano, S., Nakagaw, T., 2012. Gateway Vectors for Plant Genetic Engineering: Overview of Plant Vectors, Application for Bimolecular Fluorescence Complementation (BiFC) and Multigene Construction. Genetic Engineering - Basics, New Applications and Responsibilities. https://doi.org/10.5772/32009

Vercruysse, J., Baekelandt, A., Gonzalez, N., Inzé, D., 2020. Molecular networks regulating cell division during Arabidopsis leaf growth. Journal of Experimental Botany 71, 2365–2378. https://doi.org/10.1093/jxb/erz522

Vlieghe, K., Boudolf, V., Beemster, G.T.S., Maes, S., Magyar, Z., Atanassova, A., de Almeida Engler, J., de Groodt, R., Inzé, D., de Veylder, L., 2005. The DP-E2F-like Gene DEL1 Controls the Endocycle in Arabidopsis thaliana. Current Biology 15, 59–63. https://doi.org/10.1016/j.cub.2004.12.038

W, D.A.C., Danisman, S., Wal, F. van der, Dhondt, S., Waites, R., Folter, S. de, Bimbo, A., Dijk, A.D.J. van, Muino, J.M., Cutri, L., Dornelas, M.C., Angenent, G.C., Immink, R.G.H., 2012. Arabidopsis Class I and Class II TCP Transcription Factors Regulate Jasmonic Acid Metabolism and Leaf 159, 1511–1523. https://doi.org/10.1104/pp.112.200303

Wang, S., Li, W., Liu, S., Xu, J., 2016. RaptorX-Property: a web server for protein structure property prediction. Nucleic acids research 44, W430–W435. https://doi.org/10.1093/nar/gkw306

Weßling, R., Epple, P., Altmann, S., He, Y., Yang, L., Henz, S.R., McDonald, N., Wiley, K., Bader, K.C., Gläßer, C., Mukhtar, M.S., Haigis, S., Ghamsari, L., Stephens, A.E., Ecker, J.R., Vidal, M., Jones, J.D.G., Mayer, K.F.X., ver Loren Van Themaat, E., Weigel, D., Schulze-Lefert, P., Dangl, J.L., Panstruga, R., Braun, P., 2014. Convergent targeting of a common host protein-network by pathogen effectors from three kingdoms of life. Cell Host and Microbe 16, 364–375. https://doi.org/10.1016/j.chom.2014.08.004

Weßling, R., Panstruga, R., 2012. Rapid quantification of plant-powdery mildew interactions by qPCR and conidiospore counts. Plant Methods 8, 35. https://doi.org/10.1186/1746-4811-8-35

Wildermuth, M.C., 2010. Modulation of host nuclear ploidy: A common plant biotroph mechanism. Current Opinion in Plant Biology 13, 449–458. https://doi.org/10.1016/j.pbi.2010.05.005

Wildermuth, M.C., Steinwand, M.A., McRae, A.G., Jaenisch, J., Chandran, D., 2017. Adapted Biotroph Manipulation of Plant Cell Ploidy. Annual Review of Phytopathology 55, 537–564. https://doi.org/10.1146/annurev-phyto-080516-035458

Yang, L., Teixeira, P.J.P.L., Biswas, S., Finkel, O.M., He, Y., Salas-Gonzalez, I., English, M.E., Epple, P., Mieczkowski, P., Dangl, J.L., 2017. Pseudomonas syringae Type III Effector

HopBB1 Promotes Host Transcriptional Repressor Degradation to Regulate Phytohormone Responses and Virulence. Cell Host and Microbe 21, 156–168. https://doi.org/10.1016/j.chom.2017.01.003

Zhang, J., Li, L., Lv, Q., Yan, L., Wang, Y., Jiang, Y., 2019. The fungal CYP51s: Their functions, structures, related drug resistance, and inhibitors. Frontiers in Microbiology 10. https://doi.org/10.3389/fmicb.2019.00691

Table 1. *G. orontii* TCP-targeting effectors selected for spray-induced gene silencing. [1]*G. orontii* MGH1 genome accessed through MycoCosm (Grigoriev et al., 2014), [2](Bernhofer et al., 2018), [3](Weßling et al., 2014).

Effector	Copy number[1]	Annotation[1,2]	*G. orontii* MPIPZ OEC-TCP interactions identified via yeast-two hybrid[2]	OEC homologs in other species[1,3]
OEC14	2	RNAse-like effector, nuclear localization signal (RIKRR)	TCP20	Powdery mildews including *G. cichoracearum, E. pisi, E. necator*
OEC21	2	RNAse-like effector	TCP14, TCP15, TCP20, HB21, CSN5A	Powdery mildews including *G. cichoracearum, E. pisi*
OEC27/ OEC39	7	RNAse-like effector	TCP9, TCP14, TCP15	Powdery mildews including *G. cichoracearum*
OEC59/ OEC68	2		TCP20, TPR8	Powdery mildews including *G. cichoracearum, E. pisi, E. necator*
OEC60/ OEC61	2	glycosyl hydrolase family 17 (GH17)	TCP13, TCP14, CSN5A, SBP	Powdery mildews including *G. cichoracearum, E. necator, E. pisi, B. graminis* f. sp. *hordei,* and *B. graminis* f. sp. *triticum* (BEC1005); Other fungal pathogens, GH17 domain-containing proteins are widely present and secreted in fungi however the region upstream of the GH17 domain (containing *G. orontii* MPIPZ OEC60 or OEC61 sequence) has only been identified in powdery mildews
OEC70	2		TCP9, TCP14, CSN5A, ASIL1, RCN1, UBQ-like gene	Powdery mildews including *G. cichoracearum, E. pisi, E. necator*
OEC119	2		TCP14, TCP20, RCN1, PP2AA2	Powdery mildews including *G. cichoracearum*

Table 2. TCP transcription factor gene information and targeting effectors. [1](Lopez et al., 2015), [2](Weßling et al., 2014).

Arabidopsis thaliana TCP[1]	Gene Locus	TCP interactions identified via yeast-two hybrid[2]
TCP9 (Class I)	AT2G45680	OEC27, OEC39, OEC49, OEC70, OEC76
TCP13 (Class II)	AT3G02150	OEC45, OEC61
TCP14 (Class I)	AT3G47620	OEC16a, OEC21, OEC27, OEC35, OEC39, OEC45, OEC55, OEC60, OEC70, OEC101, OEC110, OEC117, OEC119, OEC120, OEC123, OEC125
TCP15 (Class I)	AT1G69690	OEC21, OEC39
TCP20 (Class I)	AT3G27010	OEC14, OEC21, OEC68, OEC77, OEC119

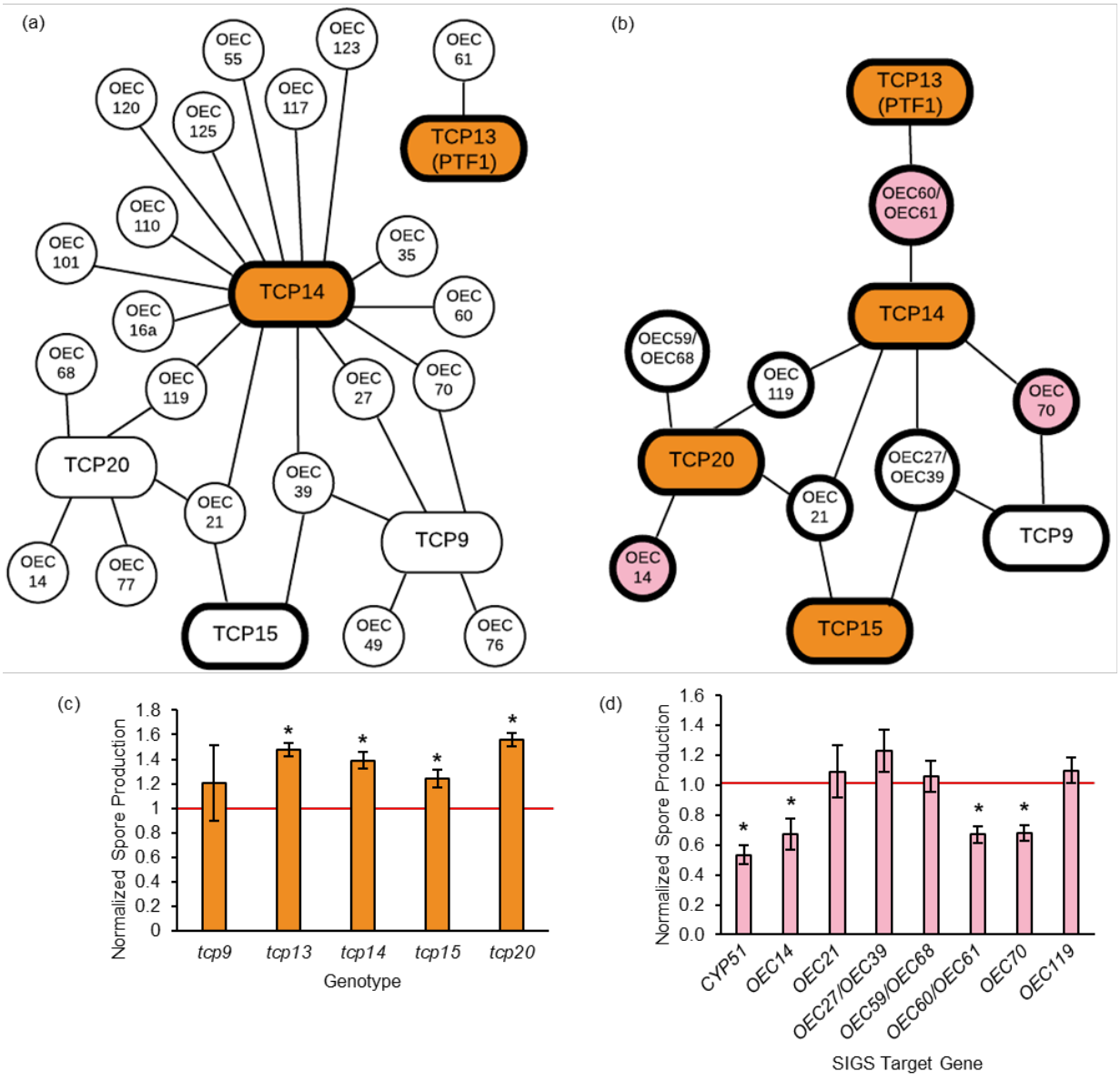
(a)
OEC 55
OEC 123
OEC 61
OEC 120
OEC 117
OEC 125
TCP13 (PTF1)
OEC 110
OEC 101
OEC 35
TCP14
OEC 60
OEC 16a
OEC 68
OEC 119
OEC 27
OEC 70
TCP20
OEC 39
OEC 21
TCP9
OEC 14
OEC 77
TCP15
OEC 49
OEC 76
(b)
TCP13 (PTF1)
OEC60/ OEC61
TCP14
OEC59/ OEC68
OEC 119
OEC 70
TCP20
OEC27/ OEC39
OEC 21
TCP9
OEC 14
TCP15
(c)
Normalized Spore Production
1.8
1.6
1.4
1.2
1
0.8
0.6
0.4
0.2
0
tcp9
tcp13
tcp14
tcp15
tcp20
Genotype
(d)
Normalized Spore Production
1.6
1.4
1.2
1.0
0.8
0.6
0.4
0.2
0.0
CYP51
OEC14
OEC21
OEC27/OEC39
OEC59/OEC68
OEC60/OEC61
OEC70
OEC119
SIGS Target Gene

Fig. 1. Powdery mildew infection assays identify *A. thaliana* TCP transcription factor and *G. orontii* effector (OEC) genes contributing to spore production. (a) TCP-OEC Protein interaction map and associated powdery mildew spore production phenotypes Interactions were identified by yeast-two hybrid using *G. orontii* MPIPZ effectors (Weßling et al., 2014). Effector homologs not identified in *G. orontii* MGH1 are omitted. The genetic contribution to spore production of all genes inside bolded shapes were measured in *G. orontii* MPIPZ infection of *A. thaliana* experiments. TCP ovals shaded if associated adult *tcp* mutant has enhanced powdery mildew spore production. *tcp15* mutant seedlings have enhanced disease susceptibility (Weßling et al., 2014). (b) *G. orontii* MGH1 effector-TCP interactions inferred from *G. ororntii* MPIPZ interactions (Weßling et al., 2014) investigated in this study. The genetic contribution to spore production of all genes inside bolded shapes were measured in *G. orontii* MGH1 infection of *A. thaliana* adult plant experiments. TCP ovals shaded if associated *tcp* mutant has enhanced powdery mildew spore production. OEC circles are shaded to indicate less spore production when homologs of OECs were targeted using spray-induced gene silencing. (c) *G. orontii* MGH1 spore production on T-DNA insertion *tcp* mutants. Average normalized spore production of $n \geq 6$ displayed ±SE. (d) Spore production of *G. orontii* MGH1 when targeting homologs of OECs using spray-induced gene silencing. *CYP51* is included as a positive control gene required for fungal growth. Average normalized spore production of $n \geq 3$ displayed ±SE. *$p<0.05$ by Student's T-Test (unpaired, 2-sided).

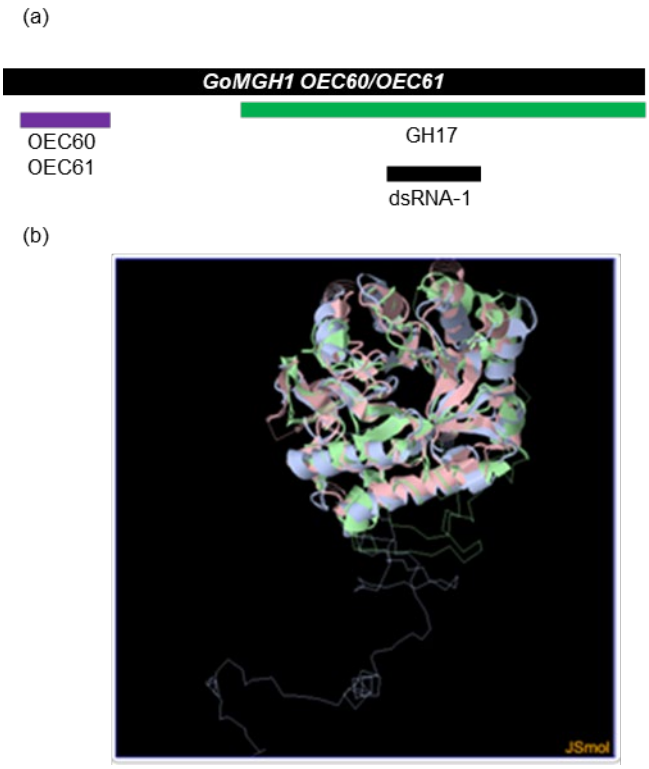

Fig. 2. *G. orontii* MGH1 OEC60/OEC61 homologs have a glycosyl hydrolase family 17 domain. (a) *G. orontii* MGH1 *OEC60/OEC61* is 1359 bp. GH17 domain is present at 502-1338 bp. *G. orontii* MPIPZ OEC60/OEC61 homology extends over 55-227 bp. (b) RaptorX protein structure prediction (Wang et al., 2016) model for *G. orontii* MGH1 protein ID 4531743 (blue) aligned with Barley endoglucanase (GH17) (green, PDB ID:1ghs) and *Rhizomucor miehei* glycoside hydrolase family 17 beta-1,3-glucanosyltransferase which had the highest scored protein structure in the Protein Databank (Pink, PBD ID: 4wtp).

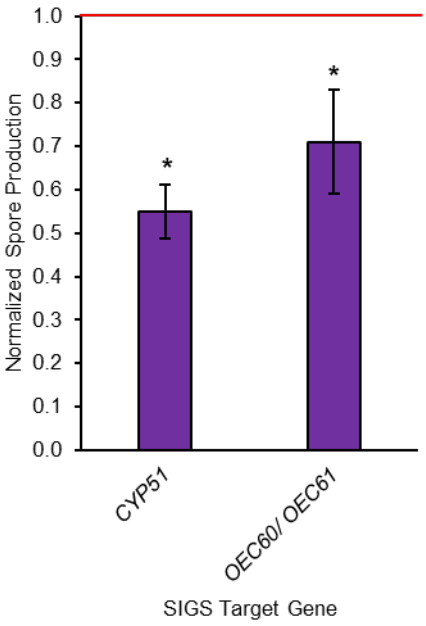

Fig. 3. Long dsRNA targeting homolog of *OEC60/OEOC61* in *E. necator* reduces spore production on *V. vinifera* leaf discs. Average normalized spore production displayed from n=4. Spore suspension concentrations were normalized to the input tissue weight (g) before being normalized to the control. *CYP51* is included as a positive control gene required for growth. Error bars ± SEM. *$p<0.05$ by Student's T-Test (unpaired, 2-sided) compared to control.

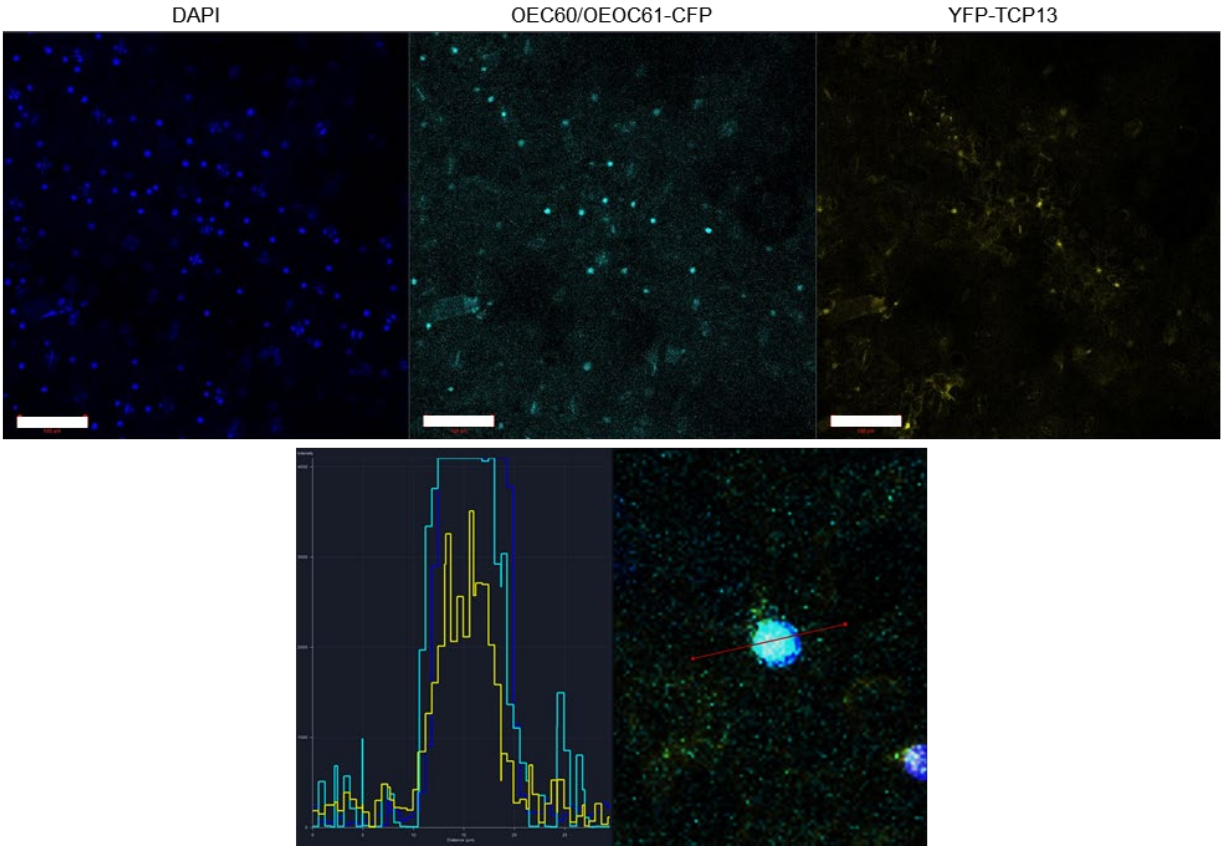

Fig. 4. *G. orontii* MGH1 homolog of OEC60/OEC61 colocalizes with TCP13 in plant nuclei. YFP-TCP13 and OEC60/OEC61-CFP were co-expressed in *Nicotiana benthamiana* leaf tissue using Agrobacterium-mediated transient expression. Before microscopy, DAPI was infiltrated into tissue to stain DNA and highlight the nuclei. Top panel: Individual fluorescence channels of co-infiltrated leaf tissue. Scale bar is 100 µm. Bottom panel: Red vector (30 µm) drawn through a nucleus of a merged image from top panel shows strong nuclear accumulation of fluorescence signal for DAPI, YFP, and CFP channels.

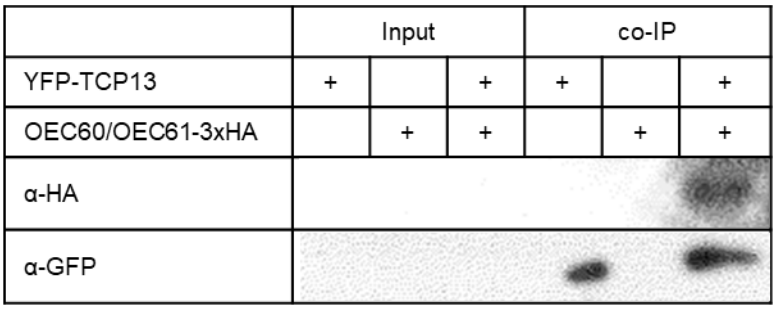

Fig. 5. *A. thaliana* TCP13 interacts *in planta* with *G. orontii* MGH1. YFP-TCP13 and OEC60/OEC61-3xHA were co-expressed in *Nicotiana benthamiana* leaf tissue using Agrobacterium-mediated transient expression. Co-immunoprecipitation was performed to purify GFP-containing protein complexes. Western blot shows HA and GFP detection.

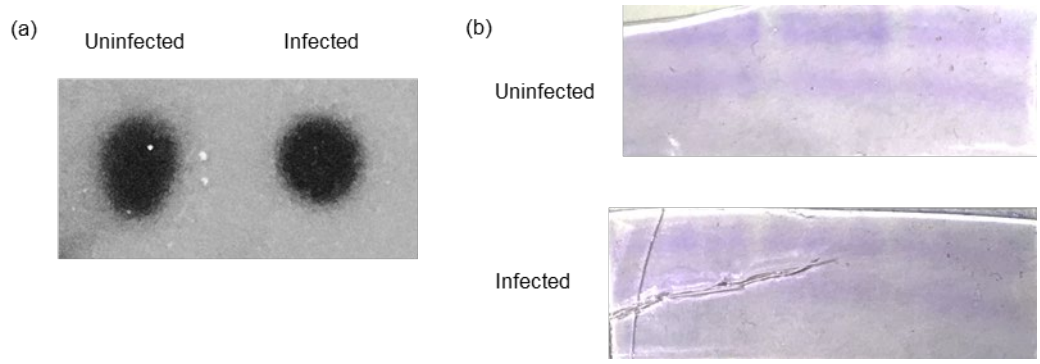

Fig. 6. Co-immunoprecipitation of *G. orontii* MGH1 homolog of OEC60/OEC61 from *A. thaliana* transgenic plants expressing OEC60/OEC61-MYC successfully precipitates multiple proteins. (a) Western blot confirms precipitation of MYC-tagged protein from infected and uninfected *A. thaliana* leaf tissue. (b) Coomassie-stained SDS-PAGE gel shows multiple protein bands indicating multiple proteins co-immunoprecipitated with OEC60/OEC61-MYC.

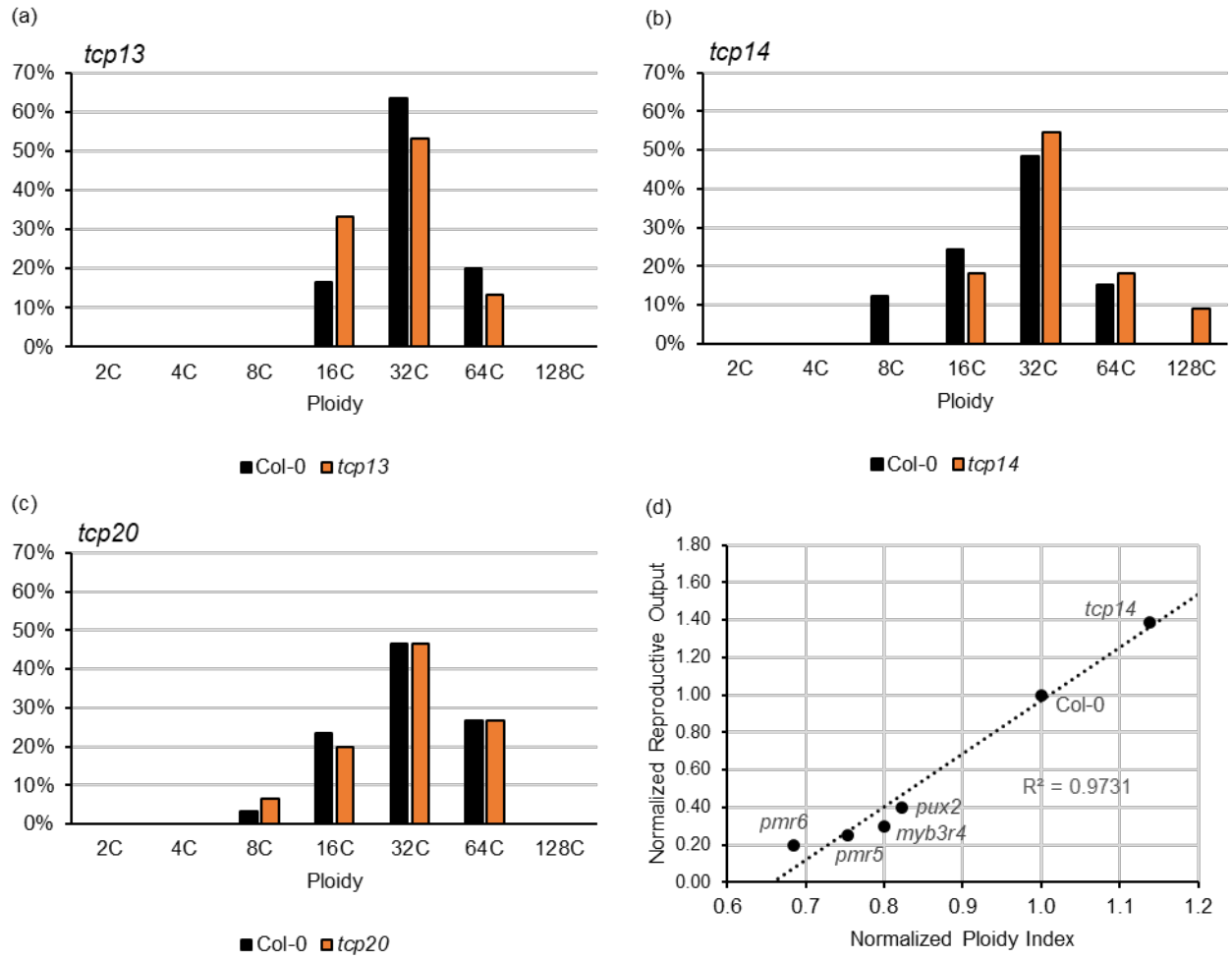

Fig. 7. *tcp14* mutant has elevated ploidy at the site of powdery mildew infection that is correlated with the enhanced spore production supported by this mutant. (a-c) DNA content distributions of mesophyll cells underlying powdery mildew infection site of *tcp13* (a), *tcp14* (b), *tcp20* (c). n=30 nuclei from one experiment. Statistical significance determined by Mann-Whitney Test for Two Independent Samples with $p<0.05$. (d) Normalized reproductive output (conidiophore/colony for *pmr5, pmr6, pux2,* and *myb3r4* (Chandran et al., 2013) or spore production for *tcp14*) plotted against normalized mesophyll ploidy index at the site of *G. orontii* MGH1 infection of *A. thaliana* at 5 dpi.

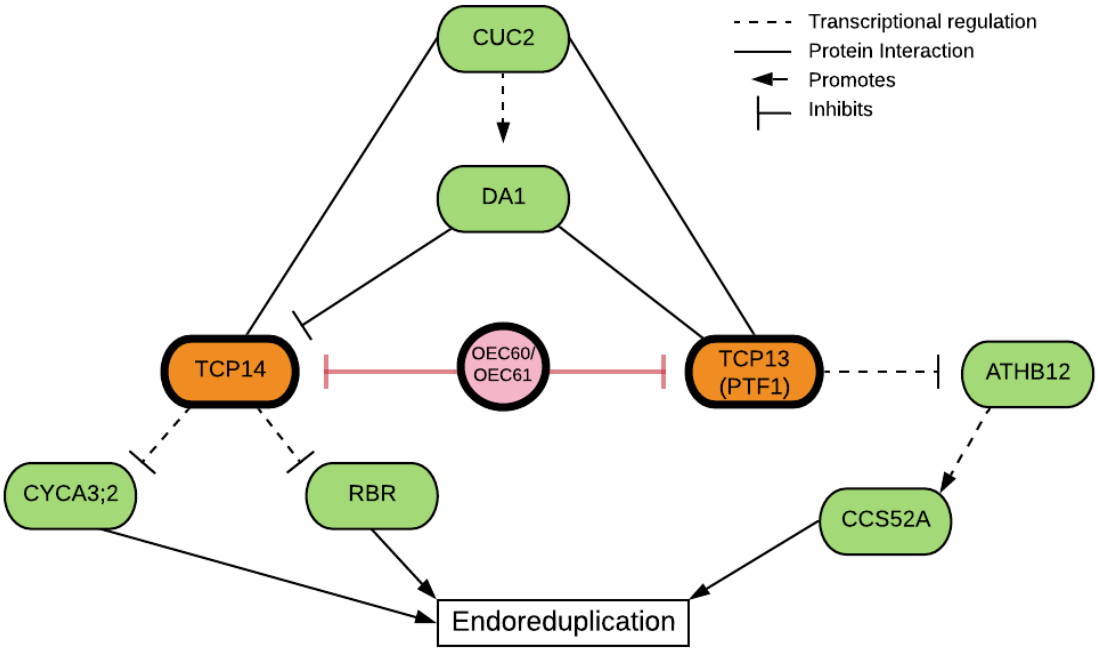

Fig. 8. Proposed simple model of TCP13 and TCP14 mediated powdery mildew-induced endoreduplication. Red lines indicate proposed relationships. OEC60/OEC61 is proposed to interact with TCP14 and TCP13 to limit their activity. OEC60/OEC61 activity could modulate TCP13 and TCP14 interaction with CUC2 to increase *DA1* expression. This could promote DA1 activity to degrade TCP14, a known negative regulator of endoreduplication which suppresses expression of *RBR* and *CYCA3;2*. TCP13 inhibition/degradation could increase the expression of *ATHB12*, a positive regulator of *CCS52A2* involved in endoreduplication. The limited model does not include all potential impacts of TCP14 and TCP13 inhibition/degradation. See text for additional details.

SI Table 1. Powdery mildew gene information. [1]*G. orontii* MGH1 and *E. necator* c genomes accessed through MycoCosm (Grigoriev et al., 2014).

Powdery Mildew Species	Gene	Protein ID[1]	Annotated Domains[1]	Enzyme Commission Number (EC)[1]	Secretion Signal by SignalP[1] (Amino Acid Cleavage Site)	Gene Length (bp)
Golovinomyces orontii MGH1	*CYP51*	2912305	cytochrome P450	1.14.14.154	N	1578
		2918117	cytochrome P450	1.14.14.154	N	1578
	OEC14	4149374			Y (19/20)	654
		4151953			Y (23/24)	642
	OEC21	4150772			Y (22/23)	531
		1829066			Y (22/23)	531
	OEC 27/ OEC 39	4300314			Y (22/23)	453
		4465085			Y (22/23)	453
		4575775			Y (22/23)	489
		1624466			Y (20/21)	363
		4163222			Y (22/23)	489
		4148210			Y (22/23)	363
		5230192			Y (22/23)	486
	OEC 59/ OEC 68	4590467			Y (58/59)	633
		5337153			Y (18/19)	819
	OEC 60/ OEC 61	4531743	glycosyl hydroase family 17	3.2.1.58	Y (18/19)	1359
		4808639	glycosyl hydroase family 17	3.2.1.58	Y (18/19)	1359
	OEC 70	5103140			Y (18/19)	318
		5394824			Y (18/19)	318
	OEC119	743938			Y (25/26)	495
		2411758			Y (25/26)	378
Erysiphe necator c	*CYP51*	1462	cytochrome P450	1.14.14.154	N	1575
	OEC 60/ OEC 61	2081	glycosyl hydroase family 17	3.2.1.58	Y (18/19)	1353

SI Table 2. TCP13 and TCP14 protein interactions in common. Interactions identified in BioGRID (Stark et al., 2006).

Common TCP13 and TCP14 protein interactions			
AT1G03040	AT2G25620	AT4G10240	AT1G76760
AT1G04250	AT2G29580	AT4G16780	AT1G77920
AT1G05710	AT2G31070	AT4G17460	AT2G02060
AT1G07360	AT2G32160	AT4G18390	AT2G02450
AT1G08970	AT2G33290	AT4G27330	AT2G03500
AT1G11650	AT2G33610	AT4G29100	AT2G04038
AT1G13450	AT2G33710	AT4G33450	AT2G04890
AT1G14030	AT2G33835	AT4G34740	AT2G13570
AT1G14920	AT2G33860	AT4G34990	AT2G17950
AT1G16640	AT2G36000	AT4G35250	AT5G66940
AT1G17590	AT2G36026	AT4G36260	AT5G67180
AT1G19270	AT2G37000	AT4G36540	AT3G50700
AT1G19860	AT2G38130	AT4G37180	AT3G51080
AT1G20700	AT2G40260	AT4G37740	AT3G55980
AT1G23420	AT2G41690	AT4G37940	AT3G57230
AT1G24625	AT2G41940	AT5G04820	AT3G61920
AT1G26780	AT2G45680	AT5G05120	AT4G00870
AT1G28360	AT2G45850	AT5G05790	AT4G01460
AT1G30210	AT2G46130	AT5G06160	AT4G01920
AT1G30460	AT2G46735	AT5G08070	AT4G08150
AT1G30490	AT2G47450	AT5G09750	AT5G63090
AT1G30500	AT2G47700	AT5G12980	AT5G65210
AT1G35490	AT3G01220	AT5G14170	AT5G42470
AT1G35560	AT3G01970	AT5G17300	AT5G42910
AT1G46480	AT3G07740	AT5G17800	AT5G51910
AT1G53230	AT3G11580	AT5G23000	AT5G53950
AT1G58100	AT3G13960	AT5G23280	AT5G54360
AT1G66810	AT3G15030	AT5G25160	AT5G59570
AT1G68150	AT3G15210	AT5G25220	AT5G59990
AT1G68360	AT3G16250	AT5G26650	AT5G60120
AT1G69570	AT3G19070	AT5G26749	AT5G60970
AT1G69690	AT3G21150	AT5G27910	AT5G61380
AT1G69810	AT3G24490	AT5G28640	AT5G39660
AT1G72210	AT3G24520	AT5G35900	AT3G49940
AT1G72570	AT3G27010	AT5G37260	AT1G75520
AT1G75080	AT3G47620	AT5G38800	

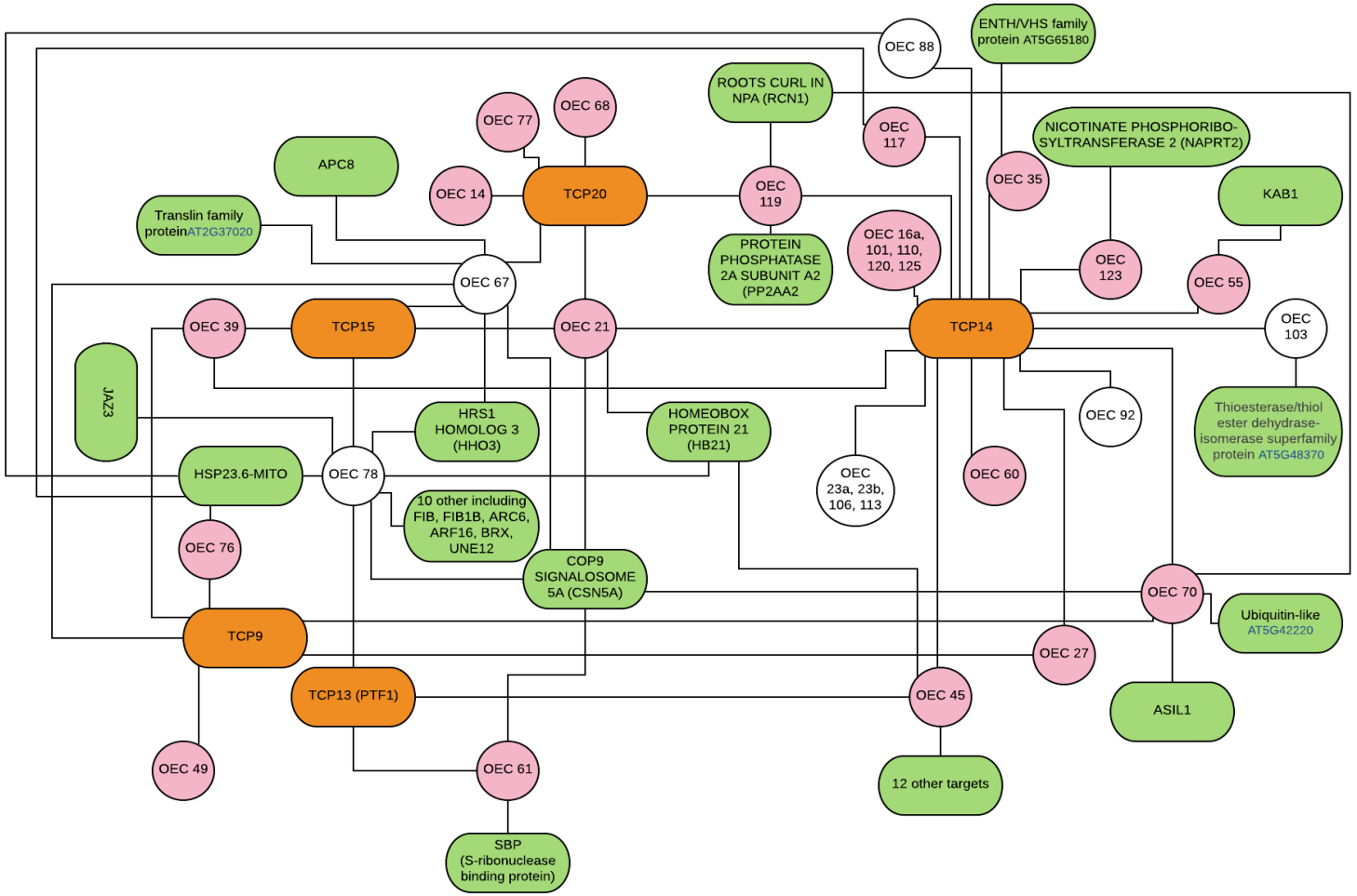

SI Fig. 1. The TCP-targeting *G. orontii* MPIPZ effector (OEC) interactome identified by (Weßling et al., 2014). This includes protein-protein interactions with TCP-targeting *G. orontii* MPIPZ effectors (OECs) identified in the study. Homologs of purple/shaded OECs have been identified in *G. orontii* MGH1. Homologs of white/unshaded OECs have not been identified in *G. orontii* MGH1. Multiple genes are sometimes listed in one bubble fit all the interactors.

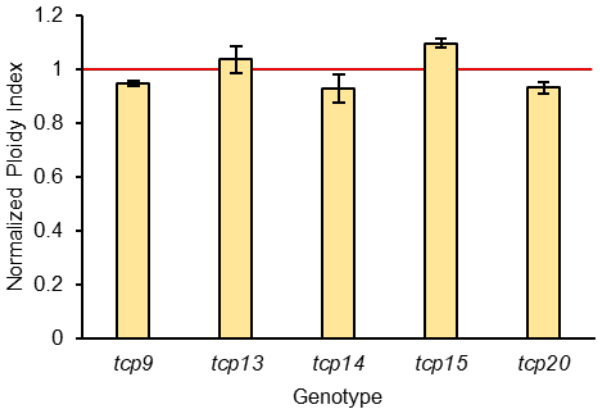

SI Fig. 2. Whole leaf ploidy analysis of adult *A. thaliana tcp* mutants. Ploidy distributions were determined using flow cytometry to measure DAPI fluorescence signal of nuclei isolated from the 8th leaf of 4.5 week old uninfected plants. Normalized average Ploidy Index ((%2C*0)+(%4C*1)+(%8C*2)+(%16C*3)+(%32C*4)+(%64C*5)) is displayed for n=3 from one experiment. A Student's T-test (unpaired, 2-sided) was used to determine statistical significance ($p<0.05$). An independent experiment showed similar results.

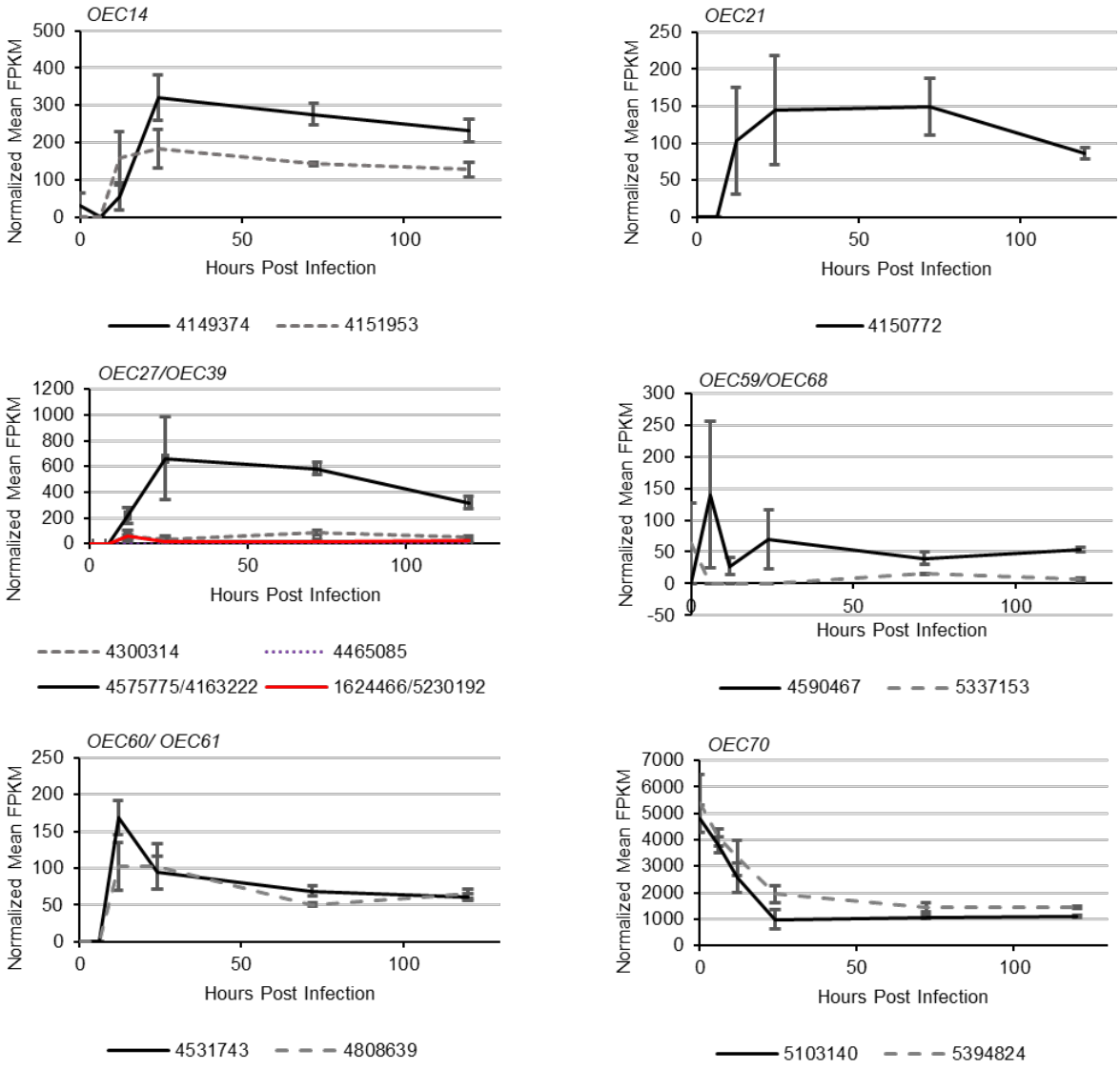

SI Fig. 3. *G. orontii* MGH1 effector expression during infection at 0, 6, 12, 24, 72, and 120 hours post infection. Mean normalized FPKM (fragments per kilobase of exon per million reads) with n=3 is displayed for each gene, ±SEM, for each gene indicated by protein ID for *G. orontii* MGH1 v4.0 annotated and accessed through MycoCosm (Grigoriev et al., 2014). Gene copies are omitted if not identified in RNA-Seq.

Chapter 5: Conclusion

Summary and Future Directions

Interrogation into the genetic and metabolic interactions between *G. orontii* and *A. thaliana* reveals a highly fine-tuned interface at the intersection of metabolism, defense, and the cell cycle. The complete mechanisms underlying these processes still remains to be uncovered, but the research described here provides insight and additional tools to further uncover how powdery mildews alter host physiology to facilitate nutrient acquisition (Fig. 1). Genetics in both the plant and fungal side of this plant pathogenic interaction are perturbed to elucidate how the powdery mildew infection site supports the reproduction of powdery mildew fungi. The powdery mildew, *G. orontii* MGH1 now has a published high-resolution genome that has been annotated by the Joint Genome Institute and accessed through MycoCosm (Grigoriev et al., 2014). This was utilized to identify and prioritize genes of interest to examine and eventually design primers for cloning and synthesizing RNAs for gene silencing. Combined with the genetic resources available for *A. thaliana* this plant pathogen interaction provides a great system to explore the important factors mediating pathogenesis to provide a deeper understanding of this complex symbiosis.

Previous work in the Wildermuth lab uncovered *G. orontii* MGH1 relies on host endoreduplication to fuel its reproduction (Chandran et al., 2013, 2010) and as a result, specific metabolic pathways are upregulated in response to infection. In Wildermuth et al., 2017, we further explore microbe-induced endoreduplication and found it is a widespread phenotype observed in plant tissue surrounding the infection site of biotrophs (Appendix 1). Induced endoreduplication transforms the host tissue into a feeding site for nutrient uptake. Evolutionary distant microbes promote this transformation to support their colonization, development, and proliferation. Manipulation of endocycle entry at the G_2/M transition point is a common intervention point to induce endoreduplication (Wildermuth et al., 2017). Enhanced endoreduplication is associated with enhanced metabolic capacity. With this in mind, we explored the pyruvate dehydrogenase (PDH) bypass, an upregulated metabolic pathway at the powdery mildew infection site. We hypothesized metabolites from this pathway are important in supporting powdery mildew reproduction. In Chapter 2, we found PDH bypass enzymes are important in supporting the growth of the fungus, however, the viability and development of powdery mildew growing on PDH bypass mutant plants is not impacted, indicating fungal asexual reproduction is constrained and regulated by the metabolic capacity of the host. The proliferation of the fungus is tied to the PDH bypass capacity in a dosage-dependent manner. Additionally, we found carbon derived from the plant PDH bypass is incorporated into spore lipids. Future work will explore what metabolites specifically are acquired by powdery mildews and how they sense metabolite availability to fine tune their development. The PDH bypass produces lipid precursors, but it is unknown what lipid intermediate(s) make it into the fungus before fungal manipulation. For example, this intermediate could be the precursor itself (Acetate/Acetyl-CoA), free fatty acids, mono-/di-/tri-acyclglycerols, phospholipids, a specific derivation of the aforementioned, or a combination. There is also the question if endoreduplication simply increases the metabolic output providing all these metabolites for the fungus or if there is specific manipulation from the fungus to provide certain chemistries. This work will build our understanding of pathogen requirements which can help us design intervention points to prevent disease.

In Chapter 3, we developed a rapid discovery platform to identify genes in powdery mildew fungi that promote pathogenesis. This allowed us to also more rapidly study powdery mildew genetics as there are constraints in manipulating an obligate biotroph with no known culturing methods to propagate it independent of the host. Using RNA interference, we can spray dsRNA targeting powdery mildew genes onto infected plants to limit powdery mildew growth. We identified several novel gene targets in *G. orontii* and translated these methods and targets to *E. necator*, the cause of grape powdery mildew. Gene targets are now being used to inform applied research into controlling powdery mildew disease of agriculturally important plants, particularly for grapevine which is a $3.8 billion industry annually in California alone (Fuller et al., 2014). Powdery mildew is the most prevalent and costly grape disease in the state for wine grapes as well as raisin and table grapes. *E. necator* is often controlled by rotating treatments of sulfur and various fungicides. Although disease is usually effectively managed to produce a desirable crop, there is a need for additional fungicides with novel modes of action to minimize resistance emergence in the field (Frenkel et al., 2015). Sulfur is quite effective and cheap but there are health risks associated with application to the workers and the surrounding communities (Raanan et al., 2017). There are also limitations in using current fungicides late in the season due to minimum residue limitations which can prevent the use of a crop. RNA pesticides may provide superior benefits to what is currently on the market. RNA may be safer than traditional fungicides as they can be designed target specific organisms are readily degraded in the environment (Bramlett et al., 2020). Using our system, we plan to identify more conserved powdery mildew targets and improve the efficacy of spray-induced gene silencing to determine if it is a viable control method in the field (e.g. for grapevine powdery mildew.

Genetic contributors to powdery mildew-induced endoreduplication have been identified (Chandran et al., 2010; 2013; Wildermuth et al., 2017), however, genetic investigations into this process have been restricted to the host plant. Using methods developed in Chapter 3, powdery mildew-host interactions could be perturbed from the pathogen side of the interaction to uncover powdery mildew genetic contributors of growth and manipulation of the host cell cycle. *G. orontii* effectors that interact with cell cycle regulators via yeast 2-hybrid were prioritized for this study (Weßling et al., 2014). Host plant TCP transcription factors are known regulators of growth and development with some members having direct described roles in suppressing endoreduplication, namely TCP14 and TCP15 (Peng et al., 2015). There are 24 members of this protein family in *A. thaliana*, and they often appear to be redundant in function, with the need for multiple *TCP* genes to be disrupted to see a phenotype. TCPs are divided into two classes, class I and class II which have been categorized as behaving antagonistically: class I TCPs promote growth, while class II TCPs suppress growth (Lopez et al., 2015). Despite these generalities, we identified TCPs with individual contributions to powdery mildew disease and powdery mildew-induced endoreduplication and found members belonging to different classes (TCP13 and TCP14) to similarly impact powdery mildew asexual reproduction. This aligns with a recent comprehensive study of *A. thaliana* TCPs. van Es and colleagues described the role of TCPs in plant development over the complete *A. thaliana* lifecycle (2019). They suggest the broad categorization of opposite functions for class I and II TCPs needs revision. Furthermore, they show closely related TCPs do not necessarily have full genetic redundancy due to the complexity of interactions of TCPs that is context dependent (van Es et al., 2019). The powdery mildew infection site provides a unique context to explore functional TCP nodes as we examine an induced response in mature fully expanded leaves; thereby limiting some of the redundancy observed for TCP nodes during normal

plant development. Our analysis reveals *TCP13, TCP14, TCP15,* and *TCP20* are all suppressors of powdery mildew proliferation and furthermore that *TCP14* is a suppressor of powdery mildew-induced endoreduplication. This is especially significant given, both *TCP14* and *TCP15* need to be disrupted to enhance leaf ploidy; individual mutants have wildtype ploidy (Peng et al., 2015). Powdery mildew OEC60/OEC61 targets both class I and class II TCPs, TCP13 and TCP14 which have a highly overlapping set of known protein interactors. Future work will reveal what proteins interact with OEC60/OEC61 in *A. thaliana* to further investigate the link between effectors and TCP-mediated powdery mildew endoreduplication. Homologs of OEC60/OEC61 are found in plants and fungi due to the presence of a glycosyl hydrolase family 17 domain (Gaudioso-Pedraza and Benitez-Alfonso, 2014); the small N-terminal domain originally identified by Weßling et al., 2014. When OEC60/OEC61 is silenced, powdery mildew spore production is reduced in both *G. orontii* and *E. necator*. This is significant as powdery mildew genetic targets in a model system translated to an agriculturally important crop. Further work should be done to explore the role of the GH17 domain in TCP interactions and pathogenicity outside powdery mildews.

With the rapid spray-induced gene silencing assay developed, which does not require plasmid construction or plant transformation, it increases the scope of research one can perform in the context of powdery mildew genetics and provides additional tools to uncover the link between host endoreduplication and successful powdery mildew infection (Fig. 1). Endoreduplication is a fascinating phenomenon to explore in the context of parasitism. Discoveries made in the powdery mildew system build our understanding of metabolic enhancement via induced-endoreduplication given its evolutionary convergence among biotrophs and specific tissues to increase metabolism, extending findings outside of plant pathogen relationships. Given the findings are beginning to be tested in agriculturally relevant plants and reflect what is observed in other parasitic interactions, we hope this research can enhance our ability to combat these infections.

References

Bramlett, M., Plaetinck, G., Maienfisch, P., 2020. RNA-Based Biocontrols—A New Paradigm in Crop Protection. Engineering 6, 522–527. https://doi.org/10.1016/j.eng.2019.09.008

Chandran, D., Inada, N., Hather, G., Kleindt, C.K., Wildermuth, M.C., 2010. Laser microdissection of Arabidopsis cells at the powdery mildew infection site reveals site-specific processes and regulators. Proceedings of the National Academy of Sciences of the United States of America 107, 460–465. https://doi.org/10.1073/pnas.0912492107

Chandran, D., Rickert, J., Cherk, C., Dotson, B.R., Wildermuth, M.C., 2013. Host Cell Ploidy Underlying the Fungal Feeding Site Is a Determinant of Powdery Mildew Growth and Reproduction. Molecular Plant-Microbe Interactions 26, 537–545. https://doi.org/10.1094/MPMI-10-12-0254-R

Frenkel, O., Cadle-Davidson, L., Wilcox, W.F., Milgroom, M.G., 2015. Mechanisms of resistance to an azole fungicide in the grapevine powdery mildew fungus, Erysiphe necator. Phytopathology 105, 370–377. https://doi.org/10.1094/PHYTO-07-14-0202-R

Fuller, K.B., Alston, J.M., Sambucci, O.S., 2014. The value of powdery mildew resistance in grapes: Evidence from California. Wine Economics and Policy 3, 90–107. https://doi.org/10.1016/j.wep.2014.09.001

Gaudioso-Pedraza, R., Benitez-Alfonso, Y., 2014. A phylogenetic approach to study the origin and evolution of plasmodesmata-localized glycosyl hydrolases family 17. Frontiers in Plant Science 5, 1–14. https://doi.org/10.3389/fpls.2014.00212

Grigoriev, I. v., Nikitin, R., Haridas, S., Kuo, A., Ohm, R., Otillar, R., Riley, R., Salamov, A., Zhao, X., Korzeniewski, F., Smirnova, T., Nordberg, H., Dubchak, I., Shabalov, I., 2014. MycoCosm portal: Gearing up for 1000 fungal genomes. Nucleic Acids Research 42, 699–704. https://doi.org/10.1093/nar/gkt1183

Lopez, J.A., Sun, Y., Blair, P.B., Mukhtar, M.S., 2015. TCP three-way handshake : linking developmental processes with plant immunity. Trends in Plant Science. https://doi.org/10.1016/j.tplants.2015.01.005

Peng, Y., Chen, L., Lu, Y., Wu, Y., Dumenil, J., Zhu, Z., 2015. The Ubiquitin Receptors DA1 , DAR1 , and DAR2 Redundantly Regulate Endoreduplication by Modulating the Stability of TCP14 / 15 in Arabidopsis 27, 649–662. https://doi.org/10.1105/tpc.114.132274

Raanan, R., Gunier, R.B., Balmes, J.R., Beltran, A.J., Harley, K.G., Bradman, A., Eskenazi, B., 2017. Elemental sulfur use and associations with pediatric lung function and respiratory symptoms in an agricultural community (California, USA). Environmental Health Perspectives 125, 1–8. https://doi.org/10.1289/EHP528

van Es, S.W., van der Auweraert, E.B., Silveira, S.R., Angenent, G.C., van Dijk, A.D.J., Immink, R.G.H., 2019. Comprehensive phenotyping reveals interactions and functions of Arabidopsis thaliana TCP genes in yield determination. Plant Journal 99, 316–328. https://doi.org/10.1111/tpj.14326

Weßling, R., Epple, P., Altmann, S., He, Y., Yang, L., Henz, S.R., McDonald, N., Wiley, K., Bader, K.C., Gläßer, C., Mukhtar, M.S., Haigis, S., Ghamsari, L., Stephens, A.E., Ecker, J.R., Vidal, M., Jones, J.D.G., Mayer, K.F.X., ver Loren Van Themaat, E., Weigel, D., Schulze-Lefert, P., Dangl, J.L., Panstruga, R., Braun, P., 2014. Convergent targeting of a common host protein-network by pathogen effectors from three kingdoms of life. Cell Host and Microbe 16, 364–375. https://doi.org/10.1016/j.chom.2014.08.004

Wildermuth, M.C., Steinwand, M.A., McRae, A.G., Jaenisch, J., Chandran, D., 2017. Adapted Biotroph Manipulation of Plant Cell Ploidy. Annual Review of Phytopathology 55, 537–564. https://doi.org/10.1146/annurev-phyto-080516-035458

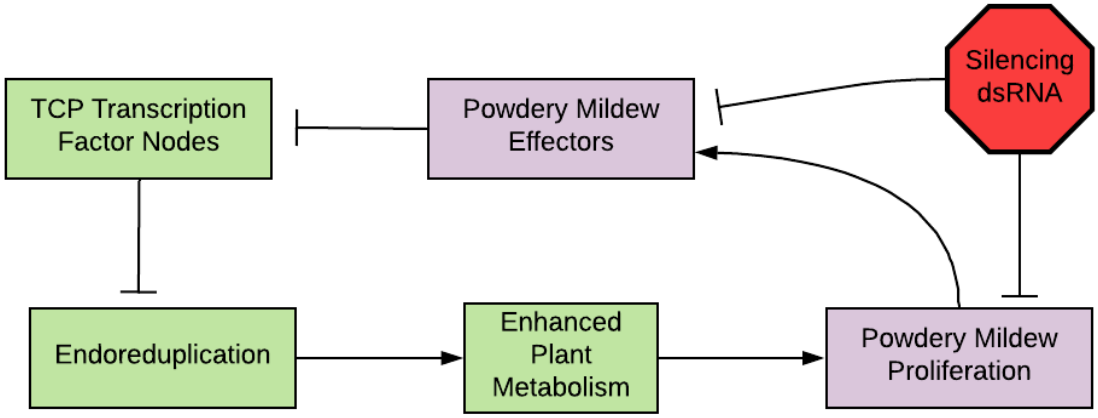

Fig. 1. Powdery mildew proliferation is promoted by ploidy-associated shift in host primary metabolism (Chapters 1-2; Appendix 1). Endoreduplication modulators, like TCP transcription factors and powdery mildew effectors that target them, modulate host susceptibility to powdery mildew (Chapter 4). Topical RNA targeting powdery mildew genes can suppress powdery mildew proliferation via effectors that target TCPs (shown above) or other means (Chapter 3-4).

Appendices

Appendix 1: Adapted Biotroph Manipulation of Plant Cell Ploidy published in Annual Review of Phytopathology

Appendix 2: Protocol for fungal spore neutral lipid comparison using flow cytometry

Appendix 3: Adult *Arabidopsis thaliana* powdery mildew spore quantification protocol

Appendix 4: Quantification of *A. thaliana* powdery mildew infection site ploidy protocol

Appendix 1: Adapted Biotroph Manipulation of Plant Cell Ploidy published in Annual Review of Phytopathology

The following review article was published in *Annual Review of Phytopathology*. All authors granted permission to include it in this dissertation.

Wildermuth, M.C., Steinwand, M.A., McRae, A.G., Jaenisch, J., Chandran, D., 2017. Adapted Biotroph Manipulation of Plant Cell Ploidy. Annual Review of Phytopathology 55, 537–564. https://doi.org/10.1146/annurev-phyto-080516-035458

Preface

My role in this publication included the research and write-up of biotrophic effectors which coordinate cell cycle modification in the host plant.

Adapted Biotroph Manipulation of Plant Cell Ploidy

Mary C. Wildermuth,[1] Michael A. Steinwand,[1] Amanda G. McRae,[1] Johan Jaenisch,[1] and Divya Chandran[2]

[1] Department of Plant & Microbial Biology, University of California, Berkeley, California 94720; email: mwildermuth@berkeley.edu
[2] Regional Center for Biotechnology, NCR Biotech Science Cluster, Faridabad, India 121001

Keywords

endoreduplication, cell cycle, ploidy, biotroph, effector

Abstract

Diverse plant biotrophs that establish a sustained site of nutrient acquisition induce localized host endoreduplication. Endoreduplication is a process by which cells successively replicate their genomes without mitosis, resulting in an increase in nuclear DNA ploidy. Elevated ploidy is associated with enhanced cell size, metabolic capacity, and the capacity to differentiate. Localized host endoreduplication induced by adapted plant biotrophs promotes biotroph colonization, development, and/or proliferation. When induced host endoreduplication is limited, biotroph growth and/or development are compromised. Herein, we examine a diverse set of plant-biotroph interactions to identify (*a*) common host components manipulated to promote induced host endoreduplication and (*b*) biotroph effectors that facilitate this induced host process. Shared mechanisms to promote host endoreduplication and development of nutrient exchange/feeding sites include manipulation centered on endocycle entry at the G2-M transition as well as yet undefined roles for differentiation regulators (e.g., CLE peptides) and pectin/cell wall modification.

Introduction

Plant biotrophs are pathogenic or mutualistic microorganisms and pests that colonize and obtain nutrients from living plant cells without killing them. In so doing, plant biotrophs often manipulate the host plant cell cycle to facilitate their colonization, development, and/or proliferation. **Figure 1** illustrates the evolutionary diversity of these plant biotrophs and the range of cell fates that are

manipulated as part of their interaction with a host plant. Biotroph-induced cell division and/or hyper cell expansion (hypertrophy) often results in visible phenotypes such as tumors and galls, as observed for the α-proteobacterium *Agrobacterium tumefaciens* (46), the basidiomycete smut fungus *Ustilago maydis* (17), the Fijivirus *Rice black-streaked dwarf virus* (113), parasitic root nematodes (29), and nodules formed in the α- and β-proteobacterial rhizobia-host symbioses (83). There is evidence that plant biotrophs (e.g., *Agrobacterium* and *Ustilago* spp.) have converged on common mechanisms to promote host cell division and/or hypertrophy, such as manipulation of the plant growth hormones auxin and cytokinin to induce tumor/gall formation (15, 77, 88). Likewise, the *Xanthomonas campestris* pv. *vesicatoria* effector AvrBs3 and the *Carlavirus Chrysanthemum virus B* protein P12 each induce expression of the plant growth–promoting bHLH transcription factor UPA20 to induce leaf mesophyll cell hypertrophy (63, 80).

In contrast to the visible phenotypes associated with induced plant cell division and hypertrophy, biotroph-induced endoreduplication is typically observed at the microscopic level. Thus, it has only recently been identified as a common strategy used by diverse biotrophs to promote their colonization, development, and proliferation (27, 137). Endoreduplication is a variation of the cell cycle in which cells replicate their DNA but do not go through mitosis; each endocycle results in doubled DNA content that is typically accompanied by a corresponding increase in nuclear and cellular size. In plants, endoreduplication is an integral part of development typically associated with postmitotic growth of plant organs such as roots, the hypocotyl, and leaves. It is also a part of terminal differentiation in large single cells such as trichomes and in organs with enhanced metabolic capacity such as endosperm and fruit (16, 76, 110).

Mutualistic biotrophs [e.g., rhizobia (68) and arbuscular mycorrhizal fungi (AMFs) (11)] and parasitic biotrophs [e.g., powdery mildew (PM) fungi (24), root nematodes (29), and the *Begomovirus Cabbage leaf curl virus* (CaLCuV) (5)] induce localized host endoreduplication to promote their colonization, development, and/or proliferation (**Figure 2**). In each of these interactions, induced host endoreduplication is limited to 2–4 cycles and is associated with a localized source- sink change and a sustained site of nutrient acquisition/exchange. Furthermore, where examined, induced host endoreduplicated cells exhibit decondensed chromatin and a proportional increase in nuclear size consistent with active gene expression and enhanced metabolic capacity (137). By contrast, host endoreduplication induced as a part of a genotoxic stress or resistance response is typically associated with condensed chromatin and no proportional increase in nuclear size. Induced endoreduplication in this situation tends to occur via activation of DNA damage check- points. Genotoxic stress–/resistance–induced endoreduplication likely serves to protect genome integrity, prevent the transmission of deleterious mutations, and/or provide a compensatory means of supporting growth in the absence of cell division (e.g., 42, 57). What then is the function of localized host endoreduplication induced by an adapted plant biotroph? In the case of CaLCuV, viral replication is seen in cells with induced endoreduplication, and host DNA replication machinery used in endoreduplication is required for viral replication (5, 90). Similarly, rhizobia involved in symbiotic nodulation engage in host endoreduplication as part of symbiosome development to facilitate bacterial differentiation to form functional nitrogen-fixing nodules (131) (**Figure 2**). In the case of AMFs, the role of induced endoploidy is less clear but likely functions to physically facilitate infection, accommodate arbuscules in cortical parenchyma cells, and meet the extensive nutritional demands of the fungus. The PM *Golovinomyces orontii* induces host endoreduplication specifically in mesophyll cells underlying its feeding

structure (housed in the epidermal cell) to support the metabolically demanding process of asexual reproduction (24, 25). Both root-knot and root-cyst nematodes promote the formation of large multinucleated and polyploid feeding cells by activating a combination of mitotic and endoreduplication cycles in plant root vascular parenchyma cells (29) (**Figure 2**). Endoreduplication appears to both facilitate feeding site development and allow for an enhanced supply of nutrients to the parasitic nematodes.

In all cases, when induced host-endoreduplication is limited, the colonization, development, and/or proliferation of the biotroph are impaired (27, 137). As indicated above, it appears that induced host endoreduplication may play a variety of roles in these interactions: to accommodate the developing biotroph; to provide host machinery and cues for biotroph DNA replication, development, and differentiation; to provide host machinery and cues to support coordinated host cell differentiation to form a feeding/nutrient exchange site; and to support the nutritional demands of the biotroph during metabolically demanding phases of its life cycle. Not only does increased DNA content result in enhanced transcription and translation and an overall increase in the biosynthetic capacity of the infected cell, but particular metabolic and regulatory pathways exhibit preferentially enhanced nonadditive ploidy-associated transcription (137). This could result from an endoreduplication-associated alteration of genome structure (101) or the transcription of certain genes being particularly sensitive to dosage (140).

Although endoreduplication is a crucial component of these biotroph-plant interactions, our understanding of the host proteins and processes manipulated to achieve biotroph-induced endoreduplication, as well as effectors (biotroph-secreted compounds and proteins) used by the biotroph in this endeavor, remains limited. Herein, we examine current knowledge and explore emergent themes focused on biotroph-induced endocycle entry and progression in compatible hosts. Other cell cycle manipulations (e.g., cell division or fusion) that may accompany endoreduplication as part of a specific biotroph-plant interaction are not examined in detail. Furthermore, biotroph inhibition of plant defense and programmed cell death is not addressed. Refer to Le Fevre et al. (77) for a general review on modulation of host cell biology by plant pathogens. Similar to biotroph-induced plant cell division and hypertrophy, we present evidence that plant biotrophs have converged on common mechanisms to promote host endoreduplication, including the manipulation of the host anaphase-promoting complex and modulation of core cell cycle transcriptional machinery. A yet undefined role for differentiation regulators, such as CLAVATA3/embryo-surrounding region (CLE) peptides, and for pectin/cell wall modifications as part of this process is also suggested.

The Plant Endocycle Machinery

The canonical mitotic cell cycle comprises four sequential phases, G1 (gap 1), S (DNA synthesis), G2 (gap 2), and M (mitosis); DNA is duplicated during the S phase and duplicated chromosomes are segregated into two daughter cells during the M phase (111). In contrast, endoreduplicating cells, which undergo repeated cycles of DNA replication (G-S) in the absence of mitosis, double their genomes without chromosomal separation and cell division, resulting in mononucleate polyploid cells with multiples of the 2*C* DNA content (e.g., 4*C*, 8*C*, 16*C*, etc.). Herein, we briefly describe major components of the plant endocycle focused on endocycle entry and progression as relevant to biotroph-induced plant endoreduplication. For recent, more-detailed reviews of plant endocycle components, please refer to References 10, 18, 27, 33, and 50.

During plant development, the switch from the mitotic cell cycle to the endocycle involves integrated regulation of the cell cycle machinery. Downregulation of B-type cyclin-dependent kinase (CDKB)-cyclin (CYC) complexes is sufficient to trigger exit from mitosis and entry into the endocycle in dividing cells. This can occur via targeted proteolysis of mitotic cyclins, transcriptional downregulation of mitotic CDKs or CYCs, and/or inhibition of CDK activity by CDK inhibitors (CKI) (18, 33). In the case of biotroph manipulation of quiescent cells, re-entry into the cell cycle is also required.

The anaphase-promoting complex/cyclosome (APC/C) E3-ubiquitin ligase plays a central role in endoreduplication initiation via targeted proteolysis of specific mitotic cyclins such as CYCB1;1 and CYCA2;3 (55). In plants, the cell cycle switch 52 (CCS52) proteins, which are functional homologs of Cdh1 and *Drosophila melanogaster* Fzr, act as substrate-specific activators of the APC/C complex to positively promote entry into the endocycle via mitotic CYC degradation (55). Loss- of-function *ccs52* mutants exhibit reduced ploidy, whereas *CCS52* overexpression enhances ploidy (7, 73, 74). Retinoblastoma-related protein (RBR), a master regulator of cell division and differentiation, interacts with specific E2F and MYB3R transcription factor partners to promote mitosis or endoreduplication (31, 66, 67, 81). In actively dividing cells, *CCS52* expression is repressed by RBR-E2FA-DPA (dimerization partner A) or the atypical E2F transcription factor DEL1/E2FE (73, 81). Meanwhile, hyperphosphorylation of MYB3R4 by CDKB-CYCBs promotes mitotic progression via transcriptional activation of pro-mitotic genes, including CYCBs (2, 51).

As the endocycle progresses, repeated cycles of G-S presumably require alternating low and high levels of A-type cyclin-dependent kinases (CDKAs). Low CDKA levels are required for licensing of replication origins by the origin replication complex during early G1, whereas high CDKA levels drive S-phase transcription (33). The kinase inhibitor protein (KIP)-related (KRP) family of CDK inhibitors have emerged as likely candidates for driving these oscillating cycles of CDKA activity (60, 109, 126). In general, overexpression of KRPs in mitotically active cells was shown to stimulate endoreduplication, whereas overexpression in postmitotic cells such as trichomes resulted in reduced ploidy (109, 135). The apparent opposite effect on endoreduplication may be explained by the dose-dependent nature of KRPs and the cellular context in which they are expressed. Tight regulation of KRP levels is therefore critical. Accordingly, KRP proteins are under the posttranslational control of Skp-Cullin-F-Box (SCF) and Cullin-RING (CRL) classes of ubiquitin ligases (92, 106). Loss-of-function mutants in an F-Box protein FBL17 and a knockdown mutant of CULLIN4 displayed strong reduction in endoreduplication levels, possibly by reducing KRP proteolysis.

Another important player during endoreduplication progression is DNA topoisomerase VI, the plant homolog of the archaeal DNA topoisomerase. DNA topoisomerases play an important role in decatenation of replicated chromosomes and therefore may be required to untangle replicated DNA during successive rounds of endoreduplication (117). An analysis of *Arabidopsis* mutants of four different subunits of this complex, RHL1/HYP7, RHL2, RHL3/BIN3/HYP6, and MIDGET/BIN4, found that DNA topoisomerase VI is not required for mitotic activity or endoreduplication entry; instead, it is required for successive rounds of replication during endocycle progression (19, 65, 119, 120). In general, single mutants of the different topoisomerase VI

subunits had severe dwarf phenotypes and reduced ploidy levels in endoreduplicating cells such as trichomes, leaves, and the hypocotyl as a result of incomplete endoreduplication.

Endoreduplication Induced by Plant Biotrophs

Adapted plant biotrophs manipulate and/or utilize known components of the plant cell cycle to promote localized host endoreduplication. In addition, these biotroph-plant interactions have elucidated novel cell cycle players and new roles for previously identified core cell cycle regulators. Below, we discuss the diverse set of interactions, shown in **Figure 2**, in which an adapted biotroph induces localized plant cell endoreduplication to support its colonization, development, and/or proliferation. **Figure 3** integrates findings from these interactions and presents a simplified model depicting the (proposed) function of identified host factors in adapted biotroph-induced endocycle entry and progression. **Table 1** details both plant host and microbial proteins/factors with known or putative roles in biotroph-induced plant cell endoreduplication.

Legume-Rhizobia Symbiosis

The symbiotic interaction between rhizobia and leguminous plants results in the formation of nitrogen-fixing root nodules, which provide plants with nitrogen and rhizobia with carbon and other nutrients. During nodule organogenesis, lipochitooligosaccharide signals released by the rhizobia, known as Nod factors, stimulate inner root cortical cells to reinitiate mitosis and form a nodule meristem. Nodules produced by the *Sinorhizobium meliloti–Medicago* interaction contain a persistent meristem (indeterminate nodules) that maintains a population of actively dividing cells throughout the life of the nodule (62) (**Figure 2**). By contrast, nodules produced by the *Mesorhizobium loti–Lotus japonicus* interaction contain a transiently active meristem (determinate nodules). Meristem formation in indeterminate nodules is followed by a differentiation program in which cells continuously exit from the meristem and undergo several rounds of endoreduplication with a concomitant gradual increase in cell volume. Rhizobia contained within infection threads invade these large endoreduplicated cells, where they are engulfed in host-membrane-derived compartments via endocytosis to form symbiosomes. As the nodule matures, bacteria within these symbiosomes elongate, endoreduplicate, and terminally differentiate into nitrogen-fixing bacteroids. The symbiosome is the site of nitrogen fixation and functions in nutrient exchange between the host and the bacteroid. The mature nodule is therefore a complex structure consisting of three main zones: an apical rhizobia-free meristematic zone (ZI), a central endoreduplicated symbiosome-harboring zone (ZII), and a terminal bacteroid-containing nitrogen-fixing zone (ZIII) (68) (**Figure 2**).

The plant APC/C activator CCS52A was the first regulator to be implicated in endoreduplication in differentiating root nodules (23). *Medicago truncatula CCS52A* expression is activated prior to nodule differentiation and expressed throughout the endoreduplication-competent ZII of mature nodules (107, 131). RNAi downregulation of *CCS52A* expression in *M. truncatula* did not affect early nodule primordia formation and colonization but instead dramatically decreased nodule ploidy (**Table 1**; **Figure 3**). Furthermore, the lack of endoreduplication prevented bacteroid differentiation and nitrogen fixation, which led to premature senescence and eventual disintegration of the whole organ (131), indicating that endoreduplication is integral to the proper development and function of nodules. In the *M. loti–L. japonicus* interaction, DNA topoisomerase VI plays a role in endocycle progression, as mutants in two DNA topoisomerase VI subunits, *VAG1/RHL1*

and *SUNERGOS1/RHL2*, produce nodules with decreased proportions of endoreduplicated cells (121, 141) (**Table 1**; **Figure 3**).

The calcium/calmodulin-dependent protein kinase (CaCMK) DMI3 is essential for relaying calcium signals triggered upon Nod factor recognition to the nucleus and inducing symbiotic gene expression (86). *M. truncatula*–interacting protein of DMI3 (IPD3) interacts with DMI3 in ZII of mature nodules and controls the expression of a subset of genes required for symbiosome formation (94). Mutations in *MtIPD3* result in two types of defective nodules: small with infection threads arrested at the cortex and elongated but defective in endoreduplication (56, 85, 94) (**Table 1**). In addition, a number of plant small peptides that regulate nodule initiation and/or development could potentially impact biotroph-induced host cell endoreduplication. These include early nodulin 40 (ENOD40), CLE peptides, short peptides 12 or 13 amino acids in length that regulate plant cellular differentiation (12) (**Table 1**), and C-terminally encoded peptides (34). Although a role for these plant peptides in induced host endoreduplication has not yet been established, plant nodule–specific cysteine-rich (NCR) peptides that promote bacterial endoreduplication and terminal differentiation into nitrogen-fixing bacteroid have been identified (34).

Parasitic Root Nematode-Induced Host Endoreduplication

Parasitic biotrophic plant nematodes co-opt the host cell cycle machinery to induce the formation of two different types of feeding sites within plant roots. Root-knot nematode-induced giant cells are surrounded by parenchymatic vascular tissue cells that are actively asymmetrically dividing in a disordered manner to form root swellings known as galls. In contrast, root-cyst nematodes generate one large syncytium that accumulates multiple nuclei through the fusion of adjacent cells in which mitosis is reinitiated (29, 72). Cells in both types of feeding sites undergo endoreduplication to produce large polyploid nuclei, which are accompanied by a corresponding increase in cell size (**Figure 2**).

Similar to the rhizobia-host interaction, root-knot and root-cyst nematode feeding site development utilizes the plant APC/C activators CCS52 and DNA topoisomerase VI to promote the endocycle (**Table 1**; **Figure 3**). Strong phenotypes were observed for knockdown mutants in the DNA topoisomerase VI subunit *RHL1*, particularly in the case of syncytia (30) (**Table 1**; **Figure 3**). The root-knot nematode was able to penetrate but could only form tiny multinucleate giant cells in *rhl1* knockdown mutants. The root-cyst nematode was unable to even trigger syncytium formation, suggesting endoreduplication is required for syncytia initiation (30). *CCS52A1* and *CCS52B* are highly expressed in galls and syncytia, whereas the CCS52 repressor *DEL1* is weakly expressed throughout feeding site development (30, 39). Knockdowns of *CCS52* genes resulted in smaller giant cells and syncytia, smaller nuclei, and delayed nematode development, whereas overexpression of *DEL1* similarly resulted in smaller giant cells containing smaller nuclei, malformed syncytia, and reduced nematode reproduction (30).

In addition, the KRP family of CDK inhibitors plays an important role in giant cell development (129, 130). Three of the seven *Arabidopsis* KRPs (*KRP2*, *KRP5*, and *KRP6*) normally expressed in root vascular tissues are also expressed in galls after nematode infection. Phenotypes of knockouts and overexpressors of *KRP1* and *2* suggest they function in suppressing G1-S progression associated with mitosis, whereas KRP6 may function primarily in the suppression of endocycle progression (**Table 1**; **Figure 3**). Loss-of-function *krp2* mutants formed giant cells with a greater

number of nuclei and an increased number of neighboring proliferating cells compared with wild type; however, no effect on nematode reproduction was observed, suggesting that in some cases the increased number of nuclei may compensate for the lack of endoreduplication in giant cell nuclei (129, 130). By contrast, overexpression of *KRP2* or *KRP1* (which is typically not expressed in galls) resulted in smaller giant cells with fewer nuclei and reduced cell division of neighboring cells, indicating that ectopic expression of KRPs can block mitosis (130). A significant decrease in nematode reproduction compared with the wild type was observed in both overexpression (OEX) lines (**Table 1**). By contrast, *KRP6* OEX lines formed smaller giant cells with a higher number of lower ploidy nuclei and increased proliferation of neighboring cells (127, 128), suggesting that KRP6 can suppress endocycle progression and promote mitosis. Furthermore, there is evidence to support a special role for cytokinesis inhibition by KRP6 that is particularly relevant to root-knot nematode multinucleated giant cell formation and acytokinetic mitosis (127, 128). Although these data are compelling, misexpression of mitotic and endocycle regulators can be particularly hard to interpret in systems such as nematode feeding site development where both processes occur.

Parasitic root nematodes manipulate their host environment through the secretion of bioactive compounds (e.g., hormones and CLE-like peptides) and effector proteins that they deliver directly to the host via a syringe-like stylet (98). A number of these have potential functions in biotroph-induced endoreduplication. For example, nematode-secreted CLE peptides play a critical role in promoting feeding site development (49, 58, 134) (**Table 1**). Furthermore, nematode infectivity or syncytium size was reduced in *Arabidopsis* CLE receptor mutants, suggesting plant CLE signaling pathways have been hijacked by the nematodes to promote their growth and development (87). This is contrasted with plant CLE peptides acting as a negative control on nodulation in the legume-rhizobia symbiosis (34, 89). Root nematodes can also secrete cytokinins, which may activate CCS52A1 expression and promote endoreduplication (123), and double mutants in host cytokinin receptors *ahk2*,*3* or *ahk3*,*4* exhibit reduced syncytium size (114). Localized auxin levels also appear to play a role in the root nematode–host interactions, as plants deficient in auxin transport (e.g., *PINs*, *AUX1*, *LAX3*) (48, 71, 75) reduce both root-knot and root-cyst infectivity. In addition, the root-cyst nematode effector *Hs19C07* interacts with auxin influx transporter *AtLAX3* to increase accumulation of auxin and expression of cell wall–remodeling enzymes during syncytium formation (75) (**Table 1**).

Pectin composition/modification could influence endoreduplication via an impact on cytokinesis, cell wall expansion, or signaling (61) (**Figure 3**). The secreted root-cyst nematode cellulose-binding protein HsCBP interacts with and enhances the activity of *Arabidopsis* pectin methylesterase 3 (AtPM3) to facilitate syncytium development (54). Furthermore, secreted pectate lyases are found across nematode species (125), and silencing these genes reduced nematode infectivity (97). Additional predicted nematode effectors with potential roles in cell cycle regulation include a CDC48-like protein and an SKP1-like protein, silencing of which resulted in a >50% reduction in developing females (9, 102, 116). SKP1-mediated proteolysis (e.g., of KRP) could im- pact endocycle entry and/or progression (44), whereas the CDC48-like effector, an AAA-ATPase, could function to regulate cell division, expansion, and/or differentiation (95).

Arbuscular Mycorrhizal Fungal Symbiosis

AMFs (Order: Glomales) are obligate symbionts within roots of most land plants. AMFs provide the plants with phosphorus while acquiring carbon from the plant. Specific signaling events that parallel the rhizobia symbiosis promote AMF colonization of the plant root. Fungal penetration of plant epidermal cells by specialized appressoria called hyphopodia allows for intercellular fungal hyphal growth that follows the pre-penetration apparatus until the fungus reaches the inner cortex. The hyphae then grow laterally until it induces pre-penetration apparati in an inner cortical cell, which allows the hyphae to enter this cell. In inner cortical cells, highly branched arbuscules develop and fill up most of the infected cortical parenchyma cell (52, 96) (**Figure 2**). The arbuscules are transitory sites of nutrient exchange. As old arbuscules degrade, hyphae colonize additional cortex cells and form new arbuscules.

A number of studies suggest that AMF-induced host ploidy is a common feature (27). For example, tomato, pea, and leek root cortical cells colonized by the AMF showed enhanced ploidy compared to uninfected controls (11, 41, 103). Also, a broad survey of AMF-colonized roots from diverse plants found 22 of the 25 species tested exhibited endopolyploid root nuclei compared to controls (6). AMFs trigger changes in both plant root epidermal and cortical cells that have been associated with endoreduplication. For example, nuclei movement (from cell periphery to the center), increased nuclear volume, and chromosome decondensation are commonly observed in AMF-infected cells of different plant species (6, 11, 41, 43, 138).

For the AMF interaction, proteins involved in initial signaling, host cell remodeling and colonization, nutrient (e.g., sugar and phosphorus) transport, and host defense suppression have been identified (96); however, AMF manipulation of the cell cycle remains largely unexplored. Similar to rhizobial Nod factor induction of an infection thread in the legume-rhizobia symbiosis, AMF lipochitooligosaccharide mycorrhizal factors (Myc factors) promote development of the pre-penetration apparatus, which is thought to be an evolutionary precursor of the infection thread (93, 96). The involvement of CaCMK is conserved in both systems, as is its interacting protein, IPD3/CYCLOPS (**Table 1**). *ipd3*/*cyclops* mutants show reduced AMF colonization compared to wild-type plants, with no arbuscules formed in *ipd3* mutants despite the presence of fungal hyphae (56, 139). As *ipd3 Medicago* mutants exhibit reduced nodule endoreduplication, a similar role for IPD3/CYCLOPS and Myc factor-induced signaling in AMF endoreduplication should be explored.

Although the functions of proteins such as CCS52 in AMF-induced endoreduplication have not been examined, Tahiri-Alaoui et al. (122) proposed a role for CULLIN-4 (CUL4) as a regulator of AMF-induced endoploidy based on the preferential induction of *CUL4* in AMF-colonized roots and a putative role for similar CULLINs in the regulation of the cell cycle via ubiquitin proteolytic degradation. CUL4 was subsequently determined to be a major regulator of endoreduplication in *Arabidopsis* trichomes (106). Although the APC/C complex appears to dominate control over endocycle entry by degrading mitotic cyclins, the Cullin-RING E3 ubiquitin ligase (CRL)-CUL4 complex is important for regulating endocycle progression (106) and should be further examined in the AMF symbiosis and other interactions discussed herein (**Figure 3**).

Finally, auxin perception is also required for arbuscule development: The auxin reporter DR5-GUS is preferentially expressed in root cells containing arbuscules; *miR393*, which sup- presses auxin signaling, is downregulated during AMF symbiosis; and overexpression of *miR393* resulted

in a strong defect in arbuscule formation (38) (**Table 1**). Localized enhanced auxin responses are also observed in developing syncytia in the root-cyst nematode–plant host interaction and in the rhizobial-legume symbiosis (15). Temporally and spatially defined cellular control over active forms of auxin and their transport and signaling likely acts to promote localized cell division or limit the extent of endoreduplication.

Powdery Mildew-Induced Host Endoreduplication

Unlike the previous interactions, the PM fungi exclusively infect aboveground tissues of plants. Family members have adapted to a wide variety of plants, including *Arabidopsis thaliana* (45). The PM life cycle of *G. orontii* on *Arabidopsis* leaves consists of (*a*) germination of the fungal spore (conidium) on the leaf surface, (*b*) penetration of the host epidermal cell wall, (*c*) establishment of a specialized feeding structure (the haustorium) in the penetrated epidermal cell within one day post inoculation (dpi), (*d*) surface hyphal growth, and (*e*) formation of asexual reproductive structures (conidiophores) containing new spores at 5 dpi. Continued colony growth includes development of an extensive surficial hyphal network with multiple secondary haustoria and conidiophores (70). Endoreduplication occurs specifically in the mesophyll cells underlying the epidermal cell containing the fungal feeding structure at 5 dpi, concomitant with the metabolically demanding process of asexual reproduction (24, 25) (**Figure 2**). Furthermore, the extent of fungal reproduction is highly correlated with the ploidy index of mesophyll cells underlying the haustorium-containing epidermal cell (25). Together, these data support induced localized host endoreduplication as a means of providing the adapted fungus with the metabolites it requires for asexual reproduction. Below, we further detail mutants with altered mesophyll leaf cell ploidy and PM reproduction. It should be noted that defense activation does not appear to be responsible for the reduced PM reproduction of these mutants (25, 132, 133). Association of induced host endoreduplication with asexual reproduction has not yet been examined for other adapted PM-host interactions. Interestingly, epidermal cell endoreduplication was associated with an early resistance response in an incompatible PM-barley interaction with features consistent with responses to genotoxic stress (8).

Global expression profiling and quantitative reverse transcription polymerase chain reaction of cells laser-microdissected from the *G. orontii–Arabidopsis* infection site at 5 dpi showed localized enhanced expression of *MYB3R4*, *CCS52A*, and the CDC48-interactor *PUX2* (24, 27).

Loss-of-function *myb3r4* mutants supported reduced PM asexual reproduction with fewer conidiophores per colony compared to wild type (24) (**Table 1**). Furthermore, the PM-induced ploidy increase was abrogated in the *myb3r4* mutant, suggesting that MYB3R4 function is required for induced endoreduplication that promotes PM reproduction. Hyperphosphorylated MYB3R4, via specific CDKB-CYC complexes, is a transcriptional activator of a number of G2-M-specific genes, promoting mitosis and cytokinesis (51) (**Figure 3**). At the PM infection site, a number of MYB3R4 targets, which are normally activated and/or required during mitosis and cytokinesis, including mitotic cyclin CYCB1;2 and PLEIADE, exhibited decreased expression at the PM infection site. This suggested that un(der)phosphorylated MYB3R4 might act to repress mitosis (and cytokine- sis) and promote the endocycle at the PM infection site (24, 137). The phosphorylation status of MYB3R in other eukaryotic systems changes the composition of the multisubunit cell cycle regulatory complex (e.g., DREAM complex) (108), revealing dual functionality of MYB3Rs. Very recently, it was discovered that *Arabidopsis* MYB3R1 could

function as an activator or repressor of mitosis depending on the cellular context (66, 67). Consistent with un(der)phosphorylated MYB3R4 function to promote endoreduplication at the PM infection site, preliminary analysis of *ccs52A* null mutants showed a small but significant reduction in PM reproduction (27) (**Table 1**). Thus, CCS52 function could promote mitotic cyclin degradation and the un(der)phosphorylated form of MYB3R4 (**Figure 3**). DEL1, a negative regulator of *CCS52A* gene expression and of endoreduplication in dividing cells, was not expressed at the PM infection site (24, 26), which is consistent with PM infection of postmitotic cells in mature leaves and the fact that host cell mitosis is not initiated as part of the PM interaction. Phenotypes of *del1* knockouts and overexpressors elucidated the impact of DEL1 on preinfection (basal) gene expression that promoted defense (26). Although this provided insight on the functional role of DEL1 in actively dividing cells, it is not directly relevant to the adapted PM infection site.

Plant ubiquitin X (PUX) 2 can act as an adapter for the interaction of AtCDC48 and SYP31 when they co-localize at the plane of cell division during cytokinesis (99, 100). *pux2* mutants ex- hibit reduced mesophyll basal leaf cell ploidy compared to wild-type plants; however, PM-induced endoreduplication still occurs (25) (**Table 1**). This suggests that PUX2 can promote endoreduplication during leaf development, perhaps through an inhibitory impact on cytokinesis (**Figure 3**), but that it is not required for PM-induced endoreduplication. Similarly, PM asexual spore production is markedly reduced when grown on *powdery mildew resistant* (*pmr*) *6 Arabidopsis* leaves that have lower basal ploidy in mesophyll cells but still undergo PM-induced endoreduplication (25, 132) (**Table 1**). For both *pux2* and *pmr6*, because PM-induced endoreduplication starts at a lower mesophyll ploidy level, the final ploidy in cells underlying the haustorial complex is lower than that in the wild type (25). PMR6 is a pectate-lyase domain-containing protein with an unusual C-terminal domain (132). Although pectin lyase activity has not been demonstrated, given its similarity to pectin lyases, PMR6 is likely to modify pectin via direct action on a pectin substrate or via binding of pectin (132). Indeed, mutants in *pmr6* have altered cell wall composition, as do *pmr5* mutants (132, 133).

Pectin plays an important role in polar cell-growth processes, including cytokinesis and cell wall expansion (61), and is also targeted for modification by root nematode effectors [e.g., HsCBP (54) and secreted pectate lyases (97, 125)], as discussed above. We do not yet understand how slight modifications to pectin or other cell plate/wall components impact cytokinesis and cell wall expansion. However, we do know that both endoreduplication and cell expansion are altered in *pmr6* and *pmr5* (25, 132, 133).

PMR5 is a plant-specific trichome birefringence-like (TBL) protein. TBL proteins have been shown to mediate pectin esterification and the synthesis and deposition of secondary wall cellulose (13, 14). Microarray analysis of *pmr5* mutants suggests that PMR5 may play a role in coordinating differentiation and cell cycle responses mediated by HD-Zip and MYB3R transcription factors (25). Similar to *myb3r4* mutants, *pmr5* mutants did not exhibit PM-induced endoreduplication (25) (**Table 1**). *pmr5* supported less PM reproduction than *myb3r4* and exhibited lower PM-induced mesophyll ploidy than *myb3r4*. Given these phenotypes and the finding that MYB3R4 target genes exhibit altered expression in *pmr5*, it is likely that PMR5 acts upstream of MYB3R4 in controlling PM-induced endoreduplication (25) (**Figure 3**).

Arabidopsis proteins interacting with *G. orontii* effector candidates (OEC) were identified by yeast two-hybrid (Y2H) with subsequent evaluation of T-DNA insertion lines in those genes of interest (136). Mutants in four of these *Arabidopsis* target genes (*TCP13–15* and *APC8*) with known/putative roles in cell cycle regulation exhibited altered *G. orontii* reproduction (**Table 1**). However, ploidy phenotypes have not yet been examined in the context of the PM infection for any of these mutants. A number of different OECs showed the capacity to interact with the TEOSINTE-BRANCHED 1 (TCP) transcription factor class I family members TCP13–15 (136). TCPs generally promote cell division via induction of mitotic cyclins; however, their role is broader, as TCPs can also impact cell expansion, endoreduplication, and differentiation in cell cycle phase- and context-dependent manners (84). TCP15 repressor lines exhibited enhanced ploidy in trichomes, leaves, and the hypocotyl, consistent with a role for TCP15 in promoting mitosis and inhibiting the endocycle (78). Accordingly, *tcp15* mutants supported more PM reproduction (136). TCP14 repressor lines, however, displayed opposite ploidy phenotypes depending on the cellular context: Trichomes exhibited enhanced ploidy and branching, whereas leaves showed a delayed onset of endoreduplication (64). TCP13 apparently acts during early leaf development/differentiation (35). Mutants in *tcp13*, *14*, and *15* each allowed for more PM growth and reproduction (136), suggesting they may act synergistically to promote proliferation and repress endoreduplication. This could explain why TCP13, 14, and 15 are all targeted by multiple *G. orontii* effectors. Interestingly, OEC67 interacts with TCP15 and the anaphase-promoting complex subunit APC8 via Y2H (136). In this context, OEC67 could help modulate temporal, cell-specific control of TCP15 degradation via APC8. However, *apc8* mutants support enhanced PM reproduction (136), suggesting additional complexity (e.g., 142).

Cabbage leaf curl virus Parasitism

CaLCuV is a bipartite single-stranded DNA virus in the genus *Begomovirus* of the *Geminiviridae* family that infects a broad range of Brassicaceae members, including cabbage and *Arabidopsis* (105) (**Figure 2**). CaLCuV encodes seven proteins: a capsid protein, two viral replication proteins (Rep and Ren), a transcriptional activator protein (TrAP), a movement protein (MP), a nuclear shuttle protein (NSP), and AC4, which exhibits significant divergence within the begomoviruses and is associated with suppression of RNA silencing. Begomoviruses do not encode a DNA polymerase, and thus they require host replication components from dividing or endoreduplicating cells (e.g., 90). CaLCuV infects differentiated leaf mesophyll cells and induces host endoreduplication to provide the components needed for viral replication (5, 90).

Host proteins and processes that mediate the CaLCuV interaction have been identified by (*a*) Y2H studies, (*b*) co-immunoprecipitation, (*c*) altered expression in microarray studies, and (*d*) screening of *Arabidopsis* mutant collections (105) (**Table 1**). CaLCuV replication-associated proteins Rep and Ren interact with a number of host proteins, including essential components of the host DNA replisome such as RBR and proliferating cell nuclear antigen (PCNA), the processivity factor for DNA polymerase delta (21). Viral protein interaction with RBR is critical to CaLCuV infectivity; Rep mutants compromised in RBR binding exhibit a dramatic reduction in viral DNA replication and disease symptoms (1, 3, 69) (**Table 1**). Furthermore, Rep is sufficient to induce *PCNA* expression supporting viral replication (91). *PCNA* expression is suppressed in differentiated cells, and release of this suppression occurs through viral protein interaction with RBR to release E2F-mediated repression of PCNA (36, 37). RBR interacts with E2FA, B, or C and MYB3R partners

to promote mitosis or endoreduplication (**Figure 3**). Overexpression of E2FB and CYCD, both of which promote the mitotic cell cycle, greatly reduced CaLCuV infection, whereas overexpression of E2FC or E2FA, which facilitate the endocycle, did not impact infection (5) (**Table 1**). Taken together, these suggest that viral interaction with RBR relieves repression of E2FC and E2FA, displacing E2FB, resulting in the activation of S-phase genes and an increase in endocycling cells (5) (**Figure 3**). MYB3R4 may play a role in promoting endoreduplication in response to CaLCuV, as its expression was enhanced in response to the viral TrAP protein (79). The PM *G. orontii* and CaLCuV both induce mesophyll cell endoreduplication in differentiated cells of mature leaves; therefore, un(der)phosphorylated MYB3R4 may promote host endoreduplication in the CaLCuV-host interaction, as proposed for the PM interaction (24, 137) (**Figure 3**). Furthermore, TrAP downregulation of the G2-M-promoting APC3 subunit HOBBIT could help limit mitotic cell cycle activation and promote entry into the endocycle in this context (79, 112). TrAP also altered expression of specific genes associated with cell wall biogenesis/modification, including enhanced expression of a pectin methylesterase inhibitor protein and the cellulose synthase AtCSLD6 and decreased expression of the TBL-domain containing protein 7 (79). Functional testing of mutants in these genes, as well as *pmr5* and *pmr6*, to see whether they alter CaLCuV infectivity and host mesophyll endoreduplication could support a common role for pectin/cell wall modification in localized host mesophyll endoreduplication associated with both CaLCuV and powdery mildew parasitism (**Figure 3**).

By screening an *Arabidopsis* transposon-based enhancer/gene trap collection for enhanced expression in response to CaLCuV infection, the *CRUMPLED LEAF* gene was identified as promoting CaLCuV infection (124). *CRUMPLED LEAF* is also referred to as *CAA33*, constitutive activator of AAA-ATPase (115). The CAA33 protein is localized to the chloroplast outer envelope, and *caa33* mutants are dwarfed with reduced cell division, early/aberrant entry into the endocycle, dysfunctional plastids, and stress activation; their leaves are curled and crumpled, similar to the symptoms of a CaLCuV infection (4, 59, 124). Silenced *CAA33* lines accumulated less virus at 12 dpi and exhibited greatly reduced symptoms, whereas *CAA33* overexpressor lines were more susceptible to CaLCuV infection with more rapid and extensive symptom development (124); leaf mesophyll ploidy was not evaluated. How CAA33 functions in facilitating CaLCuV replication and movement remains unclear, but the rescue of some mitotic *caa33* defects by sucrose (59) suggests that it may integrate source/sink metabolism with cell cycle fates.

Conclusions and Future Directions

Evolutionarily distant plant biotrophs have converged on induced endoreduplication as a mechanism to support their colonization, development, and/or proliferation in distinct host tissue and cell types. Elevated ploidy is generally associated with enhanced cell size, metabolic capacity, and the capacity to differentiate. Similar roles are observed for biotroph-induced localized host cell endoreduplication: accommodation of the developing biotroph; provision of host machinery and cues for biotroph DNA replication, development, and differentiation; provision of host machinery and cues to support coordinated host cell differentiation to form a feeding/nutrient exchange site; and enhanced metabolic capacity to meet the nutritional demands of the biotroph during metabolically demanding phases of its life cycle.

In these independently evolved interactions, biotrophic resource demand is a sink that requires enormous nutrients from its host source, similar to nutrient mobilization from the endopolyploidy

endosperm to support embryogenesis. Differentiation is closely associated with endoreduplication in plant development. Interestingly, it is apparent that finely tuned cross talk between the biotroph and host plant can facilitate both (*a*) host endoreduplication and differentiation of feeding/nutrient exchange sites and (*b*) biotroph endoreduplication and differentiation. Furthermore, plant biotrophs have evolved mechanisms that mimic endogenous plant control of differentiation (e.g., via CLE-like peptides and modulation of cytokinin and auxin).

Host factors required for biotroph-induced endoreduplication highlight shared points of manipulation centered on endocycle entry at the G2-M transition (**Figure 3**), with central cell cycle regulators such as RBR-E2F-MYB3Rs and APC/C as targets. In addition, manipulation of cytokinesis seems to be favored, perhaps via pectin modification. Pectin composition/modification could influence endoreduplication via an impact on cytokinesis, cell wall expansion, or signaling (61), and there is (preliminary) evidence to support a role for pectin composition/modification in all three parasitic biotroph-plant host interactions discussed herein.

Genomes for these adapted plant biotrophs are now available, and functional studies are under way to identify effectors and their targets and functions. The highly localized and timed secretion of biotrophic effectors can effectively reduce undesired impacts and pleiotropy associated with manipulation of cell cycle components. Furthermore, these effectors often function in a dominant fashion, allowing insights into cell cycle modulation and cellular differentiation programs that are nearly impossible to unravel in the context of development. Although elucidation of host proteins and processes manipulated to achieve biotroph-induced endoreduplication is gaining momentum, our understanding of the metabolic underpinning and impact of endoreduplication remains limited. Important questions for the future include the following: How does endoreduplication result in enhanced metabolic capacity in the context of these interactions, and how is endoreduplication linked to source/sink changes and differentiation?

Disclosure Statement

The authors are not aware of any affiliations, memberships, funding, or financial holdings that might be perceived as affecting the objectivity of this review.

Acknowledgements

This work was supported by US National Science Foundation (NSF) grants (IOS-0958100 and MCB-1617020) to M.C.W., an NSF Graduate Research Fellowship to M.A.S., and Regional Centre for Biotechnology core funds to D.C.

Literature Cited

1. Ach RA, Durfee T, Miller AB, Taranto P, Hanley-Bowdoin L, et al. 1997. RRB1 and RRB2 encode maize retinoblastoma-related proteins that interact with a plant D-type cyclin and geminivirus replication protein. Mol. Cell. Biol. 17:5077–86
2. Araki S, Ito M, Soyano T, Nishihama R, Machida Y. 2004. Mitotic cyclins stimulate the activity of c-Myb- like factors for transactivation of G2/M phase-specific genes in tobacco. J. Biol. Chem. 279:32979–88
3. Arguello-Astorga G, Lopez-Ochoa L, Kong KJ, Orozco BM, Settlage SB, Hanley-Bowdoin L. 2004. A novel motif in geminivirus replication proteins interacts with the plant retinoblastoma-related protein. J. Virol. 78:4817–26

4. Asano T, Yoshioka Y, Kurei S, Sakamoto W, Sodmergen, Machida Y. 2004. A mutation of the CRUM- PLED LEAF gene that encodes a protein localized in the outer envelope membrane of plastids affects the pattern of cell division, cell differentiation, and plastid division in Arabidopsis. Plant J. 38:448–59
5. Ascencio-Iba´n˜ez JT, Sozzani R, Lee TJ, Chu TM, Wolfinger RD, et al. 2008. Global analysis of Arabidopsis gene expression uncovers a complex array of changes impacting pathogen response and cell cycle during geminivirus infection. Plant Physiol. 148:436–54
6. Bainard LD, Bainard JD, Newmaster SG, Klironomos JN. 2011. Mycorrhizal symbiosis stimulates en- doreduplication in angiosperms. Plant Cell Environ. 34:1577–85
7. Baloban M, Vanstraelen M, Tarayre S, Reuzeau C, Cultrone A, et al. 2013. Complementary and dose-dependent action of AtCCS52A isoforms in endoreduplication and plant size control. New Phytol. 198:1049–59
8. Baluska F, Bacigalova K, Oud JL, Hauskrecht M, Kubica S. 1995. Rapid reorganization and microtubular cytoskeleton accompanies early changes in nuclear ploidy and chromatin structure in postmitotic cells of barley leaves infected with powdery mildew. Protoplasma 185:140–51
9. Bellafiore S, Shen Z, Rosso M-N, Abad P, Shih P, Briggs SP. 2008. Direct identification of the Meloidogyne incognita secretome reveals proteins with host cell reprogramming potential. PLOS Pathol. 4:e1000192
10. Berkmans B, De Veylder L. 2009. Transcriptional control of the cell cycle. Curr. Opin. Plant Biol.12:599–605
11. Berta G, Fusconi A, Sampo` S, Lingua G, Perticone S, Repetto O. 2000. Polyploidy in tomato roots as affected by arbuscular mycorrhizal colonization. Plant Soil 226:37–44
12. Betsuyaku S, Sawa S, Yamada M. 2011. The function of the CLE peptides in plant development and plant-microbe interactions. Arabidopsis Book 9:e0149
13. Bischoff V, Nita S, Neumetzler L, Schindelasch D, Urbain A, Eshed R, et al. 2010. TRICHOME BIRE- FRINGENCE and its homolog At5g01360 encode plant-specific DUF231 proteins required for cellulose biosynthesis in Arabidopsis. Plant Physiol. 153:590–602
14. Bischoff V, Selbig J, Scheible WR. 2010. Involvement of TBL/DUF231 proteins into cell wall biology. Plant Signal. Behav. 5:1057–59
15. Boivin S, Fonouni-Farde C, Frugier F. 2016. How auxin and cytokinin phytohormones modulate root microbe interactions. Front. Plant Sci. 7:1240
16. Bourdon M, Pirrello J, Cheniclet C, Coriton O, Bourge M, et al. 2012. Evidence for karyoplasmic homeostasis during endoreduplication and a ploidy-dependent increase in gene transcription during tomato fruit growth. Development 139:3817–26
17. Brefort T, Doehlemann G, Mendoza-Mendoza A, Reissmann S, Djamei A, Kahmann R. 2009. Ustilago maydis as a pathogen. Annu. Rev. Phytopathol. 47:423–45
18. Breuer C, Braidwood K, Sugimoto K. 2014. Endocycling in the path of plant development. Curr. Opin. Plant Biol. 17:78–85
19. Breuer C, Stacey NJ, West CE, Zhao Y, Chory J, et al. 2007. BIN4, a novel component of the plant DNA topoisomerase VI complex, is required for endoreduplication in Arabidopsis. Plant Cell 19:3655–68
20. Caillaud MC, Dubreuil G, Quentin M, Perfus-Barbeoch L, Lecomte P, de Almeida Engler J, et al. 2008. Root-knot nematodes manipulate plant cell functions during a compatible interaction. J. Plant Physiol. 165:104–13

21. Castillo A, Collinet D, Deret S, Kashoggi A, Bejarano ER. 2003. Dual interaction of plant PCNA with geminivirus replication accessory protein (Ren) and viral replication protein (Rep). Virology 312:381–94
22. Catoira R, Galera C, de Billy F, Penmetsa RV, Journet EP, et al. 2000. Four genes of Medicago truncatula controlling components of a Nod factor transduction pathway. Plant Cell 12:1647–66
23. Cebolla A, Vinardell JM, Kiss E, Ola´h B, Roudier F, et al. 1999. The mitotic inhibitor ccs52 is required for endoreduplication and ploidy-dependent cell enlargement in plants. EMBO J. 18:4476–84
24. Chandran D, Inada N, Hather G, Kleindt CK, Wildermuth MC. 2010. Laser microdissection of Arabidopsis cells at the powdery mildew infection site reveals site-specific processes and regulators. PNAS 107:460–65
25. Chandran D, Rickert J, Cherk C, Dotson BR, Wildermuth MC. 2013. Host cell ploidy underlying the fungal feeding site is a determinant of powdery mildew growth and reproduction. Mol. Plant-Microbe Interact. 26:537–45
26. Chandran D, Rickert J, Huang Y, Steinwand MA, Marr SK, Wildermuth MC. 2014. Atypical E2F transcriptional repressor DEL1 acts at the intersection of plant growth and immunity by controlling the hormone salicylic acid. Cell Host Microbe 15:506–13
27. Chandran DC, Wildermuth M. 2016. Modulation of host endocycle during plant-biotroph interactions. In The Enzymes, Vol. 40: Developmental Signaling in Plants, ed. C Lin, S Luan, pp. 65–103, Burlington, MA: Academic
28. de Almeida Engler J, Favery B, Engler G, Abad P. 2005. Loss of susceptibility as an alternative for nematode resistance. Curr. Opin. Biotechnol. 16:112–17
29. de Almeida Engler J, Gheysen G. 2013. Nematode-induced endoreduplication in plant host cells: Why and how? Mol. Plant-Microbe Interact. 26:7–24
30. de Almeida Engler J, Kyndt T, Vieira P, Van Cappelle E, Boudolf V, et al. 2012. CCS52 and DEL1 genes are key components of the endocycle in nematode-induced feeding sites. Plant J. 72:185–98
31. Desvoyes B, Ramirez-Parra E, Xie Q, Chua N-H, Gutierrez C. 2006. Cell type–specific role of the retinoblastoma/E2F pathway during Arabidopsis leaf development. Plant Physiol. 140:67–80
32. de Veylder L, Beeckman T, Beemster GTS, Krols L, Terras F, et al. 2001. Functional analysis of cyclin- dependent kinase inhibitors of Arabidopsis. Plant Cell 13:1653–68
33. de Veylder L, Larkin JC, Schnittger A. 2011. Molecular control and function of endoreplication in development and physiology. Trends Plant. Sci. 16:624–34
34. Djordjevic MA, Mohd-Radzman NA, Imin N. 2015. Small-peptide signals that control root nodule number, development, and symbiosis. J. Exp. Bot. 66:5171–81
35. Efroni I, Blum E, Goldschmidt A, Eshed Y. 2008. A protracted and dynamic maturation schedule underlies Arabidopsis leaf development. Plant Cell 20:2293–306
36. Egelkrout EM, Mariconti L, Settlage SB, Cella R, Robertson D, Hanley-Bowdoin L. 2002. Two E2F elements regulate the proliferating cell nuclear antigen promoter differently during leaf development. Plant Cell 14:3225–36
37. Egelkrout EM, Robertson D, Hanley-Bowdoin L. 2001. Proliferating cell nuclear antigen transcription is repressed through an E2F consensus element and activated by geminivirus infection in mature leaves. Plant Cell 13:1437–52

38. Etemadi M, Gutjahr C, Couzigou JM, Zouine M, Lauressergues D, et al. 2014. Auxin perception is required for arbuscule development in arbuscular mycorrhizal symbiosis. Plant. Physiol. 166:281–92
39. Favery B, Complainville A, Vinardell JM, Lecomte P, Vaubert D, et al. 2002. The endosymbiosis-induced genes ENOD40 and CCS52a are involved in endoparasitic-nematode interactions in Medicago truncatula. Mol. Plant-Microbe Interact. 15:1008–13
40. Favery B, Quentin M, Jaubert-Possamai S, Abad P. 2016. Gall-forming root-knot nematodes hijack key plant cellular functions to induce multinucleate and hypertrophied feeding cells. J. Insect Pathol. 84:60–69
41. Fusconi A, Lingua G, Trotta A, Berta G. 2005. Effects of arbuscular mycorrhizal colonization and phosphorus application on nuclear ploidy in Allium porrum plants. Mycorrhiza 15:313–21
42. Gegas VC, Wargent JJ, Pesquet E, Granqvist E, Paul ND, Doonan JH. 2014. Endopolyploidy as a potential alternative adaptive strategy for Arabidopsis leaf size variation in response to UV-B. J. Exp. Bot. 65:2757–66
43. Genre A, Chabaud M, Faccio A, Barker DG, Bonfante P. 2008. Prepenetration apparatus assembly precedes and predicts the colonization patterns of arbuscular mycorrhizal fungi within the root cortex of both Medicago truncatula and Daucus carota. Plant Cell 20:1407–20
44. Genschik P, Marrocco K, Bach L, Noir S, Criqui M-C. 2014. Selective protein degradation: a rheostat to modulate cell-cycle phase transitions. J. Exp. Bot. 65:2603–15
45. Glawe DA. 2008. The powdery mildews: a review of the world's most familiar (yet poorly known) plant pathogens. Annu. Rev. Phytopathol. 46:27–51
46. Gohlke J, Deeken R. 2014. Plant responses to Agrobacterium tumefaciens and crown gall development. Front. Plant Sci. 5:155
47. Gomez SK, Harrison MJ. 2009. Laser microdissection and its application to analyze gene expression in arbuscular mycorrhizal symbiosis. Pest Manag. Sci. 65:504–11
48. Grunewald W, Cannoot B, Friml J, Gheysen G. 2009. Parasitic nematodes modulate PIN-mediated auxin transport to facilitate infection. PLOS Pathol. 5:e1000266
49. Guo Y, Ni J, Denver R, Wang X, Clark S. 2011. Mechanisms of molecular mimicry of plant CLE peptide ligands by the parasitic nematode Globodera rostochiensis. Plant Physiol. 157:476–84
50. Gutierrez C. 2009. The Arabidopsis cell division cycle. Arabidopsis Book 7:e0120.2009
51. Haga N, Kato K, Murase M, Araki S, Kubo M, et al. 2007. R1R2R3-Myb proteins positively regulate cytokinesis through activation of KNOLLE transcription in Arabidopsis thaliana. Development 134:1101–10
52. Harrison MJ. 2012. Cellular programs for arbuscular mycorrhizal symbiosis. Curr. Opin. Plant Biol. 15:691–98
53. Hershko A. 1999. Mechanisms and regulation of the degradation of cyclin B. Philos. Trans. R. Soc. Lond. B 354:1571–76
54. Hewezi T, Howe P, Maier TR, Hussey RS, Mitchum MG, et al. 2008. Cellulose binding protein from the parasitic nematode Heterodera schachtii interacts with Arabidopsis pectin methylesterase: cooperative cell wall modification during parasitism. Plant Cell 20:3080–93
55. Heyman J, de Veylder L. 2012. The anaphase-promoting complex/cyclosome in control of plant devel- opment. Mol. Plant. 5:1182–94

56. Horva´th B, Yeun LH, Domonkos A, Hala´sz G, Gobbato E, et al. 2011. Medicago truncatula IPD3 is a member of the common symbiotic signaling pathway required for rhizobial and mycorrhizal symbioses. Mol. Plant-Microbe Interact. 24:1345–58
57. Hu Z, Cools T, De Veylder L. 2016. Mechanisms used by plants to cope with DNA damage. Annu. Rev. Plant Biol. 67:439–58
58. Huang G, Allen R, Davis EL, Baum TJ, Hussey RS. 2006. Engineering broad root-knot resistance in transgenic plants by RNAi silencing of a conserved and essential root-knot nematode parasitism gene. PNAS 103:14302–6
59. Hudik E, Yoshioka Y, Domenichini S, Bourge M, Soubigout-Taconnat L, et al. 2014. Chloroplast dysfunction causes multiple defects in cell cycle progression in the Arabidopsis crumpled leaf mutant. Plant Physiol. 166:152–67
60. Jegu T, Latrasse D, Delarue M, Mazubert C, Bourge M, et al. 2013. Multiple functions of Kip-related protein5 connect endoreduplication and cell elongation. Plant Physiol. 161:1694–705
61. Jiang L, Wang H, Zhuang X, Wang X, Law HY, Zhao T, et al. 2016. Demonstration of a distinct pathway for polar exocytosis for plant cell wall formation. Plant Physiol. 172:1003–18
62. Jones KM, Kobayashi H, Davies BW, Taga ME, Walker GC. 2007. How rhizobial symbionts invade plants: the Sinorhizobium-Medicago model. Nat. Rev. Microbiol. 5:619–33
63. Kay S, Hahn S, Marois E, Hause G, Bonas U. 2007. A bacterial effector acts as a plant transcription factor and induces a cell size regulator. Science 318:648–51
64. Kieffer M, Master V, Waites R, Davies B. 2011. TCP14 and TCP15 affect internode length and leaf shape in Arabidopsis. Plant J. 68:147–58
65. Kirik V, Schrader A, Uhrig JF, Hulskamp M. 2007. MIDGET unravels functions of the Arabidopsis topoisomerase VI complex in DNA endoreduplication, chromatin condensation, and transcriptional silencing. Plant Cell 19:3100–10
66. Kobayashi K, Suzuki T, Iwata E, Magyar Z, Bogre L, Ito M. 2015. MYB3Rs, plant homologs of Myb oncoproteins, control cell cycle–regulated transcription and form DREAM-like complexes. Transcription 6:106–11
67. Kobayashi K, Suzuki T, Iwata E, Nakamichi N, Suzuki T, et al. 2015. Transcriptional repression by MYB3R proteins regulates plant organ growth. EMBO J. 34:1992–2007
68. Kondorosi E, Kondorosi A. 2004. Endoreduplication and activation of the anaphase-promoting complex during symbiotic cell development. FEBS Lett. 567:152–57
69. Kong LJ, Orozco BM, Roe JL, Nagar S, Ou S, et al. 2000. A geminivirus replication protein interacts with the retinoblastoma protein through a novel domain to determine symptoms and tissue specificity of infection in plants. EMBO J. 19:3486–95
70. Kuhn H, Kwaaitaal M, Kusch S, Acevedo-Garcia J, Wu H, Panstruga R. 2016. Biotrophy at its best: novel findings and unsolved mysteries of the Arabidopsis–powdery mildew pathosystem. Arabidopsis Book 14:e0184
71. Kyndt T, Goverse A, Haegeman A, Warmerdam S, Wanjau C, et al. 2016. Redirection of auxin flow in Arabidopsis thaliana roots after infection by root-knot nematodes. J. Exp. Bot. 67:4559–70
72. Kyndt T, Vieira P, Gheysen G, de Almeida-Engler J. 2013. Nematode feeding sites: unique organs in plant roots. Planta 238:807–18
73. Lammens T, Boudolf V, Kheibarshekan L, Zalmas LP, Gaamouche T, et al. 2008. Atypical E2F activity restrains APC/CCCS52A2 function obligatory for endocycle onset. PNAS 105:14721–26

74. Larson-Rabin Z, Li Z, Masson PH, Day CD. 2008. FZR2/CCS52A1 expression is a determinant of endoreduplication and cell expansion in Arabidopsis. Plant Physiol. 149:874–84
75. Lee C, Chronis D, Kenning C, Peret B, Hewezi T, et al. 2011. The novel cyst nematode effector protein 19C07 interacts with the Arabidopsis auxin influx transporter LAX3 to control feeding site development. Plant Physiol. 155:866–80
76. Lee HO, Davidson JM, Duronio RJ. 2009. Endoreplication: polyploidy with purpose. Genes Dev. 23:2461–77
77. Le Fevre R, Evangelisti E, Rey T, Schornack S. 2015. Modulation of host cell biology by plant pathogenic microbes. Annu. Rev. Cell Dev. Bio. 31:201–29
78. Li ZY, Li B, Dong AW. 2012. The Arabidopsis transcription factor AtTCP15 regulates endoreduplication by modulating expression of key cell-cycle genes. Mol. Plant 5:270–80
79. Liu L, Chung HY, Lacatus G, Baliji S, Ruan J, Sunter G. 2014. Altered expression of Arabidopsis genes in response to a multifunctional geminivirus pathogenicity protein. BMC Plant Biol. 14:302
80. Lukhovitskaya NI, Solovieva AD, Boddeti SK, Thaduri S, Solovyev AG, Savenkov EI. 2013. An RNA virus-encoded zinc-finger protein acts as a plant transcription factor and induces a regulator of cell size and proliferation in two tobacco species. Plant Cell 25:960–73
81. Magyar Z, Horvath B, Khan S, Mohammed B, Henriques R, et al. 2012. Arabidopsis E2FA stimulates proliferation and endocycle separately through RBR-bound and RBR-free complexes. EMBO J. 31:1480– 93
82. Marois E, Van den Ackerveken G, Bonas U. 2002. The Xanthomonas type III effector protein AvrBs3 modulates plant gene expression and induces cell hypertrophy in the susceptible host. Mol. Plant-Microbe Interact. 15:637–46
83. Maro´ ti G, Kondorosi E. 2014. Nitrogen-fixing Rhizobium-legume symbiosis: Are polyploidy and host peptide–governed symbiont differentiation general principles of endosymbiosis? Front. Microbiol. 5:326
84. Mart´ın-Trillo M, Cubas P. 2010. TCP genes: a family snapshot ten years later. Trends Plant Sci. 15:31–39
85. Maunoury N, Redondo-Nieto M, Bourcy M, Van de Velde W, Alunni B, et al. 2010. Differentiation of symbiotic cells and endosymbionts in Medicago truncatula nodulation are coupled to two transcriptome- switches. PLOS ONE 5:e9519
86. Mitra RM, Gleason CA, Edwards A, Hadfield J, Downie JA, et al. 2004. A Ca2+/calmodulin-dependent protein kinase required for symbiotic nodule development: gene identification by transcript-based cloning. PNAS 101:4701–5
87. Miyawki K, Tabata R, Sawa S. 2013. Evolutionarily conserved CLE peptide signaling in plant develop- ment, symbiosis, and parasitism. Curr. Opin. Plant Biol. 16:598–606
88. Morrison EN, Emery RJN, Saville BJ. 2015. Phytohormone involvement in the Ustilago maydis–Zea mays pathosystem: Relationships between abscisic acid and cytokinin levels and strain virulence in infected cob tissue. PLOS ONE 10:e0130945
89. Mortier V, Den Herder G, Whitford R, Van de Velde W, Rombauts S, et al. 2010. CLE peptides control Medicago truncatula nodulation locally and systemically. Plant Physiol. 153:222–37
90. Nagar S, Hanley-Bowdoin L, Robertson D. 2002. Host DNA replication is induced by geminivirus infection of differentiated plant cells. Plant Cell 14:2995–3007

91. Nagar S, Pedersen TJ, Carrick KM, Hanley-Bowdoin L, Robertson D. 1995. A geminivirus induces expression of a host DNA synthesis protein in terminally differentiated plant cells. Plant Cell 7:705–19
92. Noir S, Marrocco K, Masoud K, Thomann A, Gusti A, et al. 2015. The control of Arabidopsis thaliana growth by cell proliferation and endoreplication requires the F-Box protein FBL17. Plant Cell 27:1461–76
93. Oldroyd G. 2013. Speak, friend, and enter: signaling systems that promote beneficial symbiotic associa- tion in plants. Nat. Rev. Microbiol. 11:252–63
94. Ovchinnikova E, Journet EP, Chabaud M, Cosson V, Ratet P, et al. 2011. IPD3 controls the formation of nitrogen-fixing symbiosomes in pea and Medicago spp. Mol. Plant-Microbe Interact. 24:1333–44
95. Park S, Rancour DM, Bednarek SY. 2008. In planta analysis of the cell cycle–dependent localization of AtCDC48A and its critical roles in cell division, expansion, and differentiation. Plant Physiol. 148:246–58
96. Parniske M. 2008. Arbuscular mycorrhiza: the mother of plant root endosymbioses. Nat. Rev. Microbiol. 6:763–75
97. Peng H, Cui J, Long H, Huang W, Kong L, et al. 2016. Novel pectate lyase genes of Heterodera glycines play key roles in the early stage of parasitism. PLOS ONE 11:e0149959
98. Quentin M, Abad P, Favery B. 2013. Plant parasitic nematode effector target host defense and nuclear functions to establish feeding cells. Front. Plant Sci. 4:53
99. Rancour DM, Dickey CE, Park S, Bednarek SY. 2002. Characterization of AtCDC48. Evidence for multiple membrane fusion mechanisms at the plane of cell division in plants. Plant Physiol. 130:1241–53
100. Rancour DM, Park S, Knight SD, Bednarek SY. 2004. Plant UBX domain-containing protein 1, PUX1, regulates the oligomeric structure and activity of Arabidopsis CDC48. J. Biol. Chem. 279:54264–74
101. Raynaud C, Mallory AC, Latrasse D, Je´gu T, Bruggeman Q, et al. 2014. Chromatin meets the cell cycle. J. Exp. Bot. 65:2677–89
102. Rehman S, Gupta VK, Goyal AK. 2016. Identification and functional analysis of secreted effectors from phytoparasitic nematodes. BMC Microbiol. 16:48
103. Repetto O, Massa N, Gianinazzi-Pearson V, Dumas-Gaudot E, Berta G. 2007. Cadmium effects on populations of root nuclei in two pea genotypes inoculated or not with the arbuscular mycorrhizal fungus Glomus mosseae. Mycorrhiza 17:111–20
104. Replogle A, Wang J, Bleckmann A, Hussey RS, Baum TJ, et al. 2011. Nematode CLE signaling in Arabidopsis requires CLAVATA2 and CORYNE. Plant J. 65:430–40
105. Rojas M, Hagen C, Lucas WJ, Gilbertson RL. 2005. Exploiting chinks in the plant's armor: evolution and emergence of geminiviruses. Annu. Rev. Phytopathol. 43:361–94
106. Roodbarkelari F, Bramsiepe J, Weinl C, Marquardt S, Novak B, et al. 2010. Cullin 4-ring finger-ligase plays a key role in the control of endoreplication cycles in Arabidopsis trichomes. PNAS 107:15275–80
107. Roux B, Rodde N, Jardinaud MF, Timmers T, Sauviac L, et al. 2014. An integrated analysis of plant and bacterial gene expression in symbiotic root nodules using laser-capture microdissection coupled to RNA sequencing. Plant J. 77:817–37
108. Sadasivam S, DeCaprio JA. 2013. The DREAM complex: master coordinator of cell cycle–dependent gene expression. Nat. Rev. Cancer 13:585–95

109. Schnittger A, Weinl C, Bouyer D, Scho¨ binger U, Hu¨ lskamp M. 2003. Misexpression of the cyclin- dependent kinase inhibitor ICK1/KRP1 in single-celled Arabidopsis trichomes reduces endoreduplication and cell size and induces cell death. Plant Cell 15:303–15
110. Schweizer L, Yerk-Davis GL, Phillips RL, Srienc F, Jones RJ. 1995. Dynamics of maize endosperm development and DNA endoreduplication. PNAS 92:7070–74
111. Scofield S, Jones A, Murray JAH. 2014. The plant cell cycle in context. J. Exp. Bot. 65:2557–62
112. Serralbo O, Pe´rez-Pe´rez JM, Heidstra R, Scheres R. 2006. Non-cell-autonomous rescue of anaphase- promoting complex function revealed by mosaic analysis of HOBBIT, an Arabidopsis CDC27 homolog. PNAS 103:13250–55
113. Shen J, Chen X, Chen J, Sun L. 2016. A phloem-limited fijivirus induces the formation of neoplastic phloem tissues that house virus multiplication in the host plant. Sci. Rep. 6:29848
114. Siddique S, Radakovic Z, de la Torre CM, Chronis D, Nova´k O, et al. 2015. A parasitic nematode releases cytokinin that controls cell division and orchestrates feeding site formation in host plants. PNAS 112:12669–74
115. Simkova´ K, Kim C, Gacek K, Baruah A, Laloi C, Apel K. 2012. The chloroplast division mutant caa33 of Arabidopsis thaliana reveals the crucial impact of chloroplast homeostasis on stress acclimation and retrograde plastid-to-nucleus signaling. Plant J. 69:701–12
116. Sindhu AS, Maier TR, Mitchum MG, Hussey RS, Davis EL, Baum TJ. 2009. Effective and specific in planta RNAi in cyst nematodes: expression interference of four parasitism genes reduces parasitic success. J. Exp. Bot. 60:315–24
117. Singh BN, Sopory SK, Reddy MK. 2004. Plant DNA topoisomerases: structure, function, and cellular roles in plant development. Crit. Rev. Plant Sci. 23:251–69
118. Sobczak M, Golinowski W, Grundler FMW. 1997. Changes in the structure of Arabidopsis thaliana roots induced during development of males of the plant parasitic nematode Heterodera schachtii. Eur. J. Plant Pathol. 103:113–24
119. Sugimoto-Shirasu K, Roberts GR, Stacey NJ, McCann MC, Maxwell A, Roberts K. 2005. RHL1 is an essential component of the plant DNA topoisomerase VI complex and is required for ploidy-dependent cell growth. PNAS 102:18736–41
120. Sugimoto-Shirasu K, Stacey NJ, Corsar J, Roberts K, McCann MC. 2002. DNA topoisomerase VI is essential for endoreduplication in Arabidopsis. Curr. Biol. 12:1782–86
121. Suzaki T, Ito M, Yoro E, Sato S, Hirakawa H, et al. 2014. Endoreduplication-mediated initiation of symbiotic organ development in Lotus japonicus. Development 141:2441–45
122. Tahiri-Alaoui A, Lingua G, Avrova A, Sampo` S, Fusconi A, et al. 2002. A cullin gene is induced in tomato root forming arbuscular mycorrhizae. Can. J. Bot. 80:607–16
123. Takahashi N, Kajihara T, Okamura C, Kim Y, Katagiri Y, et al. 2013. Cytokinins control endocycle onset by promoting the expression of an APC/C activator in Arabidopsis roots. Curr. Biol. 23:1812–17
124. Trejo-Saavedra DL, Vielle-Calzada JP, Rivera-Bustamante RF. 2009. The infective cycle of Cabbage leaf curl virus (CaLCuV) is affected by CRUMPLED LEAF (CRL) gene in Arabidopsis thaliana. Virol. J. 6:169
125. Vanholme B, van Thuyne W, Vanhouteghem K, de Meutter J, Cannoot B, Gheysen G. 2007. Molecular characterization and functional importance of pectate lyase secreted by the cyst nematode Heterodera schachtii. Mol. Plant Pathol. 8:267–78

126. Verkest A, Manes CL, Vercruysse S, Maes S, Van Der Schueren E, et al. 2005. The cyclin-dependent kinase inhibitor KRP2 controls the onset of the endoreduplication cycle during Arabidopsis leaf develop- ment through inhibition of mitotic CDKA;1 kinase complexes. Plant Cell 17:1723–36
127. Vieira P, de Almeida Engler J. 2015. The plant cell inhibitor KRP6 is involved in multinucleation and cytokinesis disruption in giant-feeding cells induced by root-knot nematodes. Plant Signal. Behav. 10:e1010924
128. Vieira P, De Clercq A, Stals H, Van Leene J, Van De Slijke E, et al. 2014. The cyclin-dependent kinase inhibitor KRP6 induces mitosis and impairs cytokinesis in giant cells induced by plant-parasitic nematodes in Arabidopsis. Plant Cell 26:2633–47
129. Vieira P, Engler G, de Almeida Engler J. 2013. Enhanced levels of plant cell cycle inhibitors hamper root-knot nematode-induced feeding site development. Plant Signal. Behav. 8:e26409
130. Vieira P, Escudero C, Rodiuc N, Boruc J, Russinova E, et al. 2013. Ectopic expression of Kip-related proteins restrains root-knot nematode-feeding site expansion. New Phytol. 199:505–19
131. Vinardell JM, Fedorova E, Cebolla A, Kevei Z, Horvath G, et al. 2003. Endoreduplication mediated by the anaphase-promoting complex activator CCS52A is required for symbiotic cell differentiation in Medicago truncatula nodules. Plant Cell 15:2093–105
132. Vogel JP, Raab TK, Schiff C, Somerville SC. 2002. PMR6, a pectate lyase-like gene required for powdery mildew susceptibility in Arabidopsis. Plant Cell 14:2095–106
133. Vogel JP, Raab TK, Somerville CR, Somerville SC. 2004. Mutations in PMR5 result in powdery mildew resistance and altered cell wall composition. Plant J. 40:968–78
134. Wang J, Replogle A, Hussey R, Baum T, Wang X, et al. 2011. Identification of potential host plant mimics CLAVATA3/ESR (CLE)-like peptides from the plant-parasitic nematode Heterodera schachtii. Mol. Plant Pathol. 12:177–86
135. Weinl C, Marquardt S, Kuijt SJ, Nowack MK, Jakoby MJ, et al. 2005. Novel functions of plant cyclin- dependent kinase inhibitors, ICK1/KRP1, can act non-cell-autonomously and inhibit entry into mitosis. Plant Cell 17:1704–22
136. Wessling R, Epple P, Altmann S, He Y, Yang L, Henz SR. 2014. Convergent targeting of a common host protein-network by pathogen effectors from three kingdoms of life. Cell Host Microbe 16:364–75
137. Wildermuth MC. 2010. Modulation of host nuclear ploidy: a common plant biotroph mechanism. Curr. Opin. Plant Biol. 13:449–58
138. Williamson B. 1970. Induced DNA synthesis in orchid mycorrhiza. Planta 92:347–54
139. Yano K, Yoshida S, Mu¨ ller J, Singh S, Banba M, et al. 2008. CYCLOPS, a mediator of symbiotic intracellular accommodation. PNAS 105:20540–45
140. Yoo MJ, Liu X, Pires JC, Soltis PS, Soltis DE. 2014. Nonadditive gene expression in polyploids. Annu. Rev. Genet. 48:485–517
141. Yoon HJ, Hossain MS, Held M, Hou H, Kehl M, et al. 2014. Lotus japonicus SUNERGOS1 encodes a predicted subunit A of a DNA topoisomerase VI that is required for nodule differentiation and accom- modation of rhizobial infection. Plant J. 78:811–21
142. Zheng B, Chen X, McCormick S. 2011. The anaphase-promoting complex is a dual integrator that regulates both microRNA-mediated transcriptional regulation of Cyclin B1 and degradation of cyclin B1 during Arabidopsis male gametophyte development. Plant Cell 23:1033–46

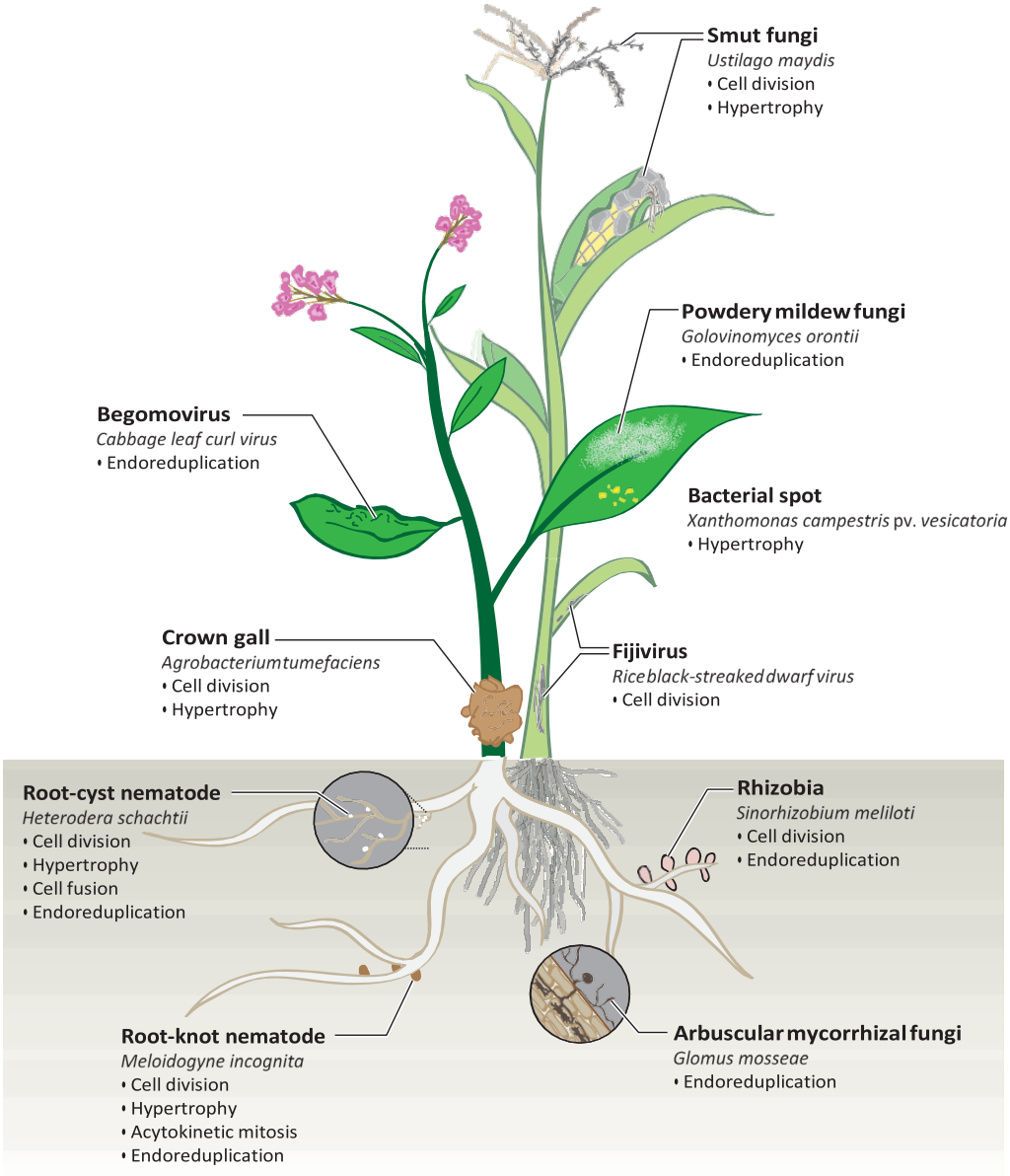

Figure 1. Diverse plant biotrophs manipulate the host cell cycle to promote their colonization, development, and proliferation. Manipulated cell fates of susceptible hosts include enhanced cell division, hypertrophy (hyper cell-expansion), acytokinetic mitosis (cytokinesis does not occur, resulting in two separate nuclei within one cell for each event), endoreduplication (cytokinesis and cell division do not occur, resulting in DNA content increased by 2*C* with each cycle), and cell fusion. Note that cell death is not induced by plant biotrophs. Examples shown reflect the evolutionary diversity of the biotrophs as well as the range of manipulated cell fates: *Ustilago maydis* on maize (17), *Golovinomyces orontii* on *Arabidopsis thaliana* (24), *Cabbage leaf curl virus* on *A. thaliana* (5), *Xanthamonas campestris* pv. *vesicatoria* on pepper (82), *Agrobacterium tumefaciens* associated with many hosts (46), *Rice black-streaked dwarf virus* on maize (113), *Heterodera schachtii* on *A. thaliana* (118, 29), *Sinorhizobium meliloti* on *Medicago truncatula* (83), *Meloidogyne incognita* on *A. thaliana* (29, 40), and *Glomus mosseae* on tomato (11). Note that *Xanthomonas campestris* pv. *vesicatoria* is a hemibiotroph; hypertrophy is induced as part of its biotrophic colonization.

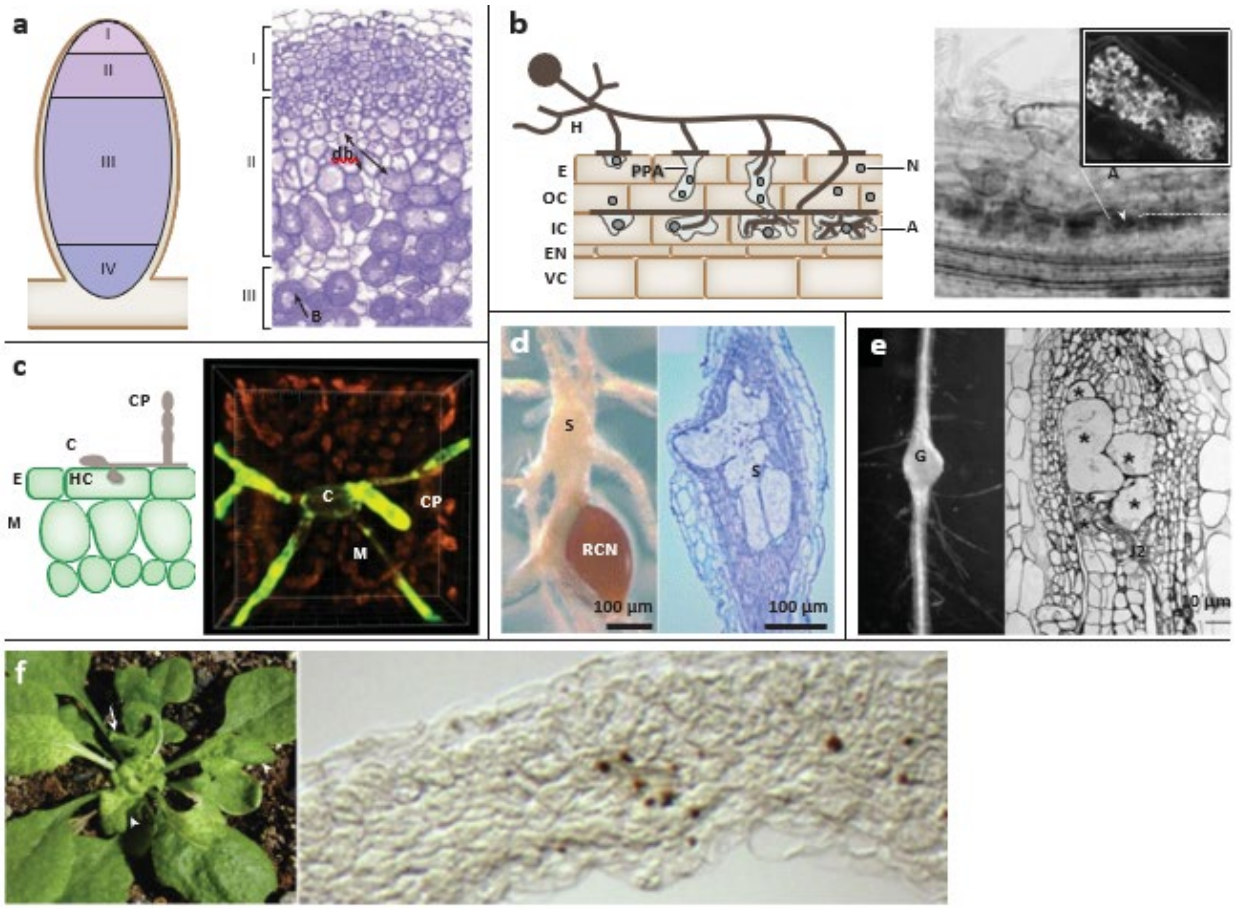

Figure 2. Plant-biotroph interaction sites with endoreduplicated cells associated with biotrophic nutrient acquisition. (*a*) Nodule development in *Medicago truncatula*. The structure of an indeterminate nodule showing the meristematic zone (I), infection zone (II), symbiotic zone (III), and senescence zone (IV). Longitudinal section of a *M. truncatula* root nodule showing growth and differentiation of symbiotic cells (from 68). In zone II, symbiotic cells enter successive endoreduplication cycles. In zone III, the symbiotic cells are terminally differentiated and packed with mature bacteroids, and they fix nitrogen. (*b*) Arbuscular mycorrhizal fungus (AMF) development in *M. truncatula* roots. The adhesion of a fungal hyphopodium to the root surface triggers formation of pre-penetration apparati (PPAs) in the contacted epidermal cell. This initiates PPA formation in the underlying outer cortical cell. The fungus then grows intercellularly, laterally along the root axis, and penetrates inner cortex cells with PPAs resulting in the development of branched arbuscules, as in Reference 43. Light micrograph of an *M. truncatula* root colonized with *Glomus versiforme* with inset of a cortical cell with arbuscules (modified from 47). (*c*) Powdery mildew infection of *Arabidopsis*. *Arabidopsis* leaf infected with *Golovinomyces orontii* 5 days post inoculation (dpi). The fungus penetrates the host epidermal cell and forms a haustorial complex (HC) through which it acquires nutrients. Further growth and reproduction of the fungus result in the formation of surficial hyphae and conidiophores bearing conidia. Endoreduplication is observed in enlarged mesophyll cells underlying the infected epidermal cell. Laser confocal microscopy image of an *Arabidopsis* leaf infected with *G. orontii* at 5 dpi shows a single fungal colony in green and autofluorescent chloroplasts in the underlying mesophyll cells in red. (*d*) (*Left*) Syncytium induced by root-cyst nematode (RCN) (from 28). (*Right) Arabidopsis* roots infected with *Heterodera schachtii* 5 dpi and a longitudinal section of the root with syncytium are shown. (*e*) *Arabidopsis* root infected with the root-knot nematode (RKN) *Meloidogyne incognita* results in the formation of a root gall. Longitudinal section at 7 dpi shows multinucleate giant cells (∗) and the juvenile RKN (J2) (from 20). (*f*) (*Left) Cabbage leaf curl virus* symptoms on *Arabidopsis* rosette leaves at 12 dpi. (*Right*) Distribution of CaLCuV virus visualized by immunolocalization of Rep/AL1 in transverse section of leaf 9 of infected plant at 12 dpi. Panels *a–e* are adapted from *Curr. Opin. Plant Biol.* 13, Wildermuth MC, Modulation of host nuclear ploidy: a common plant biotroph mechanism, 449–458, 2010, with permission from Elsevier. Panel *f* is adapted with permission from the American Society of Plant Biologists, Global analysis of *Arabidopsis* gene expression uncovers a complex array of changes impacting pathogen response and cell cycle during geminivirus infection, Ascencio-Iba´n˜ ez JT, Sozzani R, Lee TJ, Chu TM, Wolfinger RD, et al., *Plant Physiol.* 148:436–454, 2008; permission conveyed through Copyright Clearance Center, Inc. Abbreviations: A, arbuscule; B, bacteroid; C, conidia; CP, conidiophore; db, developing bacteroid; E, epidermal cell; EN, endodermis; G, root gall; H, hyphopodium; IC, inner cortex; M, mesophyll cell; N, nucleus; OC, outer cortical cell; S, syncytium; VC, vascular cylinder.

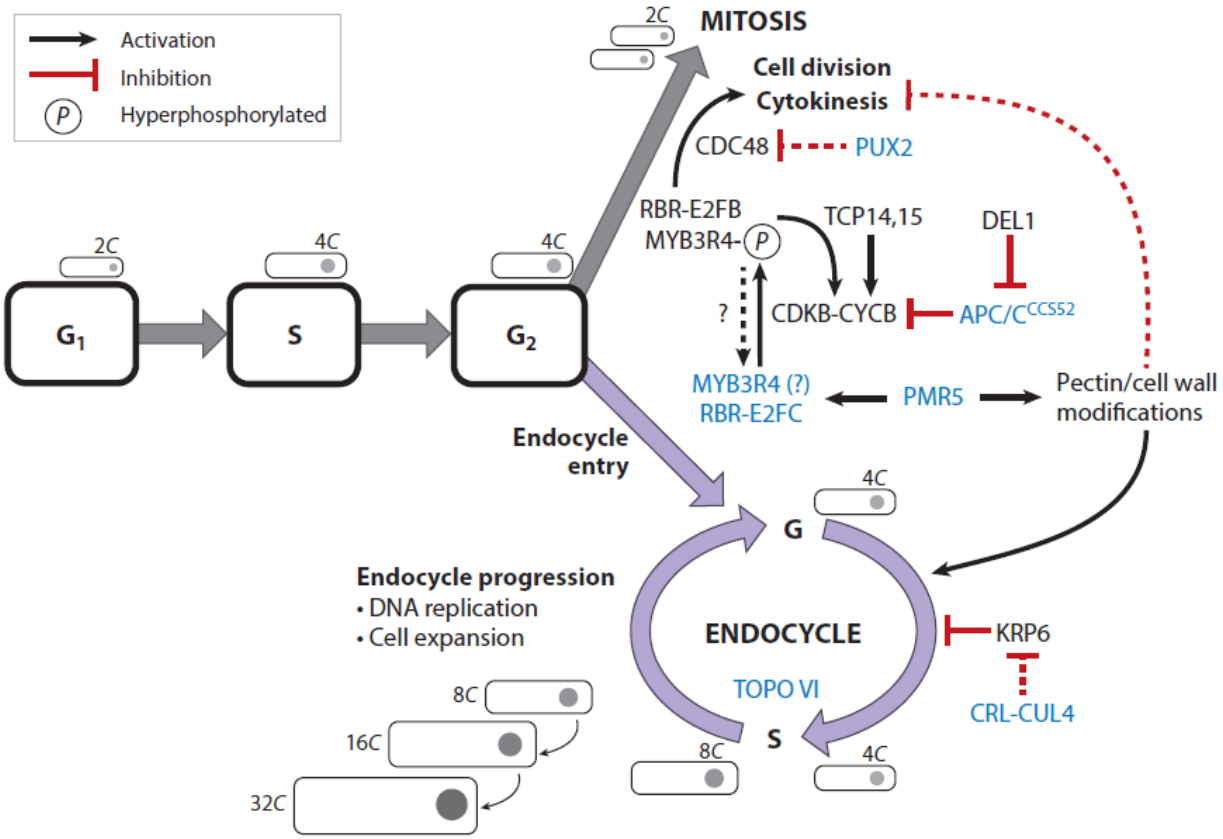

Figure 3. Modulation of host cell cycle machinery by adapted plant biotrophs to promote endoreduplication. The mitotic cell cycle progresses through gap (G) and DNA synthesis (S) phases to mitosis (M). The endocycle is a variant of the cell cycle in which DNA is replicated but mitosis does not occur, resulting in a doubling of DNA content with each endocycle round. A simplified model showing the proposed function of identified host factors in promoting endocycle entry and progression is presented. Endocycle entry is controlled at the G2-M boundary to promote the endocycle and inhibit mitosis in the specific context of each interaction. MYB3R4-P is the promitotic hyperphosphorylated form of MYB3R4; hyperphosphorylation by the B-type cyclin-dependent kinase-cyclin B (CDKB-CYCB) complex is shown. CDK-CYC complexes other than CDKB-CYCB and E2F dimerization partners are omitted for simplicity. Inhibition of CDKB-CYCB complex accumulation promotes endoreduplication. This can be achieved through (*a*) degradation of CDKB-CYCB via the activated APC/CCCS52 complex, (*b*) decreased expression of *CDKB* or *CYCB* via degradation or inhibition of promitotic transcriptional activators MYB3R4-P, TCP14, and TCP15, or (*c*) inhibition of cyclin-dependent kinase activity via CDK inhibitors, such as KRP2 (*not shown*). RBR1-MYB3R-E2FC repressive complexes restrict the expression of M-phase genes in G1-S (66, 67) (*not shown*). Here, we propose that un(der)phosphorylated MYB3R4 complexed with RBR-E2FC inhibits M-phase gene expression to promote the endocycle. Although factors that control CDKB-CYCB accumulation and thus MYB3R4-P are known, direct MYB3R4-P dephosphorylation via a phosphatase remains a theoretical possibility. PMR5 likely acts upstream of MYB3R and HDZips (*not shown*) to promote endoreduplication and cell expansion (25). In addition to PMR5, PMR6 and PME3 (*not shown*) also modify pectin/cell wall with impacts that suggest an inhibitory effect on mitosis (cytokinesis) and promotion of the endocycle. Similarly, PUX2 is an adapter of the AAA-ATPase CDC48 that is co-localized to the cell division plane during cytokinesis (99, 100). Endocycle progression involves repeated cycles of G-S, which presumably require alternating low and high levels of A-type cyclin-dependent kinase (CDKA)-CYC to allow licensing of replication origins and S-phase transcription, respectively. CRL-CUL4 proteolysis of KRPs, which inhibit specific CDK complexes, could then promote or inhibit endocycle progression in a context-dependent manner, as proposed for KRP6. DNA replication appears to specifically utilize DNA topoisomerase VI (TOPO VI). Proteins in blue promote endoreduplication. Dashed lines are proposed functions. Please refer to **Table 1** and the text for additional detail.

Table 1. Proteins and other factors with known or putative roles in biotroph-induced plant cell endoreduplication

Host target	Role in cell cycle	Biotroph effector interacting with/impacting host target	Gene expression in interaction	Plant mutant/overexpression (OEX) phenotype	Reference
Rhizobia symbiosis					
CCS52A	APC/C activator	ND	Expressed in nodule ZII	Downregulation of *CCS52A* reduced ploidy in nodules; smaller/aborted nodules unable to fix nitrogen	131
VAG1/RHL1	DNA topoisomerase VI subunit A	ND	Expressed in proliferating cortical cells in nodule ZI	*vag1* mutant has reduced ploidy in formed nodules and no increase in ploidy in outermost cortical cells; many infection threads failed to reach cortical cells; fewer nodules and colonized cells	121
SUNERGOS1/ RHL2	DNA topoisomerase VI subunit A	ND	ND	*sunergos1* mutant has reduced ploidy in nodules; many infection threads failed to reach cortical cells; less-developed nodule primordia and smaller nodules	141
CLAVATA3/ embryo-surrounding region (CLE) peptides	Controls proliferation and differentiation in development	ND	*MtCLE13* expressed early in nodule development; *MtCLE12* and *MtCLE13* are expressed in differentiating nodules and nodule apex	OEX of *MtCLE13* or *MtCLE12* impedes nodule development	89
IPD3 (interacting protein of DMI3)	Unknown	NOD factor	Expressed in nodule ZII and ZIII	Mutant shows reduced ploidy in nodules (similar to control roots) and blocked symbiosome formation	85, 94
DMI3 [calcium/ calmodulin-dependent kinase (CaCMK)]	Unknown	NOD factor	Expressed maximally in nodule ZII	Mutant fails to initiate symbiotic gene expression or cell divisions for nodule formation	86

(*Continued*)

Table 1 (*Continued*)

Host target	Role in cell cycle	Biotroph effector interacting with/impacting host target	Gene expression in interaction	Plant mutant/overexpression (OEX) phenotype	Reference
Root nematode parasitism					
CCS52A1 (AT4G22910), CCS52A2 (AT4G11920), CCS52B (AT5G13840)	Activator of APC/C; promotes endocycle	ND	Expressed in giant cells and syncytia	Mutants showed reduced size of nuclei and misformed feeding sites, whereas OEX results in higher ploidy in giant cells and syncytium than that in the WT	30
DEL1/E2FE (AT3G48160)	Atypical E2F transcription factor; supresses entry into endocycle through repression of CCS52	ND	Low expression in giant cells and syncytia	Root-cyst nematodes (RCN): OEX and mutant show malformed, small syncytia. Root-knot nematode (RKN): OEX and mutant show small giant cells with little cytoplasm	30
RHL1 (AT1G48380)	Subunit of DNA topoisomerase VI	ND	ND	Mutant exhibits reduced ploidy; no syncytia formation by RCN, whereas RKN formed minute giant cells	30, 119
KRP1 (AT2G23430)	CDK inhibitor; promotes mitosis	ND	Not expressed during feeding site development but expressed in endoreduplicating leaf cells	Infected mutant shows increased number of nuclei and abnormal neighboring vascular cells; OEX lines exhibited reduced size and nuclei count in giant cells and reduced mitotic division in neighboring cells	129, 130
KRP2 (AT3G50630)	CDKA inhibitor; promotes mitosis	ND	Highly expressed during feeding site development	Infected mutant line shows increased number of nuclei and abnormal neighboring vascular cells; OEX lines exhibited reduced size and nuclei count in giant cells and reduced mitotic division in neighboring cells	32, 129, 130
KRP6 (AT3G19150)	CDK inhibitor, promotes mitosis; apparent role in cytokinesis/ endocycle inhibition	ND	Strongly expressed in developing galls, with reduced expression prior to endocycle entry	OEX lines exhibit decreased size of giant cells; increased number of nuclei but with lower ploidy index than that in the WT	128

(*Continued*)

Table 1 (*Continued*)

Host target	Role in cell cycle	Biotroph effector interacting with/impacting host target	Gene expression in interaction	Plant mutant/overexpression (OEX) phenotype	Reference
LAX3 (AT1G77690)	Auxin efflux protein	Hs19C07	Expression upregulated in cells to be incorporated into feeding structure	Mutant lines deficient in auxin transport support fewer RCN	71, 75
PME3 (AT5G47500)	Pectin methylesterase	HsCBP	Expression upregulated upon infection	Mutant line supports less RCN growth	54
Pectin	Pectin modifications may impact cell plate and division, cytokinesis, and expansion	Secreted pectate lyases (PELs)	ND	RNAi of nematode *PELs* reduced number of nematode feeding sites and reproduction; no data on plant mutant phenotype	97
CLV2 (AT1G65380), BAM1 (AT5G65700), BAM2 (AT3G49670)	Meristem identity	Secreted CLE peptides	*CLV2* expression increased in syncytia fed upon by parasitic nematodes	Secreted CLEs were modified by the host plant cell and interacted with CLV2 and related BAM1 plant receptors in transient expression system; treatment with secreted CLEs altered root development; no data on plant mutant phenotype	49, 104
Arbuscular mycorrhizal fungi symbiosis					
IPD3/ CYCLOPS	CaCMK-interacting protein	ND	Expressed in dividing cortical cells and nodule	In mutant lines, hyphal growth penetrated the roots yet failed to form arbuscules	56, 139
microRNA393	Downregulates auxin receptors	ND	*miRNA393* downregulation occurs upon colonization; Strong DR5-GUS expression observed in cells with arbuscules	*miRNA393* OEX lines exhibit reduced expression of *miRNA393* targets (auxin receptors *TIR1* and *AFB2*) and underdeveloped arbuscules	38
DMI3 (CaCMK)	Unknown	Myc factor	ND	Mutant shows mycorrhizal growth arrested at appressorium stage	22

(*Continued*)

Table 1 (*Continued*)

Host target	Role in cell cycle	Biotroph effector interacting with/impacting host target	Gene expression in interaction	Plant mutant/overexpression (OEX) phenotype	Reference
Powdery mildew parasitism					
MYB3R4 (AT5G11510)	TF; hyperphosphorylated form activates mitosis	ND	*MYB3R4* shows PM infection site-specific expression; targets of MYB3R4 were downregulated specifically at the infection site	Mutant supports lower reproductive growth of PM; PM-induced ploidy is not observed in mesophyll cells underlying the infection site	24, 25
PUX2 (AT2G01650)	AAA-ATPase CDC48 interactor; associated with cytokinesis	ND	*PUX2* shows PM infection site-specific expression	Mutant supports lower reproductive growth of PM; basal mesophyll ploidy is lower than that in the WT; PM-induced ploidy occurs in the mesophyll cells underlying the infection site, but the final ploidy level in these cells is lower than that in the WT	24, 25
PMR5 (AT5G58600)	Trichome birefringence family member; plant specific	ND	Unchanged	Mutant supports lower reproductive growth of PM; basal mesophyll ploidy similar to that in the WT; however, PM-induced ploidy is not observed	24, 25
PMR6 (AT3G54920)	Pectate lyase like; plant specific	ND	Unchanged	Mutant supports lower reproductive growth of PM; basal mesophyll ploidy is lower than that in the WT; PM-induced ploidy occurs in the mesophyll cells underlying the infection site, but the final ploidy level in these cells is lower than that in the WT	24, 25
CCS52A1 (AT4G22910)	Activator of APC/C; promotes endocycle	ND	Induced at site of infection	Preliminary analysis of null mutants showed a small but significant reduction in PM reproduction	27

(*Continued*)

Table 1 (*Continued*)

Host target	Role in cell cycle	Biotroph effector interacting with/impacting host target	Gene expression in interaction	Plant mutant/overexpression (OEX) phenotype	Reference
TCP13 (AT3G02150)	TF; in class of leaf development regulators active during the primary stage of leaf morphogenesis	Interacts with OEC 45, 61, and 78; supported by Y2H	Unchanged	Mutant at both seedling and mature stages supports enhanced PM reproduction; constitutive expression of a miRNA targeting *TCP 5*, *13*, and *17* resulted in larger leaves and proximal expansion of the blade into the petiole domain	24, 35, 136
TCP14 (AT3G47620)	TF; regulates cell proliferation in leaf and floral organs	Interacts with OEC 113, 125, 45, 88, 120, 101, 23, 21, 110, 16, 60, 103, 106, 35, 119, 117, 92, 23, 55, and 39; supported by Y2H	Unchanged	Mutant at both seedling and mature plant stage supports enhanced PM reproduction; *TCP14* repressor lines exhibit enhanced ploidy and branching in trichomes; leaves show delayed onset of endoreduplication	24, 64, 78, 136
TCP15 (AT1G69690)	TF; regulates expression of CYCA2;3 and retinoblastoma protein (E2F transcriptional regulator driving G1 to S); promotes cell division	Interacts with OEC 21, 39, 67, and 78; supported by Y2H	Unchanged	Mutant at the seedling stage supports enhanced PM reproduction; *TCP* repressor lines exhibit enhanced ploidy in trichomes, leaves, and the hypocotyl	24, 64, 78, 136
APC8, CDC23 (AT3G48150)	Anaphase-promoting complex subunit; ubiquitination of cell cycle proteins	Interacts with OEC 67; supported by Y2H	Unchanged	Mutant at the seedling stage supports enhanced PM reproduction	24, 53, 136
***Cabbage leaf curl virus* parasitism**					
RBR (AT3G12280)	Retinoblastoma-related protein; master regulator of cell fate	Interacts with viral Rep and Ren proteins to alter E2F-specific interactions and cell cycle outcomes; promotes expression of genes in S phase and endocycle	Unchanged	When Rep-RBR binding was reduced, viral DNA replication and symptoms were dramatically reduced	1, 3, 5, 69

(*Continued*)

Table 1 (*Continued*)

Host target	Role in cell cycle	Biotroph effector interacting with/impacting host target	Gene expression in interaction	Plant mutant/overexpression (OEX) phenotype	Reference
E2FB (AT5G22220)	TF; promotes mitosis	ND	ND	OEX line did not allow viral replication or disease and had greatly reduced cell ploidy in mature leaves	5
E2FC (AT1G47870)	TF; promotes endocycle	ND	Induced by infection	OEX had minimal impact on viral replication or disease; mature leaf ploidy was similar to that in the WT	5
E2FA (AT2G36010)	TF; promotes S-gene synthesis	ND	Unchanged	OEX had minimal impact on viral replication or disease; mature leaf ploidy was similar to that in the WT	5
CYCD3;1 (AT4G34160), CYCD3;2 (AT5G67260), CYCD3;3 (AT3G50070)	Cyclin D; promotes synthesis of S-phase genes	ND	*CYCD3;1*, unchanged; *CYCD3;2*, reduced by infection; *CYCD3;3*, ND	*CYCD3;1* OEX did not allow viral replication or disease; *cycd3;1,2,3* triple mutant supported viral replication similar to that in the WT	5
PCNA	Proliferating cell nuclear antigen; DNA replication	Interacts with viral Rep and Ren proteins	Induced by infection	Rep1 is sufficient to induce PCNA	91
CAA33/ CRUMPLED LEAF (AT5G51020)	Constitutive activator of AAA-ATPase	ND	Induced by infection	Silenced *CAA33* lines accumulate less virus and shows reduced symptoms; *CAA33* OEX supports more virus and symptoms; ploidy was not examined in these lines; *caa33* mutants are dwarfed in stature with reduced cell division, early/ aberrant entry into the endocycle, and curled and crumpled leaves	4, 59, 124

Abbreviations: APC/C, anaphase-promoting complex/cyclosome; ND, not determined; OEC, *Golovinomyces orontii* effector candidate; PCNA, proliferating cell nuclear antigen; PM, powdery mildew; RBR, retinoblastoma-related protein; TF, transcription factor; WT, wild type; Y2H, yeast two-hybrid.

Appendix 2: Protocol for fungal spore neutral lipid comparison using flow cytometry

Growth conditions and powdery mildew infection

Arabidopsis thaliana plants were grown in an alternating pattern of wildtype and mutant genotypes within each box to ensure equal growing conditions and even infection upon inoculation. At 4 weeks, *A. thaliana* was tower inoculated with a moderate inoculum (2 half covered leaves at 10-14 days post infection (dpi) of *Golovinomyces orontii* MGH1 per box. After sitting for 10 minutes, the plants were returned to the growth chamber.

Spore collection

Three fully expanded mature leaves were harvested per plant with a total of 9 plants per genotype at 9 dpi. 30 mL 0.01% Tween-80 in water was added to leaves in 50 mL Falcon tube and vortexed for 30 seconds to liberate spores. Spore suspensions were filtered through 40 µm mesh and centrifuged at 4000 x g.

Enrich spores using sucrose gradient

To be able to gate spores in suspensions containing a significant amount of plant debris, a sucrose gradient may be required. This is particularly useful at early time points in infection with a low initial inoculum when the spore yield is low. To remove plant debris, the spore pellet was layered on top of a sucrose gradient (750 µL each layer: 20%, 30%, 40%, 50%, and 60% sucrose) and centrifuged at 4000 x g for 5 minutes. Below is a sucrose gradient with a spore suspension layered on top after it had been centrifuged at 4000 x g for 5 min. Spores have repeatedly been found to be enriched around the 20-30% sucrose layers, though spores are found in each layer. The 60% layer had the most debris (ex. dirt, mycelia). The layers corresponding to approximately 20-30% were collected for analysis. The enriched spore suspension is brought up to a volume of 1 mL with water, then split into stained and unstained aliquots for flow cytometry.

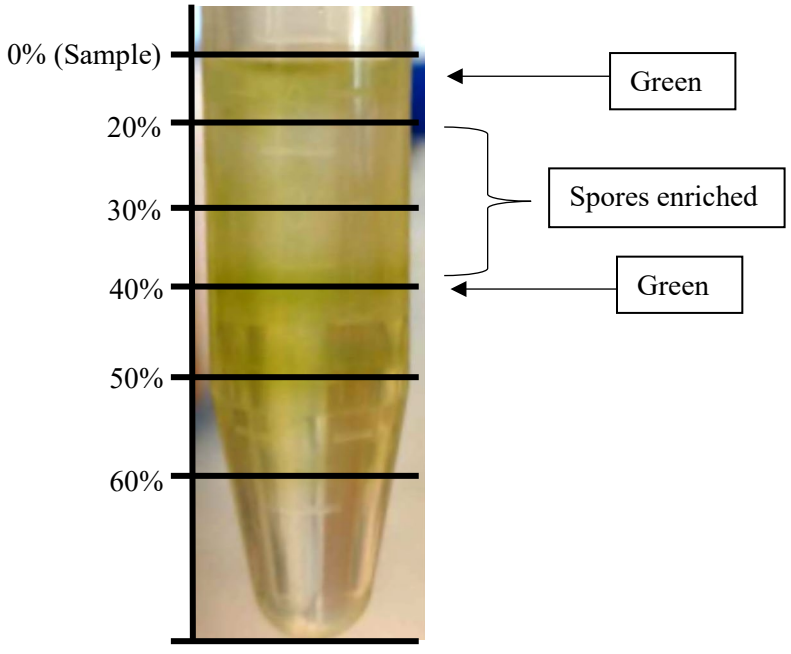

Neutral lipid staining

BODIPY 505/515 (D3921, ThermoFisher Scientific) was originally dissolved in DMSO for a stock concentration of 1 mg/mL and diluted 1000X in the spore suspension to a working concentration of 1 µg/mL.

Flow cytometry and statistical analysis

Spore suspensions were run on an LSR Fortessa X20 flow cytometer. For fluorescence measurements, samples were interrogated with a 488 nm laser and signal was captured with a FITC (505LP 530/30) filter. To identify spores in suspensions, the voltage of the forward scatter (FSC) and side scatter (SSC) parameters were lowered to 100 during measurements because the spores are relatively large (15X30 µm). This allows the spores to be seen in the FSC and SSC parameters and the spore gate to be drawn. Sample acquisition was done using BD FACSDiva Software (v7.0) and subsequent gating for analysis was done using FlowJo (v10.1). The fluorescence intensity of 200 (±10%) spores were measured per replicate. Fluorescence intensity distributions were compared using Chi-Squared T(x) statistical analysis in FlowJo (v10.1) software.

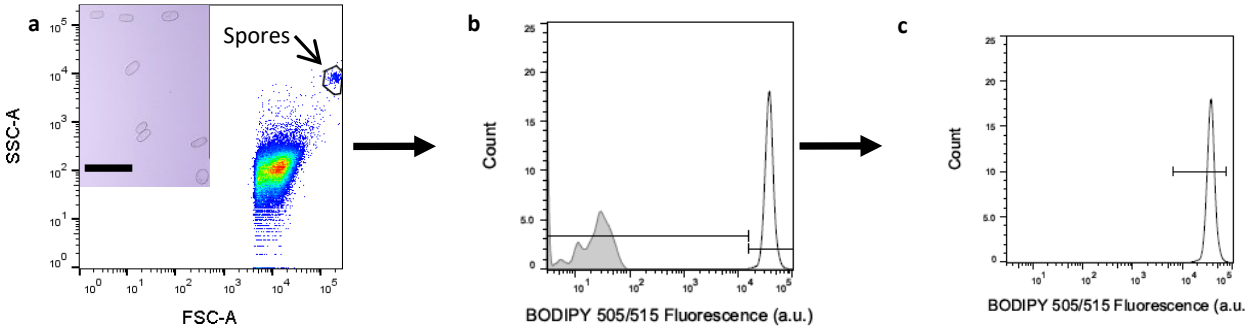

Flow cytometry gating strategy to assess *G. orontii* spore lipid content using BODIPY 505/515. (a) Spore suspension visualized by forward scatter (FSC-A) and side scatter (SSC-A) to identify spores (gated). Inset: Spores sorted by a BD Influx Sorter to verify gating methods. Scale bar is 100 µm. (b) Distribution of fluorescence measurements of stained (black) and unstained (grey) spores are compared to gate off autofluorescence. (c) Final gating for stained spores. Upper limit of gate is set at 2x the mean fluorescence for each experiment.

Appendix 3: Adult *Arabidopsis thaliana* powdery mildew spore quantification protocol

The following protocol has been optimized/adapted from Weßling and Panstruga, 2012 and Weßling et al., 2014 to phenotype *G. ororntii* MGH1 growth on *A. thaliana* adult plants.

Weßling, R. and Panstruga, R. (2012) 'Rapid quantification of plant-powdery mildew interactions by qPCR and conidiospore counts', *Plant Methods*, 8(1), p. 35. doi: 10.1186/1746-4811-8-35.

- "At 6 dpi, three samples of approximately 500 mg of seedlings were harvested per genotype. Five ml H_2O was added and spores liberated by vortexing for 30 s at maximum speed. The spore solution was filtered through Miracloth (Merck, Darmstadt, Germany) to remove large debris and spores were 4-fold concentrated by centrifugation (5 min, 4000 g). For each sample, spores were counted in eight 1 mm^2 fields of a Neubauer-improved haemocytometer (Marienfeld, Lauda-Königshofen, Germany) and results were averaged. Finally, spore counts were normalized to the initial weight of seedlings. Uses 18 day old seedlings and settling tower inoculation."

Weßling, R. *et al.* (2014) 'Convergent targeting of a common host protein-network by pathogen effectors from three kingdoms of life', *Cell Host and Microbe*, 16(3), pp. 364–375. doi: 10.1016/j.chom.2014.08.004.

- "Fungal infection assays. Powdery mildew infections were carried out as described previously, except that spores were harvested at 7 dpi (Weßling et al., 2012). Inoculations were either performed on 18 day old seedlings or 4-5 week old plants. Briefly, inoculations were either performed on three pots per genotype containing ~200 18 day old seedlings or four 4-5 week old plants were inoculated in a settling tower with *G. orontii* spores harvested from four leaves 14-21 dpi. Each round of inoculation included nine pots of randomized genotypes, thus all genotypes were included in three separate inoculations. After one minute incubation the pots were returned to the growth chamber. At seven dpi, three times 200 mg (older plants) or 500 mg (seedlings) plant material was harvested across pots and *G. orontii* spores isolated by shaking in water. The number of spores/g fresh weight was determined by counting eight chambers in a hemocytometer."

Adult *Arabidopsis thaliana* powdery mildew spore quantification protocol

Planting

1. Stratify *Arabidopsis thaliana* seeds (suspend seeds in 0.1% agarose at 4°C for 2-5 days).
2. Plant seeds. Grow plants in growth chambers at 22°C, 70% RH, and a 12 hour photoperiod with photosynthetically active radiation = 100 μmol/(m^2 × s).
3. Infect plants at 4-4.5 weeks with powdery mildew, *G. orontii* MGH1, at 2:00 pm using a settling tower and mesh cloth. Use a heavy dose (4 fully covered leaves at 11-14 dpi). Remove plants from settling tower after 10 minutes. Mark 3-4 leaves per plant that are fully expanded and exposed to the inoculation with toothpicks.

Spore collection

1. At 8-11 dpi, collect 10-15 fully expanded mature leaves from 4-5 plants (leaves 7-9, three leaves per plant) per genotype/treatment in a pre-tared 50 mL Falcon tube.
2. Weigh leaves in 50 mL Falcon tube.
3. Add 15 mL of 0.01% Tween-80 to tube and vortex vigorously (at max speed) for 30 seconds.
4. Use forceps to remove and shake water off leaves. Filter through a 40 μm filter (Sysmex) into a 15 mL conical tube. Rinse filter with 500 μL 0.01% Tween-80.
5. Centrifuge for 5 min. at 4000g.
6. Pour off supernatant. Blot rim of inverted tube to remove excess liquid.
7. Use low retention tips (Neptune low retention S^3 polymer tips). Resuspend with water to 200 μL - 1.2 mL depending on spore yield. Transfer to 1.5 mL low retention Eppendorf tube and count spore suspension.

Spore counting

1. Vortex to resuspend pellet and immediately pipet 10μL into hemocytometer (each hemocytometer has 2 chambers). Limit vortexing to limit spores sticking to sides of tube.
2. Count the spores within each 1 mm^2 of the Neubauer-improved hemocytometer chambers (9 total per chamber, see Fig. 1). For spores that are on the border of the grid, only count the ones on the right and bottom border. Count conidiophores as 1 (see Fig. 2). Suspension can be diluted to 200-1200 μL if too concentrated (>150 spores per 1X1 mm).

Calculations and statistics

Calculate spores/gram fresh weight. For each replicate, experimental spores/g fresh weight should be normalized to the paired wildtype/control spores/g fresh weight. Use a 2-tailed Student's T-Test (excel: =ttest(CONTROL,EXPERIMENTAL, 2,2)) to compare normalized control and experimental counts and determine p-value for statistical significance.

Neubauer-improved hemocytometer

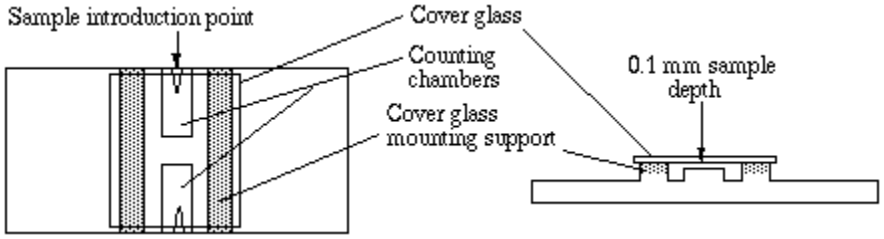

Chamber grid

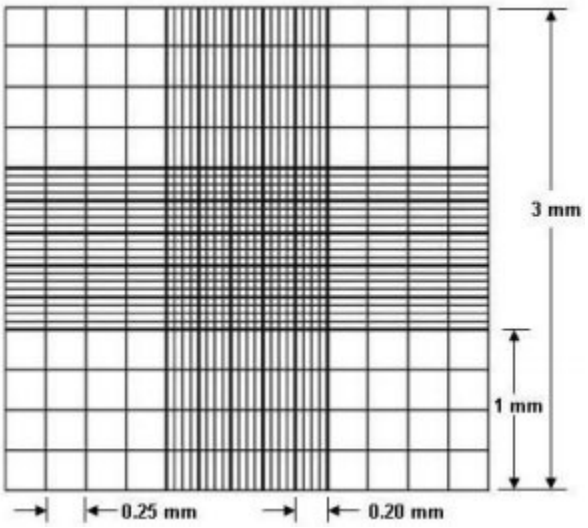

Fig. 1. Neubauer-improved hemocytometer and chamber grid layout. 10µL of spore suspension is loaded into each sample introduction point with coverslip mounted.

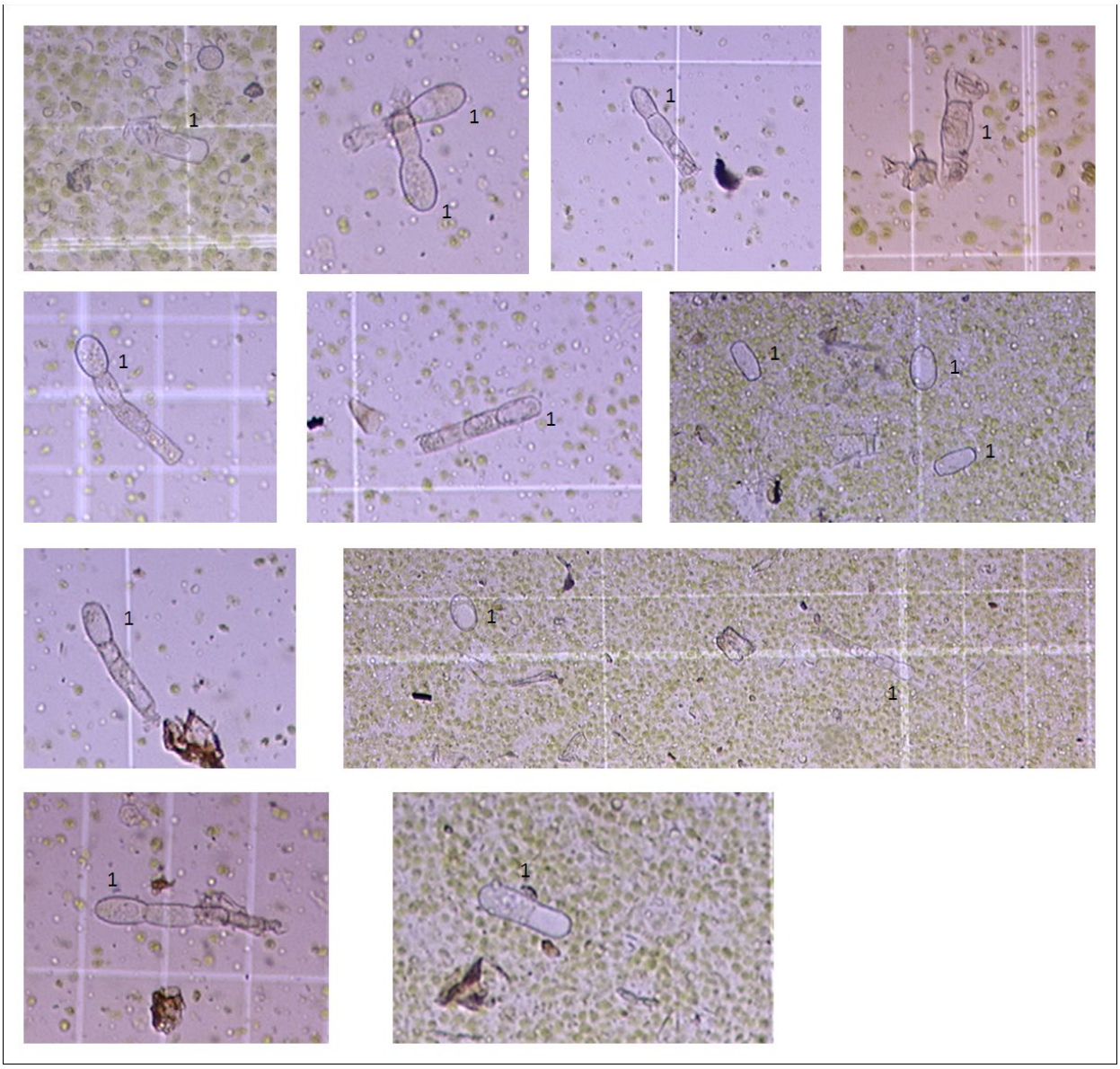

Fig. 2. Conidiophore and conidium examples. Each conidium, conidiophore, or partial conidiophore counts as 1 spore (indicated with numbers), even if multiple conidia are in a chain.

Appendix 4: Quantification of *A. thaliana* powdery mildew infection site ploidy protocol

Sample harvesting and DAPI staining

1. Fix leaf samples (3 leaves per plant into each vial, 3+ plants total) in 95% ethanol for at least 2 hours at RT or store at 4°C until use.
2. When ready to stain with DAPI, remove leaf edges using a clean razor blade and vacuum infiltrate in 1 mL of 1 μg/mL DAPI working solution in a 12-well plastic plate for 20 minutes using 200 Torr.
3. Mount leaf with trichome side up in 100 μL of 1X SYTO on a glass slide using a 18X18 mm coverslip. Only one leaf per slide.
4. Use prepared slides immediately for quantification using confocal microscopy.

DAPI: Prepare stock solution with 1 mg/mL in water. Store at -20°C wrapped in aluminum foil. Light sensitive. Prepare working concentration with 1 μg /mL in water.

SYTO 11: Prepare 5 μM working solution by adding 1 μL of 5 mM SYTO 11 dye (Molecular Probes) to 1 mL water. Store at -20°C wrapped in aluminum foil.

Confocal imaging using Zeiss LSM710

If the system is completely off, follow posted instructions for bootup of lasers (including Argon laser to visualize SYTO11) and microscope.

1. Log on to the computer using Wildermuth Lab profile and password aspir1n.
2. Start the ZEN2010 software.
3. Click "Smart Setup." Add DAPI channel and select 405 nm and "Best Signal." It is unnecessary to add a channel to capture SYTO11. SYTO11 stains the fungi for easier identification of colonies when scanning the leaf through the oculars. SYTO11 can be excited with a 488 nm laser and viewed with a FITC filter set. When capturing z-stack images, if fluorescence of SYTO11 is also captured, scans will take twice as long.
4. Click on "Acquisition" tab and set up acquisition settings (Fig. 1)
    a. In "Acquisition Mode" window, click on 1024 X 1024 "Frame Size" and "Optimal." Choose scan speed 7. Select 12-bit.
    b. Click to check Z-Stack (checkbox near top under "Acquisition" tab). Go to "Z-Stack" window. Set interval by clicking button next to "Optimum" which will auto set the slices to around 1.5 μm thick.
    c. In "Channels" window, recommend setting AU to 1 (thinner slices). Set "Digital Gain" to 1 and "Digital Offset" to 0. During the experiment you will adjust the "Gain (Master)" to the appropriate level based on which layer of cells are being imaged.
5. Load slide when the lowest objective is on (e.g. 10X). Focus sample using coarse/fine focus knob on the right side of the microscope. Use FITC filter to scan leaf for colonies. Once focused, move to 20X and adjust fine focus before adding oil and moving to the 40X objective.
6. Click the "Live" button under the "Acquisition" tab. Use fine focus to search through guard and mesophyll cell layers. To check for saturation, change color output to have red pixels indicate oversaturation and blue pixels indicate very low intensity. Identify a gain value where guard cells in the epidermal layer have good, but not saturated signal.

a. Since DAPI does not penetrate the leaf very well, the nuclei of the guard and epidermal cells typically stain more intensely than the inner mesophyll cells. Therefore, it is important to find the best DAPI channel gain settings for both layers (lower for epidermal and guard cells and higher for mesophyll cells). Use the fine focus knob to move up and down while adjusting detector gain. Epidermal cells look curly, while mesophyll cells look rounded.
b. Use 2-3 different areas on the leaf to find the optimal DAPI channel gain settings. Note them down to use for all images (ex. Gain=437 for guard cells and Gain=581 for mesophyll cells).
c. Staining intensity can vary. The protocol also works if the change in gain between layers is fixed. For example, image guard cells with gain=586 and mesophyll cells with gain=626. If the guard cell nuclei are saturated at gain=586 in another location/slide, lower the gain accordingly and image the mesophyll layer at gain=40 higher than epidermal gain.

7. While in "Live" mode, set the Z-stack interval in the "Z-Stack" window. Use the fine focus to focus just above the guard cell nuclei and click "Set Last." Use the fine focus to focus just under the mesophyll nuclei and click "Set First." End live mode.
8. Set gain to lower setting for guard cells. Click "Start Experiment" under the "acquisition" tab.
9. Watch the current image being acquired. When the Z-Stack has reached the bottom of the epidermal cell layer and the mesophyll nuclei start emerging change the gain setting to the higher value chosen for the mesophyll layer.
10. Once the z-stack is done (approximately 5 mins each scan, depends on thickness of Z), click on "save as," give the file a name, and save in a new folder for each colony. Example folders: Col-0 for tcp14 mutant>Infected>Replicate 1>Leaf 1>Colony 1. Save as a .lsm file for image processing later and as a .tif if you want to have a file for each slice that can be viewed without Imaris or other special software.
11. Perform at least 10 z-scans from different leaves for each replicate to be able to quantify at least 30 mesophyll cell nuclei.
12. Repeat procedure for uninfected samples using the same gain settings It is important to use the same settings to be able to compare the 2 different samples.
13. The number of slices for uninfected samples is typically between 35-40 and 25-30 for infected samples (since the nuclei appear to be closer to the haustorium).

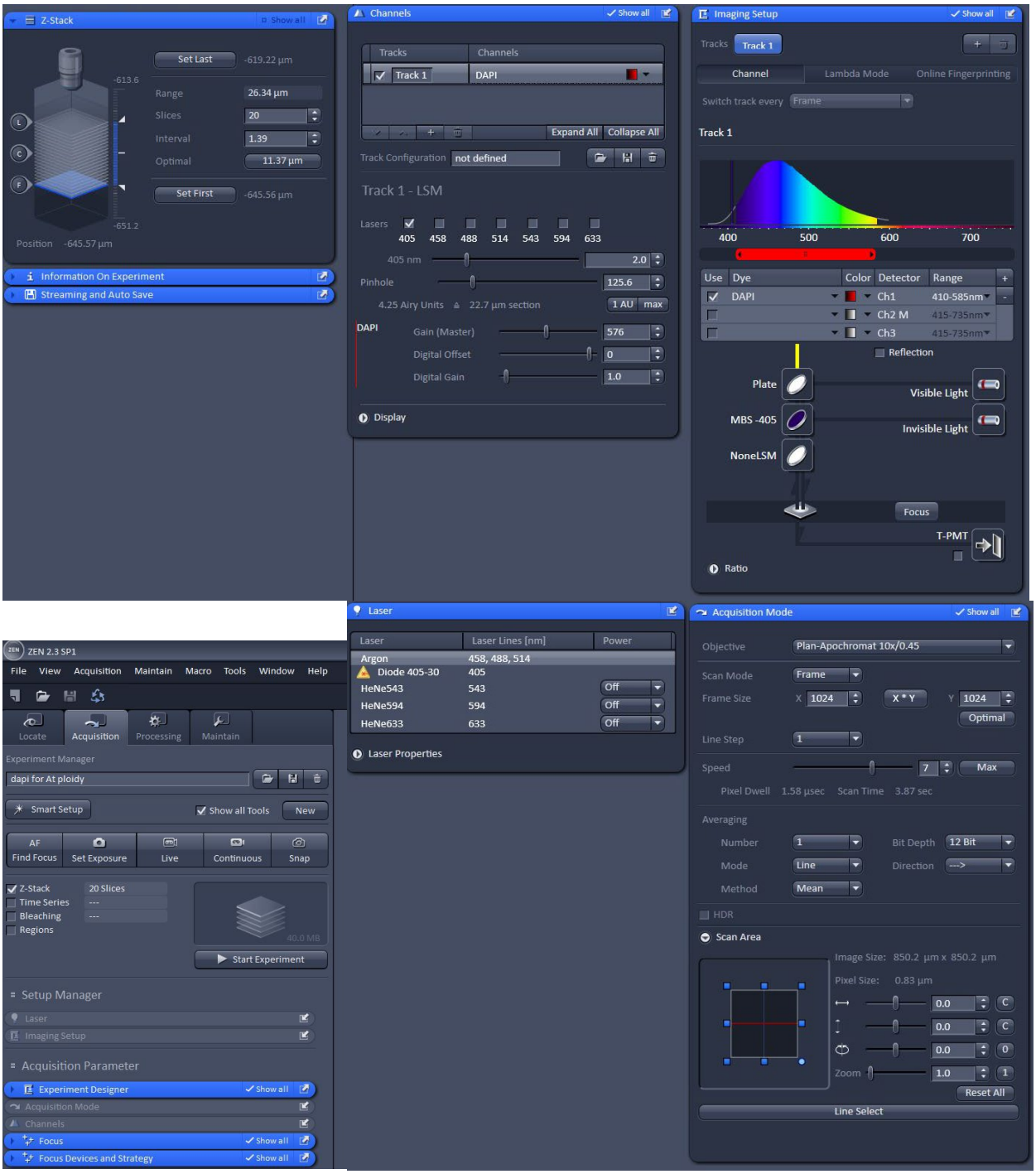

Fig. 1. Example ZEN2010 DAPI-stained mesophyll fluorescence acquisition settings using Zeiss LSM710.

Imaris-Surfaces quantification of DAPI-stained nuclei

Note: Previously Imaris-Spots was used to quantify nuclei fluorescence. Imaris-Surfaces creates a custom fitted shape over the nucleus which more accurately selects the fluorescence to quantify. This is more appropriate as guard cell nuclei are ellipsoidal and mesophyll nuclei shape vary (Fig. 2-3). Both Surfaces and Spots are used to quantify the intensity sum enclosed within the shape.

1. Save z-stack image files as a .lsm file.
2. Open Imaris 9.5.0.
3. Find file in Arena tab and open file.
4. Add new Surfaces by clicking the blue surfaces icon on the left panel or under 3D View>Surfaces.
5. Enter settings for surfaces under "Create" tab. To navigate between pages, click blue arrow (back/next):
    a. Page 1
        i. Algorithm: Under algorithm settings, check "Segment only a Region of Interest." Do not select "Process entire Image finally" or "Shortest Distance Calculation."
    b. Page 2
        i. Region of Interest: Create a tight-fitting rectangular prism around the nucleus selected for quantification by shrinking the region of interest using the pointer in X, Y, and Z plane (default ROI is entire z-stack). On the right panel, toggle between "select" and "navigate" to select the region of interest. Select allows the pointer to move the ROI and the arrows on the edge of the ROI. Navigate allows the pointer to move the z-stack to different angles and the mouse scroll zooms (zoom can also be changed in the bottom right drop-down menu). Use "Center to Selection" and "Fit to Selection" buttons in the right panel to re-center as needed.
    c. Page 3
        i. Source Channel: Select DAPI fluorescence channel under "Source Channel." Check "Smooth" and set "Surfaces Detail" to 0.2 μm. Under "Thresholding" select "Background Subtraction (Local Contrast)" and enter "Diameter of largest Sphere which fits into the Object."
        ii. To determine the diameter of the nucleus, switch to "Slice" view (click icon at top or go to View>Slice). Find the narrowest part of the nucleus by moving through the z-stack (slider button on left). In the "Measure" panel on the right select "Line." Click on the image at the edge of the nucleus to deposit a "+" and then click the other side of the nucleus to deposit another "+" laying down a line measuring the distance. The length of the line is recorded in the right panel.
    d. Page 4
        i. Threshold: Slide the left-hand threshold to manually create a cutoff of fluorescence intensity that is appropriate for the nucleus.
    e. Page 5
        i. If multiple surfaces are detected, select the surfaces of interest to be included in the surfaces created. In most cases only 1 surface will be detected. Click the green double arrow (finish).

6. Go to “Statistics” tab and under “Detailed” tab select “Specific Values” and “Intensity Sum” in the drop-down menus.
7. Record “Intensity Sum” value for ploidy analysis.
8. To re-edit surfaces, go to “Creation” tab and under “Recompute” click “Surfaces” button.
9. Repeat steps 4-7 for each nucleus quantified. In each image quantify the intensity sum for at least 1 guard cell to normalize the mesophyll values to. Multiple guard cells can be measured to get an average.
10. Save image as an .ims file to save analysis.

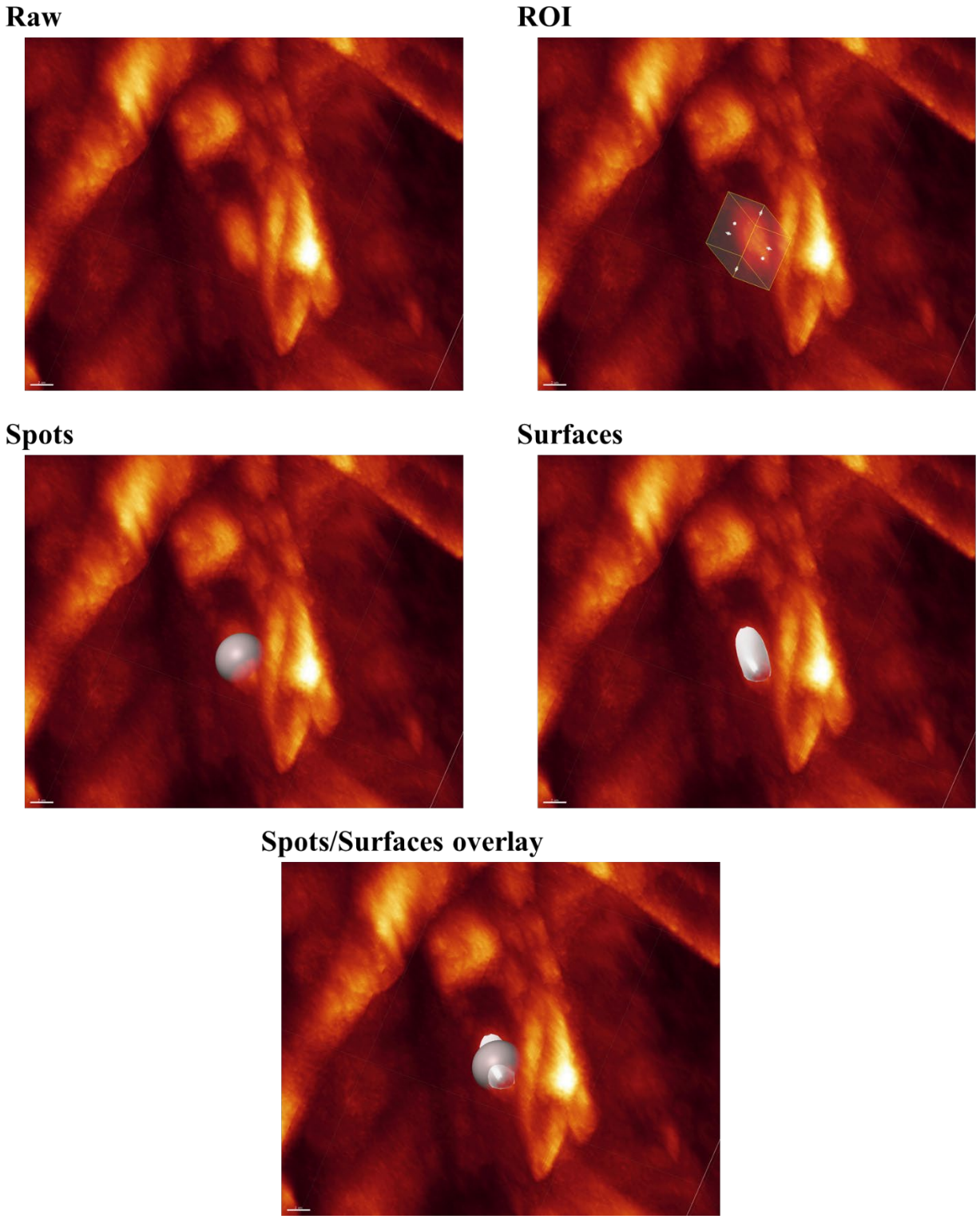

Fig. 2. Guard cell nucleus DAPI quantification. ROI=region of interest. Scale bar is 2 µm.

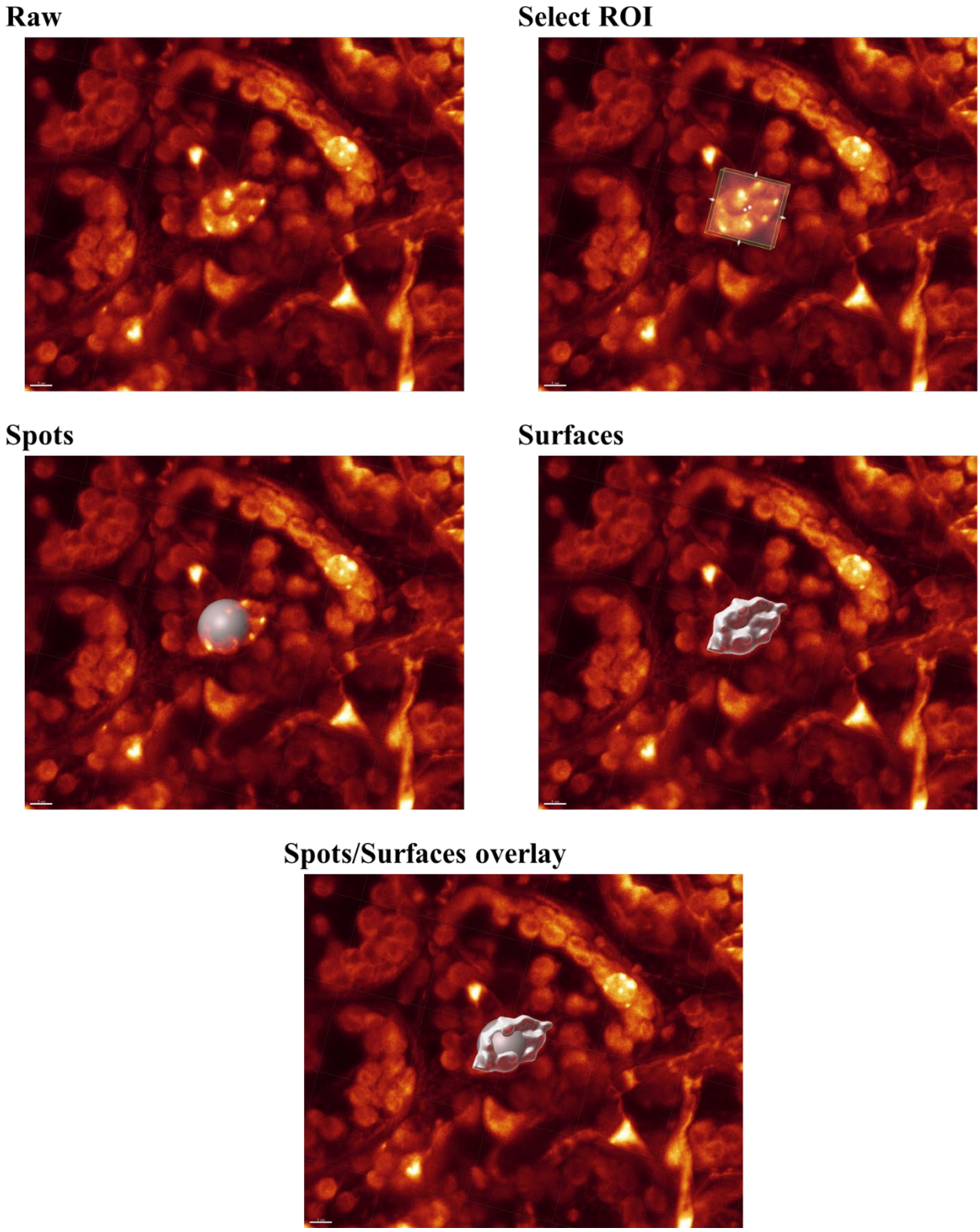

Fig. 3. Mesophyll cell nucleus DAPI quantification. ROI=region of interest. Scale bar is 5 μm.